Controlled Migration of Cells on Mechanically, Physically and Chemically Patterned Biomaterials

Vorgelegt von

Diplom-Chemie-Ingenieur

Master in Science

Gonzalo de Vicente Lucas

geb. in Madrid

Von der Fakultät II - Mathematik und Naturwissenschaften

der Technischen Universität Berlin

zur Erlangung des akademischen Grades

Doktor der Naturwissenschaften

Dr. rer. nat.

genehmigte Dissertation

Promotionsausschuss:

Vorsitzender: Prof. Dr. rer. nat. Holger Stark

Gutachterin: Prof. Dr. Ir. Marga C. Lensen

Gutachterin: Prof. Dr. rer. nat. Eva M. Eisenbarth

Tag der wissenschaftlichen Aussprache: 26. März 2015

Berlin 2015

“Science is the compass of life;
but it is not life itself”

Mikhail Bakunin

Index

List of abbreviations

α_i	Step angle with respect to the direction of the pattern
αpos_i	Step angle with respect to the direction of the pattern in positive terms
Υ	Angle of the pattern with respect to the horizontal axis of the image
Υ_{SL}	Surface tension solid/liquid
Υ_{SA}	Surface tension solid/air
Υ_{LA}	Surface tension liquid/air
µCdP	Micro-contact deprinting
µTM	Microtransfer molding
θ	Contact angle
θ_i	Step angle with respect to the horizontal
ω_{sp}	Spin speed
3BC:	PEG-b-PPG-b-PEG
3BC-µCap	Composite material of 3BC and hollow capsules
8PEG	8 Arm poly(ethylene glycol)
AFM	Atomic Force Microscopy
AuNPs	Gold nanoparticles
Blend1	Blend of PEG and 8PEG
Blend2	Blend of PEG and 3BC
BSA	Bovine Serum Albumin
c_w	Mean cosine of the directional errors
CellMAT	Cell Migration Analysis Tool
CL	Cross linker
D	Euclidean distance
$<d^2>$	Mean Square Displacement
DCM	Dichloromethane
DMF	Dimethylformamide
E	Young's modulus
ECM	Extracellular matrix
EG	Ethylene glycol

FA	Focal adhesion
FBS	Fetal Bovine Serum
FIMIC	Fill Molding in Capillaries
h_c	Critical thickness
L	Total path length
l_i	Length of the step
LbL	Layer by Layer technique
LSPR	Localized surface plasmon resonance
MIMIC	Micro-Molding In Capillaries method
MSC	Mesenchymal stem cell
NP	Nanoparticle
P	Persistence
PBS	Phosphate Buffered Saline solution
PDADMAC	Poly(diallyldimethylammonium)
PDMS	Poly(dimethylsiloxane)
PDT	Photo Dynamic Therapy
PI	Photo initiator
PEG	Poly(ethylene glycol)
PEG-µCap	Composite material of PEG and hollow capsules
PEG-µP	Composite material of PEG and solid $CaCO_3$ particles
PPG	Poly(propylene glycol)
PS	Penicillin/Streptomycin
PSS	Poly(sodium styrene sulfonate)
PVP	Polyvinyl pyrrolidone
$\vec{r}$	Position vector
RMS	Root Mean Square
S	Average migration speed
s_i	Step speed
SEM	Scanning electron microscope
T	Tracking time
t	Time

t_{penetr}	Resting time left for the blanket to penetrate inside the channels before spin-coating
$t_{pre-exp}$	Incubation time prior to cell experiment
t_{rest}	Resting time left for the blanket prior to UV-curing
t_{sp}	Spin-coating time
t_{UV}	UV-curing time
TCP	Tissue culture plate
TEM	Transmission electron microscope
TRITC	Tetramethylrhodamine isothiocyanate
V	Velocity
VBA	Visual Basic for Applications

Scope and organization of the thesis

Cell migration is a biological process very common in nature. Unicellular microorganisms need to be motile to survive as they have to reach the sources of nutrients. In multicellular organisms such as human beings, cell migration is not related that much to nutrition but mainly to the function of the cell. For example, immune cells migrate to areas infected by pathogens and attack them and osteoclasts migrate along the bones to extract the calcium needed for bodily functions, and during the process of wound healing, fibroblasts move to the wound, filling up the gap in the tissue. The abnormal migratory behavior of cancer cells can be expressed as unnecessary migration (metastasis) that can cause the appearance of tumors on new organs. From these examples, we can already discern the importance of active control of cell migration in medical areas such as tissue engineering or cancer treatment.

Different stimuli can induce and direct cell migration, e.g. topographical, mechanical or chemical cues, but the mechanisms behind the cellular response to them are still not completely understood. Cells in vivo usually encounter simultaneously several stimuli. In vitro studies can be essential to analyze the effect of those stimuli separately in order to improve our comprehension of the cellular migration. In simple terms, if we understand how cells interpret and respond to external signals, we can tailor those signals to communicate commands to the cells.

The main objective of this work was the control over the cellular migration by modification of the surface patterns presented to the cells, in particular the periodicity of them. Additionally, the interaction of fibroblasts with two different composite materials was studied. These composite materials have the potential to induce cell adhesion on specific locations and can also act as delivery vehicles for molecules such as drugs, chemoattractants or transfection agents.

This thesis is organized in the following chapters:

Chapter 1: Introduction

In this chapter the motivations of this thesis will be introduced. The different cell-substrate interactions will be described, making a special emphasis on the mechanism of cell migration and the different triggers of it, especially migration due to topographical, mechanical and chemical cues. The main tool for patterning, the **Fi**ll-**M**olding **I**n **C**apillaries (**FIMIC**) method will be described in detail and the polymeric materials used in this work. Finally, the main objectives of the thesis, supported by the information extracted from the bibliographic research, will be stated. Each experimental chapter will contain an introductory section with more specific information related to its topic.

Chapter 2: Materials and methods

Since many of the reagents, preparation methods and analytical proceeding are common to many of the experiments, they will be described in this chapter. Concrete operating conditions or chemical compositions will be stated at the Materials and Methods section of the corresponding chapter.

Chapter 3: Cell Migration Analysis Tool (CellMAT)

Migration data are typically obtained as a series of X and Y positions. Those values have to be treated to obtain migratory parameters such as migration angle, displacement or directionality. An Excel-based interface for fast analysis of the raw data to obtain those parameters which are relevant for cell migration will be presented.

Chapter 4: Controlling cell migration on Fill-Molding In Capillaries substrates

In this chapter we will present results of migration of fibroblast on topographically, elastically and chemically patterned substrates. The influence of the dimension of the pattern in the migratory behavior will be analyzed from the visual observations as well as from the typical parameters extracted from the migratory track.

Chapter 5: Fabrication of embedded patterns of elasticity

In order to study the influence of mechanical cues on the migration of cells it is necessary to generate substrates where chemical and topographical signals are suppressed. Three different methods, namely spin-coating, razor-blading and sandwiching, will be described here. The adequacy of each will be investigated, addressing the challenges found during experimentation. The work for this chapter was done with help of Paul Gruner, Bachelor in Bio- and Nanotechnology.

Chapter 6: Cell response to anti-adhesive substrates patterned with metallic nanoparticles

In this chapter the cellular response to chemical cues generated by metallic nanoparticles on the surface of anti-adhesive poly(ethylene glycol) will be analyzed. The effect of different materials, i.e. gold and silver, and shapes on the adhesion and cell viability of fibroblasts will be analyzed. Additionally, three methods for patterning of metallic nanoparticles on gels will be presented and their efficiency in terms of cell adhesion stated. Experiments for this chapter are based on a collaboration with Dr. Manar Arafeh, Çiğdem Yeşildağ, M.Sc. in Chemistry and Christoph Bartsch, B.Sc. in Chemistry.

Chapter 7: Immobilization of polymeric capsules by Fill-Molding In Capillaries for controlled interaction with adherent cells

Polymeric capsules immobilized on the surface of cytocompatible gels may also modify the chemical and mechanical properties of the material and, therefore, modify the cellular behavior. In this chapter a novel composite material containing microparticles for cell interaction will be introduced. The challenges of the processing of such samples will be explained and the observed adhesive behavior of fibroblasts, comparing it to the adhesion on samples lacking microparticles, will be described. This work was part of a collaboration with Prof. André Skirtach, which final aim is the controlled delivery of molecules to adherent cells without the necessity of biotargeting.

Chapter 1:

Introduction

1.1 Biomaterials:

A biomaterial can be defined as *"A synthetic material used to replace part of a living system or to function in intimate contact with living tissue"* [1]. Other authors open the definition to non-synthetic materials: *"A biomaterial is a nonviable material used in a medical device, intended to interact with biological systems"* [2]. Figure 1.1 illustrates some of the applications of biomaterials within the human body.

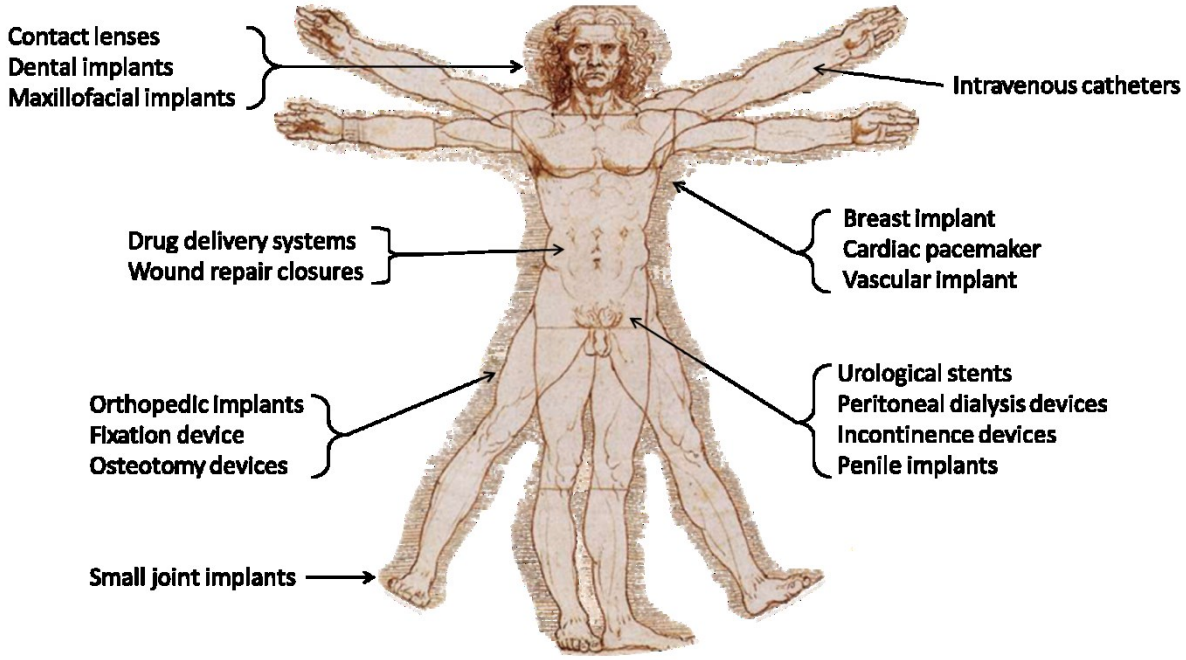

Figure 1.1: Examples of applications for replacing missing tissues or enhancing biological functions. Image based on reference [1].

While referring to biomaterials, it is important to remember that those devices which are in contact with the skin, such as artificial limbs, are not necessarily made of biomaterials, since the skin acts as a barrier between the body and the external environment.

Biomaterials have to be chosen or designed according to a set of compatibility requisites: mechanical, chemical and biological compatibility [3]. Implants must have the adequate elasticity to match the properties of the tissue where they are implanted. In the case of fixation devices for bone fracture healing or hip implants, mechanical strength is mandatory. These are two examples of mechanical requirements. At the same time, biomaterials inside the body must be chemically compatible; they are subjected to chemical attacks such as degradation and corrosion. In some cases, degradation is desirable to

remove the implant after regeneration of the tissue, but the degradation speed must be appropriate. According to the definition of biomaterials, they are intended to interact with biological systems and they must induce on them the correct reaction. This is known as biocompatibility. The exact definition is “the ability of a material to perform with an appropriate host response in a specific application” [2]. Biomaterials should, for instance, not induce immune reactions or show cytotoxic behavior; this also applies to the products derived from their degradation.

Biomaterials can be classified according to the nature of the material into several groups, e.g. metallic, ceramic, polymeric and composites [1]. Metallic biomaterials are mainly used because of their strong mechanical integrity and they are applied, among others, as stents, for dental implants and joint implants [4]. They are not biodegradable, which can be an advantage for permanent implants but a disadvantage for provisional ones [3]. Ceramic devices are extremely hard but also, due to that, they are fragile and breaks can be easily formed and spread. They can be bioinert and also biodegradable, therefore they can be employed for dental coatings, bone substitution or lining of joint implants [3]. Polymeric biomaterials have a vast spectrum of applications because of the high variability of their properties. Polymers can be hard or soft, elastic or rigid, biodegradable or bioinert, hydrophobic or hydrophilic, they can be functionalized with molecules to induce a concrete response on the cells and they can even be polymerized inside the body, leading to a perfect geometrical fitting to the affected area. Other advantages include the lower costs and the ease of fabrication. They have been used, amongst other things, for coating of wounds (artificial skin), replacement of tendons and ligaments, artificial heart valves, breast implants, dental implants, finger joints or devices for controlled drug release [3].

Composite materials are a special type of biomaterial because they combine two or more biomaterials. Each component is chosen to fulfil a specific function, combining their properties and improving the efficacy reached by the individual elements [5]. Composites find application as dental fillers, where the inorganic inclusions (ceramic) provide stiffness and the polymer provides a matrix to support the ceramic particles and permit direct polymerization at the cavity of the teeth, resulting in a complete filling of the treated area [1]. Other applications involve porous implants as scaffolds for ingrowth of tissue,

fixation devices, artificial tendons, ligaments and cartilage or joint prostheses [6]. Briefly, composites have as many potential applications as their individual components.

Hydrogels:

Hydrogels were the first cytocompatible materials successfully designed for use in the human body [7]. A hydrogel is a polymeric material containing hydrophilic groups that are able to absorb and retain large amounts of water or biological fluids inside their three-dimensional structure [8]. Hydrogels are extremely interesting as biomaterials; their properties, such as their mechanical properties, porosity or three-dimensional structure, can be tuned to match the requirements of the surrounding environment [9]. They are also highly cytocompatible thanks to their water content and physicochemical similarities to the extracellular matrix (ECM) [10]. As a result of these properties, hydrogels have been widely used for drug delivery [10] and tissue engineering applications, acting as scaffolds for cell growth during regeneration of tissues [11].

Poly(ethylene glycol) (PEG) is a highly useful hydrogel material as it can be presented as a transparent liquid before polymerization. Monomeric PEG containing acrylate groups at both ends of the chain (PEG-diacrylate) can be polymerized via radical reaction, initiated by UV radiation, which can then be micro- and nano-molded as required. The great advantages of UV-curable polymers are that the reaction can be carried out under mild conditions (room temperature or body temperature), they require short reaction times (a solid gel can be formed already after 5 minutes of irradiation), gels are formed *in situ* and the obtained materials are highly cytocompatible [12]. PEG hydrogels are transparent, brittle and relatively hard [13].

However, the most interesting property of PEG, and the reason of its extensive use in the fabrication of biomaterials, is its intrinsic anti-adhesive behavior [14–17]. Due to its high hydrophilicity, low protein adsorption occurs on the surface of PEG gels [14]. In some works, PEG was used to completely avoid non-specific protein adsorption and the consequent interaction between cell and biomaterial; for example, Wattendorf and co-workers have functionalized microcapsules with PEG in an attempt to avoid that cells can recognize the microcapsules and phagocyte them [18]. In other cases, scientists took benefit of the properties of PEG to create an inert background to study the effect of specific elements

included on the surface, e.g. gold nanoparticles, in the adhesive behavior of cells [19]. The work of Wang and colleagues shows an interesting application of the anti-adhesive properties of PEG, patterning a substrate with submicrometric features of PEG with a defined spacing between them. They created a material with "differential adhesive" properties where microbes are unable to adhere while osteoblasts adhere and spread on it [20].

Interestingly, Kim reported adhesion of fibroblasts on PEG patterned with nanopillars [21]. In their work, the nanotopography modifies the surface properties of the material turning hydrophilic PEG into hydrophobic. This behavior of nanostructured surfaces is known as the lotus effect; lotus leaves have an extremely rough surface that converts them into super hydrophobic materials. This change into hydrophobic surface modifies completely the interaction protein-surface allowing protein adsorption and consequent cell adhesion.

Previous work from our group showed that, also in presence of micrometric structures such as channels or pillars, PEG hydrogels were not cell-repellent anymore and fibroblast adhered and spread [22–24]. In this case, the hydrophilicity of PEG was maintained; hence no changes on the adsorption of proteins should have been expected. This divergence from the observations on flat PEG substrates may be explained at two levels: At a molecular level, structured substrates indeed induced differences on the protein adsorption; Roach demonstrated that the surface curvature was able to stabilize or denaturalize adsorbed proteins [25]. At a cellular level, the structure increased the available surface for adhesion per unit of volume, which led to a larger amount of accessible anchoring points. Despite that the underlying reason of this adhesive effect is not fully understood, these results highlight the fact that the chemistry alone of PEG coatings are not enough to guarantee anti-adhesive surfaces, but the structures on the surface must also be taken into consideration.

PEG-based polymers also have other interesting properties. Block co-polymers of PEG and poly(propylene glycol) (PPG) present different wettability and hydrophilicity properties from the original **PEG** hydrogels depending on the composition of PPG present in the monomers [26]. In this way, hydrogels with better cell adhesive properties can be synthetized. The work of Hsu is an example of variation of PEG composition to tune the properties of the final polymer[27]. Multi-arm PEG monomers can also be used to form

hydrogels. Due to the lower cross-linking density of the polymerized network, compared with low molecular weight linear PEG, these materials are softer than linear PEG hydrogels but maintain their anti-adhesive properties.

Hydrogels are not necessary prepared only with pure polymers. Blends of polymers can also be used. Blends of PEG, a tri-block co-polymer PEG-b-PPG-b-PEG (**3BC**) and an 8-Arm PEG monomer (**8PEG**) were already used in our group for preparing cytocompatible hydrogels [28]. One of the advantages of using these blends materials is that their properties can be tuned, for example, the hydrophobicity or the swelling behavior of the hydrogel by varying the ratio of the pure polymer constituents.

1.2 Cell-substrate interaction:

Cells behave according to their nature and surrounding environment. Consequently, adherent cells, such as fibroblasts, will adhere, but only if the substrate is suitable for it. The selection of one biomaterial over another is not a trivial issue; by choosing a substrate with the adequate properties, modifications on different types of cellular responses such as proliferation [29], differentiation [30], cellular death [31], adhesion [21] or cell motility [15] can be induced. In this work, we focused our attention on the latter.

Cell migration can be defined as any process that involves translation of cells from one location to another [32]. It is a primary process which takes place with both unicellular and multicellular organisms. In the human body, it is implicated in many biological processes, such as morphogenesis, immune response, osteoporosis, metastasis or wound healing [15,33,34].

While studying cell mobility, we can distinguish between two different concepts: Cell motility, which is the capacity of the cell to move, and cell displacement, which is the movement from one point to another [35]. Cells can be motile without displacement. At the same time, cells can also shift their position due to external forces. In this case, there is no active migration.

Active cellular displacement requires some specific steps: When a substrate is surrounded by a biological fluid (*in vitro* or *in vivo*), the first event occurring is the

adsorption of proteins on the surface. This adsorption can be non-specific or the surface can be tailored for an specific protein [25].

The next step is the cellular adhesion. Cells use the proteins on the surface as anchoring points to link with the substrate. This union is mediated by transmembrane proteins called integrins [36]. Integrins interact with other intracellular components to form adhesion complexes, which are connected to the cytoskeleton of the cell via actin filaments [37]. These adhesion complexes, especially focal adhesions (FA), do not only act as a mere gripping point, but are also part of the sensor and locomotive system of the cells. Focal adhesion has been identified as a key component to transduce the mechanical signals from the environment into biochemical and to exert forces on it, leading to displacement of the cell [15,38–41].

The strength of these adhesions has a great influence in the migration of the cell; adhesions which are too strong are hard to break and, therefore, the movement will be slowed down or non-existent. On the other hand, if the adhesion is too weak, the cell cannot exert enough force to move [33,42,43]. In other words, to incite the cell to move, the environment has to be comfortable enough for the cells to want to be there (adhere), but not as much for them to remain in the same place (migrate).

Cell translocation is preceded by cell orientation or polarization, which means, the formation of strong adhesion points on the front of the cell and the destruction of them on the rear, which results in detachment from the material. By forming new adhesions at the front, the cell will move into a determined direction [35,42,44].

Once the cell is attached and oriented, it can start to move, but why would the cell migrate in one direction instead of another or even refuse to move and stay immobile? Differences in the environment cause also inequalities and gradients inside the cell. Those gradients induce the directionality of the cell displacement. To achieve noticeable displacement, the difference of the external driving force between the front and the rear of the cell must be strong enough to overcome the internal gradient and constant enough to permit the cell to react [35].

Cell migration can be induced by many different triggers; maybe the most commonly investigated is chemotaxis, where the cell moves by following a gradient of soluble chemical

signals [45,46] (this is referred to as haptotaxis in the case of gradients of chemical signals adsorbed on a surface). Cells are also known to respond to topographic anisotropies such as channels [47,48]. This phenomenon is called contact guidance [49]. As introduced above, cells are also able to measure the mechanical properties of the environment and migrate into areas with more adequate characteristics, a process named mechanotaxis [15,50,51]. Also, light or thermal gradients, electrostatic potentials or magnetic fields, inter alia, can all promote cellular displacement [34,52–54]. In this thesis, the attention is centered on the first three phenomena, namely haptotaxis, contact guidance and mechanotaxis. More detailed information about these types of migration is included in Chapter 4.

At this point a question may arise: Why it is so important to control the migration of cells? Tailored cellular displacement has direct applications in the field of tissue engineering. For an implant to be successful, the first necessary condition is that it allows cells to migrate into the scaffold and proliferate, reconstructing the lost tissue [55]. A more concrete example where migration and growth in a specific direction is required, is during the development of nervous systems [56]. The use of topographically patterned substrates for nerve regeneration does not only provide a scaffold to grow, but also guides it in the required direction. This strategy has shown promising results promoting and improving migration and growth of cells of the nervous system and regeneration of damaged nerve tissue [57,58]. In short, if we manage to control the migration of cells into damaged areas we will be able to improve the efficacy of the regeneration and achieve a fully functional tissue.

1.3 Soft lithography:

The mechanisms which rule the different types of cellular migration are not fully understood and further experimentation must be carried out. *In vivo*, cells encounter a complex assembly of signals (chemical, topographical, mechanical, etc.) simultaneously, but to accomplish complete understanding of their effect on the behavior of cells, their influence must be studied individually. For this reason, we must be able to prepare biomaterials where only one signal is expressed at a time.

Soft lithography is a highly useful method to generate those biomaterials. Originally developed in the early 1990s by Whitesides and co-workers, it includes different techniques with a common core: They use a patterned elastomer instead of a rigid photomask to generate gels with micropatterns and microstructures [59]. Compared to other lithographic methods such as photolithography or electro-beam lithography, soft lithography has experienced a great success in the last years because of its possibilities: Versatility (many different materials can be patterned), high resolution (features down to tens of nanometers can be reproduced), easy processing and reduced costs (no expensive equipment is required).

1.3.1 Cast-Molding

The first step of many soft lithography methods is the preparation of the patterned elastomer via cast-molding [59]. In this method, a liquid polymer is poured on a patterned silicon master. After polymerization, the solidified elastomer presents a negative replica of the features on the master (Figure 1.2). This method is already capable to reproduce structures down to the nanometric scale [60]. The only necessary condition is that the polymer must be liquid and its viscosity has to permit penetration of the structures of the master.

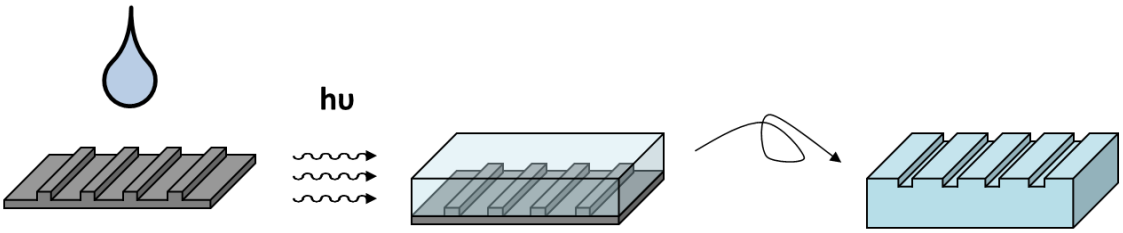

Figure 1.2: Depiction of the cast-molding technique.

A large variety of features can be replicated with this technique, such as channels, pits, pillars, squares or complex structures [61,62], but it also has its limitations. Features cannot be fabricated at any aspect ratio (height, width, separation) [59]. There are two main problems derived from the softness of the polymer and an inappropriate aspect ratio: The first phenomenon is called ***pairing*** (Figure 1.3a). The posts of the polymer stick together due to secondary interactions. This happens when the features are too high, thin and are located close to one another. The second effect is ***roof collapse*** (Figure 1.3b) and occurs when the

structures are small and largely separated. Under these conditions, the ground of the polymer (surface between features) can contact the substrate and deform the initial structure.

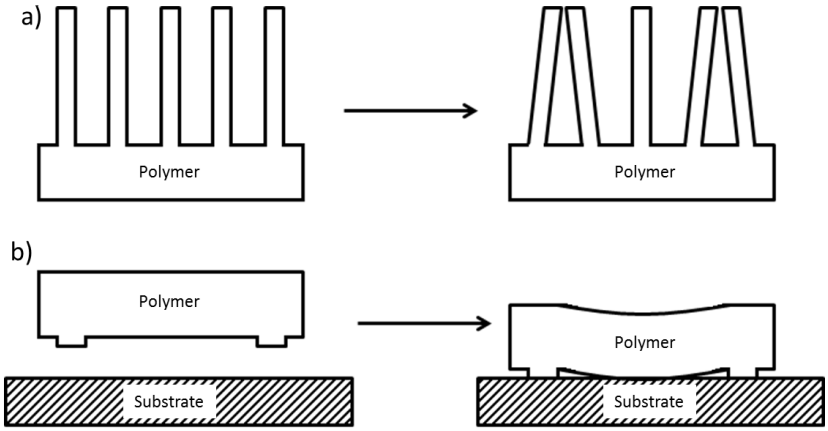

Figure 1.3: Representation of the limitations on replicating structures with soft polymers: a) pairing, b) roof collapse.

Another phenomenon to be considered is the ***shrinking***. Depending on the material and the polymerization method, the volume of the solid replica will be smaller than that of the liquid precursor. Poly(dimethylsiloxane) (PDMS), for example, is known to shrink around 1% [59] while UV-cured polymers reduce their volume in the order of 10% [63]. This is due to the conversion of secondary interactions, such as Van der Waals forces, into covalent bonds, which are more compact.

Substrates prepared by cast-molding are perfectly suitable for the study of the influence of topographic features since the structures are created on the surface of a homogeneous material, i.e. the chemistry and elasticity of the bulk material are not modified by the creation of the pattern.

1.3.2 Fill-Molding In Capillaries (FIMIC) method

In the past years, a new soft lithographic method has been developed in our group: The **Fi**ll-**M**olding **I**n **C**apillaries (**FIMIC**) method. First reported by Díez, this technique enables us to obtain topographically smooth samples with sharply defined chemical and/or elastic patterns on the surface [64]. It shares some similarities with the micro-molding in capillaries (MIMIC) method [65]. The starting point is the fabrication of a channel patterned sample (**mold**) by cast-molding. Then, the mold is placed face down on a smooth surface (typically a

clean glass slide). A drop of a secondary liquid polymer (**filler**) is placed close to the entrance of the channels and a small amount is carefully approached to the mold until subtle contact. At that point, the channels start being filled via capillary forces. Finally, the sample is UV-cured, resulting in a binary pattern along the surface of the material (Figure 1.4).

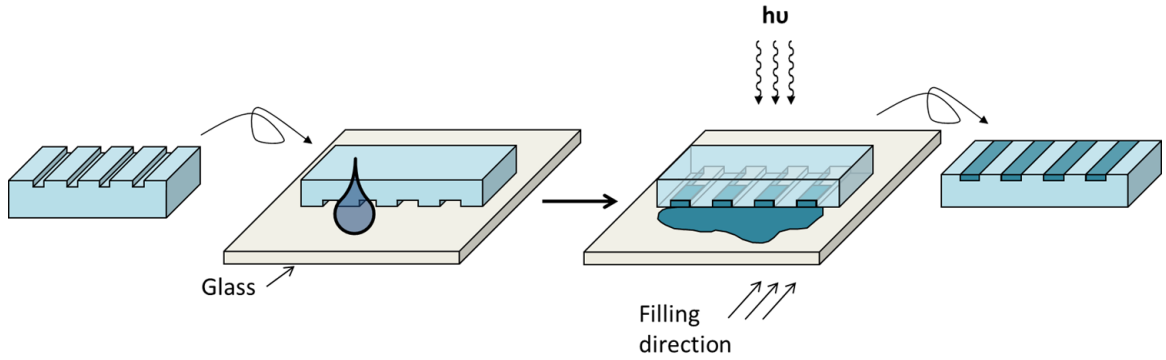

Figure 1.4: Scheme of preparation of a FIMIC sample. The mold is represented in light blue and the filler in dark blue.

The difference between MIMIC and FIMIC methods is that while in the former case the lines created by capillary filling are the final structure (the polymeric mold is removed), in the latter case, using the FIMIC method, the mold and the filled lines form together the substrate.

The polymers to be used for the FIMIC method must be in liquid state. If UV-curable polymers are used to prepare the FIMIC substrates, transparency to UV radiation must be added as a necessary condition. On the other hand, other polymerization methods such as thermic curing could be also employed.

As indicated above, mechanical patterns can be generated with this method; using the same material as mold and filler, but changing the cross-linking density of one of the components, an elastic contrast can be generated on the surface of the gel. This approach has already been applied in our group, obtaining mechanical 2D patterns which can be measured with Atomic Force Microscopy (AFM) [64,66]. Díez et al. used FIMIC samples to study the influence of mechanically patterned PEG on cellular adhesion. They demonstrated that not only topographic but also elastic patterns modify the anti-adhesive properties of PEG, since fibroblasts showed a clear preference for those lines containing a stiffer material [64].

Chemical patterns can also be created by this technique when the mold and filler material are different. Components can be chosen to fit special requirements such as cell affinity or swelling degree. For instance, when a cell-adherent material is used in combination with PEG, the adhesion of cells is controlled and directed exclusively to the lines of the adhesive material [66]. The capillary filling can be used as well to generate composite materials of PEG-based polymers and nanoparticles, such as those made from calcium phosphate or gold, thus introducing biofunctional particles inside the channels [67,68].

Fabrication of FIMIC samples has two main concerns, the formation of scum-layer and the delamination of the filled lines. In some cases, the filler material not only penetrates the channels (Figure 1.5a) but also form a film covering the pattern and connecting the channels (Figure 1.5b). This happens when the contact between the top of the structures and the glass before filling is not complete, for example as a result of the presence of particles of dust. In this way, the filler is not restricted to the channels anymore but forms a continuous coating between glass and mold.

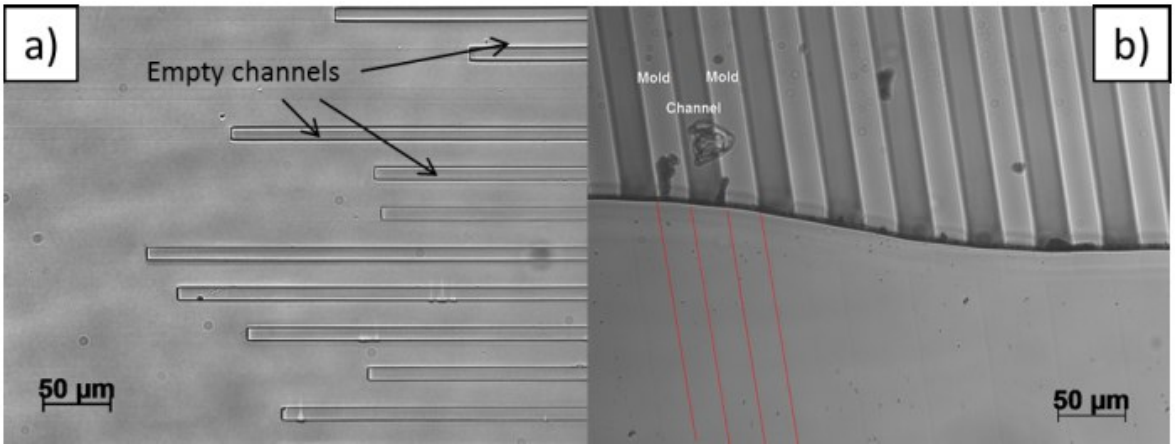

Figure 1.5: Optical image of a FIMIC sample (a) and a sample with scum-layer (b). The presence of scum-layer can be detected by a continuous line connecting the channels at the filling front. The red lines in b represent the position of mold and filled stripes.

Delamination is a problem derived from the differences in the swelling degree of mold and filler material. When submerged in an aqueous medium, the hydrogel swells, incorporating water to its network and increasing its volume. Materials with a different swelling degree will incorporate different amounts of liquid and will “grow” at different rates. If the filling material has a greater swelling degree than the mold, it may happen that

the volume of the hydrated material cannot be contained anymore inside the channel and the stripe detaches from the mold (Figure 1.6).

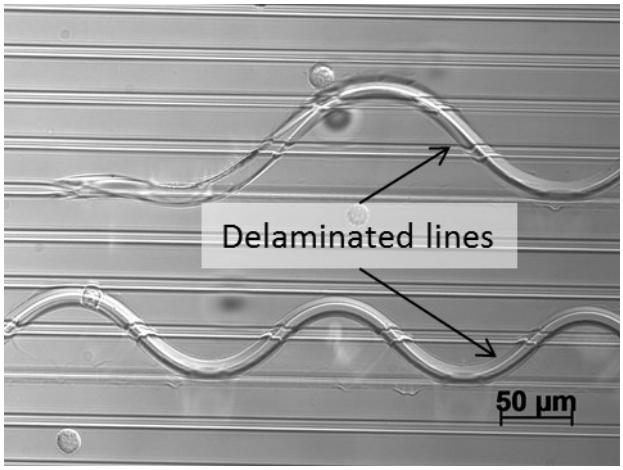

Figure 1.6: Optical image of a FIMIC sample presenting delamination of two lines.

FIMIC samples are not perfectly smooth. AFM analysis showed that in dry state there is a slight topography between 100 nm and 400 nm within the channels [66]. This is due to the shrinking of the filler polymer after UV-curing, which creates a depression on the surface at the filled lines. After hydration of the samples, this topography can be increased or reduced depending on the swelling degree of mold and filler. According to these results, we can select the materials used for filler and mold in order to keep the topography as low as possible. However, the use of different materials implies the creation of chemical patterns. To solve this issue, we have reported the use of blend materials of different polymers [28]. The advantage of these blends is that we can tune the physical properties of the material by changing the relative composition of the constituents, keeping similar chemical properties. Using this approach, the topography can be dramatically reduced.

It is also important to consider the aspect ratio of the topography on FIMIC samples; the width-height aspect ratio in dry state is 1:0.04 (400 nm in a 10 µm width line) in the worst of the cases. To the best of our knowledge, nobody has reported cell studies on structures with similar aspect ratios and due to their reduced dimensions it may be that the cells are not affected by them. On the other hand, the geometry (convexity/concavity) may affect the cells. Park studied this effect, concluding that fibroblasts avoid concave geometries (pit-like), migrating preferentially to the top of convex ones (hills) [69]. However, the aspect ratio of the features used in their work was larger than our system (1:0.25) and the results may not be comparable.

In this thesis, we investigated the migration of fibroblasts on topographically, mechanically and chemically patterned substrates. We aimed to understand the effect of the dimensions of the patterns in terms of direction, speed and persistence of the displacement. For this purpose, we prepared substrates using cast-molding and the FIMIC method. We also studied three methods to obtain samples with an embedded pattern of elasticity, where the pattern was covered with a thin film, ensuring that a topographically and chemically homogeneous surface was presented to the cells, overcoming the limitations of the FIMIC samples. These materials can be of great use in the study of the cellular response to mechanical cues. Finally, we introduced two composite systems with PEG-based polymers and micro- and nanoparticles. We investigated the adhesive behavior of fibroblast on those materials and their possible application to direct and enhance cell migration.

Chapter 2:

Materials and Methods

Most of the materials and some methods were common to every experimental chapter of the present work. For better organization, they are explained in this section. Concrete operating conditions and composition of the materials are outlined in the Materials and Methods section of the corresponding chapter.

2.1 Materials

2.1.1 Hydrogels

The following polymers were used during the experimentation:

- Poly(ethylene glycol) diacrylate (**PEG**) (Sigma-Aldrich, M_w 575 Da): Provided as a liquid pre-polymer (Figure 2.1).
- Triblock co-polymer of Poly(ethylene glycol) and Poly(propylene glycol) (PPG), PEG-b-PPG-b-PEG (**3BC**) (Sigma-Aldrich, M_w 4400 Da): Provided as a liquid pre-polymer (Figure 2.1).
- 8-Arm Poly(ethylene glycol)-OH (**8PEG**) (Jenkem Technology USA, M_w 15 kDa): Provided as a solid (Figure 2.1).
- Blend of **PEG** and **8PEG** (**Blend1**) in a mass rate of 1:1: The blend was solid at room temperature.
- Blend of **PEG** and **3BC** (**Blend2**) in a mass rate of 33:66: The blend was liquid at room temperature.

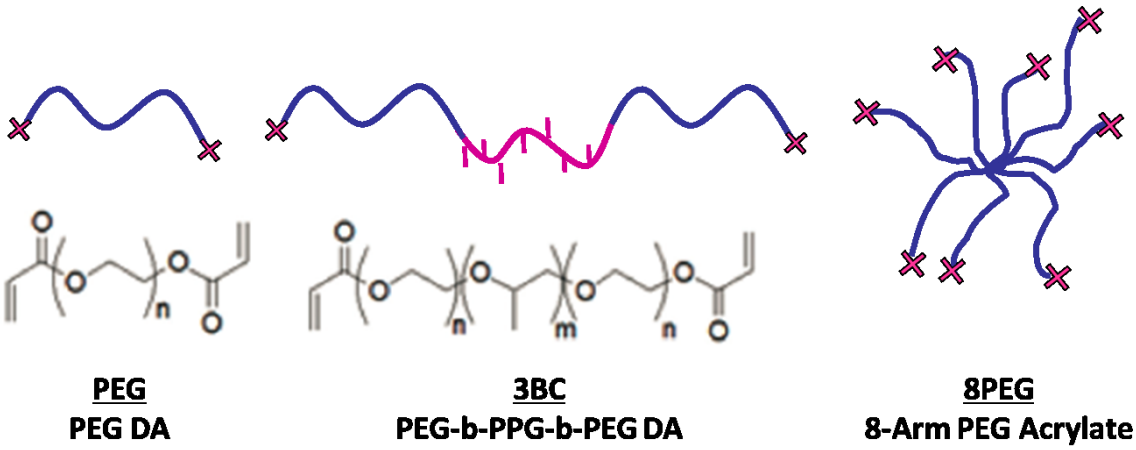

Figure 2.1: General structure of PEG-based monomers: Poly(ethylene glycol) diacrylate (PEG), block co-polymer diacrylate (3BC) and 8-arm PEG acrylate (8PEG). The stars at the end of the chains represent acrylate groups.

The PEG-based polymers were supplemented with 1% of 2-hydroxy-4'-(2-hydroxyethoxy)-2-methylpropiophenone (PI) (Sigma-Aldrich, M_w 224.26 $gmol^{-1}$), a photo-initiator, to achieve UV-curing. The PI was added to the pre-polymer, heated at 50°C for 30 minutes and mixed with the help of sonication.

In some cases, a cross-linker, namely pentaerythritol triacrylate (Sigma-Aldrich, M_w 298 $gmol^{-1}$) (CL), was added to the pre-curing mix (0% - 10%) to modify the cross-linking density of the PEG-based polymers and, therefore, the stiffness of the material.

The concentration of photo-initiator and cross-linker is expressed in weight percentage with respect to the quantity of polymer.

2.1.2 Acrylation of PEG-based polymers

In order to obtain UV-curable polymers, it is necessary to add acrylate groups to the end of the polymer chains. This acrylation was necessary in the case of **3BC** and **8PEG**, since the **PEG** was purchased already in acrylated state. Reagents were provided by Sigma-Aldrich unless stated otherwise.

The acrylation procedure is explained with more detail elsewhere [66].

The polymer (**3BC** / **8PEG**) and the catalyst, K_2CO_3, were dried separately inside a vacuum oven at 95°C for 3 hours. A reflux column was set up on the reaction flask and, to avoid the presence of humidity during the reaction, the air was removed by bubbling through N_2 prior to the reaction. The catalyst, dichloromethane anhydrous (DCM), and acryloyl chloride were then added to the reaction flask. The reaction was carried out at 51°C and in absence of light for a minimum of 3 days to ensure the maximal conversion.

The products were filtered to remove the catalyst and the solvent was evaporated off under a N_2 stream. Afterwards, the filtered polymer was dropped into a beaker containing cold petroleum ether. The remaining acryloyl chloride was dissolved in petroleum ether while the polymer precipitated. The precipitate was re-suspended in DCM and poured into a sedimentation funnel with a small amount of a saturated solution of NaCl in distilled water. The organic phase dried over $MgSO_4$. After overnight drying, the $MgSO_4$ was filtered and a small amount of 4-methoxyphenol was dissolved into the filtrate, which acted as an inhibitor and avoided undesired polymerization during storage.

Finally, the flask was placed on a rotary evaporator Hei-VAP Value (Heidolph Instruments GmbH & Co. KG, Germany) and left until the solvent was removed. The polymer was stored in a flask protected from light radiation.

2.1.3 Cell culture

Mouse fibroblasts L929 (kindly provided by Dr. Lehmann, Fraunhofer Institute for Cell Therapy and Immunology, IZI, Leipzig, Germany) were cultured in RPMI 1640 medium with addition of 10% Fetal Bovine Serum (FBS) and 1% Penicillin/Streptomycin (PS) in an incubator CB150 Series (Binder GmbH, Germany) at controlled temperature (37°C) and CO_2 atmosphere (5%). Medium, sera und reagents were provided by PAA Laboratories GmbH, Germany, unless stated otherwise.

2.1.4 Microparticles

Microparticles prepared by the Layer-by-Layer (LbL) technique were provided by Prof. André Skirtach (Max Plank Institute of Colloids and Interfaces, Potsdam, Germany). A complete description of the method can be found in the paper of Bédard [70]. Briefly, solid templates were submerged in a solution of polyelectrolyte. Non reacted material was removed by washing and the coated template was submerged in another polyelectrolyte solution oppositely-charged. The process was repeated to obtain a multi-layered coating [71].

For our experiments, microparticles with a solid core of $CaCO_3$ were used. The particles were co-precipitated with TRITC-dextran for recognition by fluorescence microscopy and coated by a multilayer of polyelectrolytes: poly(diallyldimethylammonium) (PDADMAC, positive) and poly(sodium styrene sulfonate) (PSS, negative). These particles were robust due to the solid core and had sizes from 3 µm to 5 µm.

Hollow capsules were prepared using SiO_2 as template. After formation of the polyelectrolyte multilayer shell, the core was dissolved in HF (solution 0.3M) and the capsules were filled with TRITC-dextran [70]. The advantage of the SiO_2 templates was their monodisperse size; capsules obtained had diameters of 3 µm.

2.1.5 Metallic nanoparticles

For the studies of the influence of composite materials of **PEG** and metallic nanoparticles, the following nanoparticles were prepared (Table 2.1):

Table 2.1: Metallic nanoparticles synthetized for the preparation of composite materials with PEG. The reference indicates the bibliographic source of the synthesis method.

Structure	Shape
Sphere	Au Sphere [72]
	Au Hollow urchin-like Sphere [73]
	Ag/Au (core/shell) Sphere [74]
	Ag Sphere [74]
2D	Au Triangular nanoplate [75]
	Au Multishape plate [75]
3D	Au Tetrahedron [76]
	Au Cube [76]
	Au Decahedron [77]

A complete description of the synthesis and characterization methods of the metallic nanoparticles (NP) can be found in the recent thesis of Arafeh [68].

2.1.6 Fluorescent dyes

Fluorescein sodium salt (λ_{ex} = 490 nm, λ_{em} = 514 nm) was purchased at Sigma-Aldrich and used for recognition of the boundaries of the samples during fluorescent analysis of composite materials containing microcapsules.

Fluorescein diacetate (Sigma-Aldrich) was used for testing the viability of cells when cultured on our hydrogels. Inside living cells, it will be degraded to fluorescein (λ_{ex} = 490 nm, λ_{em} = 514 nm)

Propidium iodide (λ_{ex} = 540 nm, λ_{em} =608 nm) purchased at Fluka was used in combination with fluorescein diacetate for Live/Dead assays. It is a fluorescent molecule that binds to the nucleic acid of cells. This substance cannot penetrate the membrane of

healthy cells and, therefore, it is used to stain those ones with damaged membranes, including dead cells.

FITC-dextran (M_w 70 kDa) (λ_{ex} = 490 nm, λ_{em} = 514 nm) was used to increase the contrast between mold and filler while using the sandwich method. The election of a dye linked to a high molecular weight molecule was done in order to avoid diffusion of the dye from the filler material to the mold during polymerization.

As previously described, microparticles were labelled with tetramethylrhodamine-dextran (TRITC-dextran) (λ_{ex} = 552 nm, λ_{em} =579 nm) for easy recognition via fluorescent microscopy.

2.2 Preparation of the samples for cell studies

For characterization studies, the samples were placed on microscope or cover slides and the adhesion took place through secondary interactions. For this reason, it was extremely important to work in a clean environment, since the deposition of particles on the glass led to incomplete adhesion of the sample, or, when deposited on the sample, disturbed the analysis and caused erroneous interpretations of the results.

2.2.1 UV-Curing of PEG-based polymers

One of the properties of the PEG-based polymers used for this work is that they are UV-curable. As stated in the introduction (see Chapter 1), the advantage of this polymerization method is that it can be carried out under mild conditions (i.e. room temperature), requires short reaction time, gels are formed *in situ* and the products are highly cytocompatible [12]. The polymerization was carried out via a radical reaction (Figure 2.2). The UV-radiation creates a radical on the photo-initiator (PI) (initiation). This radical reacts with the acrylate group present at the end of the PEG chains and generates another radical. The new radical reacts with a new PEG chain, binding them chemically (propagation). The reaction finishes when the radical ending of one chain recombines with another radical (termination).

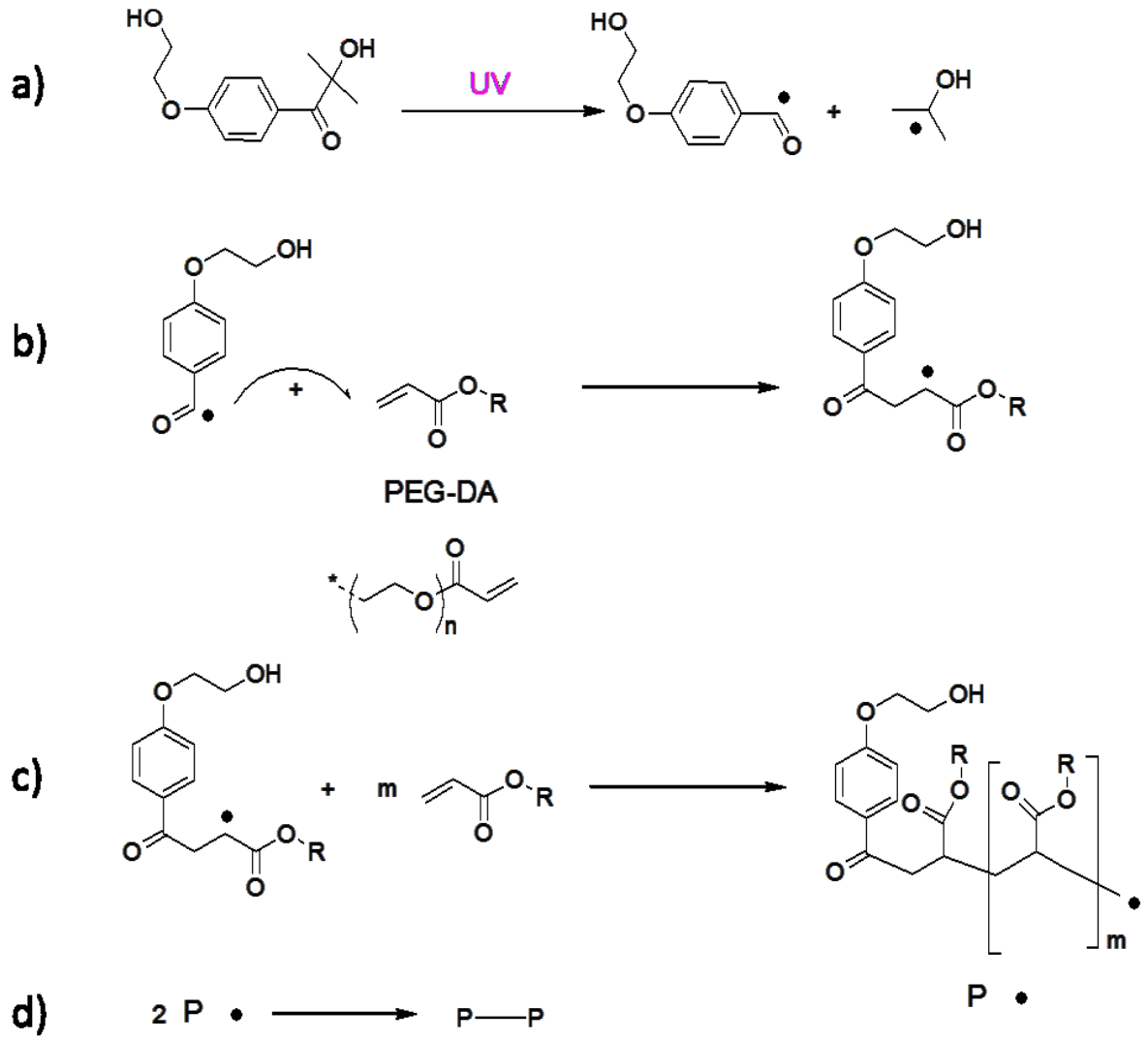

Figure 2.2: Scheme of the radical reaction of polymerization. a) Initiation. b) Reaction. c) Propagation. d) Termination.

The termination step occurred frequently and new photo-initiation was required. The UV-source was kept activate during the whole process. This time was noted as t_{UV}.

2.2.2 Preparation of the Mold (Cast Molding [59,60])

With the term "**mold**" we refer to a negative copy of a structured silicon master made of a polymeric material. The molds were prepared using the cast-molding technique, which is briefly described here.

A drop of the pre-curing mix was placed on top of a topographically structured silicon master (Amo GmbH, Germany) which was previously fluorinated with trichloro(1H,1H,2H,2H-perfluorooctyl) silane 97% (Sigma-Aldrich). The drop was covered

with a cover slip (Carl Roth GmbH, Germany) and left to completely fill the channels. Afterwards, the polymer was UV-cured (Figure 1.2). The UV-curing time varied with the finality of the mold (for preparation of FIMIC samples or for experimentation on topographically patterned substrates among others) between 5 minutes and 30 minutes. The concrete time will be stated for each case. The UV-polymerization can be inhibited by the presence of O_2 and, therefore, is carried out under N_2 atmosphere. On the other hand, O_2 can act as a catalyst of the reaction at high temperature.

In the case of **8PEG** and blends containing that polymer, we worked at 80°C in order to melt the solid pre-curing mix. The silicon master, cover slips and pipettes used were also warmed up to avoid solidification before curing. To keep the temperature of the system stable during the curing, the master was placed on top of an aluminum block, which was also warmed up to 80°C.

During this work, the molds were labelled with a three-number code. This code described the characteristic distances of the topographic structure, namely width of the channels, distance between them and height of the hills (w-d-h) (Figure 2.3).

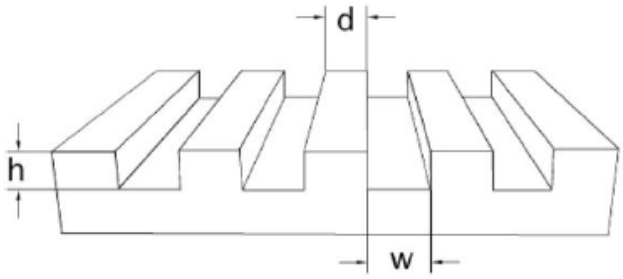

Figure 2.3: Topographic structure of a mold with the three characteristic distances; w-d-h.

2.2.3 Fill Molding In Capillaries method (FIMIC)

To prepare the FIMIC samples, first we had to generate a mold. In this case, to avoid delamination (see Chapter 1), the material was UV-cured for less than 10 minutes. After that time, the sample was solid enough to work with it, but some acrylate groups remained unreacted and could be used to chemically link the mold and the filler material, hereafter referred to as "**filler**". The mold was placed face down on a clean glass slide. Since the channels were filled via capillary force, it was mandatory to use a liquid polymer as filler. A

small amount of the filler was eased towards the side of the mold until slight contact with it. Once the channels were filled, the sample was UV-cured again (Figure 1.4, page 11).

In the case of FIMIC samples, the first two numbers of the three-numbered code of the mold indicated the size of the filled lines and the size of the mold lines.

Different combinations of mold and filler were used throughout this thesis and they are indicated in the corresponding chapter.

2.2.4 Embedding patterns of elasticity

Several techniques were employed to obtain a smooth surface with a pattern of elasticity underlying the surface. In this section, "blanket" will make reference to the material used to embed the pattern of elasticity.

2.2.4.1 Spin-coating:

The samples were placed on the rotor plate of a spin-coater SCK-100 (Instras Scientific, USA). The fixation to the plate was made using a double-sided tape; therefore, to protect the sample from destruction, we placed it on a cover slip. After adding the polymer, the spin-coater was turned on at a determined spin speed; the speed and time used are specified for each case. Finally, the blanket was cured.

2.2.4.2 Razor-blade:

For preparing samples via Microtransfer Molding (μTM) a drop of filler material is placed on top of a topographically patterned sample. After the topography was filled, the excess was removed by scraping [78]. Nevertheless, after removal of the excess, a thin layer, in the order of 100 nm, still covered the sample between the filled structures [59,78]. In the original work, that film is removed in order to print only the patterned structure as isolated islands. In our case, the film was desirable and it was expected to provide a smooth and chemically homogeneous surface while allowing detection of the underlying elasticity.

In analogy to the µTM, a drop of blanket material was placed on top of the sample and spread along the surface using a razor-blade parallel to the pattern. The excess was removed at the edge of the sample. The blanket was cured afterwards.

2.2.4.3 Sandwich method:

The name of this method comes from the experimental construction (Figure 2.4). The substrate (S) was placed on a glass slide. Then, a drop of the blanket material (B) was placed on top of the topography and covered with another glass slide. The substrate and the blanket play the role of the ham and the cheese, while the glass slides act as bread slices to create the sandwich. The sandwich was pressed using different weights. The load was placed on a microscope slide lying on top of the sample. Using this methodology, it was ensured that the pressure was homogeneously distributed along the surface of the substrate. The higher the pressure was, the more blanket overflowed to the sides, i.e. surplus of coating material was removed, and the thinner the coating was. By controlling the weight, we controlled the thickness of the blanket.

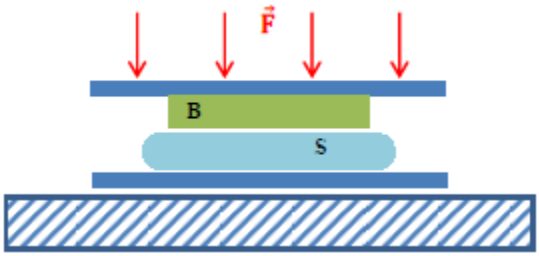

Figure 2.4: Schematic representation of the "Sandwich method". B represents the blanket material and S the substrate. F is the pressing force exerted by the load placed over the blanket.

This method is similar to the replica-molding [59] since in both methods a topographically structured polymer is used as mold, which is covered with a second polymer (replica). Nevertheless, in our case the thickness of the replica was intended to be controlled and mold and replica were stayed together by chemical binding, forming the sample.

2.3 Analytical methods:

2.3.1 Atomic Force Microscopy (AFM)

An Atomic Force Microscope (AFM) NanoWizard II (JPK Instruments AG., Germany) was used to analyze the topography and the stiffness of the samples. Images were edited with NanoWizard IP Version 3.3a (JPK instruments AG., Germany)

2.3.1.1 Topographic Imaging:

Imaging in dry state was done in intermittent and contact mode. The AFM probes used for those modes were TAP150 Al-G (Budget Sensors, Innovative Solutions Bulgaria Ltd., Bulgaria) and ContAl (Budget Sensors, Innovative Solutions Bulgaria Ltd., Bulgaria) respectively. For imaging on swollen state, a probe PNP TR 20 (NanoWorld AG., Switzerland) was employed.

2.3.1.2 Force Spectroscopy:

Force Mapping was used as a qualitative tool to identify patterns of elasticity or to confirm modifications on the elastic properties of the surface by addition of micro- and nanoparticles to the substrate. Measurements in dry state were carried out with a ContAl probe, while for swollen state a PNP TR 20 was used. The cantilever was calibrated before each set of measurements.

2.3.2 Optical Imaging

Optical images were obtained using an Observer Z1 microscope (Carl Zeiss, Germany) with an objective 20x, and analyzed using the AxioVision V4.8.2 software package (Carl Zeiss, Germany).

While imaging cross-sections, a problem arose: The slices of sample hardly stood perpendicularly to the microscope slide. To solve this inconvenience, we created a sample-holder (Figure 2.5). The sample was attached, through Van der Waals forces, to the cover

glass, which was perpendicular to the microscope slide. The screw permitted to correct the orientation of the sample in case it was not correctly placed.

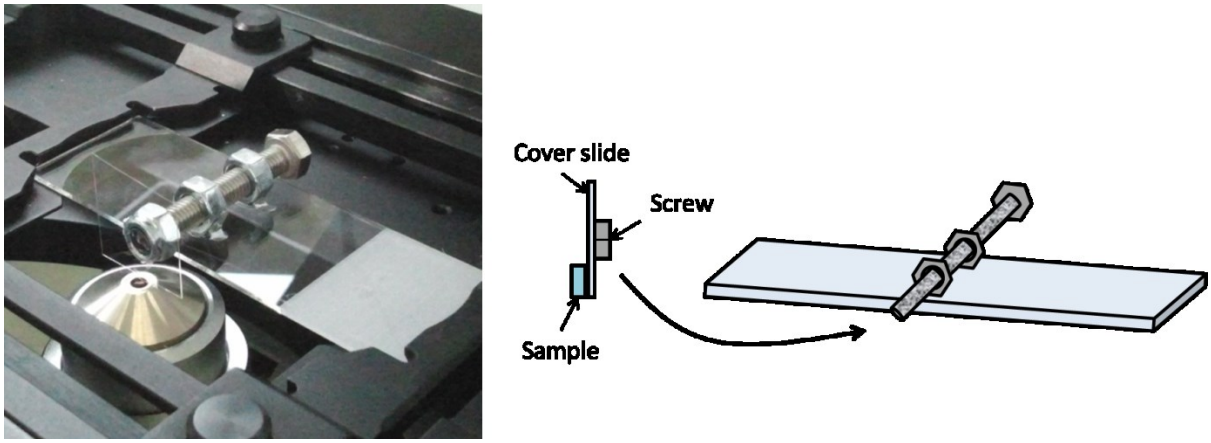

Figure 2.5: Sample holder for imaging cross-section.

2.3.3 Fluorescence microscopy:

As in the case of optical images, fluorescence images were obtained using an Observer Z1 microscope with an objective 20x, and analyzed using the AxioVision V4.8.2 software package.

Confocal and 3D images were made using a Leica TCS SP5 II Confocal Microscope (Leica, Germany) with a 20x and a water immersion objective 63x. Images were analyzed and processed using the program Bioimage XD (Free software).

2.3.4 Scanning Electron Microscopy (SEM)

Scanning Electron Microscopy was used to image adherent cells on **PEG** substrates modified with metallic nanoparticles. For this purpose, the samples containing adherent fibroblasts were dried by using solutions of acetone with increasing concentrations (30%, 50%, 70%, 90%, 95% and 99.9%, v/v) and finally placed into a critical point drying chamber. The samples were coated with gold and imaged with the equipment provided by the Zentraleinrichtung Elektronenmikroskopie from the Technical University Berlin (Zelmi, TU Berlin).

2.4 Cell experiments

2.4.1 Preparation of cells

For every cell experiment described in this work, preparation of the cells was necessary, i.e. detachment of the cells from the culture flask and seeding on the samples.

Cells growing in a cell culture flask (SPL Live Sciences Inc., Korea) were washed with Phosphate Buffered Saline solution (Dulbecco's PBS) and treated with Trypsin-EDTA for 2 minutes at 37°C to detach cells from the flask. After that, fresh medium was added to neutralize the poisoning effect of Trypsin-EDTA and the suspension of cells was centrifuged at 1300 rpm and 4°C for 5 minutes. The supernatant was removed and the pellet was re-suspended in fresh medium.

2.4.2 Cell migration

The samples were sterilized via submersion in ethanol, placed on 15 µL-Slide 8-well for cell culture (IBIDI GmbH, Germany) and left in PBS overnight to ensure complete hydration.

After preparation of the cells (see above), the concentration was determined using a counter chamber Marienfeld Superior (Paul Marienfeld GmbH & Co. KG, Germany). A new suspension containing 50000 cell/mL was prepared. PBS was sucked out from the incubation plates and 300 µL of the cell suspension were seeded on the samples. The samples were incubated at 37°C and 5% CO_2 for 1 hour ($t_{pre\text{-}exp}$).

After pre-incubation, the samples were placed in new incubation plates and 300 µL of fresh medium was added. This pre-incubation step was done to remove non-adherent cells. The samples were incubated again in an inverse microscope Observer Z1 microscope with an integrated Incubator XL (PeCon GmbH, Germany) at 37°C and 5% CO_2 atmosphere.

Time-lapse images were acquired at intervals of 10 minutes during 14 hours, using a 20x objective. Cell tracking information from the videos was obtained using the manual cell tracking plug-in available for Image J (Free software). The data were further interpreted using a self-made analysis tool described in Chapter 3 (CellMAT). Adherent cells exert traction forces on the material and modify the elastic properties of the surrounding

substrate [15,38,79]. To assess that the observed migration track was exclusively due to the hydrogel properties, only isolated cells, i.e. not in contact with other cells, were studied.

2.4.3 Adhesion Test

For the cell adhesion experiments, the samples were sterilized in ethanol, placed in 15 µL-Slide 8-wells for cell culture (IBIDI GmbH) and left in PBS overnight to ensure complete hydration. Cells were prepared as described above, obtaining a suspension containing 30000 cell/mL. PBS was sucked out from the incubation plates and 300 µL of the cell suspension were seeded on the samples. The samples were incubated at 37°C and 5% CO_2 for 24 hours.

After incubation, the cells were fixed, prior to microscope observation; the medium was removed and the samples were gently washed with PBS two times. Formaldehyde 4% (Roti®-Histofix 4% Carl Roth GmbH & Co, KG) was added and left for 30 minutes. Finally, the samples were washed with PBS before observation.

2.4.4 Live/Dead assay

To analyze the cytotoxicity of our polymeric materials, we applied a Live/Dead assay based on the use of fluorescein diacetate and propidium iodide. A solution was prepared containing 10% of fluorescein diacetate in acetone (0.5 mg/mL), 10% of propidium iodide in PBS (0.5 mg/mL and 80% PBS. The samples were prepared as for an adhesion experiment. After incubation at 37°C and 5% CO_2, the medium was gently removed and the sample was covered with the dye solution.

In this assay, the fluorescein diacetate (non-fluorescent) penetrated the cells and was enzymatically degraded to fluorescein which is fluorescent. Only living cells can carry out this transformation and, therefore, stain green. On the other hand, fluorescent propidium iodide cannot penetrate the cell membrane to bind with the nucleic acids. Consequently only dead cells, or those with their membrane damaged, can be stained in red with propidium iodide (Figure 2.6).

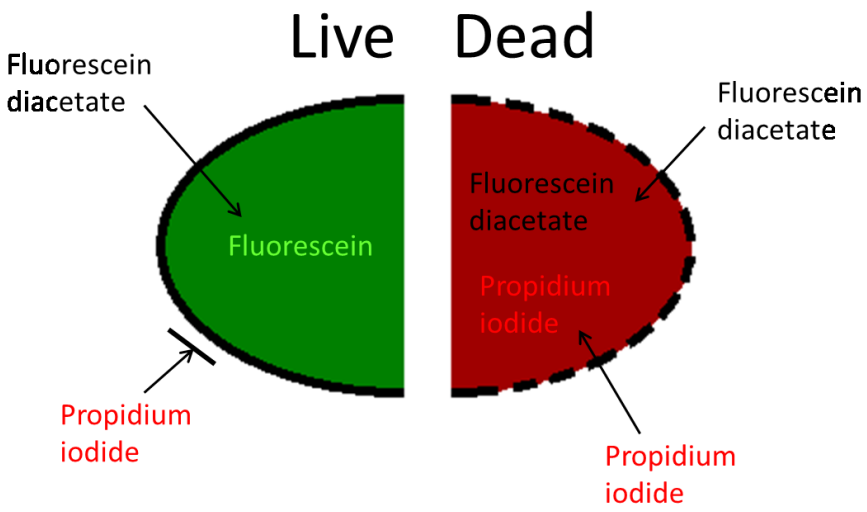

Figure 2.6: Schematic representation of the Live/Dead assay. On the left side, a living cell transforming the fluorescein diacetate into fluorescent fluorescein and blocking the propidium iodide. On the right side, a dead cell stained by the propidium iodide linked to the genetic material.

The number of viable and dead cells was quantified by fluorescence microscopy. According to the regulation DIN EN ISO 10993-5 2009 [80], materials showing a reduction of cell viability higher than 30% are considered cytotoxic. Other sources refine this criterion, defining the range from 100% to 80% viability as non-cytotoxic and from 80% to 70% as slightly cytotoxic.

Chapter 3:

Cell Migration Analysis Tool (CellMAT)

3.1 Introduction:

Cell migration can be easily observed and recorded by time-lapse imaging with an optical microscope. However, the migration of large numbers of cells cannot be efficiently presented by showing images of the tracks of every single cell; this would result in publications with endless pictures which would be open to interpretation from the reader. Therefore, some parameters have been introduced to describe the migratory behavior of cells and to support comparison between different systems.

Cell migration has been traditionally described using the "Random walk model". This model aims to describe the movement of a walker (molecule, animal, cell, etc.) which can choose any direction after each step [81]. A special case is "persistent random walk", where the direction of the next step is correlated to the previous steps [81]. This model introduces the concept of persistence as a measure of the correlation between the direction of successive steps [82,83]. Adapting the equation of the mean square displacement ($<d^2(t)>$) of a pure random walk model to the case of persistent movement, the following expression is obtained [83]:

$$< \boldsymbol{d^2(t)} > = \boldsymbol{2S^2P\left\{t - P\left[1 - e^{-t/P}\right]\right\}} \qquad \textbf{Eq. 3.1}$$

where *S* is the average migration speed and *P* the persistence time. Eq. 3.1 is generally used to estimate the value of *S* and *P* by fitting the experimental data of tracked cells as done by DiMilla and other authors [84–87].

Using a persistent random walk model may, however, present some complications. In 1987, Dunn and Brown sketched one of the limitations of the model. They said that cells showing low persistence were not necessarily random walkers, but it may be that the imaging interval was too long to show persistence [82]. Figure 3.1 illustrates this phenomenon; both images represent the same track. The left one was obtained observing the sample every 10 minutes, while the right one presents observations each hour. The left track shows that the cell migrates persistently in the same direction for several steps before turning. If we observe the right track, the highest number of steps before a direction change

is only three steps, which, after the persistent random walk model, will be seen as bad persistence.

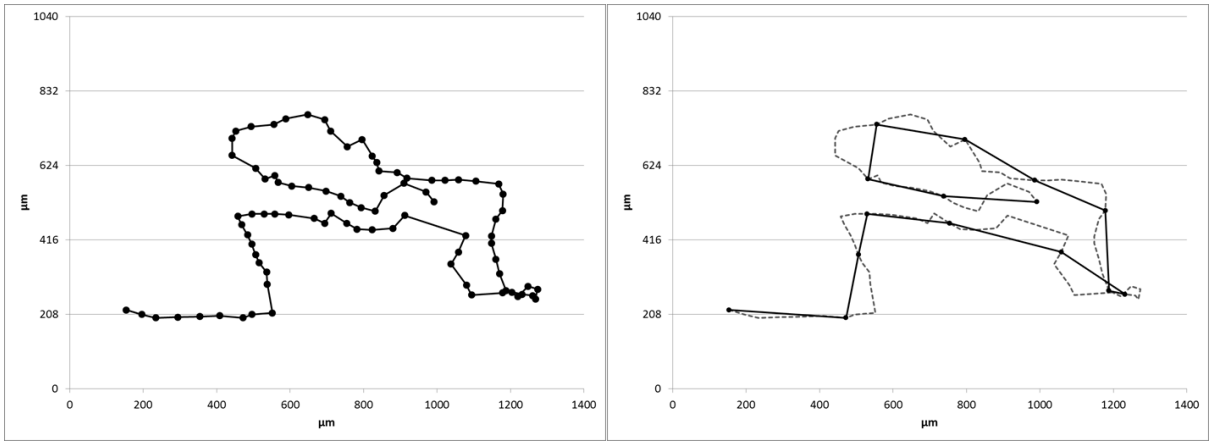

Figure 3.1: Track of a cell migrating. Images taken every 10 minutes (left), 1 hour (right).

These observations demonstrate that the accuracy of the estimation of the migration parameters *S* and *P* will depend on the sampling interval which must not be higher than the persistence time, to allow the persistent behavior to be recognized. On the other hand, the tracking duration must be carefully chosen; the complete analysis must be much longer than the persistence time to fully analyze the dynamics of the cell [84].

House and colleagues suggested a different approach to characterize and analyze migration tracks. They stated that the use of the random walk model to predict the migration of cells can produce errors in the range of the displacement. Therefore, they proposed the use of direct measured parameters to describe cell behavior [88]:

They described the **persistence time (P)** as "the longest period *P* during which a migrating cell does not change its direction by more than 15°". They considered that deviations of 15° did not constitute a drastic change of direction but small deviations over the general direction.

The **migration speed** at each time point can be calculated as the module of the velocity.

$$s_i = \left|\vec{V}(t)\right| = \frac{d\vec{r}(t)}{dt} \approx \vec{r}(t) - \vec{r}(t-1) \qquad \textbf{Eq. 3.2}$$

Where $\vec{r}(t)$ is the vector indicating the position of the cell at time t. Using Eq. 3.2, the **average migration speed (S)** can be calculated as:

$$S = \frac{\sum_{i=1}^{N} s_i}{T} \qquad \textbf{Eq. 3.3}$$

House also used the **Euclidean distance (D)** defined as the distance between the starting point and the end of the track (Figure 3.2).

$$\boldsymbol{D = |\vec{r}(T) - \vec{r}(0)|} \qquad \textbf{Eq. 3.4}$$

This parameter should not be confused with the **total path length (L)**, which is the summation of the step lengths (Figure 3.2).

$$\boldsymbol{L = \sum_{t=0}^{T} |\vec{r}(t+1) - \vec{r}(t)|} \qquad \textbf{Eq. 3.5}$$

These last two parameters can be used to calculate the **Straightness Index**, which indicates whether the cell follows a straight line or changes its direction regularly [81,89].

$$\boldsymbol{Straightness\ Index = \frac{D}{L}} \qquad \textbf{Eq. 3.6}$$

If the distance between the origin and the end of the path is similar to the total path length, this indicates that the cell followed a quasi-straight path and the straightness index will be close to 1. The disadvantage of this parameter is that its value tends towards 0 when the number of steps increases. Therefore it is not suitable to compare tracks with different number of steps [90].

According to Benhamou the straightness index defined in Eq. 3.6 can be applied for oriented migration where the objective is located at a distance D and the walker reaches it. Benhamou suggested the use of the **ratio G/L** to describe the straightness of the track for those cases where the goal was placed in the infinite (goal never reached), being G the distance between the origin and the projection of the location after *n* steps [90]. These approach suits better to the experiments presented in this thesis, where the migration was guided by a pattern but there was no goal to be reached.

G can be defined as the sum of the steps in the goal direction, were l_i is the length of the step, θ_i the angle with respect to the horizontal and γ the angle of the goal direction (in this work, the direction of the pattern):

$$\boldsymbol{G = \sum_{i=1}^{n} l_i \cos(\theta_i - \gamma)} \qquad \textbf{Eq. 3.7}$$

Considering that the efficiency of the orientation can be estimated as the mean cosine of the directional errors (c_w), this value also represents the ratio G/L.

$$\boldsymbol{c_w(\theta - \gamma) = \frac{\sum_{i=1}^{n} l_i \cos(\theta_i - \gamma)}{L} = \frac{G}{L}} \qquad \textbf{Eq. 3.8}$$

The variance of this ratio is inversely proportional to the path length, consequently the precision increases with the number of steps.

The straightness index and the ratio G/L have been defined for migration oriented to a point (the final goal). Persistence of motion could also be defined relative to a direction or pattern. In this work, the degree of orientation of migration was defined relative to a line (direction of the pattern; the cell can move parallel, perpendicular or at an angle to the direction of the pattern. Cell migration on a line parallel to the surface patterning is considered oriented, regardless of whether the direction of the motion is to the right or to the left. The parameters already introduced consider such migration inefficient, because turns of 180° results in a migration away from the initially chosen goal point. When the degree of orientation relative to a line or a pattern is desired, the straightness index and the ratio G/L can be useful to evaluate the efficiency of the movement but not as an indication of the degree of orientation of a track.

Another commonly used parameter to describe the path of a migrating cell is the **step angle (θ_i)** [85,91–93]. This can be defined as the angle of each individual step with respect to a determined direction (in our case, the direction of the pattern) (Figure 3.2).

Studying the correlation between the migration distance and the migration angle of each individual step, an idea of the orientation of the migration with respect to the pattern can be obtained [91]. To analyze this correlation, each step vector ($\overrightarrow{r}(t)$) is represented on a chart starting at position 0. In this way, the length and direction of each step can be compared with the other steps. This analysis may give a more accurate idea of the orientation than the independent analysis of the step angles; for example, if a cell moves 10 small steps (0.5 µm) perpendicularly to the pattern and 2 steps (15 µm) parallel to it, with regard to the step angles, the movement of the cell will appear as perpendicular. If the length of the steps is also taken into consideration, however, it can be seen that the perpendicular movement was negligible and the cell was actually migrating parallel to the pattern.

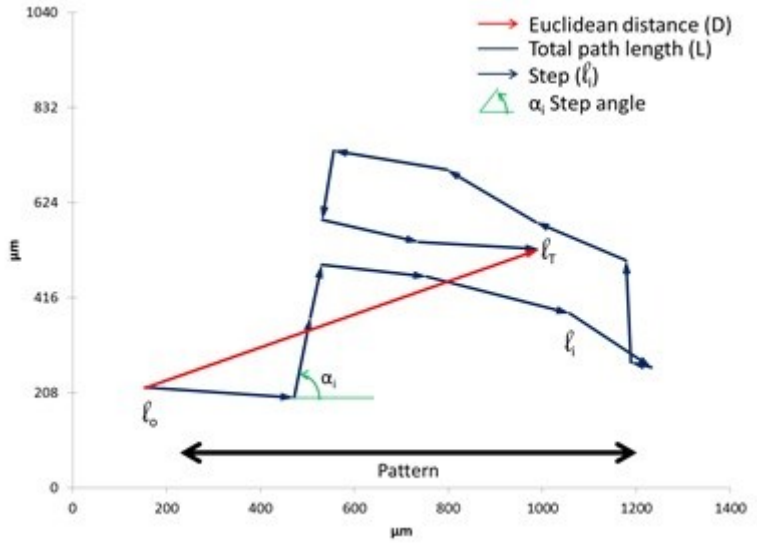

Figure 3.2: Definition of the Euclidean distance, the path length, the step distance and the step angle of a cell track.

Several software tools are available to analyze the images obtained from cell migration experiments, obtaining the tracks of the cells as well as other migration parameters.

These programs can be subdivided into two main groups: The first group includes programs which can automatically recognize each cell, detect their contour and calculate the position of the center of the cell. The advantage of these software products is that they can analyze large numbers of cells in a short time, albeit they require high resolution and, specially, high contrast images (contrast between cell and background) to work correctly. This is not a problem for experiments on flat substrates, but on structured ones the contrast obtained with phase contrast imaging is not sufficient to achieve satisfactory results. This inconvenience can be bypassed using fluorescent markers. However, fluorescent markers may damage the cells and therefore the recording time and exposure must be restricted. This in turn results in a decrease in the quality of the images [94].

The other group is formed by those programs where the cells are manually tracked. In this case, the recognition algorithm is substituted by the knowledge and experience of the experimentalist. The advantage of such an approach is that a human can more easily differentiate between adherent cells and other features such as structures or floating cells. On the other hand, the accuracy of the tracking depends on the accuracy of the definition of the position of the center of the cell and, because it is manually selected, some error may be introduced. This method is also highly time-consuming, since every single cell must be selected at each image of the recorded migration.

In this work, migration was studied on patterned substrates (with surface structural patterns); hence, the contrast between cells and background was very poor. Consequently it was very unpractical to use software based on automatic cell recognition. There are not many tools available to analyze manually-tracked migration data. The majority of such tools are oriented to the analysis of chemotaxis experiments. Therefore the standard parameters obtained with those programs are not sufficient for a complete characterization of the behavior of the cells investigated in this thesis.

For this reason, a new program was specifically created for this work. The so called CellMAT (Cell Migration Analysis Tool) is based on the most suitable parameters used in the literature. Using this tool it was possible to describe cell migration in terms that can be used to compare different experiments. With CellMAT, the speed of the data treatment was also increased (Experiments can be analyzed using only a couple of clicks).

3.2 Materials and methods:

The X and Y position of the cells on each slide was obtained using the manual tracking plugin of the open source software “ImageJ”.

For the calculation of the parameters as well as the production of the graphic representations, several macros were developed using Visual Basic for Applications (VBA), which were then executed using Microsoft Excel 2010.

The code of these macros can be found in the appendix of this thesis.

3.3 Discussion

The first necessary step to describe the cell migration was the analysis of the images of the migration experiments. ImageJ analyses the images using a plugin (Manual Tracking, Fabrice P. Cordelières, Institut Curie, Orsay, France) that records the selected position of the cell on each slide and produces a track using those data. The software already calculates the distance covered by the cell between two consecutive steps and the speed of the cell. To obtain the correct results, the time interval (time between captures) must be entered, as

well as the conversion from pixel to units (e.g. µm) for the image; the image file does not contain information about the scale, but its size is specified in pixels. To prevent errors in the analysis, the first step is to import the X and Y data from the file generated by ImageJ and to convert them into metric units, namely µm. The software CellMAT already includes the conversion factor pixel/µm for images obtained with an Observer Z1 microscope, using a 10x or 20x objective and allows the pixel/µm scaling factor to be set manually (Figure 3.3).

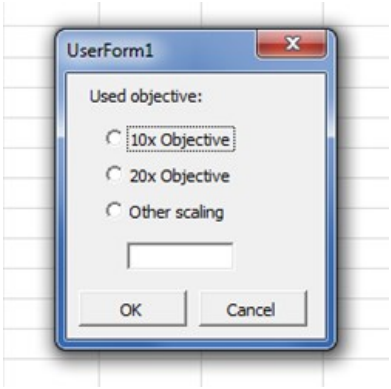

Figure 3.3: Formulary for the setting of the scaling factor.

Once the data had been converted into the correct units, CellMAT analyzes each step, calculating the distance covered (l_i), its x and y components (notated as dx_i and dy_i), the angle of the step with respect to the horizontal (θ_i) and the step speed (s_i). To calculate the step speed, the software requires the time interval, which is indicated using a message box before the calculation (Figure 3.4).

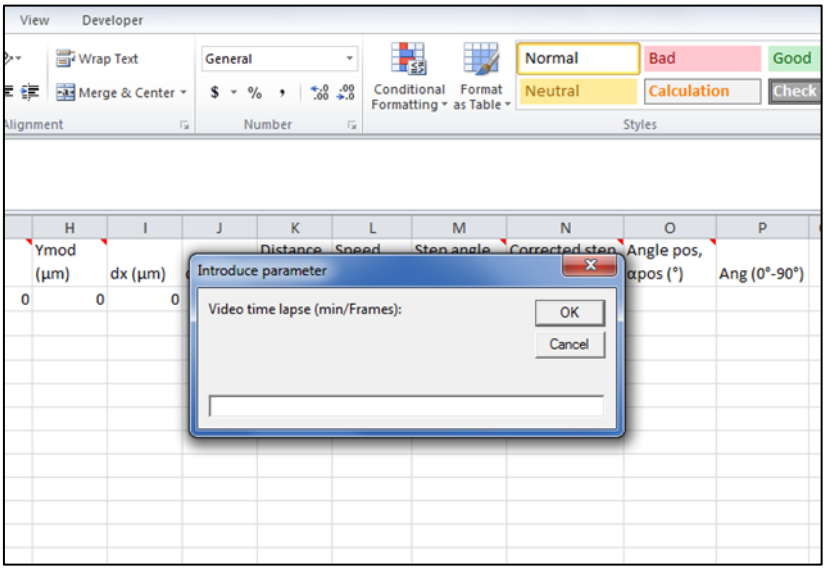

Figure 3.4: Screenshot of the message box for input of the sampling interval.

To analyze the orientation to the pattern, the step angle has to be corrected, obtaining α_i, which refers to the angle of the pattern (Υ). The angle of the pattern was defined as the angle formed between the positive X axis and the pattern. This angle was measured in the 1st or 4th quadrant, i.e. $-90° < \Upsilon \leq 90°$ (Figure 3.5). This defined the right direction as the positive direction of the movement and angles with an absolute value $|\alpha_i|$ greater than 90° were considered to be backwards or to "escape" from the goal. The pattern angle is also indicated via a message box (Figure 3.6).

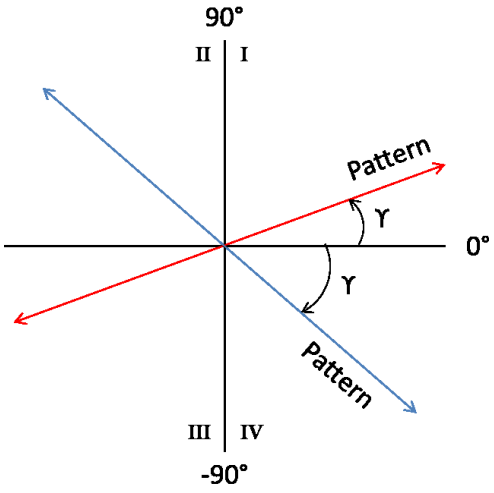

Figure 3.5: Representation of the selection of the angle to indicate the direction of the pattern. The blue and red lines represent the two possible situations: Pattern from down-left to up-right and pattern from up-left to down-right.

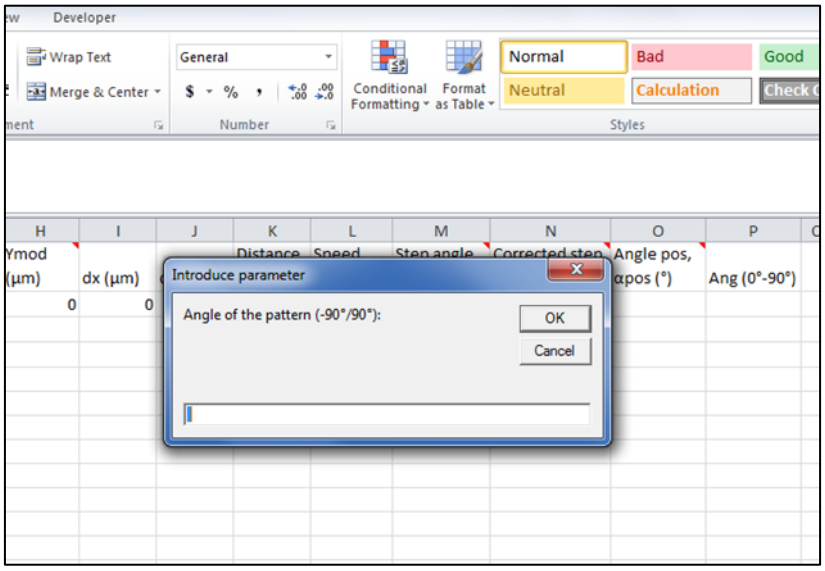

Figure 3.6: Screenshot of the message box for input of the angle of the pattern.

The step angle was corrected by subtracting the value of the pattern angle (Eq. 3.9), and finally converted into positive angles ($0° \leq \alpha_i < 360°$) (Eq. 3.10)

$$\propto_i = \boldsymbol{\theta_i} - \boldsymbol{\gamma} \qquad \textbf{Eq. 3.9}$$

$$\begin{aligned} \propto_i < \mathbf{0}^\circ \quad & \propto \boldsymbol{pos_i} = \propto_i + \mathbf{360}^\circ \\ \propto_i \geq \mathbf{0}^\circ \quad & \propto \boldsymbol{pos_i} = \propto_i \end{aligned} \qquad \textbf{Eq. 3.10}$$

Once the raw data were treated, the program analyzes the tracks. The analysis is done in two ways: graphically and numerically.

3.3.1 Graphical analysis:

The different tracks were represented on a chart with the same dimensions as the original image (Figure 3.7). They were also represented with a common origin at the position x=0, y=0 (wind rose display) with an indication of the direction of the pattern (Figure 3.8).

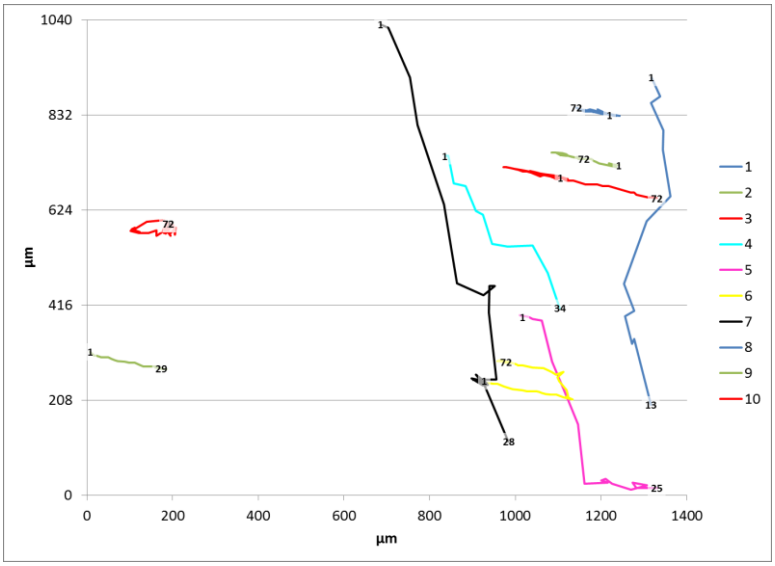

Figure 3.7: Representation of the tracks (1 to 10) using the original coordinates from the acquired images.

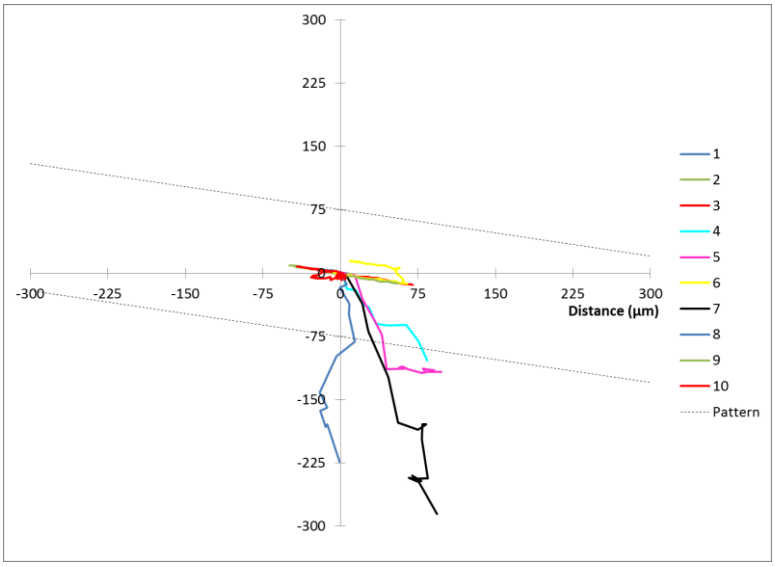

Figure 3.8: Wind rose display of the tracks (1 to 10) starting at the origin of coordinates. The dotted black lines represent the direction of the pattern.

The wind rose display gives an impression of the orientation of the tracks. Random migrations will spread in every direction, while oriented ones will be uniaxial (parallel to the pattern lines). Observing Figure 3.8 we can already say that tracks 1, 2, 3, 6, 9 and 10 were oriented in the direction of the pattern, while tracks 4, 5, 7 and 8 had a tendency to move at an angle or even perpendicularly.

As stated in the introduction, the correlation between the step length and the step angle $\left(\vec{r}(t)\right)$ also helps to characterize the orientation of the track; consequently, it was also represented by the program (Figure 3.9).

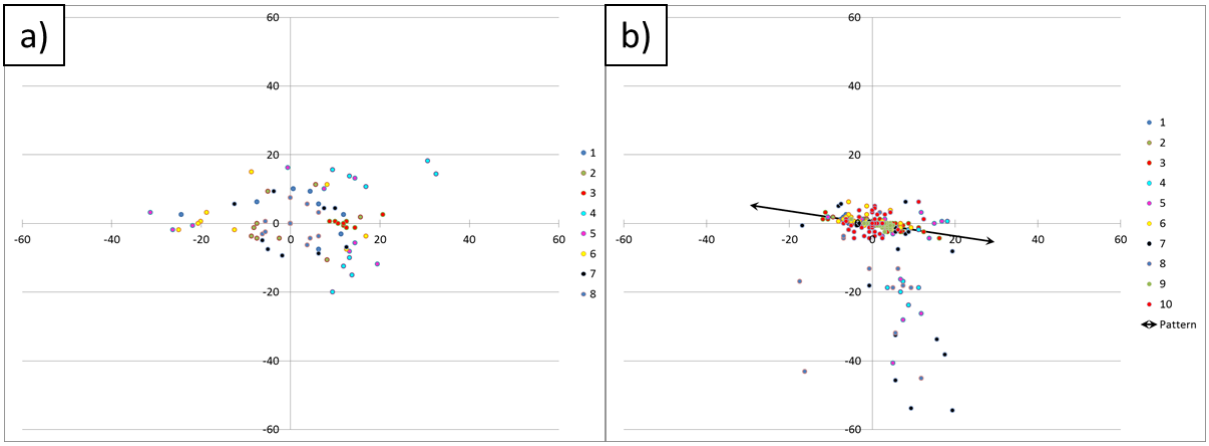

Figure 3.9: Representation of the correlation between step length and step angle of two different experiments: a) without pattern and b) with pattern (black line).

In absence of a pattern (Figure 3.9a) cells migrated randomly and no tendency to any direction can be recognized. Cell migration on a patterned substrate can be influenced by

that pattern and the steps of the movement would then be mainly oriented to its direction (Figure 3.9b).

3.3.2 Numerical analysis:

Graphic analysis methods are useful and thought to be easily understood. Nevertheless, they are dependent on the subjective interpretation of the observer. For this reason, numerical parameters have also been calculated to help an accurate interpretation of the migration data to be achieved.

The frequency of occurrence of each angle has been calculated. The positive corrected step angles (αpos_i) were sorted into four groups (Table 3.1). In order to prevent discrimination between steps "to the right" and "to the left", i.e. 0° and 180°, the angles in the 2nd and 3rd quadrant, between 90° and 270°, were converted into their mirror reflex on the 1st and 4th quadrant. Figure 3.10 illustrates this equivalence; αpos_2 measured with respect to the left side of the pattern has the same value as αpos_1 since both steps are on the same line with opposite directions. Regarding the orientation to the pattern and regardless their direction, both angles are the same.

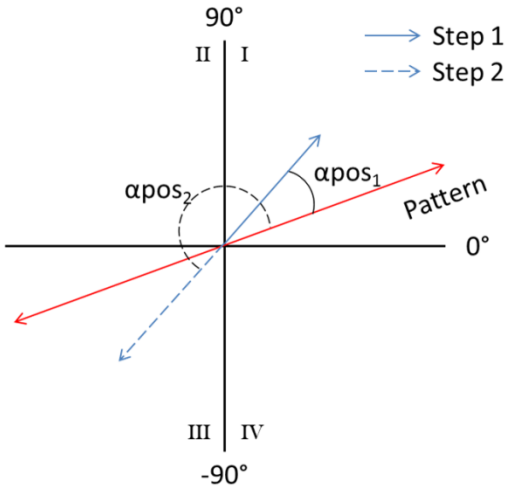

Figure 3.10: Representation of the step angle with respect to the direction of the pattern (αpos) for one step (step 1) and the corresponding step in the opposite direction (step 2). The blue lines represent the direction of the steps and the red one the direction of the pattern.

At the same time, movements "up" and "down" were similar in terms of orientation, i.e. uniaxial; if the pattern is horizontal, tracks in the direction of the positive and negative y

values were both perpendicular to the pattern. Hence the angles now contained in the 4th quadrant were also converted into their mirror reflex on the 1st quadrant (Figure 3.11).

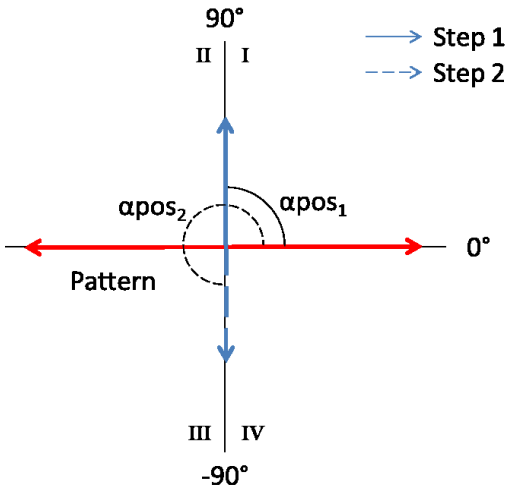

Figure 3.11: Representation of the step angle with respect to the direction of the pattern (αpos) for a step perpendicular to the pattern (step 1) and the corresponding step in the opposite direction (step 2). The blue lines represent the direction of the steps and the red one the direction of the pattern.

With these transformations, the angles were grouped to represent parallelism or perpendicularity to the pattern direction into four intervals with centers at 0°, 30°, 60° and 90°. According to House, the size of the interval was chosen to be ± 15° from the center of it [88]. The frequency of occurrence expressed as a percentage is calculated as the number of times the cell migrate with a certain angle divided by the total number of steps.

Table 3.1: Grouped step angles for the analysis of the orientation of the migration.

Group	Grouped angles
0°	$0° \leq \alpha pos_i < 15$, $165° \leq \alpha pos_i < 195°$, $345° \leq \alpha pos_i \leq 360°$
30°	$15° \leq \alpha pos_i < 45°$, $135° \leq \alpha pos_i < 165°$, $195° \leq \alpha pos_i < 225°$, $315° \leq \alpha pos_i < 345°$
60°	$45° \leq \alpha pos_i < 75°$, $105° \leq \alpha pos_i < 135°$, $225° \leq \alpha pos_i < 255°$, $285° \leq \alpha pos_i < 315°$
90°	$75° \leq \alpha pos_i < 105°$, $255° \leq \alpha pos_i < 285°$

For easier comparison, the frequency of occurrence can be represented in a chart as well (Figure 3.12). In the example it can be seen that the tracks 1, 2, 3, 6 and 9 were well oriented to the pattern, since their steps were around 80 % of the time in the direction of the feature (to the right or to the left). Track 4 showed migration at an angle and parallel to the pattern to a similar extent. The angles of tracks 5, 7 and 10 were distributed between all

intervals. The tracks did not show any orientation with respect to the pattern and were categorized as random tracks. Finally, track 8 was mainly oriented at an angle to the pattern with a tendency toward perpendicular motion.

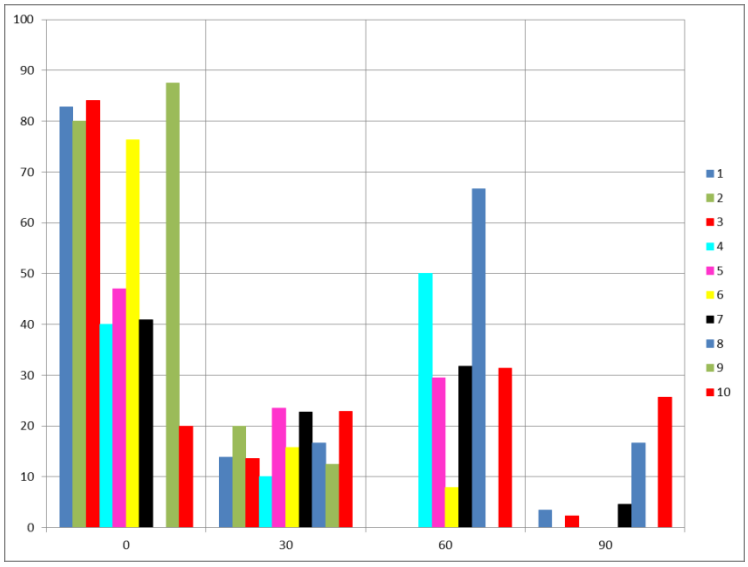

Figure 3.12: Representation of the frequency of occurrence of the step angles αpos_i grouped around the values 0°, 30°, 60° and 90°.

The analysis tool also calculated other parameters to describe the migrating behavior and represented them in form of a results table (Table 3.2).

The first two columns were made to ease the recognition of the cell and comparison with the other analytical methods. Cells were numbered in the order used to track them with ImageJ and a color code was assigned. This color code was the same which had been used by the tracking plugin of ImageJ.

The migration time or tracking time (T) was calculated as the product of the number of steps and the time interval. In some cases, migrating cells appeared in the range of the camera after the start of video recording and consequently their tracks were shorter. This must be taken into consideration; each cell track had its own value for T.

The Euclidean distance (D) and the total path length (L) were calculated according to Eq. 3.4 and Eq. 3.5 respectively. Using these values and the Eq. 3.6, the straightness index was calculated. As previously indicated, this parameter gives an idea of the efficiency of the movements in terms of straightness. For this case, cells 4, 7, 8 and 9 migrated mainly in one direction without turning back. In contrast, cells 1, 2, 3, 6 and 10 turned regularly and finished at a position relatively close to their starting points. Combining this information

with the previously presented results, we can say that cells 1, 2, 3 and 6 were not random walkers. On the contrary, they were highly oriented to the pattern. The features induced on them only a tendency for uniaxial migration and, consequently, they were free to change the direction of their movement and retrace their steps.

The ratio G/L (Eq. 3.8) gave similar values to those obtained by the straightness ratio. In this case, the values could be also negative, 0 being the worst case. The positive or negative sign of the number indicated, respectively, if the final position of the cell was located on the right or on the left side of the starting point on the pattern axis. This parameter presented tracks 4, 5, 6, 7 and 8 as more sinuous than the straightness index, because it also included the deviation with respect to the pattern direction as a variable. For this reason, tracks relatively straight but with orientations different to the pattern, such as number 8, get such a low valuation.

The average speed was also calculated as the average of the step speeds (Eq. 3.3). This is one of the most used migration parameters and is specially used to compare the effect of different environmental conditions (substrate, medium, etc.) in the migration behavior of cells. A comparison of the migration speeds between cells within the same experiment is not typically done, since it is considered that the differences are due to the individual characteristics of the cell and not due to differences in the environment. The values of every cell of an experiment were averaged and compared with cells under other experimental conditions.

Table 3.2: Table of migration parameters.

Cell	Color code	T (min)	D (μm)	L (μm)	Straightness index	Ratio G/L	Average speed (μm/min)
1	Blue	710	24.92	126.74	0.20	-0.20	0.18
2	Green	710	26.04	99.65	0.26	-0.26	0.14
3	Red	710	71.45	239.14	0.30	0.30	0.33
4	Cyan	330	133.55	152.74	0.87	0.66	0.45
5	Pink	240	152.45	224.68	0.68	0.52	0.90
6	Yellow	710	20.44	173.89	0.12	0.08	0.24
7	White	270	300.31	409.78	0.73	0.35	1.46
8	Blue	120	224.11	257.00	0.87	0.15	1.98
9	Green	280	53.17	72.14	0.74	0.74	0.25
10	Red	710	0.63	149.67	0.00	0.00	0.21

3.3.3 Software features:

The steps undertaken by CellMAT to calculate the necessary parameters for the interpretation of cell tracks are summarized in Figure 3.13.

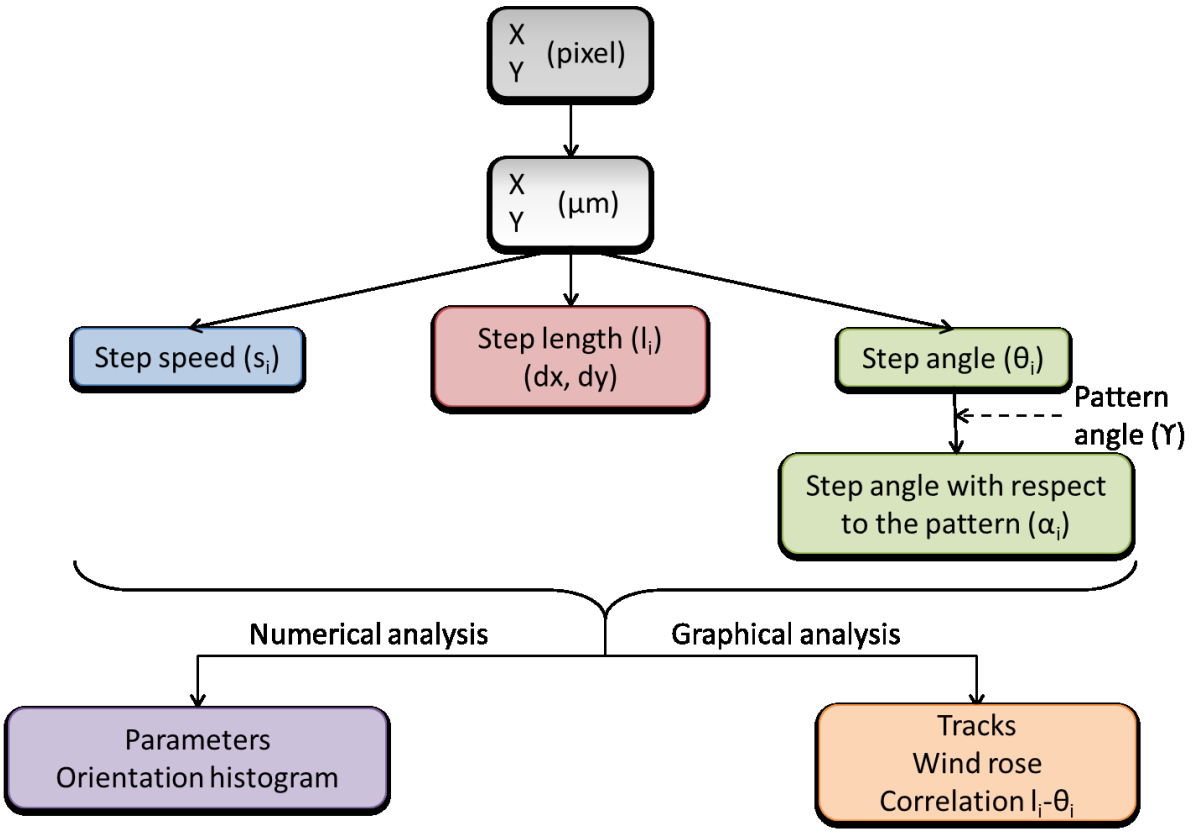

Figure 3.13: Schematic representation of the software algorithm.

The software has been tested with a plausibility and robustness check using different numbers of cell tracks, pattern angles and time intervals. The program worked correctly in all situations.

In some cases the color codification may be confusing because only seven colors were used; especially when the charts created by Excel are aimed to be used in a written report. The selection of the colors has been done to fit with the tracking images obtained by ImageJ and the tracks can be easily recognized on the Excel file by clicking on them. The colors can be manually modified in case the graphic is exported to a report.

Sometimes, the elevated number of tracks present on a file makes the interpretation of the graphic results hard. For this reason, the software included the possibility to add and remove tracks from the graphic by clicking on the corresponding checkbox (Figure 3.14).

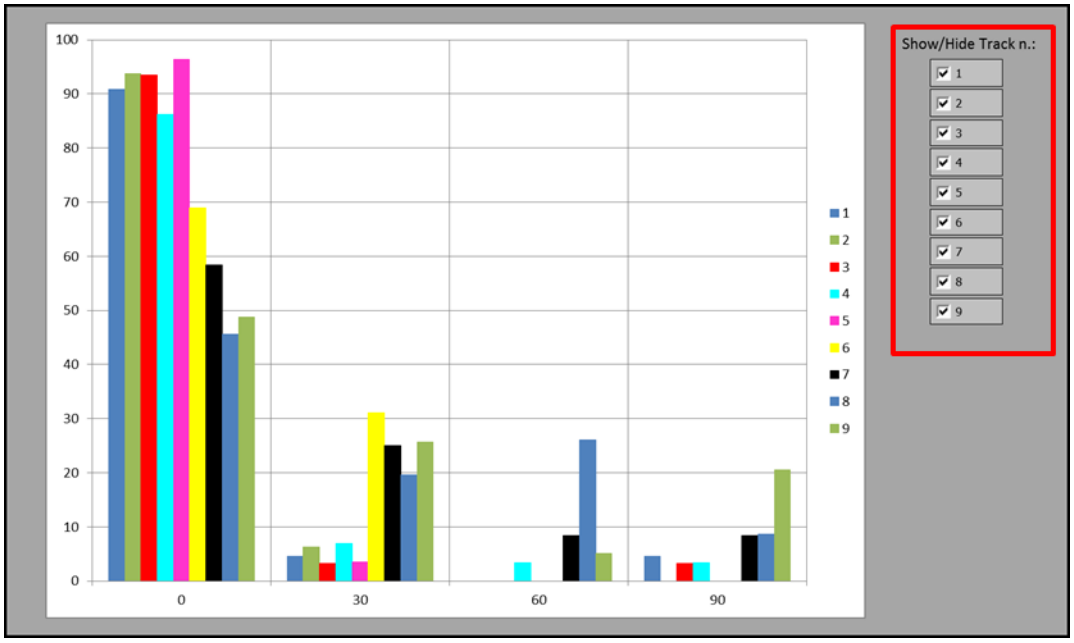

Figure 3.14: Example of a chart showing the frequency of occurrence of an angle. Highlighted with a red box is the checkbox to add and remove tracks from the chart.

These features together with parameter calculation and the generation of graphic representations made CellMAT a useful tool for fast and accurate analysis of large numbers of cell tracks on line-like patterned substrates.

3.4 Conclusions

An Excel based tool has been developed to analyze batches of cell tracks on patterned substrates with a few clicks. The program has been shown to be effective regardless of the number of tracks, direction of the pattern and acquisition interval.

The combination of the different parameters and graphic analysis overcomes the shortcomings of individual parameters and permitted an accurate interpretation of the migration paths.

The tool CellMAT has been developed to fit the specific needs of this work and, consequently, to obtain more universal analysis tools some modifications in the code of the program would be required. One possible improvement would be the inclusion of a larger database of conversion factors pixel/µm for the different microscope systems and magnification settings.

Several repetitions of each experiment are necessary to obtain statistically relevant results. These experiments are saved separately. Nevertheless the results can be treated together. To increase the speed of the data treatment, the analysis tool should be able to add several data files to the pool of data to be treated, including the possibility to set the pattern angle and time interval separately for each experiment.

Despite CellMAT still being at a very early development stage, it can already accomplish the necessary tasks to analyze cell migration and can compete with other freely available software.

Chapter 4:

Controlling cell migration on topographic and Fill-Molding in Capillaries substrates

4.1 Introduction:

As defined in Chapter 1, migration is the process through which cells actively change their position over time [32]. However, what causes cells to migrate from their original location in the first place? What triggers this movement? We have already seen that heterogeneities on the cellular environment can be recognized by the cells and stimulate their migration. Three of the main signals that influence migrating cells are topographic, mechanical and chemical signals. In this chapter we investigated the effect of those three cues on the migration of fibroblasts.

4.1.1 Contact guidance:

The fact that the topographic and physical properties of the substrates play an important role on cell behavior was first observed by Harrison at the beginning of the 20th century [95]. Mid-century, Paul Weiss introduced his concept of "contact guidance" to define the guiding action of oriented interfaces on the migration of cells [49]. This concept goes further than a mere physical effect of the topographic cues on the cells and in fact involves other internal mechanisms as well. Nowadays, many of the basic questions about those underlying mechanisms remain unsolved; however, some theories about cell recognition of the topographic cues and subsequent response have been developed [56]. Most of these hypotheses are based on the idea that the environment modifies either the components of the cellular membrane or the shape of the cells, and that this affects the cell function and behavior.

Some researchers suggest that anisotropies modify the way in which proteins interact with the surface. Proteins adsorb preferentially on low-energy surfaces and the interfacial energy is correlated to the surface roughness [96]. The protein-surface interaction also affects the structure of proteins and, consequently, their activity and stability [25]. Adhesion complexes, and especially focal adhesions, are seen as the main functional linker between the cell and the extracellular matrix (ECM) [97,98]. The location of cellular receptors on the membrane can be altered by the topographic cues as well as the cytoskeleton; cells will align to directions where the distortion of their cytoskeleton is minimized [99]. Therefore,

the cells become highly polarized and behave differently than in absence of those topographic cues [100,101].

Another effect of the presence of topography is the modification of the shape of cell. Dalby and co-workers suggest that the shape of the cell has a direct relation with its functionality via modifications in the nucleus and gene expression [102–104]. The modification of the shape is controlled by the cytoskeleton where the transduction of the external cues by the cytoskeleton is linked to the adhesion complexes. The nucleus is linked to the cytoskeleton and modifications of it will passively deform the nucleus [104]. These deformations have shown to have an effect on the chromatin structure and, therefore, on the accessibility to the genes, modifying the phenotype of the cell and its behavior [104,105].

Many kinds of anisotropies induce a response on cells [106], among others, pits [107], pillars [22], grids [86] or channels [108]. The last two present a great advantage for controlling cell migration; the cells respond to them by orienting their bodies to the topography, which is one of the first steps for migration, and can induce a preference for the movement in a determined direction [48,56,109,110]. Features such as pits or pillars can be seen by the cells as a homogeneous field of heterogeneities and they orient at any possible direction [62].

Not only the type but also the dimensions of the topography can control the direction of movement. Jeon and co-workers showed that on samples with a small grid (similar to pits) the cells migrated without special orientation [86]. When a channel-like topography (similar to grids where one of the dimensions trend to infinite) was present, the cells migrated parallel to the lines, even if they originally orientated perpendicularly [86,93]. Nevertheless, if the distance between grooves was increased, the migration could follow directions different to that of the pattern [110]. The dimension of the features also affects the migration speed of the cells; Kaiser and Jeon, both concluded that migration parallel to the pattern lines was faster than the perpendicular one [86,93].

In addition, the geometry of the substrate affects the movement of the cells. Park and co-workers tested the behavior of cells when confronted with surfaces containing concave pits and convex hills [69]. They seeded fibroblasts on samples with pits and hills with an aspect ratio width/depth of 4:1. Cells positioned inside pits moved to escape whereas cells

close to hills tried to climb them. Summarizing, concave topographies create adverse conditions for cell adhesion, while convex ones enhance it.

As already commented in Chapter 1, previous experiments in our group demonstrated that the incorporation of topographic features induced cell adhesion on intrinsically anti-adherent PEG. In this chapter we went one step further and we investigated the migratory behavior of fibroblasts adhering on those patterned PEG substrates. We expected that the conclusions extracted from the observation of the migration could shed light on the unusual phenomenon of adhesion on PEG hydrogels.

4.1.2 Mechanotaxis:

It was suggested that the capacity to recognize topographic structures is related to the ability to detect the mechanical properties of the ECM [104]. How exactly does a cell measure the elasticity of its environment? Lo and colleagues suggest that the cell carries out a “pulling test” through the focal adhesions [15]. The cell exerts forces pulling from the actin fibers connected to the focal adhesions and measures the energy consumption for generating tension as a response to the force. On soft materials, under low forces, the receptor-ligand complex can move long distances. On the contrary, on stiff substrates a small displacement of the receptors creates great tension. This tension may increase the influx of calcium ions, which leads to a higher energy consumption. Whatever the mechanism, it seems to be accepted that focal adhesions play a major role in the conversion of the mechanical signals of the environment into biochemical ones (mechanotransduction) [104,105,111].

A special type of mechanotaxis is “durotaxis”. This term was coined in 2000 by Lo and colleagues to define a preference, which certain types of cells possess for stiffer materials. These cells consequently migrated into stiffer areas of the material upon which they were positioned [15]. Durotaxis has been the object of numerous studies in the last two decades. Mechanical differences have been presented as gradients [15,85,87,112] and, most interesting in the context of this thesis, as patterns [62,113,114] on the surface of the substrate. However, external factors, i.e. external strain on the material [87] or interaction of other cells with the surface [15,111], may also alter the stiffness sensed by the cells. For

this reason, while studying the effect of mechanical cues on the behavior of individual cells, it is mandatory to avoid overpopulation of cells on the samples during the experiments. This overpopulation can falsify the observations and lead to contradictory results.

Different methods have been used to create mechanical heterogeneities on substrates in the past. Gradients of elasticity have been mainly prepared by putting two precursors into contact and letting them diffuse into one another. The composition of the precursors regulated the differences in the mechanical properties of both materials. These mixes can be created by simple contact and diffusion through one interphase [15,115] or by several contact and diffusion steps inside multi-channeled microfluidic devices [85,116]. Kuntanawat and co-workers simply modified the thickness of the film, altering the apparent elasticity of the substrate [112], since the elasticity of thin gels is affected by the underlying substrate, e.g. glass slide (see Chapter 5).

Patterns of elasticity can be prepared by coating solid structures with a relatively soft film [38,62,117,118]. These samples are based in the principle outlined in the previous paragraph. The embedded structures affect the elasticity of determined areas of the substrate, while others remain unaffected (either no solid structure is located underneath or the film thickness is high enough to hide the effect of the structure). In the work of Cortese et al., the pattern was created by utilizing the contrast between air chambers and the bulk substrate. They created topographic patterns of PDMS and covered the whole sample with a film, creating air pockets between the patterned structures [62].

Another method to generate patterns of elasticity is the control of the polymerization sites through photomasks or laser beams. In the work of Nemir et al., a base polymer was prepared and the solid gel was soaked with a solution containing a different polymer precursor. The precursor penetrated the network of the gel and was polymerized via UV-curing at determined positions with the help of a photomask. The unreacted precursor was then removed, leaving areas composed only of the base polymer [119]. In comparison, Kloxin and Hahn used a laser beam to “draw” the pattern. The difference between both methods is that while Hahn used a similar approach to Nemir, i.e. diffusing a second precursor inside a base polymer and removal of the unreacted pre-polymer [120], Kloxin used a UV-degradable cross-linker, undoing the network at the positions affected by the laser [9].

A different strategy was followed by Chou and co-workers. They created the pattern by filling the channels of a topographically patterned sample with a second polymer of different composition [113] in a similar way to the microtransfer molding (μTM) developed by Whitesides [78].

In all these examples, with the exception of Kloxin, the differences of elasticity were obtained by using two polymeric precursors of the same polymer but with different compositions. This approach presents the risk of modifying the chemistry of the surface; the chemistry of both precursors, despite of their similarity, is different and may be enough to form a chemical pattern which could override the mechanical one.

In our case, to make elastic patterns, a "channel filling" strategy was also used. We applied the **Fi**ll-**M**olding **I**n **C**apillaries (**FIMIC**) method (see Section 2.2.3 and Figure 1.4, page 11) to create elastic patterns on the surface of the substrates by filling the grooves of a previously patterned hydrogel with another liquid pre-polymer. The patterns of elasticity were generated using different concentrations of cross-linker for the mold and the filler material. The addition of the cross-linker was maintained at low levels (0% to 10%) in order to minimize the possible alteration of the surface chemistry of the materials.

By using FIMIC samples, we were able to study the migratory behavior of fibroblasts on well-defined patterns of elasticity. We also wanted to confirm the observed tendency of migration from softer to stiffer materials reported by Lo and other authors, in addition to establishing the optimal size of the pattern which can induce and accelerate cell migration, leading to the control of this cellular behavior.

4.1.3 Haptotaxis

As explained in Chapter 1, haptotaxis is a type of cell migration where the cells respond to chemical signals to orientate and move themselves. It should not be confused with chemotaxis, where the chemical agents are dissolved in the medium. In the case of haptotaxis, the cues are fixed on the surface of the migration substrate [45]. The term haptotaxis literally means "fasten arrangement" and Carter, who introduced this term, also called them "adhesion gradients" [45]; the chemical cues, also known as ligands, serve as anchoring points for cell adhesion and further displacement.

Most of the work done in the field of haptotaxis was carried out using gradients of ligands [121,122]. As a general conclusion of the migration of cell in the presence of gradients, we can say that cells move into the direction of increasing concentration of ligand (obviously in the case of chemoattractants). It can also be said that the speed of migration increases with the slope of the gradient [121], i.e. the more drastic are the concentration changes, the faster the cells move forward.

Only a few scientists investigated the effect of haptotactic patterns on cells. Harris [46] created squared patterns of adhesive material on different substrates. He found that cells migrated along the less adherent zones until they reached an adherent area. Then, cells remained confined to the adherent areas, not returning back to the less adherent ones. This phenomenon is similar to that observed on cells migrating on elastically patterned substrates [15]. When Harris reduced the size of the "haptotactic islands", he found that cells adhered to several of them at the same time, bridging the less adherent zones.

Our work contributes to the research done on such chemical patterns. Taking advantage of the capacity of the FIMIC method to use different materials at the same time, we can prepare substrates for cell culture with clearly-defined chemical patterns on the surface. Controlling the size and the periodicity of the pattern, we aimed to be able to direct cell migration.

Cell migration has been extensively studied in recent years. Unfortunately, a concrete protocol for the observation of cells does not exist. Some authors used pre-incubation times (ranging from 1 to tens of hours) in order to allow complete cell adhesion before analysis [15,42,48,86,93,123], while others start monitoring movement via video recording right after seeding. Neither is there unanimity in the length of the experiments; most of the studies can be grouped into "12 hours" [15,42,48,83,86,110,123] or "24 hours" [62,64,85,87,88,93] observations, even though the range of video lengths varies from several hours to more than one day. Jian and colleagues for instance tracked cell migration only for 4 hours [124].

Another analysis parameter, the sampling interval, has not been receiving the importance it deserves. As explained in Chapter 3, the lapse between images can modify the

subjective interpretation of the migration track and lead to erroneous results. Too long-spaced sampling can result in loss of information while short sampling intervals may not add necessarily useful information and increase the amount of data to be processed; a compromise between information and processing data must be achieved. Sampling intervals from 1 frame/min to 1 frame/30 min can be found in the literature. However, the majority of the authors use 1 frame/15 min.

On the other hand, many scientists agree that for studying the effect of the different migration triggers on individual cells, any interaction between cells must be avoided; cells can modify the apparent elasticity of the substrate [15,38,79] or serve as anchoring points. To avoid this problem, cells were seeded in low concentrations and cells contacting other cells were not taken into consideration for the analysis [42,48,85,86,124].

In the present work, we pre-incubated cells for 1 hour, avoiding the interference of floating non-adherent cells during imaging. Due to the processing capacity, we had to find an agreement between sampling interval and total length of the experiment. We decided to use a time interval of 10 minutes, which was shorter than the commonly employed of 15 minutes, but still did not overflow us with unnecessarily much information. With this imaging interval we were able to record and process migration of cells for around 14 hours. We considered 14 hours an adequate observation time, because for longer analysis, mouse fibroblast start dividing (typical doubling time around 14 hours [125]) and the migration tracks could be affected by cell-cell interactions.

4.2 Materials and methods:

In this chapter, three different types of substrates were used: topographically, elastically and chemically patterned hydrogels (Figure 4.1).

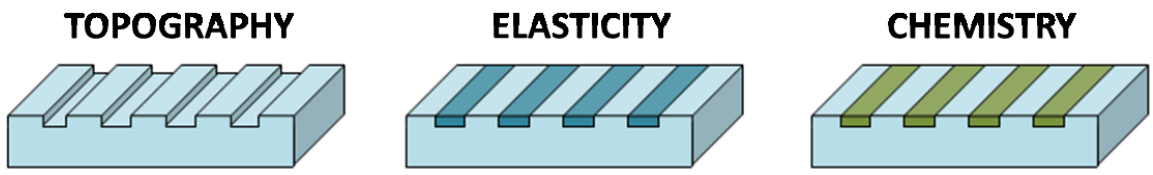

Figure 4.1: Representation of the different substrates employed for investigating cell migration.

4.2.1 Preparation of the topographic patterns:

Topographic patterns were prepared following the instructions given in Section 2.2.2. These samples were notated by a three number code, indicating the dimensions of the groove width-spacing-depth (e.g. 10-20-10)

Topographic samples were prepared without addition of cross-linker and UV-cured for 30 minutes.

4.2.2 Preparation of FIMIC samples:

Elastically and chemically patterned samples were prepared using the FIMIC method described in Section 2.2.3.

For the elastic patterns, we used combinations of **PEG, Blend1** and **Blend2** with and without addition of cross-linker (Table 4.1). Softer-in-stiffer (softer material as filler, stiffer as mold) and stiffer-in-softer patterns were prepared. The composition and dimensions of the pattern stripes for each concrete case were indicated in the following section. FIMIC samples were notated by a code, indicating the width of the filler and the mold lines (e.g. 50-10).

Table 4.1: Content of cross-linker for the formulation of the polymers for the formation of the elastic pattern.

	Content of cross-linker (% v/v)	
Material	Softer	Stiffer
PEG	0	10
Blend1	0	5
Blend2	0	5

To avoid delamination after hydration of the gels (see Chapter 1), the molds were UV-cured for 8 minutes. After filling, the samples were UV-cured another 20 minutes.

Chemical patterns were generated by filling a **PEG** mold with liquid **3BC** pre-polymer. None of the precursors were supplemented with cross-linker. As for the previously

described FIMIC samples, the UV-curing times for mold and filler were 8 and 20 minutes respectively.

Several pattern sizes were employed, being indicated in the results and discussion section. As pointed out in Chapter 2, the first number corresponded to the width of the filler lines (**3BC**) while the second designated the separation between those lines, i.e. the width of the mold lines (**PEG**).

4.2.3 Cell migration:

The protocol for cell migration was detailed in Chapter 2.

Briefly, cells were seeded on the sterile hydrogels with a concentration of 50000 cell/mL and pre-incubated at 37°C and 5% CO_2 atmosphere for 1 hour. After pre-incubation time, the samples, with the adherent cells, were placed on new culture plates and fresh medium was added. The culture chambers were incubated in a microscope-integrated incubator at 37°C and 5% CO_2 atmosphere. Cells were imaged every 10 minutes for 14 hours and 20 minutes (86 frames in total). Tracks were obtained using a Manual Tracking Tool (ImageJ) and the data were processed using a self-made analysis program (CellMAT, see Chapter 3).

4.3 Results and discussion

4.3.1 Cell migration on topographic structures:

In order to investigate the effect of topographic features of **PEG** hydrogels on the migration of fibroblasts, samples with channel structures on the surface were prepared. The dimensions of the channels, i.e. width, depth and separation (see Section 2.2.2) were varied between 10 µm and 50 µm and the migratory behavior was recorded for at least 14 hours.

The results can be grouped into narrow, medium and wide channels regarding their relation to the typical size of a mouse fibroblast, namely 10-20 µm. An average of 5 cells per image was tracked.

Figure 4.2 shows the migration tracks of fibroblasts on a substrate with dimensions 5-10-5. Narrow channels (5 µm) were smaller than the cell size. For this reason, the cells

showed two different behaviors on these samples: Some cells deformed their bodies to fit inside the channel. The migration of these cells was evidently confined to channels and the tracks fitted to a straight line (e.g. dark blue, red and white tracks). Other cells, unable to enter the channels sat on top of them, introducing only a fraction of their body as a guide. These cells had greater freedom to migrate on different directions and to cross from one channel to another (line-crossing), e.g. green and pink (center) tracks.

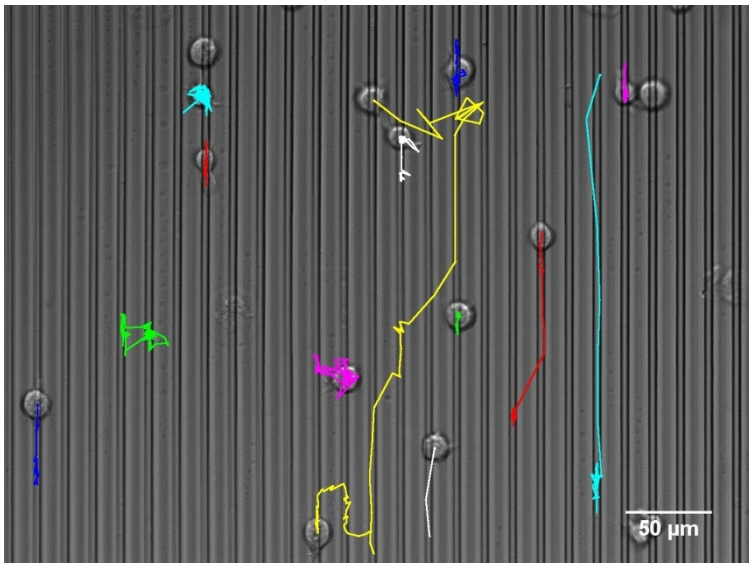

Figure 4.2: Migration tracks of fibroblasts moving on a topographically patterned PEG sample with dimensions 5-10-5.

These two kinds of migration were not completely independent. Cells were able to change their migration, entering and exiting the grooves. As a result, parts of their tracks showed extreme alignment to the direction of the lines, while others were more similar to random migration (yellow track). The persistence of these cells was relatively low (less than 70 minutes). This was due to the uniaxial homogeneity of the samples inside the channels; there were no differences between both directions of the lines. After each step, the cell analyzed their environment and found a similar substrate on both sides. The lack of additional signals made both directions favorable for further migration.

Cells migrating on these samples presented and average migration speed of **0.32 ± 0.26 µm/min**. Cells inside the channels showed a slightly reduced migration speed compared to those sitting on the surface.

When grooves with widths approximately the size of the cell were used (10 µm), we still observed confinement of cells inside the channels (Figure 4.3). The deformation of the

fibroblast necessary to fit inside the channels was lower. For this reason, the presence of cells sitting on the surface and migrating randomly on top of it was almost non-existent; substrates with these dimensions showed almost exclusively migration oriented in the channel direction.

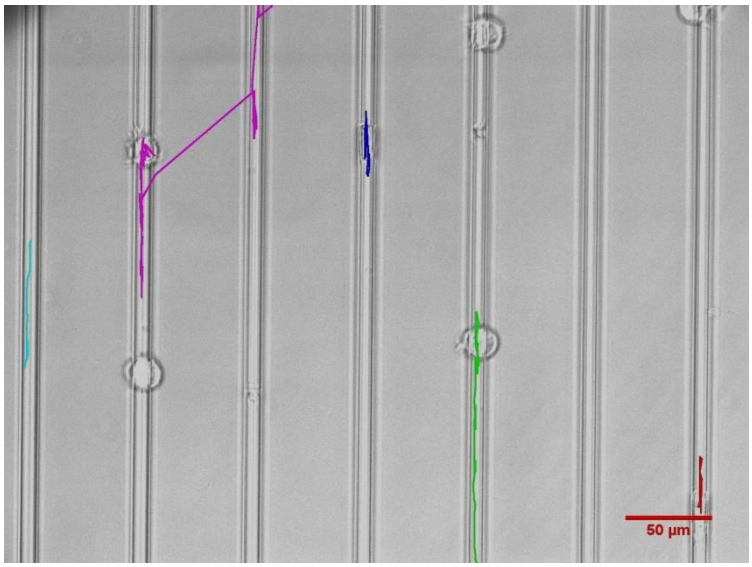

Figure 4.3: Migration tracks of fibroblasts moving on a topographically patterned PEG sample with dimensions 10-50-15.

Nevertheless, cells inside the channels were under tension and can exit them, allowing line-crossing. On the other hand, this effect can be minimized by using large spacing between channels, like 50 µm; fibroblast cannot reach the adjacent lines while anchoring at the original one. In those cases, cells were able to move to other lines by detachment and re-attachment when the new channel was reached.

As in the previous case, the values for persistence and the straightness index were low. Cells were highly aligned (Figure 4.4); however, they regularly turned around and the movement was not persistent. This explains why the tracks were so “inefficient” from the point of view of the straightness index.

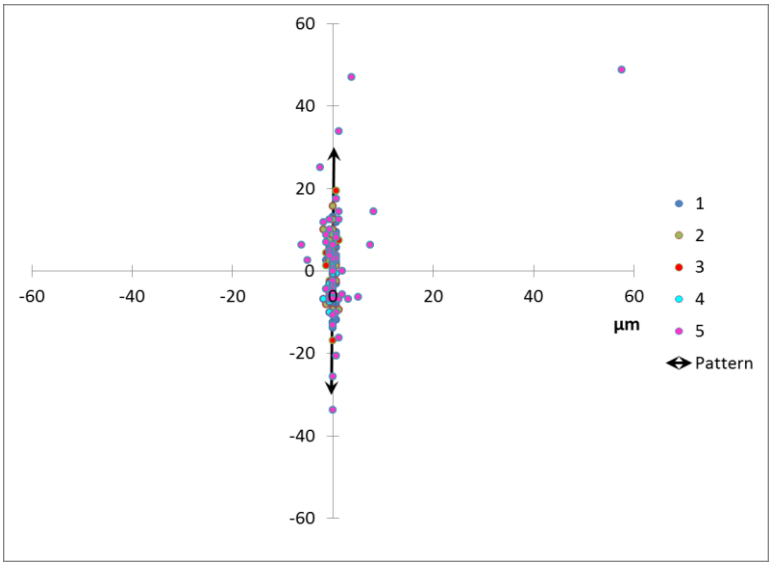

Figure 4.4: Correlation step length / step angle of cell tracks 1 to 5 on a topographically patterned PEG sample with dimensions 10-50-15.

On substrates with channels of 10 µm width cells migrated with an average migration speed of **0.45 ± 0.20 µm/min**.

If the width of the channels was increased to 20 µm, cells fitted comfortably inside them (Figure 4.5).

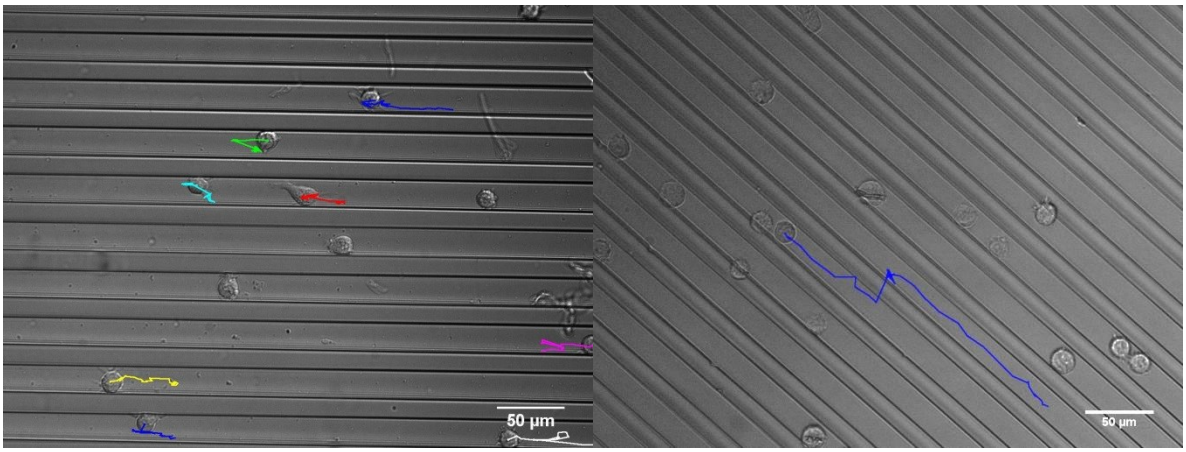

Figure 4.5: Migration tracks of fibroblasts moving on topographically patterned PEG samples with dimensions 20-10-10.

The migration still followed the direction of the pattern, although the cells had enough space to move in other directions inside the channel. For instance, the track presented in Figure 4.5 left had a persistence of 20 minutes and only 54% of the step angles were in the direction of the pattern (± 15°). The average migration speed, **0.42 ± 0.37 µm/min**, was similar to that obtained for migration on 10 µm wide grooves. .

Also in this case, the use of reduced spacing between channels, in combination with relatively low heights, allowed for line-crossing.

When substrates with channels much larger than the cell size were used, i.e. 50 µm, the observed tracks resembled those typically obtained for random migration (Figure 4.6). The fibroblasts migration was confined inside the channels. They explored the channels freely as if they were on a flat surface, varying the migration angle permanently; the step angles were distributed without any preference, such as parallel or perpendicular to the pattern direction (Figure 4.7). Only those cells migrating close to the walls of the channels showed some degree of orientation to the pattern.

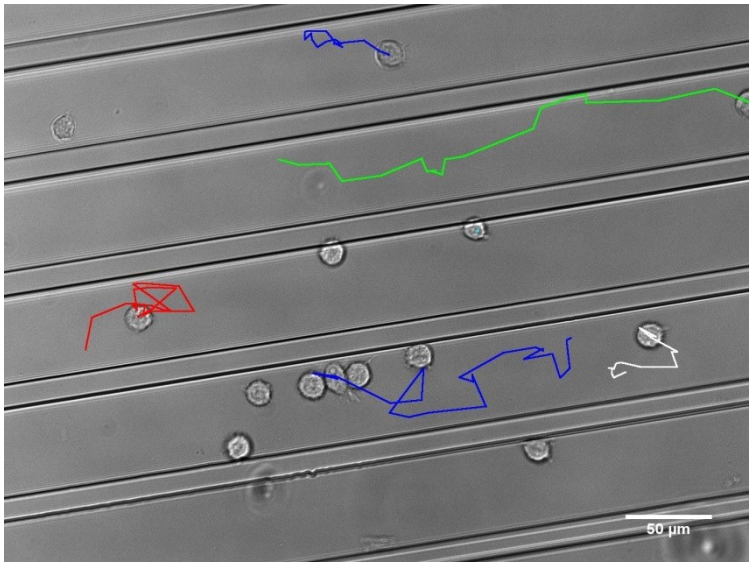

Figure 4.6: Migration tracks of fibroblasts moving on a topographically patterned PEG sample with dimensions 50-10-10.

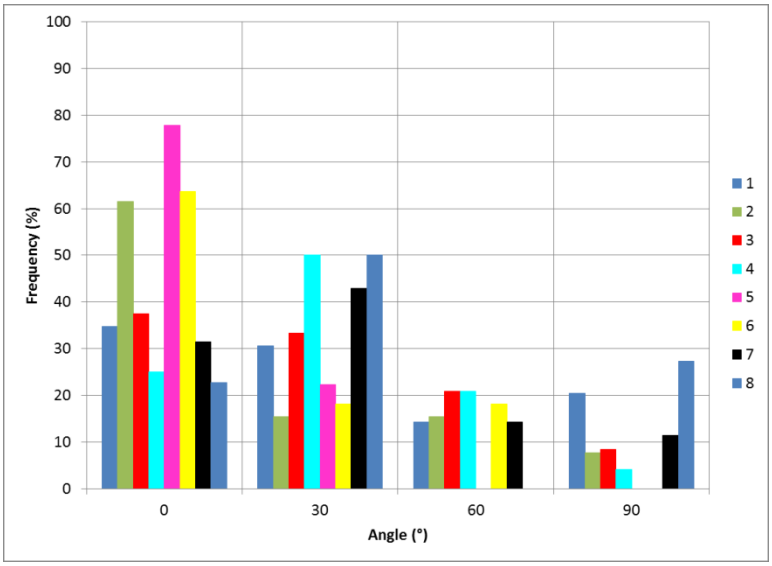

Figure 4.7: Histogram of the step angles for the tracks 1 to 8 of fibroblasts migrating on a topographically patterned PEG sample with dimensions 50-10-10.

The migration speed recorded on these samples was **0.97 ± 0.67 µm/min**.

All things considered, we observed an increased migration speed on those samples with channels wider than the cell size (20 µm or more). Cells fitting tightly inside the channels had larger surface in contact with the hydrogel, which enabled the formation of more adhesion contacts. We suggest that the elevated adhesion of cells on narrow channels resulted in slower migration speeds; as explained in Chapter 1 strong adhesions are harder to break forcing cells to migrate more slowly on more adherent substrates. This hypothesis is coherent with the observations on samples with narrow channels, where the migration of cells inside the grooves was slower than those of cells sitting on top of the topography.

Regarding the migration speed, it can be concluded that cells on wider channels migrated faster, maybe because they adhesion was weaker since the available surface for adhesion was lower (Table 4.2). The elevated value of standard deviation illustrates the fact that not all cells were migrating in the same way. Some of them migrated fast, with longer steps, while others mainly remained at their position or moved in shorter steps.

Table 4.2: Average migration speed on topographically patterned PEG samples with different dimensions.

Pattern dimensions (w-d-h) (µm)	Average migration speed (µm/min)
5-10-5	0.32 ± 0.26
10-50-15	0.45 ± 0.20
20-10-10	0.42 ± 0.37
50-10-10	0.97 ± 0.67

Figure 4.8 summarizes the migration types on topographic substrates. According to these results, we may declare that to direct fibroblast migration in the direction of channel-like topographies, the use of dimensions in the order of the cell size is recommended (between 10 µm and 20 µm). To avoid perpendicular migration (line-crossing) the grooves should be separated at least 50 µm since smaller spacing could be trespassed by spreading cells. If, on the contrary, perpendicular migration is desired, narrower channels have to be used (5 µm or less). These structures should act as anchoring points but being so narrow that the cells do not fit inside. At the same time, the next

channel should be at a distance that is reachable for the cell. Notwithstanding, migration in the direction of the pattern would not be prevented.

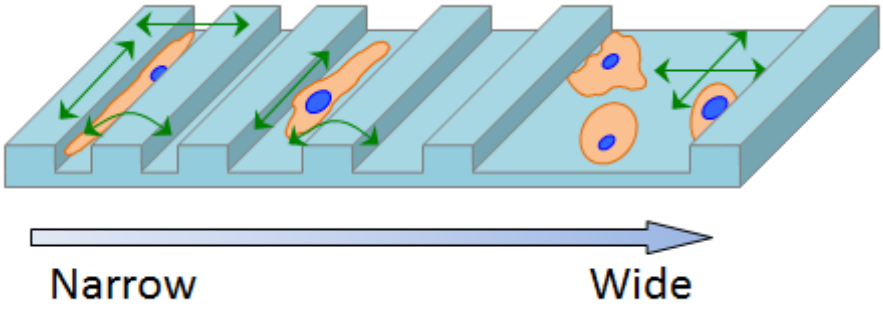

Figure 4.8: Schematic representation of the migratory behavior on topographically patterned substrates with increasing channel width.

4.3.2 Cell migration on elastically patterned samples:

4.3.2.1 Elastic patterns on PEG substrates:

In previous research we showed that not only topographic features were able to induce adhesion of fibroblasts on **PEG** substrates, but mechanical patterns also altered the adhesive properties of these materials. In this section we analyzed the effect of elastically patterned **PEG** samples on the migration of fibroblasts.

First we used FIMIC samples where the mold, prepared with **PEG** 10% CL, was filled with **PEG** 0% CL (Softer-in-stiffer). According to the durotactic behavior of fibroblasts, adhesion and migration to the mold lines, i.e. harder material, was expected.

Figure 4.9 shows the migration tracks of fibroblasts on a FIMIC sample presenting a pattern of 50 µm **PEG** 0% CL (filler) separated by 10 µm **PEG** 10% CL (mold) lines. Contrary to what we expected, cells adhered on the softer filler lines instead of on the harder mold ones. The observed migratory behavior could be attributed to the previously observed migration on wide channels, namely random migration, even though migration on the border between lines seemed to induce some degree of orientation. The migratory speed was **0.26 ± 0.14 µm/min**.

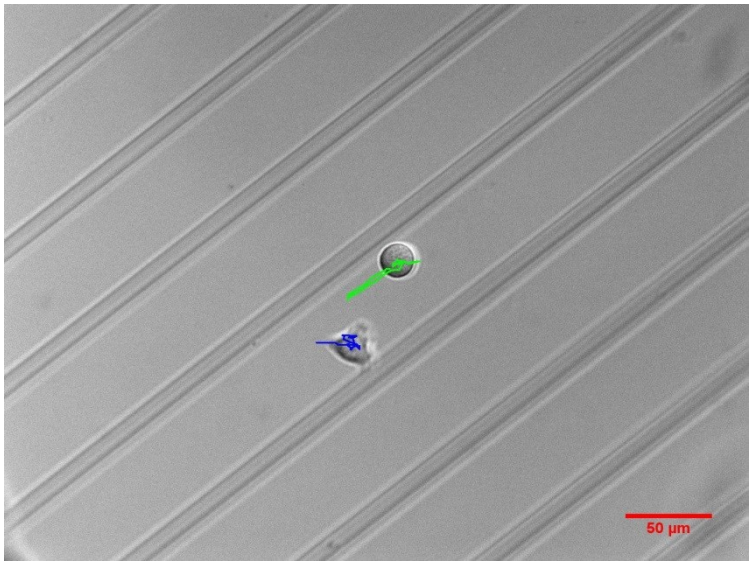

Figure 4.9: Migration tracks of fibroblasts moving on an elastically patterned PEG sample (softer-in-stiffer FIMIC sample) with dimensions 50-10.

The observed tracks on FIMIC samples differed from the results on topographic substrates on the aspect of line-crossing. Topographic features presented a physical barrier for cells to change their position to adjacent channels; cells had to spread enough to cover the distance to the top of the channel walls (depth) and to reach the new channel (separation). This hurdle was not present on the FIMIC substrates; the only hindrance for line-crossing was the width of the lines. For this reason, perpendicular migration along the sample may be possible if the dimension of the pattern is below the size of a spreading cell.

When we used a pattern dimension of 10-20 (Softer-in-stiffer) we observed cell adhesion and migration on the stiffer mold lines, as was expected (Figure 4.10).

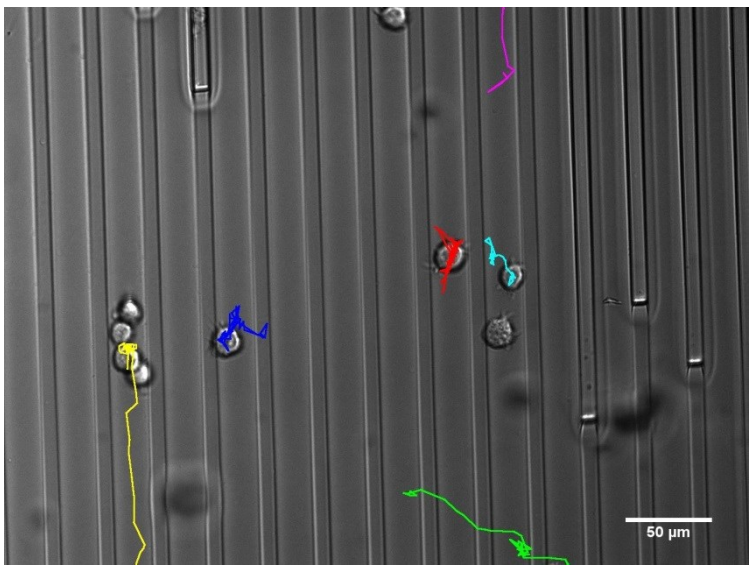

Figure 4.10: Migration tracks of fibroblasts moving on an elastically patterned PEG sample (softer-in-stiffer FIMIC sample) with dimensions 10-20.

The migratory behavior corresponded to that which was observed inside 20 µm wide channels; cells migrated with a certain degree of orientation. Nevertheless, they had enough room to explore in directions different to that of the pattern. Particularly interesting was the movement of the fibroblast represented by the green track in Figure 4.10. Because of the smoothness of the sample and the reduced spacing between attractive lines, the cell was able to reach adjacent stiffer stripes and to migrate perpendicularly to the pattern direction.

Cells migrating on these samples presented an average migration speed of **0.34 ± 0.17 µm/min**. It should be noted that on those steps corresponding to straight oriented migration (parallel or perpendicular) the speed was at least double of that observed on migration sections with random tendency.

On samples with a pattern of softer narrow lines besides wide stiffer ones (10-50), fibroblasts were also observed to adhere to the stiffer lines (Figure 4.11). As observed in the first case of this section, where the cells adhered also on the wider lines of the pattern (Figure 4.9), migration showed a predominantly random performance with regular direction changes; the persistence of the movement was under 20 minutes (2 frames). Line-crossing was frequent; however, the migration took place on the mold lines and displacements on top of filler lines were carried out by anchoring to the adjacent mold lines.

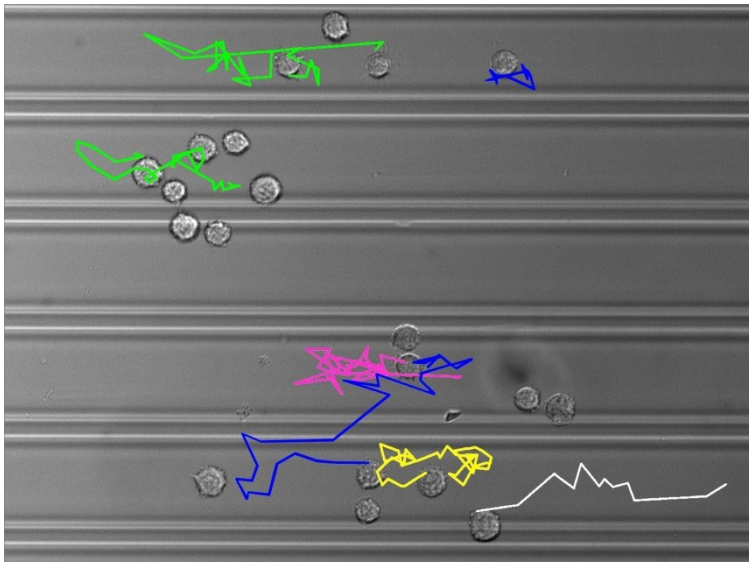

Figure 4.11: Migration tracks of fibroblasts moving on an elastically patterned PEG sample (softer-in-stiffer FIMIC sample) with dimensions 10-50.

In this case we observed a higher migration speed, with a value of **0.87 ± 0.55 m/min**.

Table 4.3 summarizes the migration speed on the different pattern dimensions. The cells on elastically patterned **PEG** substrates also showed a heterogeneous behavior; some cells migrated fast (large displacements) while others performed short steps showing a slower overall speed. These differences are reflected in the standard deviation of the average speeds.

Table 4.3: Average migration speed on elastically patterned PEG samples (softer-in-stiffer FIMIC samples) with different dimensions.

Pattern dimensions (filler-mold) (µm)	Average migration speed (µm/min)
10-20	0.34 ± 0.17
50-10	0.26 ± 0.14
10-50	0.87 ± 0.55

When the components of the pattern were inverted (Stiffer-in-softer), i.e. molds prepared with **PEG** 0% CL filled with **PEG** 10% CL, we expected to see fibroblast adhesion on the filled lines. Nonetheless, the fibroblasts adhered mainly on the mold lines.

The migration behavior was consistent with our previous observations; on 20 µm lines, oriented migration with some degree of lateral displacement was observed (Figure 4.12a). On 25-50 µm lines the cells exhibited random migration (Figure 4.12b and d). Due to the absence of a noticeable topography, cells were able to migrate into nearby stripes when the separation was in the order of the cell size or smaller. Interestingly, fibroblasts migrating on narrow lines (10 µm) showed a low degree of orientation (Figure 4.12c). In our opinion, the separation between attractive lines was reduced enough to allow line-crossing. This may explain the observed perpendicular track as well as the random one (green and blue tracks in Figure 4.12c respectively). This result supported our hypothesis of enhancement of perpendicular migration by using narrow attractive lines with reduced spacing. On the other hand, the blue track in Figure 4.12c pointed out that this kind of pattern may also induce random migration due to the absence of triggers for straight displacement.

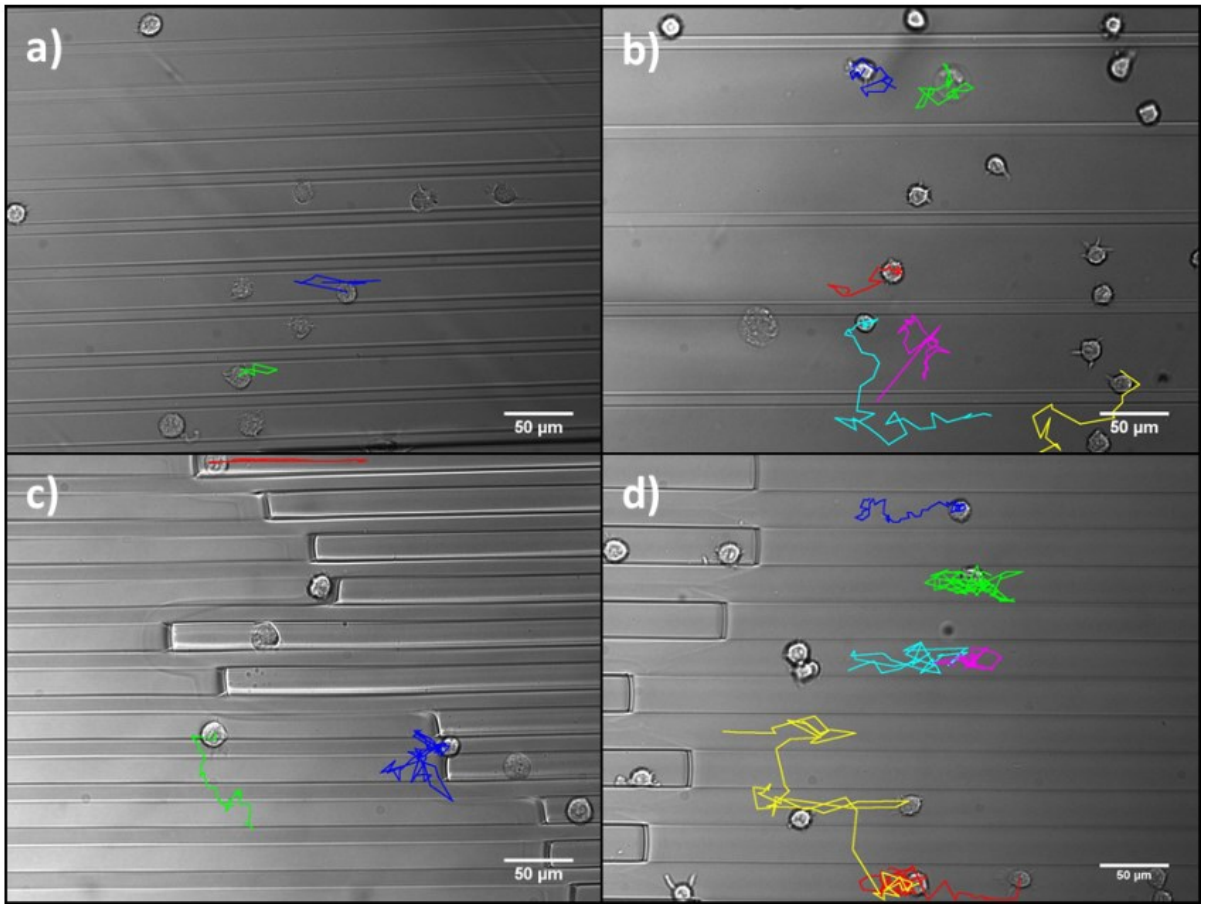

Figure 4.12: Migration tracks of fibroblasts moving on elastically patterned PEG samples (stiffer-in-softer FIMIC samples) with dimensions: a) 10-20, b) 10-50, c) 20-10 and d) 25-25.

Another interesting finding can be seen in Figure 4.12d. In this case, the size of the attractive lines was broad enough to allow random migration inside them, but at the same time, the spacing restricted the line-crossing phenomenon. As a result, the migration of the cells was geometrically restricted only by means of a mechanical pattern.

Table 4.4 summarizes the migration speed on the different pattern dimensions.

Table 4.4: Average migration speed on elastically patterned PEG samples (stiffer-in-softer FIMIC samples) with different dimensions.

Pattern dimensions (filler-mold) (µm)	Average migration speed (µm/min)
10-20	0.66 ± 0.23
10-50	0.32 ± 0.13
20-10	0.45 ± 0.16
25-25	0.62 ± 0.38

To summarize this part, the migratory behavior of fibroblasts on elastically patterned **PEG** substrates showed similarities with the observations on topographically patterned samples; cells adhering on lines with dimensions close to the cell size migrated mainly parallel to the pattern. In those cases where the separation between attractive stripes was reduced, the fibroblasts were able to bridge over those lines and, as a result, move perpendicularly to the pattern. Increasing pattern dimensions led to increasing randomness of the migration tracks. It is interesting to remark that, despite the absence of physical walls on the surface (topography much lower than the cell size), when the dimensions of the less attractive lines were larger than 25 µm, the migration was geometrically restricted and almost no line crossing was detected.

The measured migration speeds on the different substrates were statistically similar, although migration on softer mold lines was faster than on stiffer ones. This observation agreed with the theory of reduction of the migration speed on materials where the cells showed stronger adhesions (see Chapter 1).

Maybe the most intriguing observation extracted from the experimentation on elastic patterned **PEG** substrates was the preference of the cell to adhere and migrate on the mold lines, regardless their relative stiffness (the only exception to this situation was the softer-in-stiffer 50-10 sample, where the fibroblasts adhered to the filler lines that were also softer, which was also unexpected). In order to elucidate the causes for such a phenomenon (that the cells preferred to adhere to and migrate onto the mold), we investigated the protein adsorption, namely Bovine Serum Albumin (BSA), on the FIMIC samples. However no remarkable differences were detected between the degree of protein absorption on the filler and the mold lines [126].

As a second attempt, the roughness of the two phases of the pattern was analyzed; since the mold was formed against a silicon master while the filler was in contact with a glass surface, it might be possible that they presented a different roughness, inherent to the molding material (i.e. silicon master). We measured the Root Mean Square (RMS) roughness of several FIMIC samples at different positions of mold and filler lines using AFM. The obtained values were **760 ± 240 pm** and **726 ± 355 pm** for mold and filler respectively. This difference was insignificant. At the same time, to the best of our knowledge, no influence of picometric topography on the cellular behavior has ever been addressed. We suggest that

cells cannot recognize the roughness differences between the pattern lines; therefore this did not explain the observed adhesion on the mold stripes.

Nevertheless, a plausible explanation can be found in the work of Park and colleagues [69]. They found out that fibroblasts cultured on substrates with a convex / concave topography tended to escape from the concave pits migrating to the convex hills. In our case, the **PEG** FIMIC samples also presented convex / concave-like topography. In dry state the convexity corresponded to the mold lines, while the filler lines had a concave geometry.

As previously reported by our group, FIMIC samples in swollen state may present two different topographies as a result of the different degree of cross-linking between the two materials (highly cross-linked networks incorporate less water in their structure than less tightly cross-linked ones) [28,66]: When the cross-linker composition in the Mold / Filler was 0% / 10% the mold swelled more than the filler, while when the composition was 10% / 0% the filler swelled more than the mold (Figure 4.13).

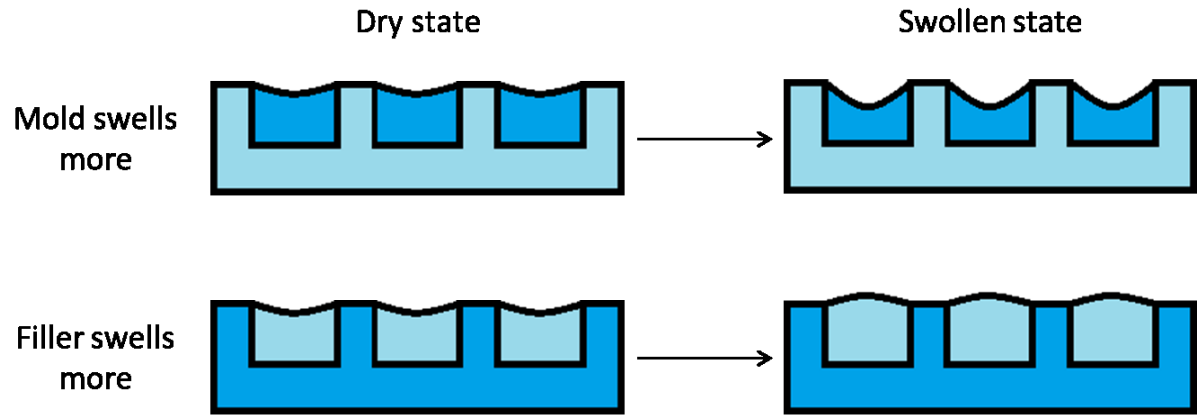

Figure 4.13: Schematic diagram outlining the topography that forms in the swollen state on FIMIC samples. Light blue represents softer materials (0% CL) and dark blue stiffer (10% CL).

For those cases where the filler swelled more than the mold (softer-in-stiffer), the cells migrated onto the mold lines (stiffer material) accordingly to the theory of durotaxis. When the mold swelled more (stiffer-in-softer), the cells migrated on the softer lines, which corresponded to the topographic hills of the sample, according to the statements of Park.

We suggest that a feasible explanation for this phenomenon can be found considering the dimensions of the topography. On stiffer-in-softer samples the topography observed in swollen state was increased when compared with that in dry state (from 200 nm to 1 µm.

Figure 4.14 left). The aspect ratio width/height of the hills, measured with AFM, was between 13:1 and 21:1. On softer-in-stiffer substrates, the original topography was levelled out and overtook, i.e. the topography was inverted and the channels stood out (Figure 4.14 right). The width/height ratios for these samples ranged between 30:1 and 42:1. The curvature on these samples was lower than on stiffer-in-softer ones (smaller ratios indicate higher topographies on shorter distances). We hypothesize that when the magnitude of the topography presented to the cells was elevated, the geometric effect ruled over the mechanical features and the cells migrated onto the hills of the surface. On the other hand, on reduced topographies, the cells migrated according to the mechanical pattern, overruling the geometric influence.

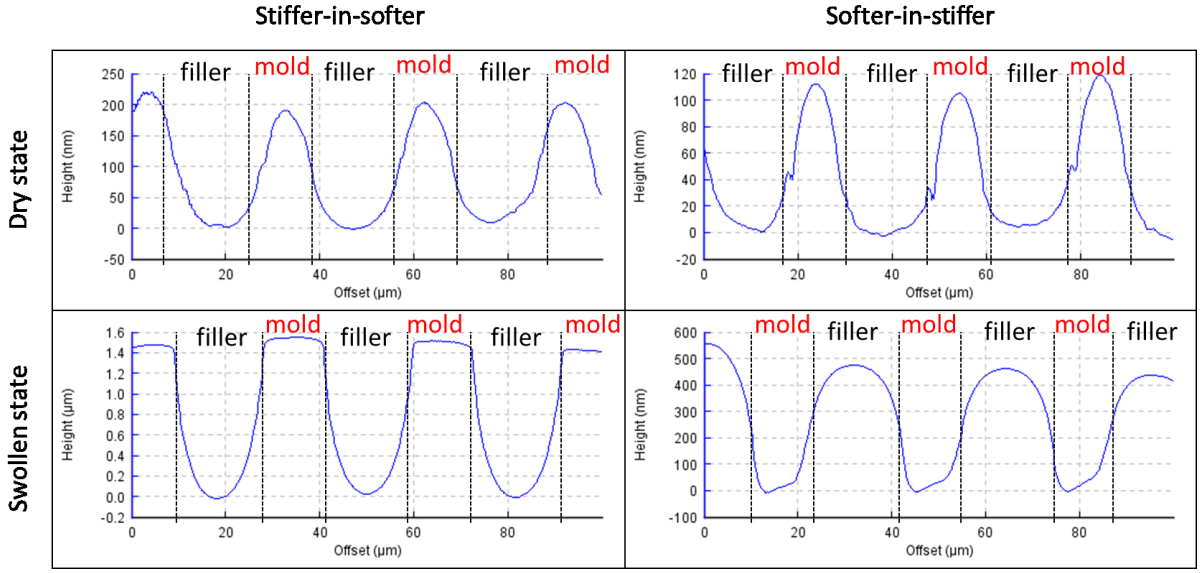

Figure 4.14: AFM topographic profiles of elastically patterned PEG samples with dimensions (filler-mold) 20-10. Left column: stiffer-in-softer samples (mold contains 0% CL and filler 10% CL). Right column: softer-in-stiffer samples (mold contains 10% CL and filler 0% CL). Upper row: Dry state. Lower row: Swollen state.

The topographic value acting as border between the geometric-controlled and the elastically-controlled zones could be extracted from the single exception to our hypothesis that was observed, namely a softer-in-stiffer sample with dimensions 50-10. In this case, topography of 600 nm along a distance of 18 µm, followed by a plateau was measured. The corresponding width/height ratio was 30:1, smaller than for the other samples of the same kind.

Summing up, we probed that cells were able to feel and respond not only to topographies with width / depth aspect ratios of 4:1 (Park's findings) but even smaller

features with ratios down to 30:1. At the same time, we demonstrated that this value (30:1) represents the border between the topographically and the elastically controlled migration; Topographic features below that value were ignored by the cells and their migration responded to the elastic pattern.

4.3.2.2 Elastically patterned substrates using PEG-based blends:

To confirm that the presence of topography was responsible for the observed discordances with the durotaxis theory, substrates lacking of such topography were required. As explained in Chapter 1, our group introduced the use of blends of PEG materials with the intention of reducing the topography present on the FIMIC samples. One of those blends was prepared mixing linear low molecular weight PEG with 8-armed PEG pre-polymer (**Blend1**). Unfortunately, these samples showed very low adhesiveness, as may be expected for pure PEG substrates. Hardly any cells were adhering on the substrates and, consequently, no migration was observed.

Polymers prepared with **PEG** and **3BC** in a blend ratio 33:66 (**Blend2**) were also previously investigated [28]. This material was less cell repellent due to the hydrophobic PPG component and, at the same time, was suitable to successfully decrease the topography inherent to the FIMIC samples. Therefore, we analyzed the migration of fibroblasts on elastically patterned samples prepared with **Blend2**.

Figure 4.15 shows the results of the migration experiments of fibroblasts on elastically patterned samples of **Blend2**. As it happened in the previous case (**PEG** in **PEG** substrates), cells adhered on the mold lines. The samples were analyzed with AFM after cell experiments and in swollen state, showing that the combination softer-in-stiffer (in other words, filler-swells-more) led to a complete levelling out of the topography present in dry state (Figure 4.16a). The absence of a topographic profile made way to the elastic pattern to control the migration. As expected, in all cases the fibroblasts adhered to the stiffer mold lines, containing 5% CL.

The samples prepared with the more-swelling material as mold (stiffer-in-softer) presented elevated topographies (in the micro-metric range) (Figure 4.16b). The width/height aspect ratio of these topographies ranged between 10:1 and 25:1. According

to our hypothesis, in such cases the geometric cues may overrule the elastic pattern and take control of the migratory behavior when the cells encounter hills with aspect ratios below 30:1 (see previous section). Confirming our hypothesis, the fibroblasts adhered to the softer mold lines, which corresponded to elevations on the surface of the stiffer-in-softer alias mold-swells-more substrates.

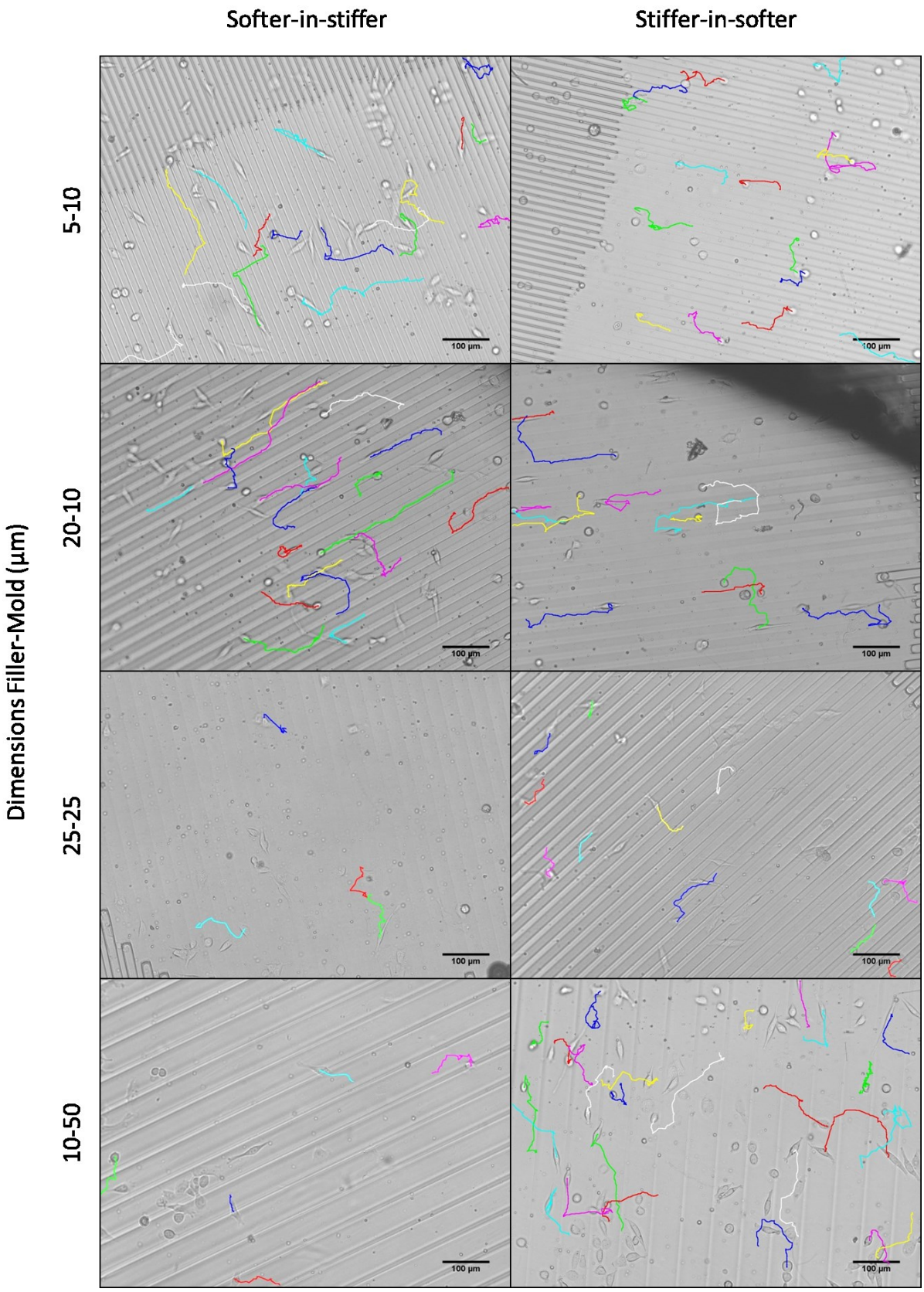

Figure 4.15: Migration tracks of fibroblasts moving on elastically patterned Blend samples. Left column: softer-in-stiffer samples (mold contains 5% CL and filler 0% CL). Right column: stiffer-in-softer samples (mold contains 0% CL and filler 5% CL).

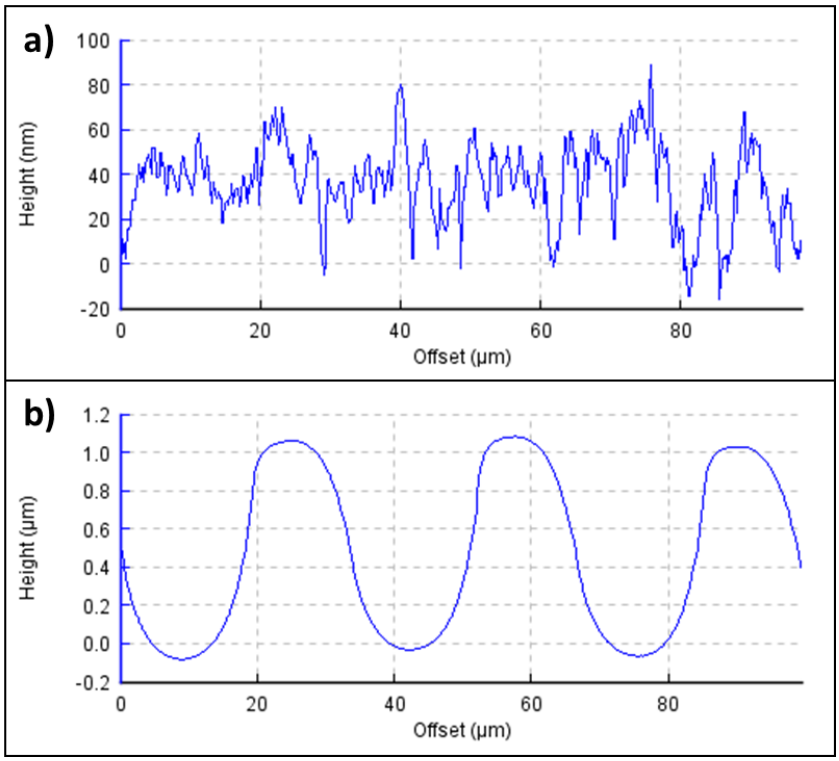

Figure 4.16: AFM topographic profiles of elastically patterned Blend samples in swollen state: a) Softer-in-stiffer FIMIC samples with dimensions (filler-mold) 5-10 and b) Stiffer-in-softer FIMIC samples with dimensions (filler-mold) 20-10.

Some differences were observed between the migratory behavior on elastically patterned substrates using either **PEG** or **Blend2** materials. **Blend2** polymers were more adherent than pure **PEG** ones and the fibroblasts adhered and spread much more on them, reaching cell sizes over 30 µm in the direction of the orientation. For this reason, while on elastically patterned **PEG** substrates with dimensions such as 10-20 or 25-25 the phenomenon of line-crossing was rare and a geometric confinement of the cells was manifest (Figure 4.10 and Figure 4.12d), on **Blend2** materials cells migrated more easily perpendicularly to the direction of the pattern. Owing to the larger spread cell size in this case, those dimensions (i.e. 20-25 µm) did not represent a significant restriction anymore to reach the adjacent lines.

As expected from previously presented results (see Section 4.3.2.1), cells migrated mainly randomly on wider lines (over 25 µm). No correlation to the direction of the pattern was detected and the tracks had low persistence values with continuous changes of direction.

On narrower, more attractive lines, we observed differences depending on the separation between those lines. Fibroblasts migrated in a more pattern-oriented manner on

samples with spacing in the order of 20 µm (Figure 4.17). Cells spread on the 10 µm lines and oriented their bodies to the direction of the pattern. During migration, the cells sat on top of the lines and, due to the high degree of spreading (long cells in the orientation axis but short in the perpendicular axis) and the separation between lines (namely 20 µm), did not contact the adjacent attractive ones. Nevertheless, perpendicular migration was also observed, to a lesser extent, on cells which stopped their movement and spread, without any notable polarization, reaching the nearby stripes over the 20 µm separation.

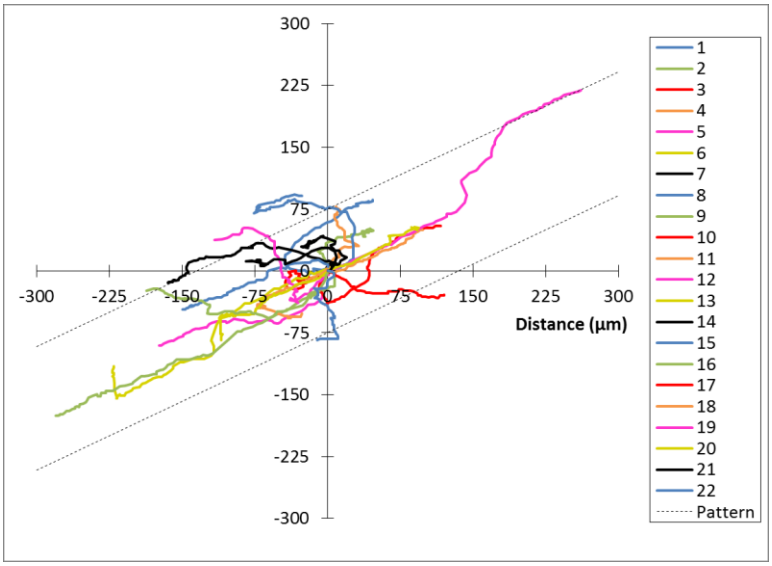

Figure 4.17: Windrose representation of the migration tracks of 22 cells on an elastically patterned Blend2 sample softer-in-stiffer with dimensions 20-10.

When the separation between more attractive lines was reduced (5 µm) a certain degree of alignment to the pattern was recorded but the separation was easily bridged and the cells presented a kind of zebra-crossing behavior, migrating perpendicularly to the pattern (Figure 4.18). This finding corroborated our hypothesis; perpendicular migration is enhanced by using narrow attractive stripes with reduced separation. On the other hand, in some cases, the cells migrated on 5-10 samples on two adjacent mold lines and this migration followed the pattern as if they were on one broader line.

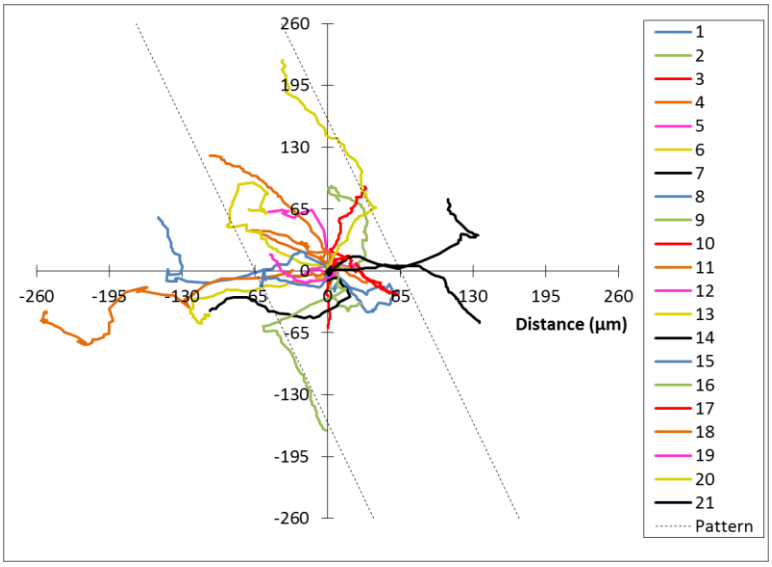

Figure 4.18: Windrose representation of the migration tracks of 21 cells on an elastically patterned Blend2 sample softer-in-stiffer with dimensions 5-10.

No significant difference was detected when relating the migration speed to the dimensions or the composition of the pattern (Table 4.5). Neither was a significant difference between the speed of parallel and perpendicular steps observed. These speeds, in spite of being close to those obtained on **PEG** FIMIC samples, were slightly lower than in the previous case. This may be due to the content of **3BC** in the **Blend2**, which increases the adhesiveness of the material and, consequently, the strength of the cellular adhesions.

Table 4.5: Average migration speed on elastically patterned Blend2 samples with different dimensions.

Pattern dimensions (filler-mold) (µm)	Average migration speed (µm/min)
5-10	0.33 ± 0.13
20-10	0.38 ± 0.12
25-25	0.43 ± 0.13
10-50	0.32 ± 0.10

To summarize the results from this set of experiments, the cell migration on elastically patterned **Blend2** hydrogels confirmed the previously observed trends (Figure 4.19): random migration occurred on wide channels while orientation occurred on narrower. Because of the high spreading degree of the fibroblasts on these materials, larger separations (at least 50 µm) were required to geometrically confine the tracks to one line (no line-crossing). On the other hand, we confirmed that small spacing in the pattern, combined with narrow stripes, increased the amount of tracks perpendicular to the pattern.

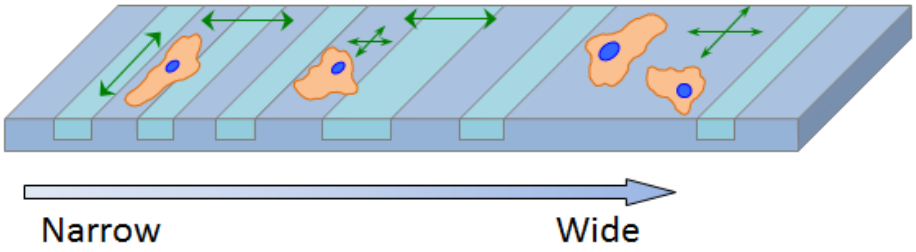

Figure 4.19: Schematic representation of the migratory behavior on elastically patterned substrates with increasing line width.

4.3.3 Cell migration on chemically patterned samples:

As indicated in Chapter 1, the FIMIC method is not only useful to generate elastic patterns, but also chemical ones. This is interesting because the majority of the research in the field of haptotaxis was done using gradients instead of clearly defined patterns, as we used here.

We prepared chemical patterns using **PEG** molds and filled them with **3BC**. We expected cell adhesion on the filled lines, since the **3BC** is less cell repellent due to the content of PPG. We varied the dimensions of the pattern, namely the width and separation of the filled channels to investigate the effect on the migration of fibroblasts.

When adherent lines of **3BC**, with sizes of 10 µm, were used in combination with anti-adhesive **PEG** lines of 20 µm in width, fibroblasts adhered as expected on the **3BC** lines (Figure 4.20).

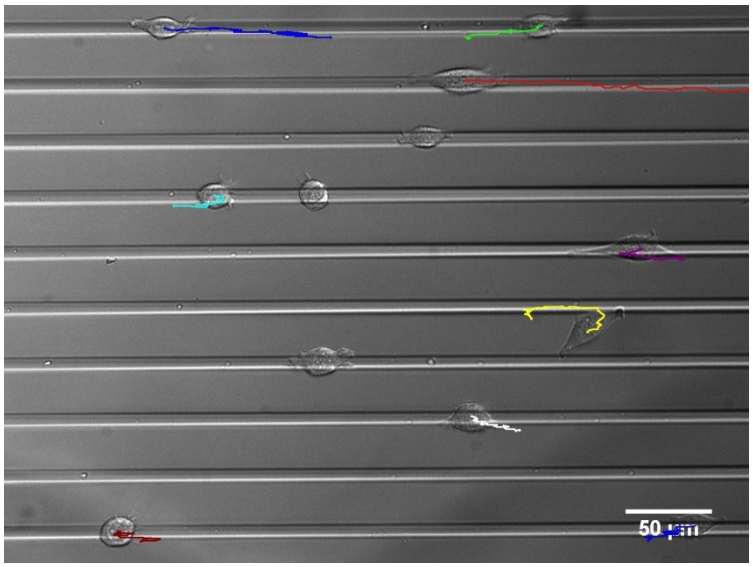

Figure 4.20: Migration tracks of fibroblasts moving on a chemically patterned sample Filler-Mold: 3BC-PEG with dimensions 10-20.

Cell migration was clearly influenced by the presence of the pattern (Figure 4.21). The cells adhered and spread along the **3BC** lines and the tracks followed the direction of the pattern. The persistence of the cells and the sinuosity of the tracks in the experiment represented by Figure 4.20 showed a persistent and straight migration. However, repetitions under similar conditions showed low degrees of persistence with frequent turns backwards. For this reason, the observations were not conclusive enough to assess an improvement in the control of forward migration.

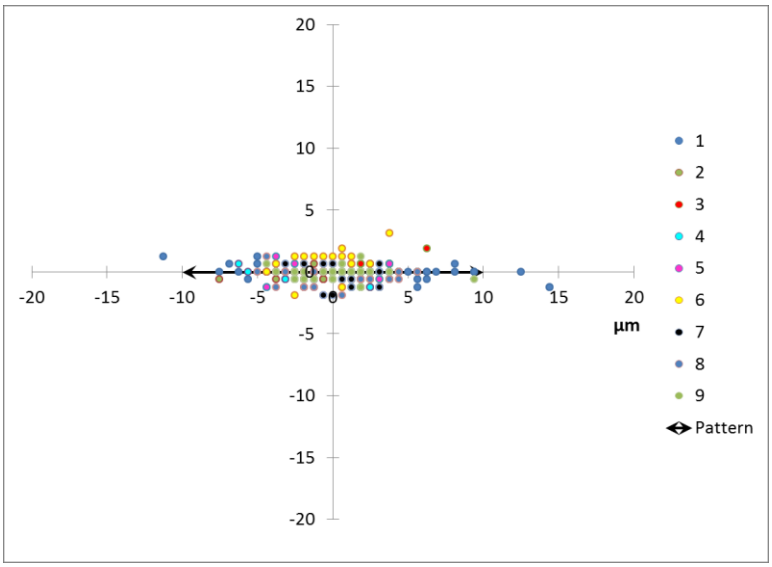

Figure 4.21: Correlation step length / step angle of cell tracks 1 to 9 on a chemically patterned sample Filler-Mold: 3BC-PEG with dimensions 10-20

Cells on these samples migrated with an average speed of **0.11 ± 0.07 µm/min**.

As observed on elastically and topographically patterned substrates, when the size of the pattern exceeded the size of the cell, the migration tracks became less oriented (Figure 4.22). In the case of 20 µm wide filled lines, cells migrated with a higher degree of orientation. Nevertheless, while on structured samples the effect of line-crossing was limited by the presence of the channel walls on FIMIC samples this restriction was not present. Line-crossing was a commonly observed phenomenon, especially when the width of the **PEG** stripes was small enough to allow line bridging; cells attached on two adjacent **3BC** lines by spreading over the intermediate **PEG** zone (Figure 4.23).

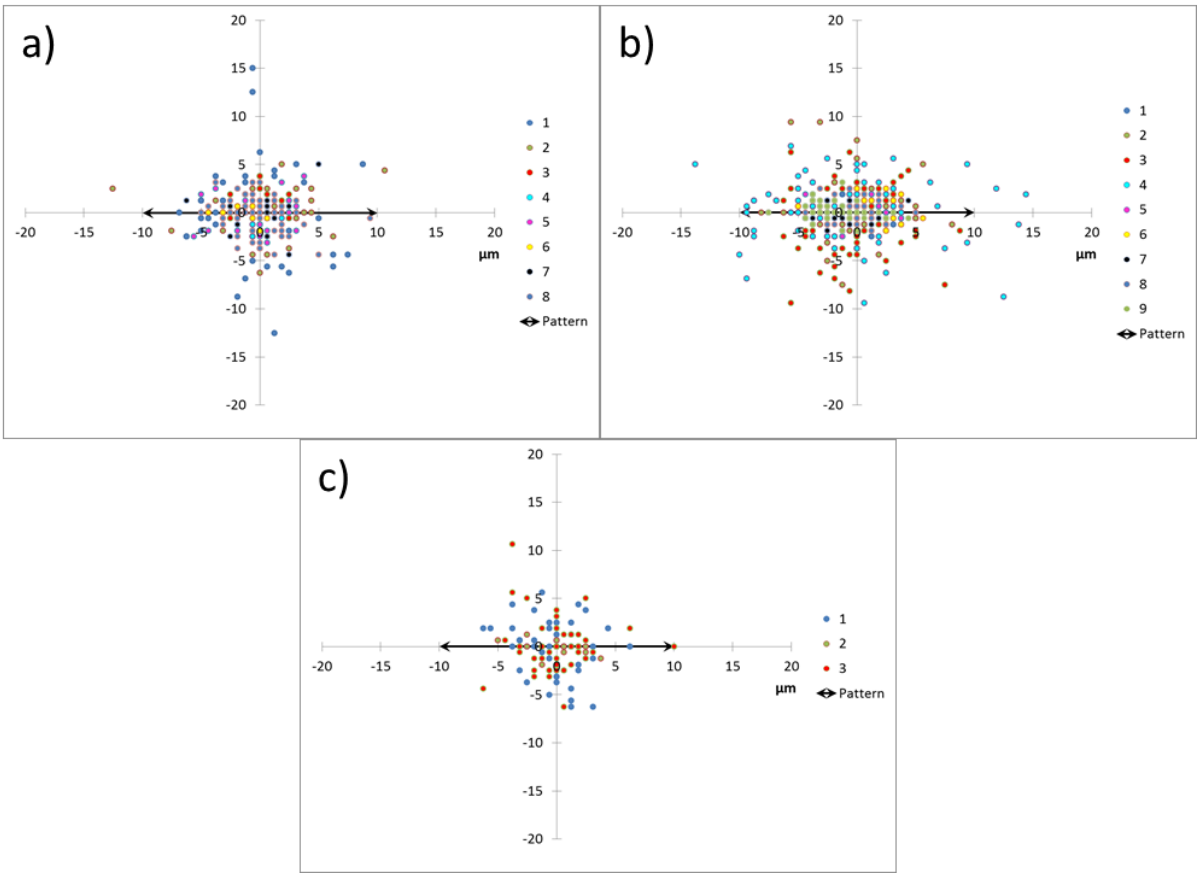

Figure 4.22: Correlation step length / step angle of cell tracks on a chemically patterned sample Filler-Mold: 3BC-PEG with dimensions: a) 20-10, b) 25-25 and c) 50-10.

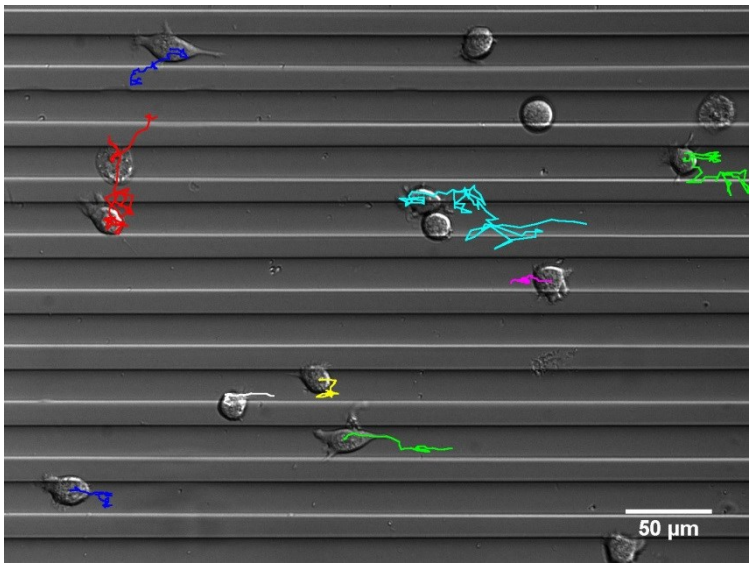

Figure 4.23: Migration tracks of fibroblasts moving on a chemically patterned sample Filler-Mold: 3BC-PEG with dimensions 20-10.

The migration speeds on 20 µm, 25 µm and 50 µm wide 3BC lines were **0.19 ± 0.15 µm/min**, **0.11 ± 0.09 µm/min** and **0.13 ± 0.07 µm/min** respectively.

Regarding the migration speed, no correlation with the dimensions of the pattern was detected. In all cases, cells migrated at a speed around **0.15µm/min**. These speeds were distinctly lower than those observed on fibroblasts migrating on topographically patterned **PEG** samples as well as on elastically patterned **PEG** and **Blend2** hydrogels. This is an expected phenomenon if we consider that the fibroblasts adhered more strongly on **3BC** than on **PEG** or **Blend2**.

Only patterns containing narrow lines of adhesive material directed cell migration in a satisfactory way. Migration parallel to the pattern was achieved by using narrow lines separated with wide anti-adhesive **PEG** stripes (Figure 4.24). Our results were inconclusive regarding the adequate dimensions to induce perpendicular migration. However, we suggest that in using adherent stripes of dimensions much below the cell size in combination with near adjacent lines, it may be possible to induce line-crossing; cell can adhere to two or even more lines at the same time. This is also true in the case of chemical patterns. The heterogeneities in the perpendicular direction may result in this direction becoming a more attractive option than the homogeneous parallel movement.

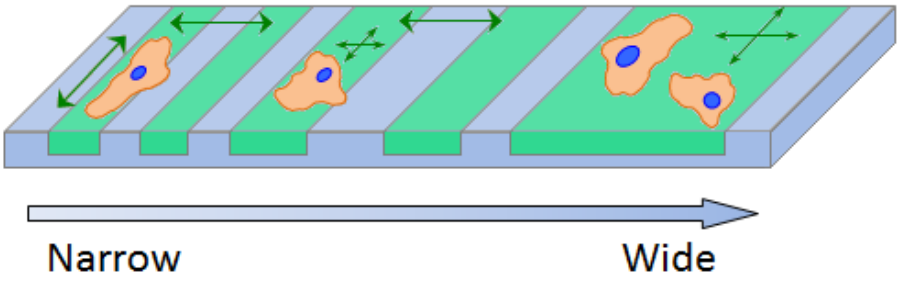

Figure 4.24: Schematic representation of the migratory behavior on chemically patterned substrates with increasing line width.

4.4 Conclusions

We analyzed the migratory behavior of mouse fibroblasts on PEG-based hydrogels containing topographic, elastic and chemical patterns. We confirmed that the presence of topographic and mechanical patterns on anti-adhesive pure PEG did not only induce adhesion of fibroblasts, but also migration. As expected, cells did not show a high degree of spreading on such materials. This was indicative for weak adhesions; however, they were strong enough to support active migration.

We observed than in all cases (topographic, mechanical and chemical patterns) cells migrated randomly on wide features (channels or smooth lines), while the alignment to the pattern direction increased at decreasing sizes of those features. When cells adhered on narrow stripes (in the order of 10 µm) and those lines were separated by a small distance, the probability of line-crossing increased and more cell migration tracks perpendicular to the pattern were observed.

On mechanical patterns prepared with **Blend2** and chemical patterns with **3BC** cells adhered and spread more. This was reflected in lower migration speeds, as a result of stronger adhesions, and in a modification of the dimensions necessary to geometrically constrain the migration parallel to the pattern, due to the larger cell size compared to cells on **PEG**.

Notably our investigation on the effect of mechanical patterns on cell migration brought interesting new results and insights. Fibroblasts responded to geometric cues when they encountered a convex / concave pattern, migrating on the hills of the topography, thereby surprisingly ignoring the mechanical pattern. Nevertheless, when smaller curvatures were measured (below a width/height aspect ratio of 30:1), the fibroblasts responded to the elastic patterns, showing the expected durotactic behavior. This was confirmed by the use of **Blend2** substrates where the filler swelled more than the mold material. In these cases the topography was completely removed by the difference in the swelling degree of both components and the cells faithfully migrated on the stiffer stripes of the samples, as they were expected to do.

This is a significant finding, since no investigation has been done to elucidate the hierarchy of predominance between mechanical and topographical cues, contrary to chemical and topographical ones. Our results can be the starting point for understanding the simultaneous effect of the different migration triggers. At the same time, based on these results, new tailored biomaterials can be synthetized with more precise control of the cellular environment, for example, on a sample containing mechanical patterns, the trigger for the migration can be switched from topography to elasticity by designing the topography of the different areas.

Chapter 5:

Fabrication of embedded patterns of elasticity

5.1 Introduction:

In the human body, each type of cell is surrounded by an environment with characteristic mechanical properties; brain has elastic modules in the order of 1 kPa, while bone tissue reaches values around 15 GPa [127]. The elastic properties of the environment influence numerous cellular processes such as contraction [98], proliferation [128], apoptosis [31] or migration [15]. Even differentiation of stem cells can be directed by the elasticity of the culture substrate [30]. As previously seen in Chapter 1, cells explore their environment through their focal adhesions, test the elastic properties of their surroundings and react accordingly to their interpretation of the mechanical signals. Unlike topographic and chemical cues, elastic cues do not have to be in direct contact with cells; inclusions under the surface of the substrate can modify the elastic properties detected by the cell without the necessity of direct contact. However, evidently, there is a limit to this detecting mechanism. Unlike Andersen's tale, cells are not princesses and cannot feel a pea under infinite mattresses. So, what is the limit to cellular deep-sensing? Many researchers have been working in the last decade in order to answer this question [111].

Deep-sensing is based in the propagation of deformations. Cells anchored to the substrate exert tensile forces on it and cause a deformation or displacement on the surface of the material (Figure 5.1). This deformation will propagate into the medium according to the Boussinesq solution for a semi-infinite substrate [129] (Figure 5.1a). When this propagation finds a second material, it will be modified due to the different mechanical properties of the second material (Figure 5.1b). The deformation generated by the cell on a substrate with an underlying second material will differ from that of the pure substrate; hence, the cell will migrate differently [130].

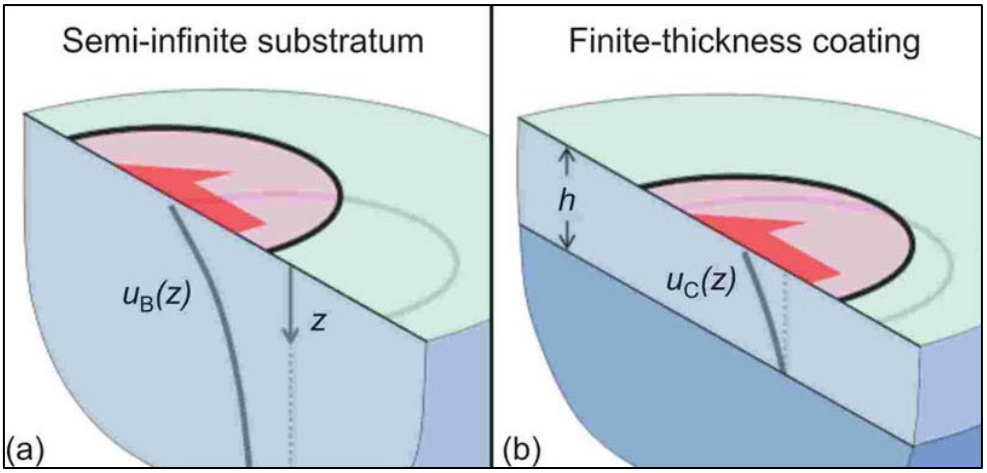

Figure 5.1: Schematic representation of the deformation cause by an adherent cell on the surface of a) a semi-infinite substrate, b) a coating of thickness h on a rigid substrate. U represents the evolution of the displacement with the distance from the origin of the deformation. Image printed with permission of the author [130]**.**

On an elastic and homogeneous material, the deformation decays inversely to the distance from the deformation source [79]. This means that at a determined depth, the deformation will be negligible and changes in the elastic properties of the material will have no further effect on it. This depth or film thickness can be defined as "critical thickness" (h_c) [130] and it is the clue to determine the scope of deep-sensing. To illustrate this concept, we can use as example the paper of Discher and co-workers, where mesenchymal stem cells (MSCs) showed greater cell spreading when cultured on thin films of polyacrylamide than on thicker ones [30]. The explanation is that MSCs on thinner substrates do not feel the original elasticity of the material (5 kPa) but this elasticity is altered by the underlying hard glass slide. Cells are therefore detecting a hybrid material, i.e. a combination of glass and polyacrylamide. On the other hand, the thickness of the thicker samples was greater than the critical thickness and, consequently, MSC behaved as though they were responding to the bulk substrate with Young's modulus (E) of 5 kPa.

Accordingly to the Boussinesq solution, the displacement is not only a function of the substrate thickness, but also of the size of the deformation area; i.e. the radius, in the case of circular deformations. Consequently, the critical thickness is related to the radius of the deformation; for large deformations, the critical thickness will be greater. There is no unanimously accepted value for the level of the deformation; some authors consider that the deformation is distributed over the whole cell; hence, h_c can vary from tens of microns

to hundred micrometers for large cells [131–133]. The mathematic model suggested by Sen and co-workers agrees with this hypothesis [134].

Other authors believe that the deformation is locally generated by the focal adhesions [135] and since they have typical sizes of 1 µm [130] the critical thickness has to be in the order of several micrometers. This theory is supported by mathematic models such as those of Maloney [130] and Merkel [79]. Experimental observations are more generous with the range of deep-sensing; Engler, Cortese and Degand tested films with thicknesses under 10 µm, reporting different cell behavior to that on thicker materials [62,118,136]. According to Maskarinec the deformation generated by a cell could be detected even at 20 µm under the surface [137]. Similar results are presented by Buxboim and Kuo, reporting cell recognition of stiffer structures underlying between 10 µm and 20 µm [117,138].

Some authors report that there is not only an upper limit for deep-sensing, but also a minimum thickness for the cell to recognize the properties of the film [38,134]. This minimal thickness has to be at least as large as the size of the deformation and, because the smallest deformations are caused by focal adhesions, this thickness is in the order of 1 µm.

Such heterogeneity in the results of the critical thickness can be explained by i) the different calculation method, i.e. mathematical estimations and empirical results, ii) the different elastic properties of the material employed and iii) the exerted force on the substrate [111]. In the case of mathematic models the magnitude of the force generating the deformation will depend on the selected parameter, while for the experimental results will depend on the cell line.

Experimentally, the modification of the elastic properties of a material due to harder inclusions underlying the surface can be measured by techniques such as Atomic Force Microscopy (AFM), using the force-spectroscopy mode. This technique generates force/distance curves at the measured points by deforming the surface with the tip (Figure 5.2). To obtain force/distance curves, the tip approaches the sample (point 1). Then the tip is attracted by the surface and feels a pulling force without changing the position (point 2). The AFM generates a pushing force which indents the surface (point 3). After indentation, the tip retracts and after passing the point 2, i.e. contact point, the still-attached surface pulls the tip, while it separates from the sample (point 4). The surface finally detaches and the force balance on the tip returns to zero (point 5). From these

curves, we can read the mechanical properties of the surface; the difference in the forces between the point 4 and 5 represents the adhesive force generated by the material (the greater this gap, the more adhesive the material). At the same time, the slope of the indentation gives an idea of the Young's modulus. Greater slopes mean more force is required to obtain the same deformation; hence stiffer materials.

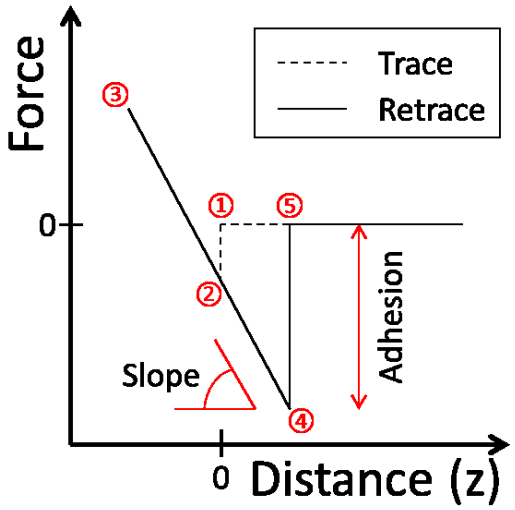

Figure 5.2: Scheme of a Force/Distance curve generated by force spectroscopy AFM. 1) Tip approach. 2) Contact. 3) Indentation. 4) Retraction. 5) Detachment.

Using indentation curves, Roduit and colleagues developed a method to analyze the elastic properties of a sample not only on the surface but also inside the bulk of the material [139]. The method is based on changes on the expected indentation curve, when the deformation reaches an area with an inclusion of another material (Figure 5.3).

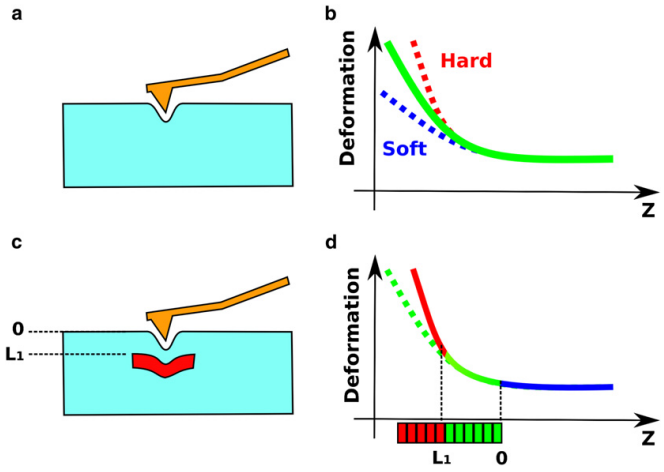

Figure 5.3: Representation of the indentation curve obtained on a material (a and b) and on the same material containing a harder inclusion (red rectangle) (c and d). Image printed with permission of the author [139]**.**

An important parameter to be considered during formation of thin films is the wetting behavior of the material. When a substrate is coated with a thin film of liquid two things may happen. The first is that the liquid can spread and cover the surface of the substrate. This process is called wetting and an example of this is water spreading on a clean glass surface. The second possibility is that after spreading, the liquid reassembles and recovers as a drop-like shape. In this case, it is said that the surface dewets as we observe with water drops on Teflon frying pans.

The wetting or dewetting of the surface depends on many factors, especially the affinity between the liquid and the substrate [140]. In the case of water, substrates with a high affinity for water are called hydrophilic, while those with a low affinity are hydrophobic materials.

When a drop of liquid is placed on the surface of a substrate three phases are present: the substrate, the coating and the environment (typically solid, liquid and air). The interaction between those phases can be represented by the surface tension (Υ_{SA}, Υ_{SL}, Υ_{LA}) and the three of them are related via the angle formed by the drop, namely the contact angle θ [141] (Figure 5.4) Measuring the contact angle between the liquid and substrate we already have an idea of the affinity between the materials.

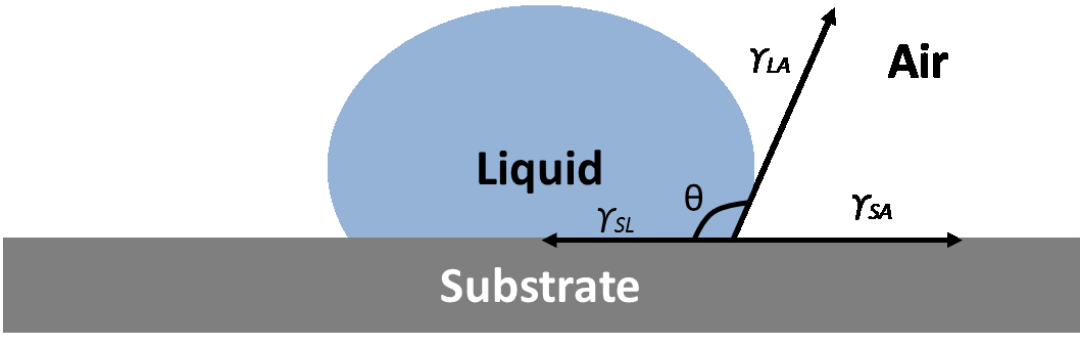

Figure 5.4: Representation of a drop on the surface of a substrate. ϒSA, ϒSL, ϒLA represent the surface tension of solid/air, solid/liquid and liquid/air respectively and θ the contact angle between liquid and solid.

However, the wettability is not only affected by the affinity between the materials. As already pointed out in Chapter 1, the presence of topography on the surface can completely alter the behavior of the substrate. This principle has been applied by Kim to change the surface properties of **PEG** from hydrophilic (contact angle ≈22.5°) to hydrophobic (contact angle ≈95°) by patterning the surface with nanopillars [21]. Consequently, the

wettability of a specific material may vary from flat substrates to structured ones, as well as among structured, depending on the characteristics of their topography.

Different strategies have been followed to generate embedded patterns of elasticity based on the coating of pre-existing stiff substrates such as glass structures [117] or spheres [117,118]. Other authors control the thickness of the coating material on a glass slide, generating a gradient of elasticity from thick coatings to thinner ones (softer to stiffer) [79,138]. Not only can glass be used as substrate, polymeric structures generated by soft lithographic methods have also been employed. Cortese and co-workers reported cellular recognition of an elastic pattern generated by covering a topographically patterned polymer with a film [62]. In their work, the elastic contrast was found between the polymer pillars and the empty niches in between.

Another possibility is to completely cover the topographically patterned hydrogels with a softer polymer ("blanket") (Figure 5.5). If the substrate originally contains channels, a line-like pattern will be obtained. The lines can be classified into two groups: Lines over former channels and lines over the hills of the mold. These lines can also be considered as thick or thin coatings on a stiff substrate respectively.

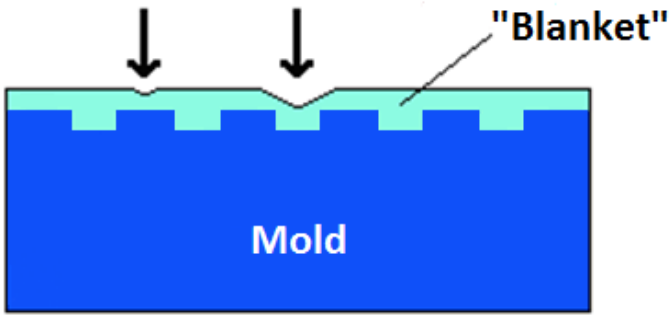

Figure 5.5: Representation of an embedded pattern of elasticity prepared by filling of a topographic substrate (dark blue) with a softer polymer (light blue).

On the other hand, **Fi**ll-**M**olding **I**n **C**apillaries (**FIMIC**) samples can already provide defined patterns of elasticity along the surface. However, to obtain this pattern, we may inadvertently also create a chemical pattern; even if the same materials were used for the mold and the filling; the different concentration of cross-linker on them could alter the chemistry of the surface. At the same time, FIMIC samples also present a topographic pattern with a typical size between 100 nm and 400 nm in dry state (see Chapter 1). When FIMIC samples are used as substrate for coating, the originally created pattern of elasticity

can be maintained and, at the same time, the blanket can be used to mask the nanometric topography while achieving homogeneous surface chemistry.

In this chapter we studied three techniques for coating of the substrate in a homogeneous and controllable manner.

Spin-Coating:

Spin-coating is a widely extended technique to create thin layers on smooth materials [118,142–144]. It uses the centrifugal forces to create homogeneous coatings on surfaces.

The main factors influencing the thickness of the layer are: spin speed (ω_{sp}), spin time (t_{sp}) and viscosity of the polymer [142,145]; the volume of the polymer has no influence on the process, provided that it is higher than a minimum value [142]. A high volume of polymer can be used to ensure homogeneity of the film, while the thickness can be adjusted with the other parameters.

Spin-coating has been applied to form PEG films [143,144], obtaining thickness ranging from hundreds of nanometers to several micrometers. Those films were prepared on flat surfaces such as glass or silicon while in the present work the film covered a pre-existing topography, i.e. the mold or the FIMIC substrate. A similar situation to the present work can be found in the literature, where Degand and colleagues successfully spin-coated PDMS on top of a glass surface covered with silica colloids of 500 nm diameter [118]. By controlling the dilution grade of the polymer into an organic solvent, they were able to reduce the thickness of the coating. This strategy could also be applied for our PEG coatings [144].

The use of spin-coating in our system can be challenging; the forces applied on the liquid affects its shape and it is known that the dissipation of forces on viscous materials requires longer time. Consequently, while spin-coating viscous materials accumulation on the side of the sample can be expected [118] and therefore the thickness of the blanket cannot be considered constant along the sample. To solve this issue, the samples were left to rest after spin-coating to form homogeneous films. On the other hand, the dewetting phenomenon also has to be taken into consideration. Long resting times may lead to dewetting and rupture of the film [140].

Another issue was the topography of the substrates; Spin-coating was originally developed to form thin films on smooth surfaces. To the best of our knowledge no studies have been done to completely fill substrates containing channel topography and to form at the same time a controlled film on top of it.

Razor-blade

To prepare samples by microtransfer molding (µTM) [78] (Figure 5.6), a topographic substrate is filled with a drop of a liquid polymer. In this method, one is only interested in the filled channels and the excess of material is removed by scraping of the surface with a block of PDMS. Nevertheless, Zhao and colleagues reported that after completing the process, a thin film (around 100 nm) remained connecting the channels.

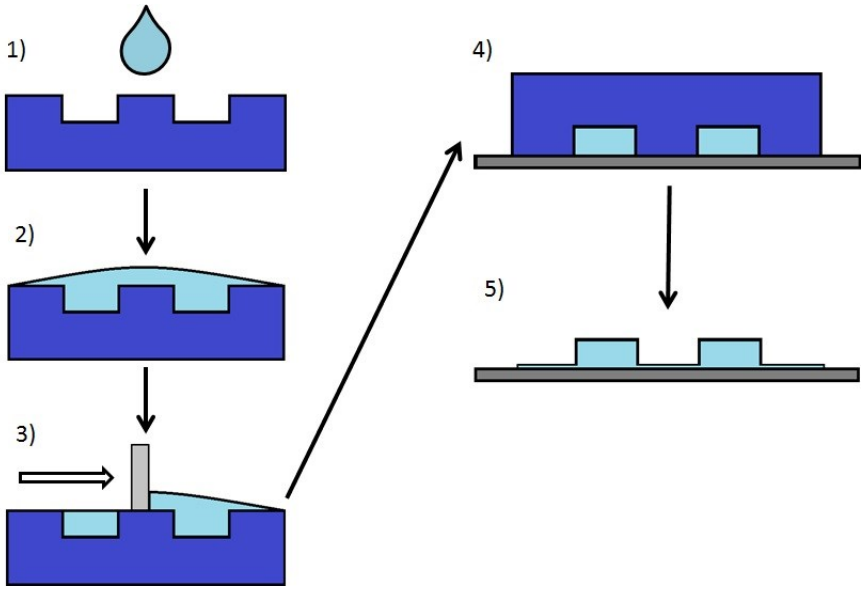

Figure 5.6: Schematic representation of the µTM method. 1, 2) Filling of the substrate, 3) Scrapping of the excess, 4) Placing on the support, 5) Removal of the substrate.

Thus, if the methodology of the µTM is followed but instead of peeling the mold away it is kept on its place, we obtain a sample with a structure embedded under a homogeneous blanket of 100 nm. Chou and colleagues used a similar method to generate patterns of elasticity with PDMS samples, but they do not report the presence of a thin coating film and their samples presented a topographic profile [113].

In the razor-blade method the wettability properties of filler and substrate also play a capital role in the formation of the thin film.

Sandwich method

After depositing a liquid pre-polymer on a topographic substrate, instead of removing the excess by scraping as in the case of the razor-blade method, a cover glass can be placed on top and pressed, in that way distributing the polymer inside the topographic features and along the surface. Eventually, the excess can be removed at the border of the sample (Figure 2.4).

This methodology has been already used to obtain thin films. In some cases, beads mixed with the liquid polymer were used to control the resulting thickness [79,130,136,138]. Some authors used the volume of the liquid polymer as parameter to control the thickness when thicker gels (greater than 5 µm) are desired [41,130,136].

We believe than the use of spheres as spacers introduces rigid inclusions under the surface and this modifies the mechanical properties detected by the cells; the cells do not respond to our line-like embedded pattern of elasticity, but to the homogeneously distributed inclusions. For this reason we used the pressing force, i.e. the load weight, as parameter to control the thickness, keeping constant the dispensed volume of blanket polymer that ensures complete coating of the substrate.

The aim of this chapter was the embedding of a pattern of elasticity under a chemically and topographically homogeneous (smooth) surface. Accordingly to the literature, we decided to create embedded patterns of elasticity under a blanket of thickness between 1 µm and 10 µm since these values are contained in every interval of cellular deep-sensing suggested by the different research groups. These samples allow the study of the effect of mechanical cues on cellular behavior in their own right; that is, without any possible interference of chemical or topographical cues. This is important to elucidate the mechanism of mechanotransduction that induces a cell response to the mechanical properties of their environment.

5.2 Materials and methods:

For these experiments, we employed two polymers, namely poly(ethylene glycol) (**PEG**) and a tri-block co-polymer PEG-b-PPG-b-PEG (**3BC**). Further description of these materials can be found in Chapter 2. Different concentrations of cross-linker (CL) were used; the percentage is indicated for each case. To avoid masking of the underlying elasticity, the blanket had to be prepared with the softer material (less CL).

Two different approaches were used for embedding the pattern of elasticity:

- Embedding of topographically patterned material ("molds"): First, molds were prepared by cast-molding as explained in Chapter 2. In this case, the blanket material filled the channels and covered the mold (Figure 5.7a). Only one assembling step was necessary; assembling of the upper layer to the mold. The advantage was that only one interface was present, i.e. between the mold and the blanket. This was important to avoid delamination (see Chapter 1). As previously described (see Chapter 2), on FIMIC samples the delamination was avoided by using short UV-curing times for the mold, leaving free acrylate groups to react with the filler polymer. This embedding strategy was similar to the preparation of FIMIC substrates in the sense that also only one contact surface was present and, consequently, the same solution could be applied.
- Embedding of FIMIC substrates: FIMIC samples were prepared as described in Chapter 2 and used as substrates. The blanket coated the surface of the FIMIC sample covering up any existing nanotopography (Figure 5.7b). In this case, we had two assembling steps; one between the filler and the mold (FIMIC) and another to attach the blanket to the substrate, hence three different materials can be used (i.e. for the mold, for the filler and for the blanket) In the simplest case, the blanket material can be the same as the one used for the filler or mold (the softest of them). However, a third formulation can be used, in this way, the materials used for the FIMIC could be selected to match the desired requirements of elasticity, in other words to generate the elastic pattern, and the blanket could be chosen regarding its cell-material interaction properties (keeping in mind that it must be softer than the underlying materials for not masking their elastic properties).

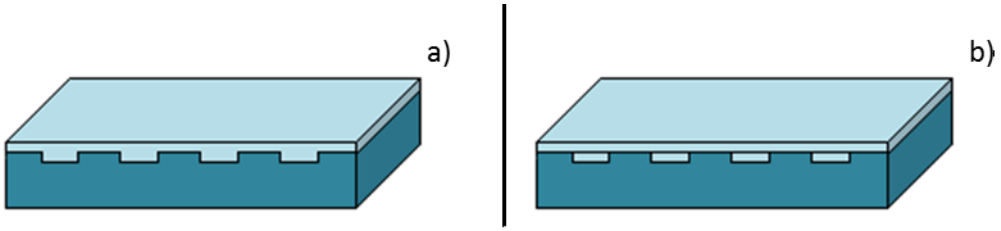

Figure 5.7: Sample with embedded pattern of elasticity: a) using a topographic sample as substrate, b) using a FIMIC sample as substrate.

5.2.1 Spin coating on topographically patterned substrates:

A pre-curing mix of **3BC** 10% CL was used to generate molds with size 10-20-10 after 8 minutes of UV-curing. Afterwards, 20 µL of **3BC** 0% CL was dropped on top of the substrates and spin-coated. The samples were left for rest (t_{rest}) before UV-curing. Some samples were left to rest before spin-coating to allow penetration of the filler inside the channels (t_{penetr}). A description of the process parameters can be found in Table 5.2.

5.2.2 Spin-coating on FIMIC samples:

For this section, FIMIC samples were prepared as indicated in Chapter 2, using **PEG** 0% CL (t_{UV} = 8 min) as mold (10-20-10) and **PEG** 10% CL (t_{UV} = 8 min) as filler. After 8 minutes, both, mold and filler, showed a solid structure. 10 µL of **3BC** 0% CL was used as coating material. The operating conditions are described in Table 5.3.

5.2.3 Razor-blade method:

The razor-blade method was tested on molds with dimensions 20-10-15 prepared with **PEG** 0% CL (t_{UV} = 5 minutes). FIMIC samples were also employed, using the same molds as in the previous case, i.e. **PEG** 0% CL, 20-10-15, t_{UV} = 5 minutes. The channels were filled with **3BC** containing 5% CL and the samples were UV-cured 15 additional minutes. Both types of samples, topographic and FIMIC, were covered with 2 µL of **3BC** 5% CL, used as blanket material. The excess was removed by a razor blade as indicated in Chapter 2.

5.2.4 Sandwich method:

Unlike other methods, this technique was applied only on mold substrates and not on FIMIC samples because of the difficulty to avoid delamination when FIMIC samples were used (no acrylate groups may remain to link with the acrylate in the blanketing material).

To analyze the homogeneity of the thickness of the substrate, molds 20-10-15 were prepared with 60 µL of **PEG** 0% CL with and without the help of a master holder (vide infra).

For the study of the influence of the load on the thickness of the blanket, molds 20-10-15 were prepared with **PEG** 0% CL and UV-cured for 5 minutes. The substrates were covered with 20 µL of blanket material (**3BC** 5% CL) and compressed between two glass slides. The combined samples, mold + blanket, were then UV-cured for 30 minutes. Five different loads were applied to the sample during UV-curing (Table 5.1)

Table 5.1: Loads applied to sandwich samples for controlling the thickness of the blanket. The glass vials were filled with distilled water and closed.

Load	Weight (g)
Cover slide	≈ 0
Microscope slide	4.80
Microscope slide + Empty glass vial	23.33
Microscope slide + Half-filled glass vial	36.60
Microscope slide + Filled glass vial	51.60

Cross-section measurements (transmission and fluorescence images) were performed using an optical microscope as described in Chapter 2. For the fluorescence images, the filler was mixed with FITC-dextran with a final concentration of 0.2 mg/mL. AFM images were obtained in contact mode using the equipment referred to in Chapter 2. The samples were analyzed in a dry state.

5.3 Results and discussion

5.3.1 Spin-coating

5.3.1.1 Spin-coating on topographically patterned substrates:

3BC is more attractive as blanket material when compared with **PEG** since a smooth film of **3BC** allows cell adhesion. In addition, it is easier to detect an underlying pattern of elasticity on **3BC** as it is softer than **PEG**. **3BC** substrates were also investigated in order to form embedded patterns of elasticity via spin-coating. We prepared molds 10-20-10 with **3BC** 10% CL, covered them with **3BC** 0% CL and spin-coated as described in Table 5.2. Experiments containing two spin-coating speeds and times corresponded to a two-step processes; the substrate was spin-coated at a determined speed (ω_{sp}) during the first period. Afterwards, the speed was modified and kept at the same value during the second period.

Table 5.2: Operating conditions for the spin-coating on 3BC molds.

Sample	t_{penetr} (h)	ω_{sp} (rpm)	t_{sp} (min)	Repetition spin-coating	t_{rest} (h)	t_{UV} (h)
SP_{mold1}	0	2000 + 4500	1 + 9	Yes	16	1
SP_{mold2}	0	4000 + 3180	1.5 + 5	Yes	16	1
SP_{mold3}	16	4500	5	No	0	2
SP_{mold4}	3	2100 + 1440	2 + 30	No	16	2
SP_{mold5}	21	360	30	Yes	2	2

In the first two cases (i.e. SP_{mold1} and SP_{mold2}) the blanketing material was deposited at the center of the substrate and spin-coated. SP_{mold1} was first spin-coated slower to distribute the polymer and then the speed was increased, aiming to obtain a thin layer. SPmold2 was spin-coated faster with the intention of forming first a thin layer and then the speed was reduced, expecting to homogenize the layer.

Even though the surface was completely covered by the drop prior to spin-coating (image not shown), after spin-coating some areas stayed uncovered. This could be already observed by eye (Figure 5.8 upper row). Both strategies, slower/faster and faster/slower,

led to similar results, namely uncoated regions. After overnight resting, the liquid coating material disappeared from the surface and presumably entered the channels. The rainbow observed on the surface of the samples (Figure 5.8 lower row) was indicative of the presence of structures which modified the refraction of the light. AFM measurements confirmed that the topography was in the range of several micrometers (image not shown).

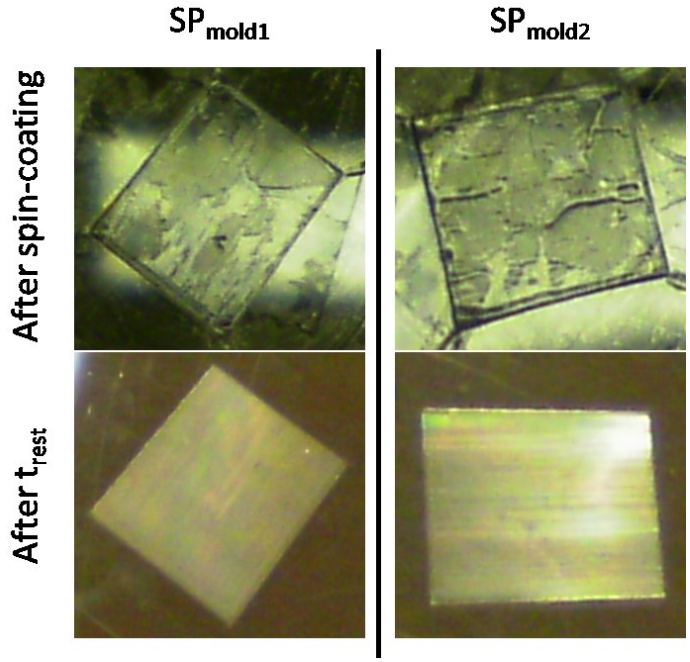

Figure 5.8: Images of spin-coated samples SP_{mold1} and SP_{mold2} after spin-coating and after overnight rest.

The presence of empty channels after spin-coating induced us to think that the high speeds used did not allow the blanketing material to penetrate the structures of the substrate. For this reason, the drop of blanketing material was allowed to penetrate the channels before spin-coating (t_{penetr}). The spin speed was varied from fast (4000 rpm) to middle (around 2000 rpm) and to slow (360 rpm) for the samples SP_{mold3}, SP_{mold4} and SP_{mold5} respectively.

First, it was investigated if the use of high speeds was adequate to form a thin film on a previously coated substrate (SP_{mold3}). The substrate was UV-cured right after spin-coating (Figure 5.9 left column).The heterogeneities in the coating were detectable by eye; regions were the lines of the topography were still visible alternated with regions coated with a film.

For the sample SP_{mold4} lower spin speeds were used (2100 rpm and 1440 rpm). It was expected that slower rotations would reduce the amount of removed blanketing polymer and form continuous coatings on the substrate. Eye observations suggested that the spin

speed was still too high and removed too much coating polymer (Figure 5.9 middle column). After overnight resting, most of the liquid polymer disappeared from the surface. The resulting sample presented a topographical pattern, which can be recognized by the rainbow formed on the surface.

Finally, it was decided to reduce the spin speed to the lowest value affordable by our equipment. It can be seen that slower spin-coating led to a larger fraction of the surface coated with the liquid polymer (Figure 5.9 right column). Nevertheless, the coating was still not complete. The sample was left in rest overnight and UV-cured. Structures on the surface were again observed. These structures, and those from samples SP_{mold4}, were analyzed with AFM and the results indicated that they were larger (more than 3 µm) than those expectable on filled channels (i.e. in the order of nanometers).

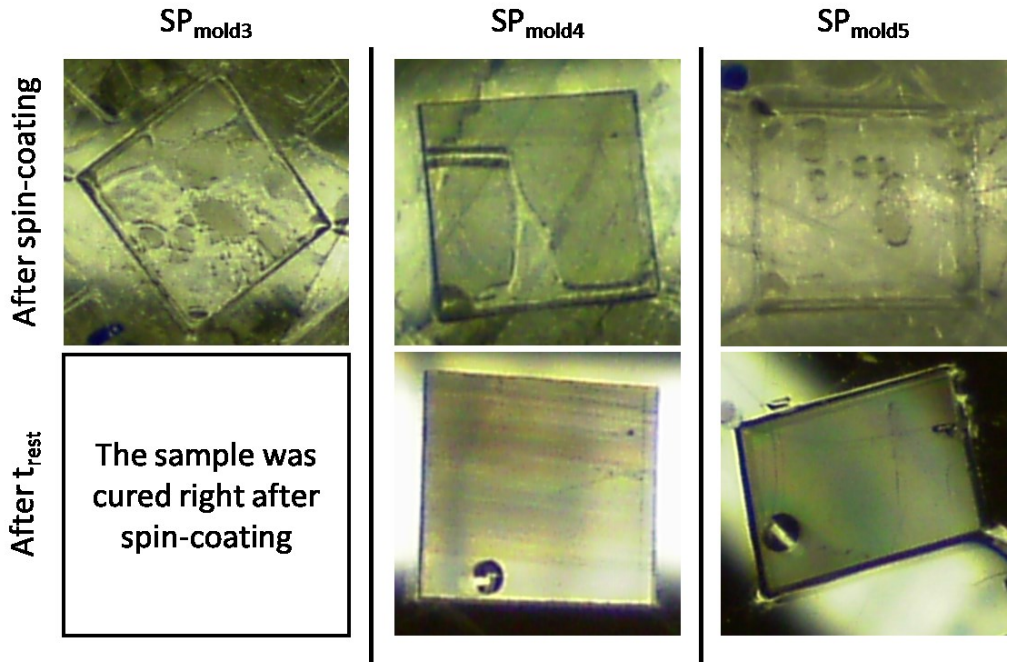

Figure 5.9: Images of spin-coated samples SP_{mold3}, SP_{mold4} and SP_{mold5} after spin-coating and after overnight rest.

The different strategies followed to create a thin film on topographically patterned substrates led to similar results, namely, unfilled channels. Two issues may be major responsible for the emptying of the channels: On one hand, dewetting of the coating film was observed after resting time. Because all the liquid polymer was connected (liquid inside the channels and on the surface of the substrate), the dewetting may drag some of the liquid inside the channels, emptying them.

Contact angle measurements were carried out, in order to investigate the dewetting of the substrates. **3BC** drops on flat and structured substrates spread immediately after contact, giving contact angles below 10°. These results a priori contradicted the observed dewetting effect. On the other side, our substrates contained not only a solid phase, but also a liquid one (the liquid material inside the channels). In such substrates the measurement of the contact angle cannot easily predict the wetting behavior.

To confirm that this dewetting-like phenomenon was able to partially empty the channels a drop with enough volume to fill the channels was placed on top of a topographically patterned substrate and left filling the sample for more than 2 days without spin-coating. At the initial time, the drop started spreading and filled the channels (Figure 5.10 left). After 63 hours, the liquid on the surface retracted and acquired a drop-like shape (Figure 5.10 right). If the dewetting-like phenomenon was not able to drag some material from inside the channels, a reduced topography could be expected (in the order of nanometers). However, a rainbow effect on the surface was already observed by eye, indicating the presence of remarkable topography. AFM analysis confirmed that the channels were at least 4 μm deep. This result confirmed that this dewetting-like effect strongly affected the filling of the channels and, therefore, the coating of the topography.

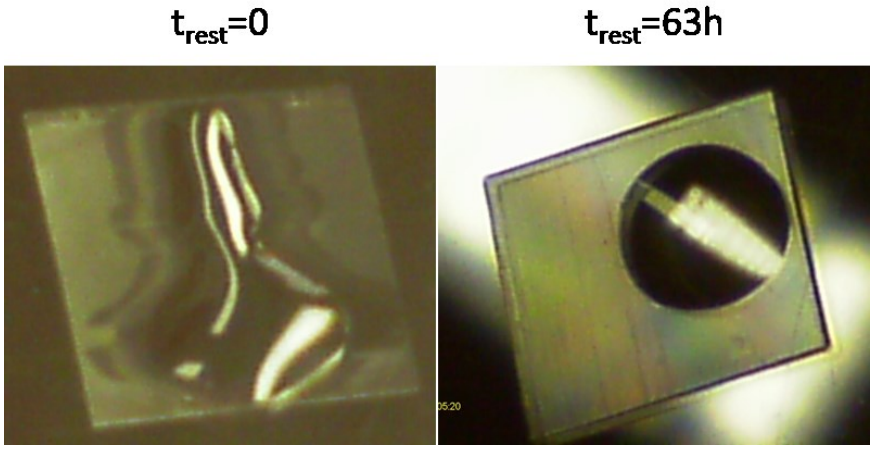

Figure 5.10: Image of a topographically patterned substrate where a drop of 3BC was deposited and left in rest at times: Left: 0 h. Right: 63 h.

On the other hand, spin-coating was intended to form thin films on smooth substrates and the presence of channels definitely modifies the way the liquid is removed from the surface. It could be assumed that centrifuge forces acting inside the channels perpendicularly to their direction may not be able to remove the liquid, which is physically

confined by the walls, but forces parallel to the pattern direction do not encounter obstacles to remove the coating material, resulting on the emptying of the channels.

Another important remark was the long UV-curing times necessary to cross-link the spin-coated film. The spin-coated samples required up to 2 hour of radiation to polymerize. The explanation for these differences in curing time between mold, filler and blanket may be that the process of re-oxygenation was more efficient on thin or less viscous films than on thick or more viscous ones, inhibiting further polymerization [12].

In short, this methodology was ineffective to achieve filling of the topographic features of the substrate and it could not be expected to be able to form a continuous coating along the surface.

5.3.1.2 Spin-coating on FIMIC samples:

Based on the results from the previous section, a new approach was chosen: The channels were filled first via FIMIC and then the samples were spin-coated to cover the nanometric topography of the FIMIC. Using FIMIC substrates, the initial topography to be filled was reduced from the micrometric to the nanometric scale. To study the effect of the different spinning conditions on the pattern of the FIMIC material, all the samples were studied using AFM before and after spin-coating treatment.

The FIMIC samples were prepared using **PEG** 0% CL (t_{UV} = 8 min) as the mold (10-20-10) and **PEG** 10% CL (t_{UV} = 8 min) as the filler. After UV-curing, **3BC** 0% CL was deposited on top and the sample was spin-coated as indicated in Table 5.3. With this methodology, the stiffer **PEG** elastic pattern was embedded under a layer of softer **3BC**.

Table 5.3: Operating conditions for the spin-coating on FIMIC substrate.

Sample	ω_{sp} (rpm)	t_{sp} (s)	t_{rest} (s)	t_{UV} (min)
SP_{FIMIC1}	1380	60	0	20
SP_{FIMIC2}	1440	60	0	20
SP_{FIMIC3}	1560	20	0	20
SP_{FIMIC4}	1440	20	10	20
SP_{FIMIC5}	1500	20	10	20
SP_{FIMIC6}	1560	60	10	20

The three first samples (SP_{FIMIC1}, SP_{FIMIC2} and SP_{FIMIC3}) were kept spinning during UV-curing, in order to stop the dewetting of the blanket. This was an attempt at "freezing" the blanket while it still covered the whole surface.

After spin-coating, the difference between grooves and hills was increased in the three cases (Figure 5.11). This was probably due to the changes in the properties of the liquid precursor during the curing (mainly the viscosity). This altered the spin-coating process and led to unexpected results. It was intended that the spin speed was kept constant. However, due to the construction of the spin-coater, it was difficult to achieve the same spin speed when speeds under 2000 rpm were used.

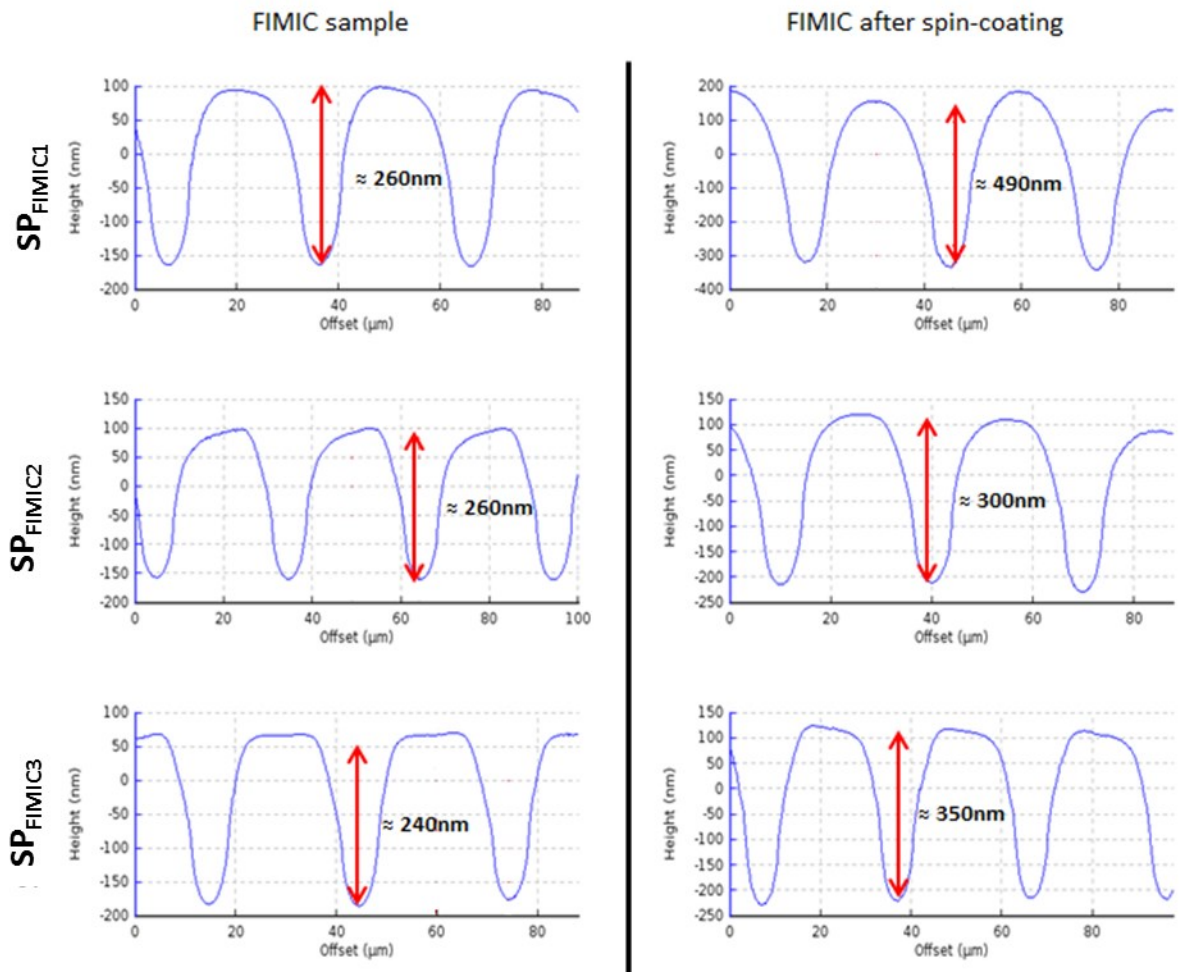

Figure 5.11: Height profile obtained with AFM in dry state. Left: FIMIC samples before spin-coating. Right: the same samples after spin-coating.

To avoid modification of the properties of the blanket during spin-coating, as observed in the previous cases (SP_{FIMIC1}, SP_{FIMIC2} and SP_{FIMIC3}), it was decided to leave the sample for a resting time before UV-curing to let the pre-curing mix form a homogeneous film over the substrate, thus losing the strains generated by the centrifuge force and returning to a resting state. This rest time should not be too long, since elevated resting times led to dewetting of the blanket and formation of drops on the surface, as seen in the previous section (Section 5.3.1.1). The samples were UV-cured after rest.

The AFM results in dry state showed a great reduction of the topography, reaching values of around 20 nm and 30 nm in the case of the samples SP_{FIMIC4} and SP_{FIMIC5} respectively (Figure 5.12). In the case of SP_{FIMIC6}, the topography experienced also a reduction, from 250 nm to 140 nm, after spin-coating. This reduction was not as large as for SP_{FIMIC4} and SP_{FIMIC5}. This difference can be easily explained by the fact that, for SP_{FIMIC6}, the

spin time was longer, leading to a removal of a larger amount of pre-curing mix and, therefore, the remaining mix was not enough to completely fill the topography.

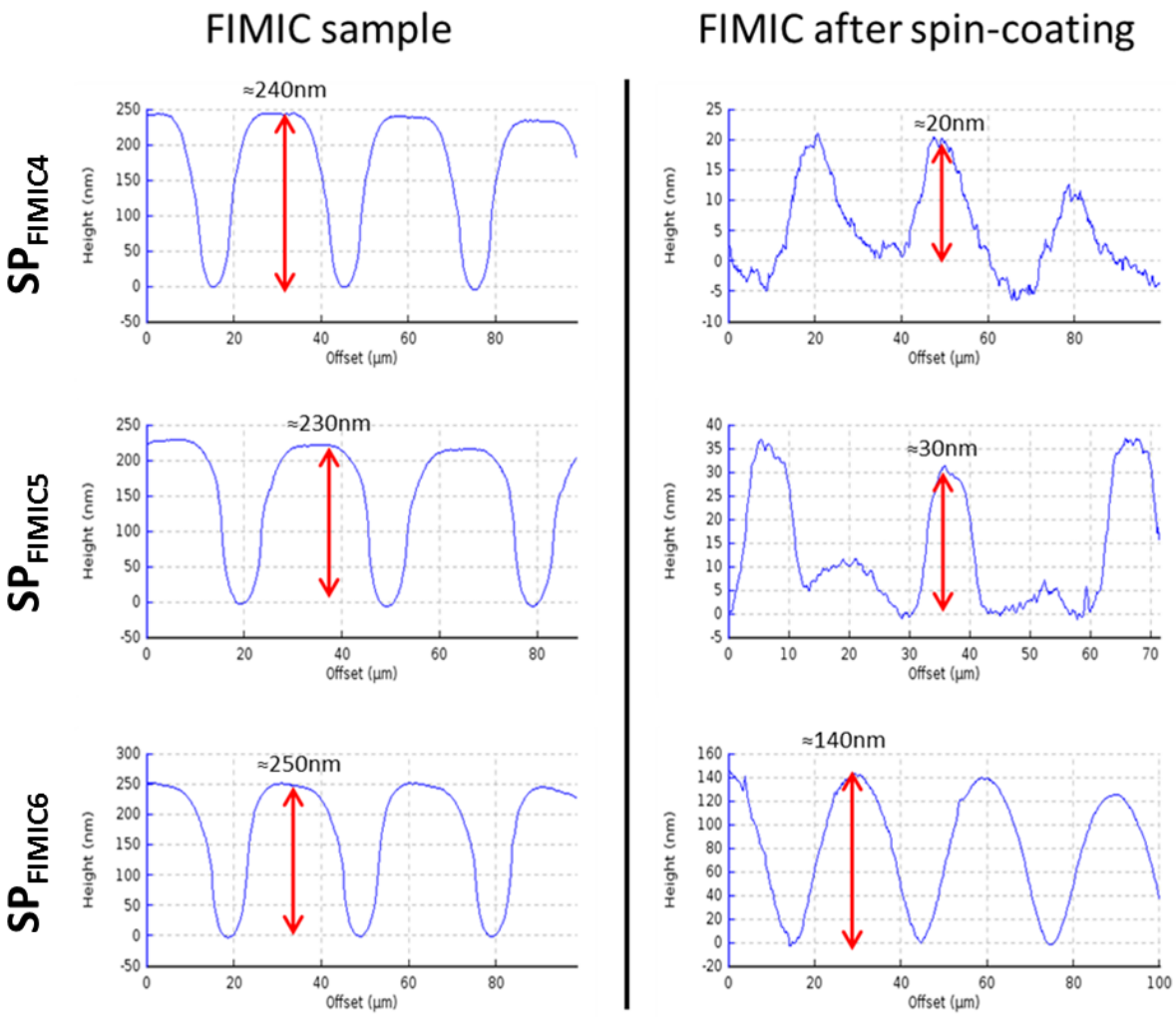

Figure 5.12: Height profile obtained with AFM in dry state. On the left column, the FIMIC samples before spin-coating. On the right column, the same samples after spin-coating with trest = 10 s.

Summarizing, during the experimentation with spin-coater the following results were observed:

- Dewetting affected the formation of thin films; long resting times allowed dewetting and consequent uncoating of the surface. Direct UV-curing during spin-coating modified the properties of the blanket and, therefore, the process of coating. Short resting times showed accumulation of the blanket on the sides of the sample.
- Spin-coating on topographically patterned molds was unable to fill completely the existing topography. The final topographic profile showed channels of 2 µm or more.

- The nanometric topography present on FIMIC samples was reduced when a short resting time was left after spin-coating.
- The reproducibility of the experiments and, consequently, the control of the thickness of the film were poor, due to the difficulty to set up the operating parameters in the equipment.

Table 5.4 summarizes the topography resulting after spin-coating on mold substrates and on FIMIC.

Table 5.4: Summary of the experimentation for generating embedded patterns of elasticity via spin-coating.

Material	Sample	t_{penetr} (h)	ω_{sp} (rpm)	t_{sp} (min)	t_{rest}	Initial topogr. (µm)	Final topogr. (µm)
3BC mold	1	0	2000 + 4500	1 + 9	16 h	10	3
	2	0	4000 + 3180	1.5 + 5	16 h	10	2
	3	16	4500	5	0 h	10	3.5 - 6
	4	3	2100 + 1440	2 + 30	16 h	10	6
	5	21	360	30	2 h	10	4
FIMIC	1	0	1380	1	0 h	0.26	0.49
	2	0	1440	1	0 h	0.26	0.30
	3	0	1560	0.2	0 h	0.24	0.35
	4	0	1440	0.2	10 s	0.24	0.02
	5	0	1500	0.2	10 s	0.23	0.03
	6	0	1560	1	10 s	0.25	0.14

5.3.2 Razor-blade method

As for the case of spin-coating, the method was tested on molds and on FIMIC samples. The molds (20-10-15) were prepared with **PEG** 0% CL. The filler for the FIMIC as well as the blanket material was **3BC** 5% CL.

5.3.2.1 Razor-blade method on topographically patterned substrates:

3BC was dropped on top of the mold, allowed to enter the channels and the excess was removed with a razor-blade parallel to the direction of the pattern. With this methodology it was expected that the channels of the mold would be filled and, at the same time, a residual layer would be left on top of the whole patterned surface, thus masking the different surface chemistry under a homogeneous blanket. This method was very experience-dependent; the razor had to be placed in the correct position and the adequate pressure had to be exerted, if not, the excess was not removed and/or the mold could be damaged.

The first observation is the elevated curing time necessary for polymerization compared to the previous fabrication method. Those samples which were UV-cured for less than 1 hour were still covered by a liquid layer; on thin films oxygen diffused more rapidly into the liquid polymer, acting as inhibitor for UV-curing. For this reason, longer exposition times were required [12].

A set of samples were analyzed with AFM in dry state, showing topography in channels ranging from 600 nm to 2.5 µm (Figure 5.13). The results indicated an incomplete filling of the channels, which may be caused by dragging off of some material from the upper layers of the channels during removal of the excess. The heterogeneity of the results at different positions of the same sample (from nanometric to micrometric topographies) could be explained by the difficulty of handling associated to the method. Additionally, some unexpected peaks were present inside the filled lines (Figure 5.13).

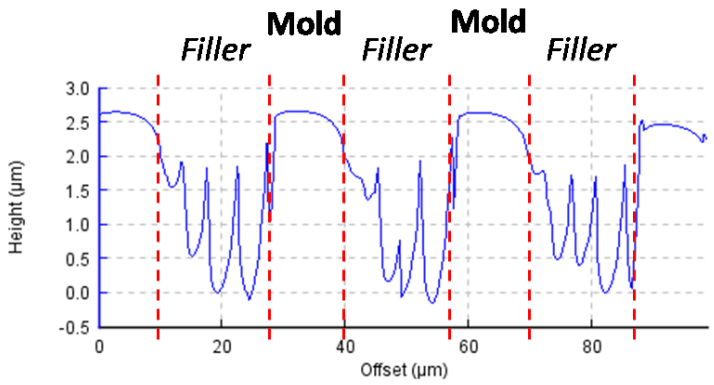

Figure 5.13: Height profile of a sample obtained by the razor-blade method on a mold after one coating (Measured in dry state by AFM). Lines representing the mold and filler lines are illustrative.

It was decided to fill the channels by consecutive coating of previously "razor-bladed" samples in order to decrease the topography after each step. The topography was indeed reduced as expected. AFM analysis on dry state showed values between 200 nm and 1 µm, which were still greater than the topography obtained on FIMIC samples (100 nm to 400 nm in dry state).

Force mapping of the samples was also carried out (Figure 5.14). Slope images showed elastic patterns in which lines with clearly different slopes for their force/distance curves could be seen. These could be related to the elastic properties of the material (Figure 5.14b). Unexpectedly, adhesion images also exhibited a pattern corresponding to the position of the mold and filled lines, even in case of reduced topography (200 nm) (Figure 5.14c). The presence of areas with different adhesive properties in combination with topographic structures may indicate that the substrate was not completely coated.

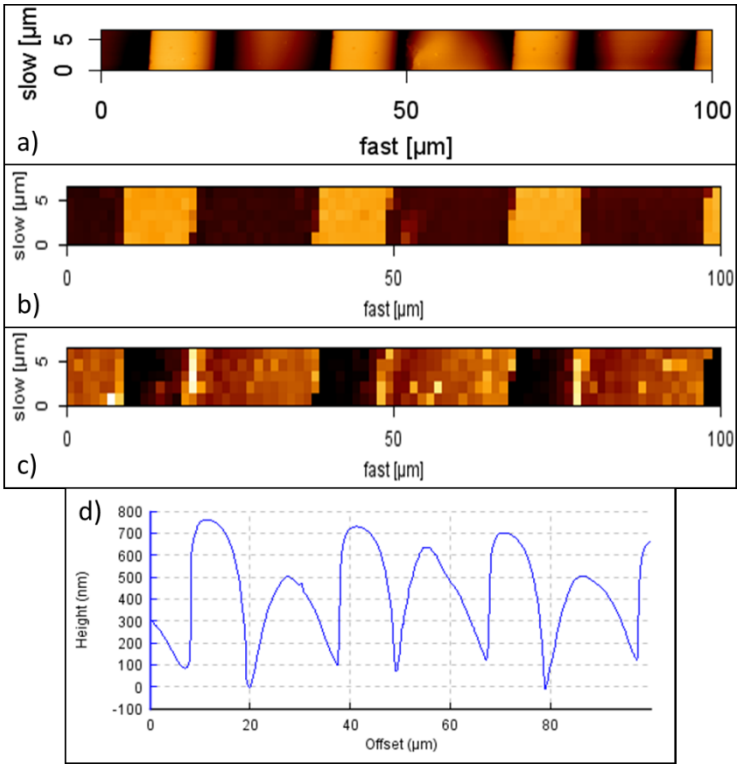

Figure 5.14: AFM analysis in dry state of razor-blade sample on a mold (20-10-15) after two razor-bade steps: a) Height image, b) Slope image, c) Adhesion image, d) Height profile.

It was concluded that razor-blading on mold substrates presented some issues: Samples were easily damaged during the process because of the fragility of the structure and the inherent brittleness of **PEG**. On the other hand, despite several filling stages to fill up the channels, the obtained topographies were still greater than those typical for FIMIC samples.

At the same time, with the necessity of consecutive filling and curing steps, the advantage of using a mold as substrate, i.e. only one interface mold-filler was present and the delamination could be prevented, was lost.

5.3.2.2 Razor-blade method on FIMIC samples:

Regarding the difficulty faced when attempting to fill the channels of the molds via razor-blading, the use of FIMIC samples, with nanometric topography, appeared to be the most suitable approach. It also had the advantage that the structures on FIMIC samples were mechanically stronger than those of topographic molds, due to their aspect ratio (hundreds of nm deep in tens of µm wide) and did not get easily damaged with the razor-blade.

FIMIC samples were prepared using **PEG** 0% CL (t_{UV} = 5 min) as the mold and **3BC** 5% CL as the filler (t_{UV} = 15 min). Any unfilled channels were cut out from the sample. Afterwards, the samples were covered with **3BC** 5% CL, the excess was removed and the polymer was UV-cured for 1 hour.

In this case, the topography reached values between 100 nm and 400 nm. Interestingly, the lines corresponding to the filled channels sticking out of the mold lines, i.e. the hills of the topography corresponded to the filled lines (Figure 5.15d). This phenomenon of "channels sticking out" could be a consequence of the different wetting properties of the two materials present on the surface. The molecules of the blanket (**3BC**) had a stronger interaction with those of the filled lines (**3BC**) than with those of the mold lines (**PEG**), resulting in a larger accumulation of the blanket material on top of the filled lines and an inversion of the topography.

In order to verify the coating of the FIMIC sample, adhesion and slope images obtained with AFM were also analyzed. On the adhesion image (Figure 5.15c), the pattern was still recognizable, but in 5 µm-width lines. Those lines corresponded to elastic pattern in Figure 5.15b and also to the second peak visible on the mold lines (Figure 5.15a and d). These lines may be artifacts generated during measurement and not really represent the surface properties of the sample. Since the AFM analysis was unable to confirm neither the presence nor the absence of a blanket, optical microscopy was also performed.

Cross-section images of the samples were unable to probe the existence of a blanket layer over the pattern (Image not shown).

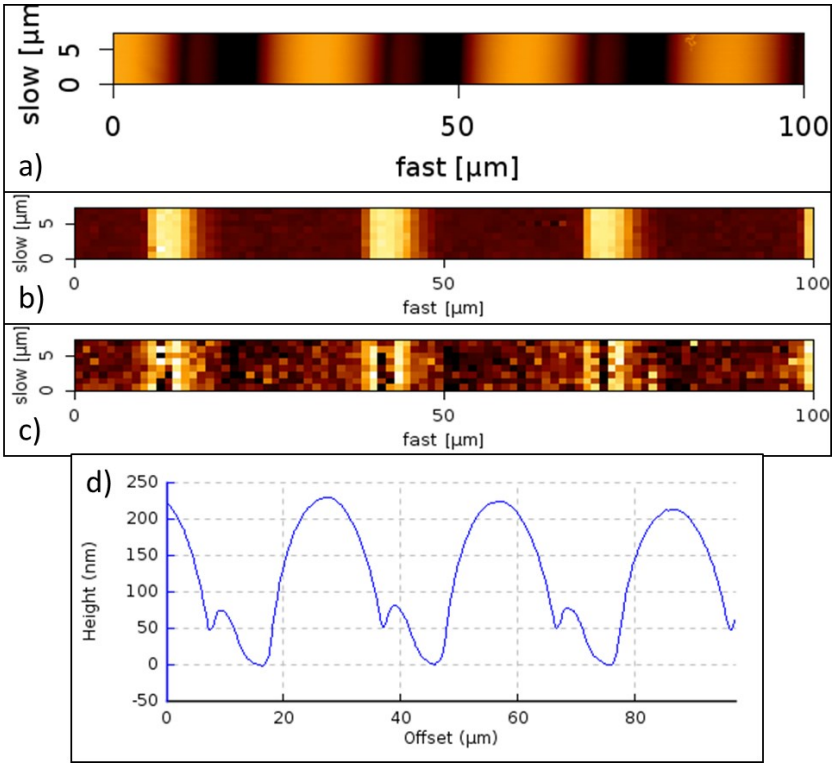

Figure 5.15: AFM analysis of razor-blade sample on FIMIC (20-10-15) in dry state: a) Height image, b) Slope image, c) Adhesion image, d) Height profile.

In summary, the use of the razor-blade method on mold substrates led to incomplete filling of the channels, contrary to our expectations based on the literature [78]. This discrepancy may have been due to the different wetting properties of the molds used; we used **PEG** while Zhao and co-workers used PDMS. Several filling steps were necessary to decrease the surface topography to values less than 1 µm. Still, no complete (continuous) coating of the substrate was achieved using this approach.

When using FIMIC substrates, it was observed that the surface topography was maintained within the range of the original samples, but it was inverted, i.e. channels stuck out of the mold. We suspect that the different wettability of filler and mold materials was responsible, inducing accumulation of the blanket on the filled lines. Nevertheless, none of the analytical methods used was able to confirm the presence of a homogeneous coating.

In general, this method manifested several disadvantages:

- The razor may damage the samples if the pressure is too high, especially on mold substrates.
- The results were not reproducible. Despite the same methodology being followed, diverse topographies were measured not only on several samples, but also at different positions of the same sample.
- At first sight, the method seems to be very simple, but in reality, the experimental application required some training; the blade must be placed with the correct angle, it must contact the whole surface equally and apply a determined pressure. These parameters must be kept constant during the removal of the excess for a homogeneous distribution of the blanket.

As a result, this method demonstrated to be laborious to control and no effective coating was obtained.

5.3.3 Sandwich method [1]

Early experiments with the sandwich method already showed that the thickness of the mold was not uniform along the sample. This affected the removal of the excess of blanket material. The blanket tended to compensate the height of the mold to create a surface parallel to the base; on areas where the mold was thinner, a thicker blanket was measured (Figure 5.16).

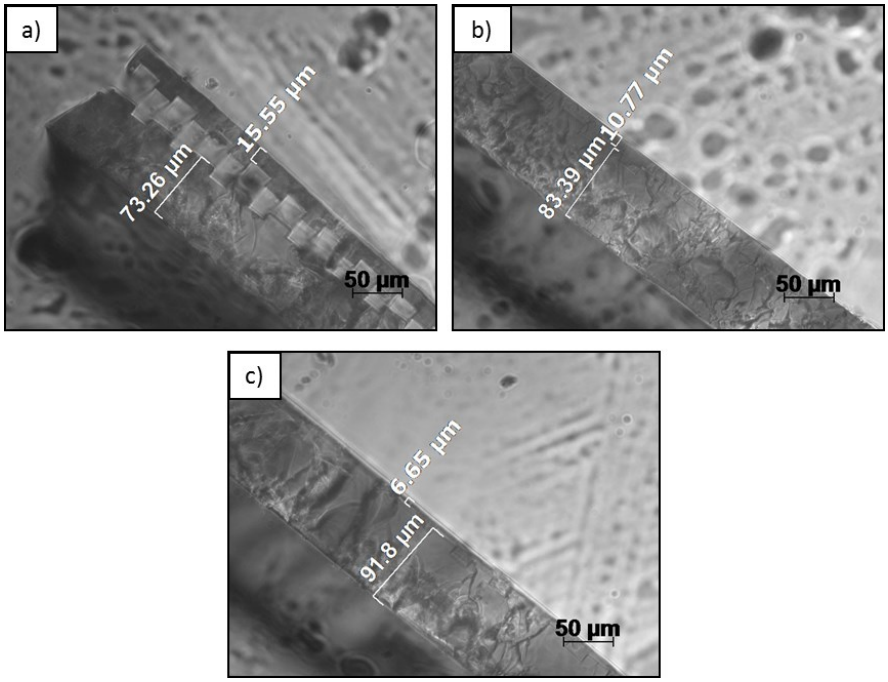

Figure 5.16: Optical images of the cross-section at different positions of a sample prepared by the sandwich method.

To solve the problem of the blanket adapting it thickness to compensate the differences in the mold, a master holder was fabricated. It consisted of an aluminum block with a square pit, upon which the master was placed. Surrounding the master there was a frame 900 µm thick over the pit base (Figure 5.17). While preparing a mold, a load could be placed on top of the cover slide. This load rested on the sides of the frame, avoiding damage to the master and, at the same time, ensured that the cover slide was placed parallel to the master.

[1] Research done in collaboration with Paul Gruner

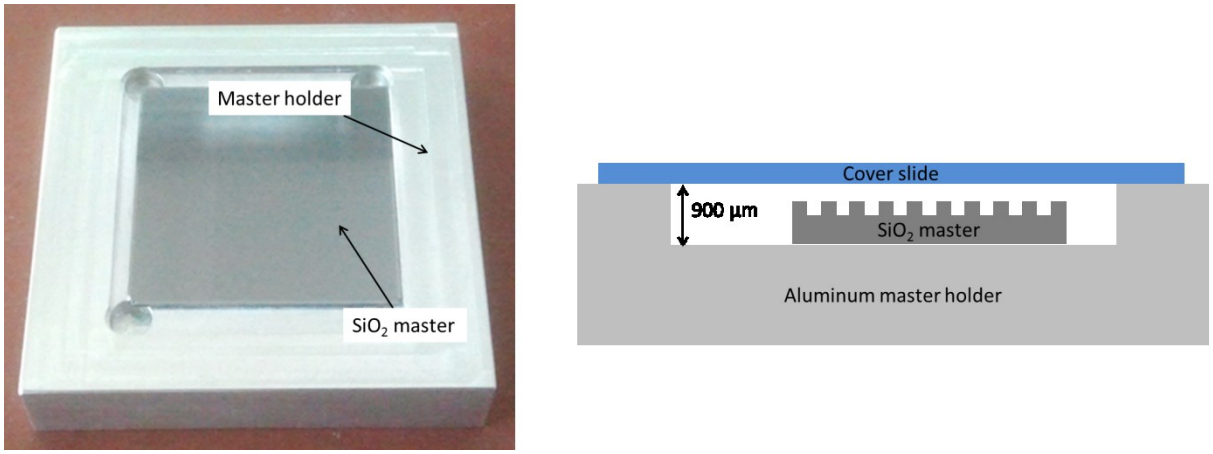

Figure 5.17: Left: Aluminum master holder with silicon master inside. Right: Schematic cross-section of the master holder.

Molds (20-10-15) with the same amount of liquid pre-polymer (60 µL of **PEG** 0% CL) were prepared, but in one case using the master holder and in the other not. After polymerization, the samples were cut and the cross-section was observed by optical microscopy. The thickness was measured at several positions along the cut and three cuts were done for each sample. Results are presented in Figure 5.18.

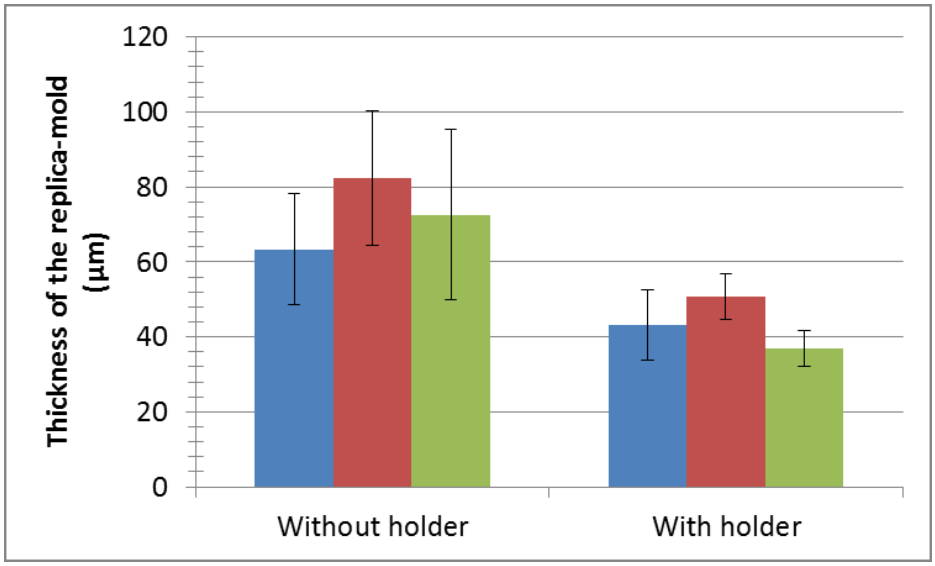

Figure 5.18: Average thickness of molds prepared with and without master holder. The columns represent repetitions of the experiment.

The standard deviation of the average thickness along the samples indicated that molds prepared without master holder had greater thickness distributions than when using the holder. Indeed, without holder, the thickness of some samples varied from 40 µm to 100 µm.

It can be seen, that repetitions of the experiment using the same conditions (right columns of Figure 5.18) did not lead to exactly the same thickness values. This was not necessarily a problem, since the coating process did not depend on the absolute value of the thickness of the substrate but on its homogeneity.

To create embedded patterns of elasticity, molds were prepared using the master holder. After polymerization, the molds were covered with **3BC** 5% CL and confined between glass slides. To reduce the number of parameters affecting the thickness of the blanket, we used the same dimensions of mold, namely 20-10-15. The molds were cut into squares measuring 10 x 10 mm and 20 µL of **3BC** were dropped on them. Different loads were applied to the samples during UV-curing to analyze the dependence of the blanket thickness to the load; increasing pressure on the sample was expected to decrease the value of the thickness.

Another method for measuring the thickness of the blanket was mixing the liquid polymer with a dye. Using dyes with high molecular weight, diffusion could be avoided and the mold and the blanket could be clearly determined by confocal microscopy. This method had a better resolution compared with the results of optical microscopy, which was of special interest for measuring thin coatings (in the order of a few micrometers) (Figure 5.19).

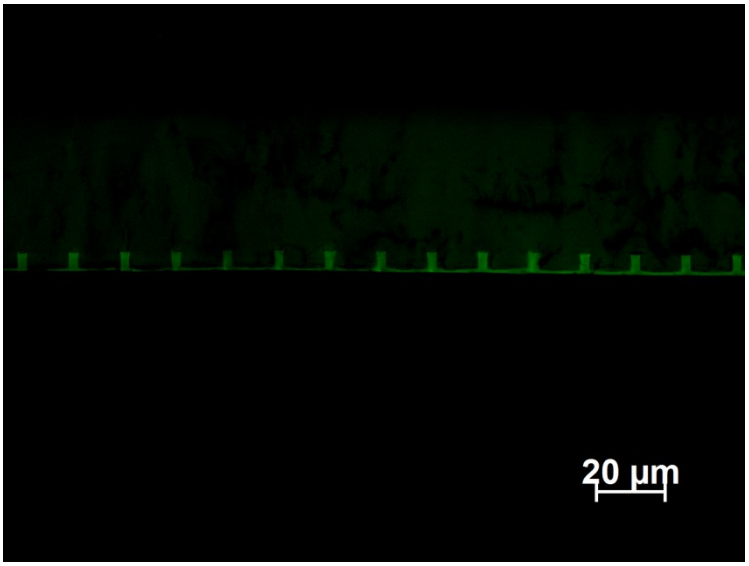

Figure 5.19: Fluorescence image of a sandwich sample using as filler a mixture of PEG 575 and FITC-dextran.

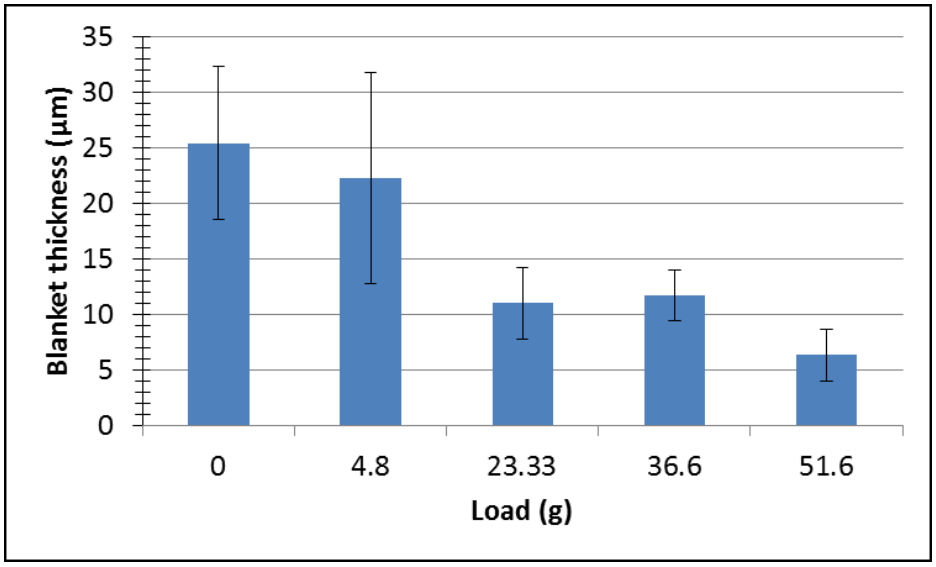

Figure 5.20: Thickness of the blanket formed via sandwich method applying different loads during UV-curing.

Figure 5.20 shows the measured thickness of samples when the load was varied. The weights corresponded to: cover slide (0 g), microscope slide (4.8 g), microscope slide + empty glass vial (23.33 g), microscope slide + glass vial half-filled with water (36.6 g), microscope slide + glass vial completely filled with water (51.6 g).

As expected, greater loads led to thinner coatings of the substrate. The thickness of the blanket was successfully reduced to values below 10 µm, which was, according to the literature, the value we chose as the deepest the cells can feel underlying features modifying the elastic properties of the surface. Not only thinner coatings were generated by increasing the load, but also the thickness along the sample was more uniform and repetitions of the experiment led to similar values, as can be deduced from the standard deviation of the results.

AFM analysis of the samples showed interesting results. Figure 5.21 was obtained from a sample where the observed blanket had a thickness of 7.69 ± 1.54 µm. The first remarkable observation was that, despite the complete coating of the mold, topography similar to that of FIMIC samples was measured (Figure 5.21a and c). It is known that after UV-curing the volume of the polymer decreases (shrinking effect) because of the conversion of Van der Waals interactions into covalent bonds [63]. In the case of PEG-based polymer this reduction is in the order of 10%. Taking into consideration that the volume of the blanket material filling and covering the channel lines was larger than that covering the mold lines, it

could expected that larger shrinking on the filled lines would occur and that depressions on the surface corresponding to those lines would form.

Force mapping revealed an elastic pattern on the surface (Figure 5.21b). The bright lines indicated areas where the slope of the Force/Distance curve of the force scan was greater, i.e. for the same exerted force less penetration was achieved and, therefore, the material was harder. The elastic behavior and the dimensions of the pattern corresponded to the composition of the sample, where the **PEG** (harder) forms lines of 10 µm width, and the **3BC** (softer) coating penetrates channels of 20 µm. As suggested, thin coatings (fewer than 15 µm) did not mask the underlying elasticity of the mold, while thicker blankets did. It was hypothesized that these elastic patterns embedded under thin layers would also be recognized by cells, which will migrate according to them.

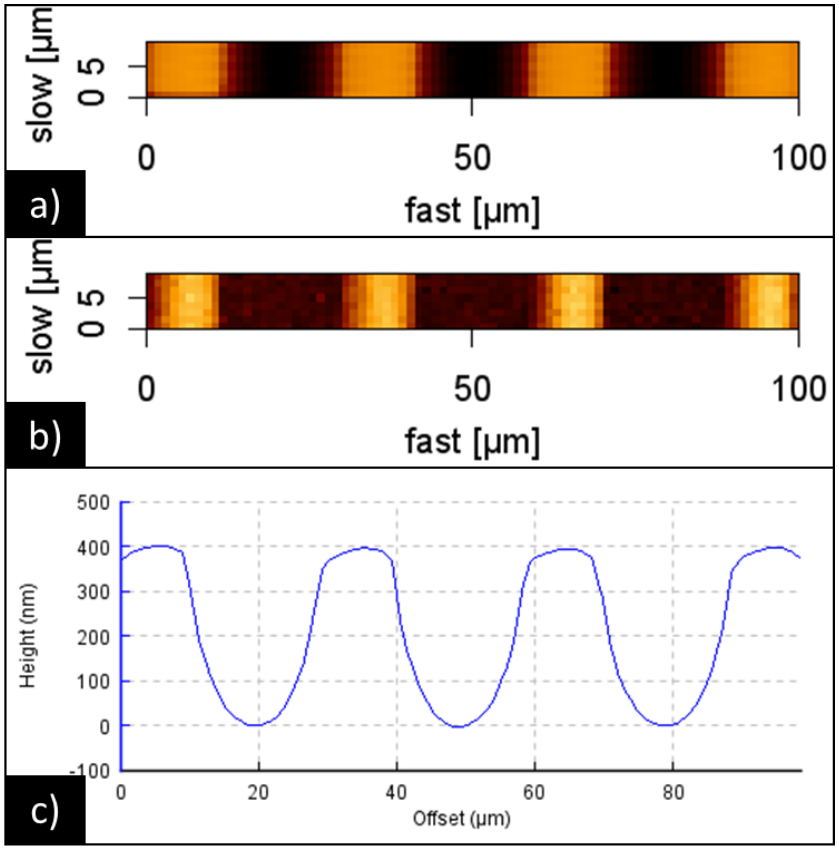

Figure 5.21: AFM analysis in dry state of a "sandwiched" sample (20-10-15): a) Height image, b) Slope image, c) Height profile.

The dimension of the mold could also play a role in the formation of the blanket; molds with wider and deeper channels require greater amounts of material to be filled, reducing the available volume for the coating. By using an excess of blanket material, we suppressed

this factor because we guaranteed complete filling of the channels and enough supply for a complete coating.

Another advantage of this method was the suppression of the dewetting effect; because the liquid blanket was constantly enclosed between the substrate below and the cover slide above, the thickness was kept constant and higher drops could not be formed.

5.4 Conclusions

5.4.1 Spin-coating:

The topographically patterned samples were covered with a liquid polymer, which filled the channels, and spin-coating was performed to distribute the coating along the surface. Several spin-speeds were used to find the optimal processing conditions to obtain a homogeneous distribution. Contrary to our expectations, AFM analysis showed incomplete filling of the substrate at low as well as at high spin-speeds. We hypothesize that the original topography was too large to be filled by spin-coating, mainly because of the action of a dewetting-like phenomenon. On the other hand, the slight topography present on FIMIC samples was effectively reduced when the blanket material was spin-coated, followed by UV-curing of the sample. We demonstrated that FIMIC samples were more adequate substrates for embedding patters of elasticity via spin-coating.

Experiments carried out in similar operating conditions showed different results. To improve the reproducibility of the method, it will be necessary to use equipment with a more accurate control of the process parameters, such as spin speed and time.

5.4.2 Razor-blade method:

Molds were coated with the blanket material and the excess was removed with the help of a razor-blade. Unexpectedly, the channels of the mold were only partially filled. After several repetitions of the process, the topography was reduced to values under the micrometric range. AFM analysis pointed to the presence of two materials, i.e. mold and filler, presumable indicative of complete coating of the mold lines by the blanket.

Razor-blading on FIMIC substrates maintained the scale of the pre-existing topography but reverted the pattern; the peaks were located on the former channels (filled lines), while the valleys corresponded to the mold lines. Optical imaging of the cross-sections was unable to confirm the presence of a blanket. Adhesion, slope and topographic images from AFM analysis induced us to think that the samples were only partially coated.

One parameter that could be changed to control the thickness of the blanket is the position of the blade. To improve this method and achieve controllable and homogeneous coating of the substrate, we suggest the development of equipment where the vertical position of the blade over the sample can be set up to the micrometric level. Mechanical displacement of the blade is also of interest, to eliminate errors due to the handling of the researcher.

5.4.3 Sandwich method:

Samples were prepared using the sandwich method. To obtain homogeneous coating thickness along the surface, molds were prepared using a mold holder specially designed for this purpose. The use of the holder improved the reproducibility of the cast-molding method. Applying different loads on the sample during UV-curing we managed to control the thickness of the blanket, i.e. higher loads lead to thinner coatings. Surprisingly, the topography present on the original FIMIC substrate was maintained despite the complete coating of the surface. We hypothesize that this topography was induced by shrinking of the polymer during UV-curing. Using this method, embedded patterns of elasticity were generated, which were measurable by AFM analysis, under a chemically homogeneous surface of a cell adhesive hydrogel.

Chapter 6:

Cell response to anti-adhesive substrates patterned with metallic nanoparticles

6.1 Introduction:

Gold and silver have been traditionally used as a measure for richness. Objects made of these two noble metals were the most valued and represented the status of their owners. In the last century, these metals became even more valuable than ever; gold and silver nanoparticles find new applications in the medical field every day, either for treatment or in diagnosis devices.

Gold nanoparticles have been investigated, amongst others, for their anti-angiogenic properties for the treatment of cancer [146] or as drug carriers [147]. They can also be used as catalysts [148] or as matrices for protein and enzyme immobilization [149]; hence, they have a great potential for being used in biosensor devices. Silver presents similar properties to gold nanoparticles, and also shares some of its applications. At the same time, silver has been extendedly used as an antimicrobial (already used in the ancient Greece). Recent research showed that the silver ions affect bacteria by increasing the permeability of the membrane and interfering with the metabolism of the cell [150].

One of the most interesting properties of the gold and silver nanoparticles is their Localized Surface Plasmon Resonance (LSPR). Briefly, electrons near the surface of the metal oscillate collectively when excited by external stimuli, generating an absorption plasmon peak [151]. The position of the LSPR peak, located near the infrared region, has a great importance in the medical field because is close to the wavelength of maximum transmission of radiation through the human tissue [152]. This property finds two different applications at the same time: It has been exploited to use gold nanoparticles for imaging and detection [153] and for photo-thermal treatment applications as well, where the gold nanoparticles can be heated up via external irradiation [147].

In addition to their use in imaging applications, gold and silver nanoparticles can also be used as selective surfaces for immobilization of proteins [149]. The importance of this application does not only rely on the capacity to fix proteins maintaining their structure and functionality [149]. Furthermore, by tuning the size of the particles down to the order of large biomolecules, the amount of absorbed molecules can be controlled, even achieving the adsorption of a single molecule per nanoparticle [154].

Various morphologies of metal nanoparticles can be synthetized, e.g. spheres [72], rods [155], plates [75], three-dimensional structures [76,77], or hollow spheres [73]. The diverse shapes of nanoparticles have different applications as a consequence of their variations in the position of the LSPR peak. At the same time, the shape of the nanoparticles can also affect the adsorption of molecules on their surface [156].

The relation between gold and silver nanoparticles and cellular organisms is a love/hate story; Gold nanoparticles are essentially considered as cytocompatible but due to their reduced size, gold nanoparticles in suspension can be taken up by cells and interact with the cellular components [157]. Some authors support that pure gold nanoparticles enter the cells via endocytosis but are unable to leave the endosomes, therefore, have no effect on the cells [158]. Other authors indicate that the question "are gold nanoparticles cytocompatible?" is not so easily answered with yes or no, but rather the toxicity is size dependent [159]. Pan and co-workers proved that gold nanoparticles of sizes below 2 nm were highly toxic. A similar size dependence can be seen with silver nanoparticles [160]. Our own (unpublished) research on the topic has shown that gold nanoparticles of sizes under 60 nm were cytotoxic and that the cytotoxic effect increased with decreasing size of particle [161].

Especially relevant for this work is the use of metallic nanoparticles as surfaces for adsorption of molecules, such as fibronectin, which are necessary for subsequent cell adhesion. Arnold and colleagues investigated the effect of the separation between anchoring points of an adherent cell using gold nanoparticles [154]. They created a pattern of nanodots on an anti-adhesive PEG background, to which a peptide sequence was adsorbed. The integrin proteins of the cells used these positions to adhere on the surface. Due to the small size of the nanoparticles, each one of them represented a single adhesive point and controlling their distribution, they managed to control the spacing of the cell adhesion complexes.

Based on this idea, we decided to incorporate metallic nanoparticles into PEG hydrogels in an attempt to modify the cell-repellent nature of the polymer at specific positions. In this chapter, we teste the cytotoxicity of composite PEG-metallic nanoparticles substrates, prepared by our newly developed transferring method [68] to verify that the composed system hydrogel/metal preserved the cytocompatibility of the individual components. We

also investigate if the inclusion of metallic nanoparticles could modify the adhesive properties of PEG hydrogels and induce cellular adhesion. Finally, we present different methods to create micropatterns (lines) of metallic nanoparticles with a well-defined size and periodicity. These chemical patterns on the surface of the substrate can be used to investigate the effect of the pattern size on the migratory process of cells in order to be able to understand and control the direction and speed of the movement.

6.2 Materials and methods:

6.2.1 Synthesis of metalling nanoparticles:

A complete description of the synthesis and characterization methods of the metallic nanoparticles (NP) can be found in the recent dissertation of Arafeh [68]. In the present work, the following metallic nanoparticles were used (Table 6.1, Figure 6.1).

Table 6.1: Metallic nanoparticles employed in the experimentation and their average sizes.

Structure	Shape	Average size
Sphere	Au Sphere	21 ± 4 nm
	Au Hollow urchin-like Sphere	206 ± 53 nm
	Ag/Au (core/shell) Sphere	192 ± 23 nm
	Ag Sphere	142 ±26 nm
2D	Au Triangular nanoplate	178 ± 41 nm
	Au Multishape plate	4.1 ± 0.9 µm
3D	Au Tetrahedron	75 ± 15 nm
	Au Cube	12 ± 2 nm
	Au Decahedron	13 ± 2 nm

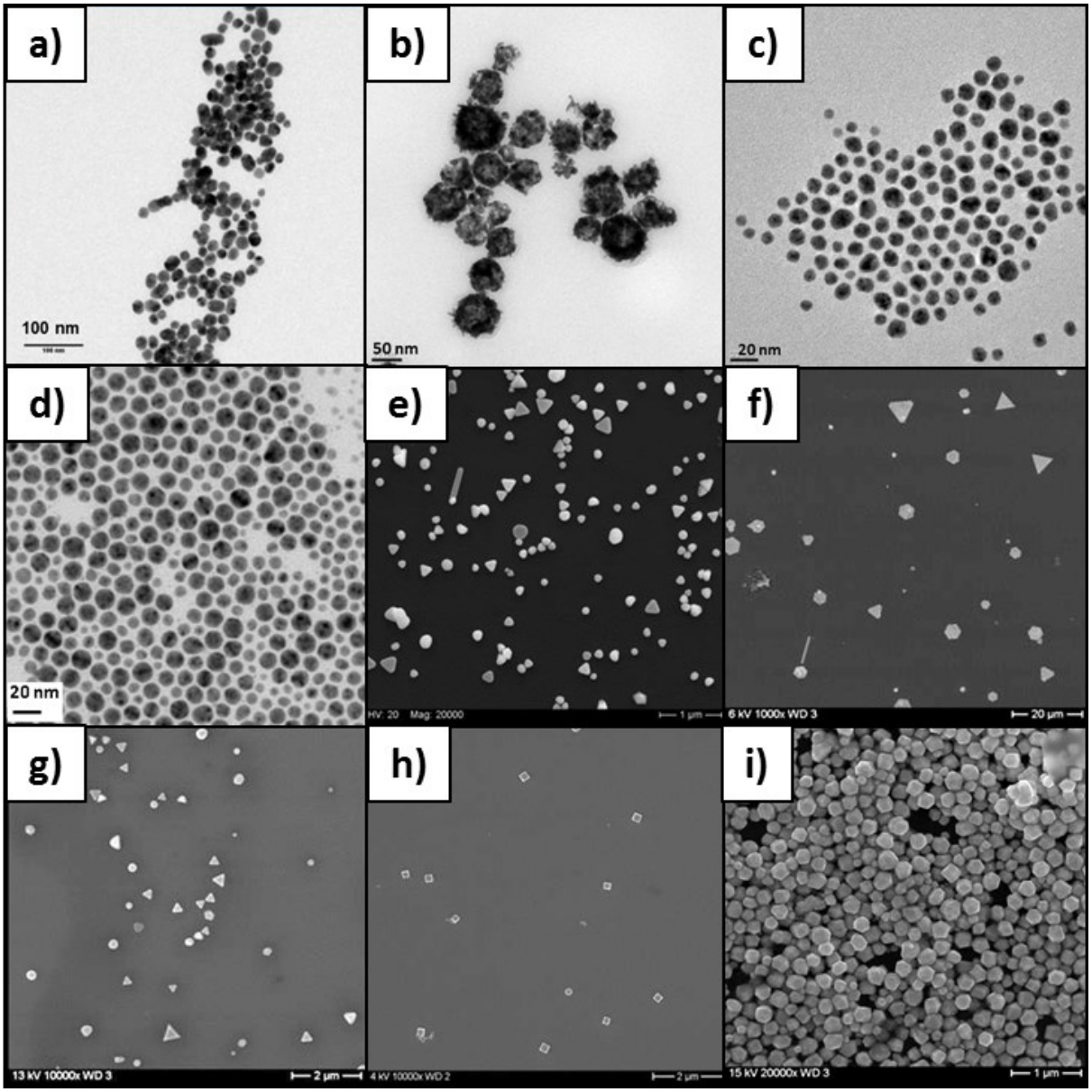

Figure 6.1: Transmission electron microscope (TEM) (Dark shape on bright background) and Scanning electron microscope (SEM) (Bright shape on dark background) images of a) Au nanospheres, b) Au hollow urchin-like nanoparticles, c) Ag/Au (core/shell) nanospheres, d) Ag nanospheres, e) Au triangular nanoplates, f) Au multishape plates, g) Au nanotetrahedrons, h) Au nanocubes and i) Au nanodecahedrons. Image printed with permission of the author [68]**.**

6.2.2 Fabrication of the composite material:

The composite materials PEG-NP were obtained through two different methods.

6.2.2.1 Transference of metallic nanoparticles to the surface of poly(ethylene glycol) gels:

This process is explained in detail elsewhere [68] and is only briefly described here.

The nanoparticles were prepared by self-assembly on the surface of an amino-silanized silicon wafer. The metallic structures were functionalized with 2-propene-1-thiol (linker). Liquid poly(ethylene glycol) (**PEG**) was dropped on top of the silicon and UV-cured. The double bond of the 2-propene-1-thiol cross-linked with the **PEG** network. As a result of this cross-linking, when the polymer was removed from the silicon, the metallic nanoparticles joined the hydrogel and formed a composite (**PEG-NP**), since the metal-thiol bond (connection between metal and gel) was stronger that the metal-amino one (connection between metal and silicon).

6.2.2.2 Physical mixing of metallic nanoparticles and poly(ethylene glycol) precursor [68]*:*

To obtain a liquid precursor of the composite material for later polymerization, a suspension of gold nanoparticles in water (**AuNPs**) was added to the pre-polymer (**PEG** 0% CL) and mixed with the help of sonication. The water of the nanoparticle suspension was removed by evaporation at 100°C for several minutes.

6.2.3 Patterning methods:

In this chapter we present three different patterning techniques:

6.2.3.1 FIMIC with composite material as filler [68]*:*

A FIMIC sample was prepared as explained in Chapter 2. As mold material we used **PEG** 0% CL, UV-cured for 8 minutes and as filler the mix **PEG**/**AuNP** (t_{UV} = 20 minutes).

6.2.3.2 FIMIC-transferring:

This method is similar to the traditional FIMIC technique. The difference was that, while in the traditional FIMIC the mold was placed on a glass surface prior to capillary filling, in this case, the mold (**PEG** 0% CL t_{UV} = 8 minutes) was placed on a silicon wafer coated with gold nanoparticles provided by Çiğdem Yeşildağ. The channels were filled with the same liquid pre-polymer used for the mold and UV-cured for 20 minutes. The gold was then expected to transfer to the filled lines by linkage of the acrylate groups of the liquid PEG

with the linker present on the gold particles (Figure 6.2). Further details about the preparation of the samples can be found in the work of Yeşildağ (unpublished Thesis).

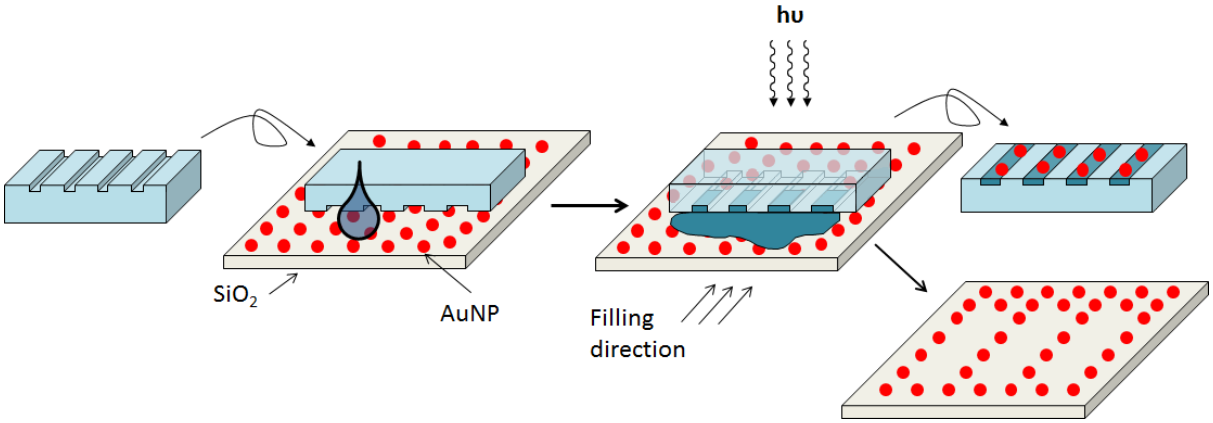

Figure 6.2: Schematic representation of the FIMIC-transferring method.

6.2.3.3 Pattern-transferring:

This approach is similar to the transferring method of Section 6.2.2.1. In this case, the pattern was previously created on the surface of the silicon substrate (prepared by the colleague Çiğdem Yeşildağ). A detailed description of the patterning method of the silicon substrate can be found in the work of Yeşildağ (unpublished).The patterned silicon wafer was used as a substrate for transferring into a **PEG** hydrogel (0% CL, t_{UV} = 30 minutes) as explained in Section 6.2.2.1 (Figure 6.3).

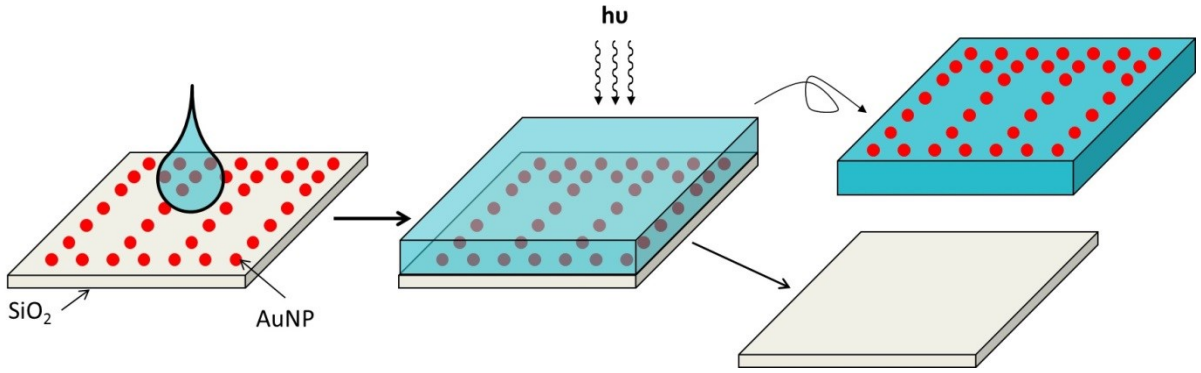

Figure 6.3: Schematic representation of the pattern-transferring method.

6.2.4 Cell studies:

Protocols indicated in Chapter 2 were followed to study the cytotoxicity and adhesion of fibroblasts L292 on the composite samples **PEG-NP**.

The samples were immersed in water for detachment of the hydrogel from the silicon wafer. Afterwards, they were sterilized in ethanol and submerged in well-plates for cell experiments containing PBS to keep them in swollen state during preparation of the suspension of cells. The PBS was substituted by 300 µL of a suspension containing 5000 cell/mL and the samples were incubated at 37°C and 5% CO_2 atmosphere. Adhesion and cytotoxicity experiments were carried out 24 hours after seeding.

For experiments of adhesion, the medium was removed, the samples washed with PBS and fixed with formaldehyde. Adhesion was observed by optical microscopy. Additionally, scanning electron microscope (SEM) images of fibroblast adhering on metallic nanoparticles were captured.

In the case of cytotoxicity experiments by the Live/Dead assay, the medium was replaced by the fluorescent solution fluorescein diacetate/propidium iodide and analyzed by fluorescence microscopy. Images were taken at random positions of the sample, the viable and dead cells summed and the percentage of viable against the total represented. For the quantification of the viability, between 500 and 3000 cells were analyzed per sample. Each material was tested at least 3 times to obtain a statistically representative result.

A positive and a negative control were also prepared on each well-plate. For the positive control, the cells were cultured without sample, i.e. on tissue culture plate (TCP). For the negative control, a drop of ethanol was added to the medium of cells growing on TCP.

6.3 Results and discussion

6.3.1 PEG-NP composite gels: [2]

6.3.1.1 Cytotoxicity studies of PEG-NP composite materials:

In this section the cytotoxicity of our new developed composite materials of **PEG** with different geometries of gold and silver nanoparticles attached on the surface was investigated. As outlined in the introduction (Section 6.1), cytotoxicity of gold nanoparticles

[2] The work described in this section was done in collaboration with Dr. Manar Arafeh.

is traditionally attributed to nanoparticles suspended in the medium and taken up by cells, where they can interfere with the biological processes and cause cellular death. It was expected that the immobilization of the particles on the surface of the gel would avoid cellular uptake; hence, the cytotoxic effect, due to the incorporation of gold nanoparticles inside the cell, should not be observed.

L929 fibroblasts were cultured on samples containing metallic nanoparticles for 24 hours. Then, the medium was removed and the fluorescent solution added.

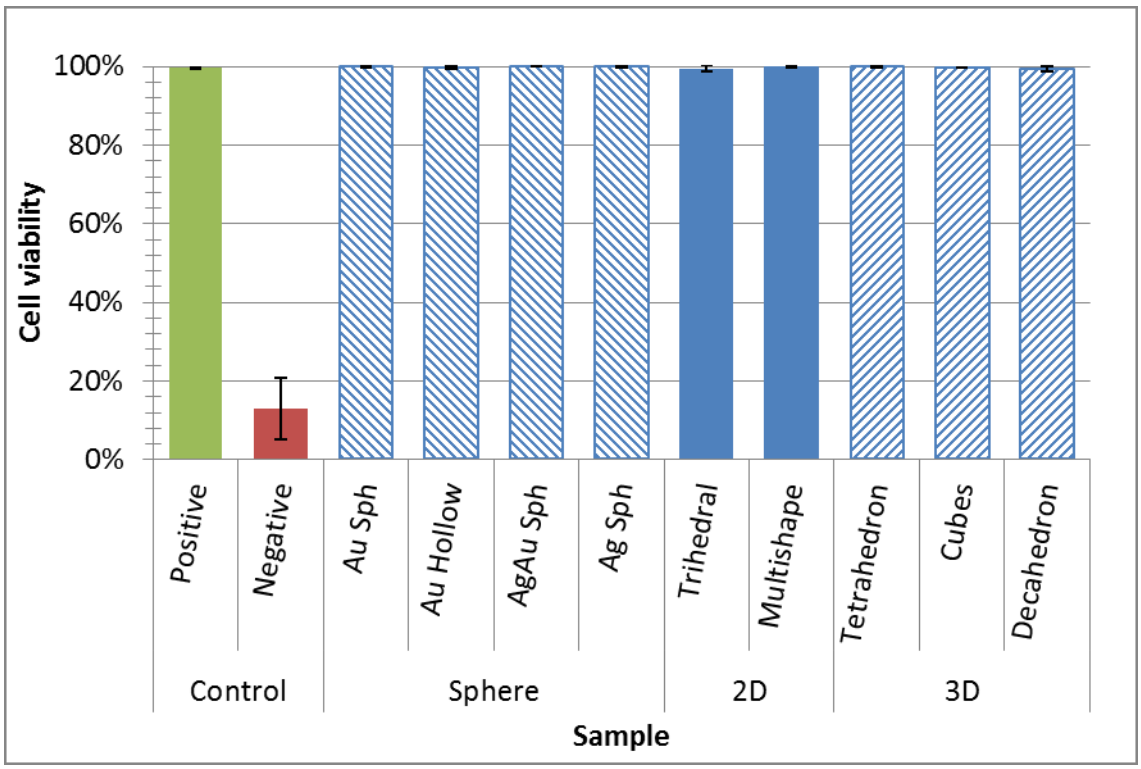

Figure 6.4: Study of the cytotoxicity of composite materials PEG-NP on fibroblasts L292. The vertical axis represents the percentage of viable cells over the total imaged (at least 270 cells).

Figure 6.4 shows the results of the experiments of cell viability on composite materials **PEG-NP**. The green and red bars represent the positive and negative control experiments, serving as reference respectively for cytocompatible and cytotoxic materials. As expected, every tested sample showed no cytotoxic effect at all. The percentage of viable cells is around 99% with negligible standard deviation (The largest value obtained was 0.8%). These results were similar to those typically obtained for cell cultured on tissue culture plates, i.e. control sample (Figure 6.5).

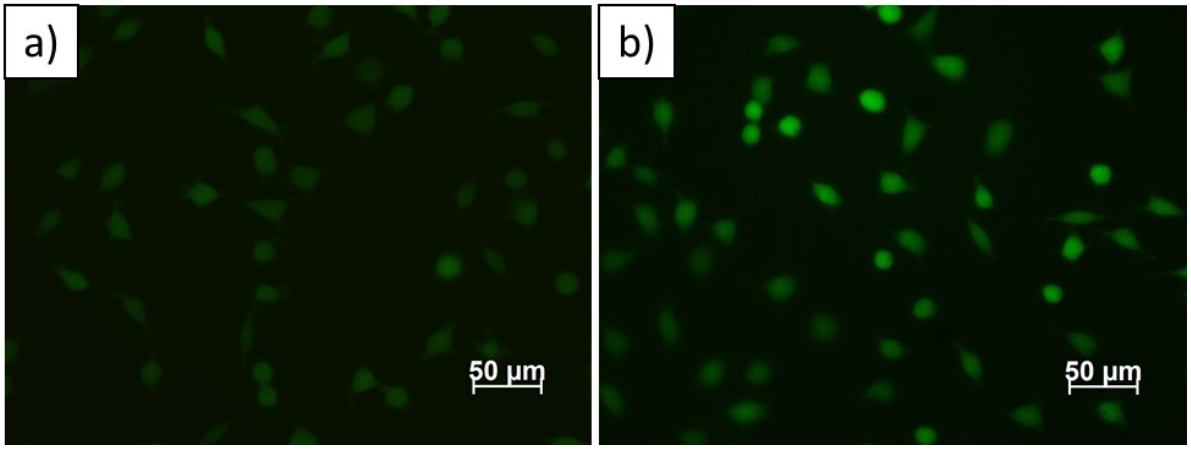

Figure 6.5: Live/Dead assay of fibroblast cultured on: a) tissue culture plate, b) a composite sample containing Au spheres.

No differences related to the shape or size of the nanoparticles could be detected. As hypothesized, the cytotoxic effect of the nanoparticles was eliminated by immobilization of them on the surface of a polymeric matrix. We can state that immobilized nanoparticles have no harmful effect on cellular cultures regardless of their size.

6.3.1.2 Adhesive behavior of fibroblast on PEG-NP composite materials:

In order to verify whether the inclusion of metallic nanoparticles on the surface of **PEG** hydrogels modified the inherent anti-adhesive properties of the substrate, we performed adhesion experiments with L929 fibroblasts. Cells were seeded and incubated 24 hours at 37°C and 5% CO_2 atmosphere. After incubation, the cells were fixed.

To quantify the effect of the nanoparticles on the adhesive behavior of the fibroblast, the cell area was measured. For each sample, around 200 cells were measured except in the control case of fibroblast on pure **PEG**, where fewer cells were found on the sample area. Live observation demonstrated that those cells were indeed non-adherent (floating) cells, according to the expected situation on such samples.

Two control experiments were carried out to reproduce the best and the worst adhesive situation, namely on tissue culture plate (TCP) (considered as an adhesive material) and on **PEG** (no adhesion). Figure 6.6a shows the typical value of the cell area in those cases: Non-adherent fibroblasts showed projected areas of around 198 ± 35 μm^2, while adherent fibroblasts showed average areas of 614 ± 220 μm^2. Adherent fibroblasts on TCP can fill areas of up to 1500 μm^2.

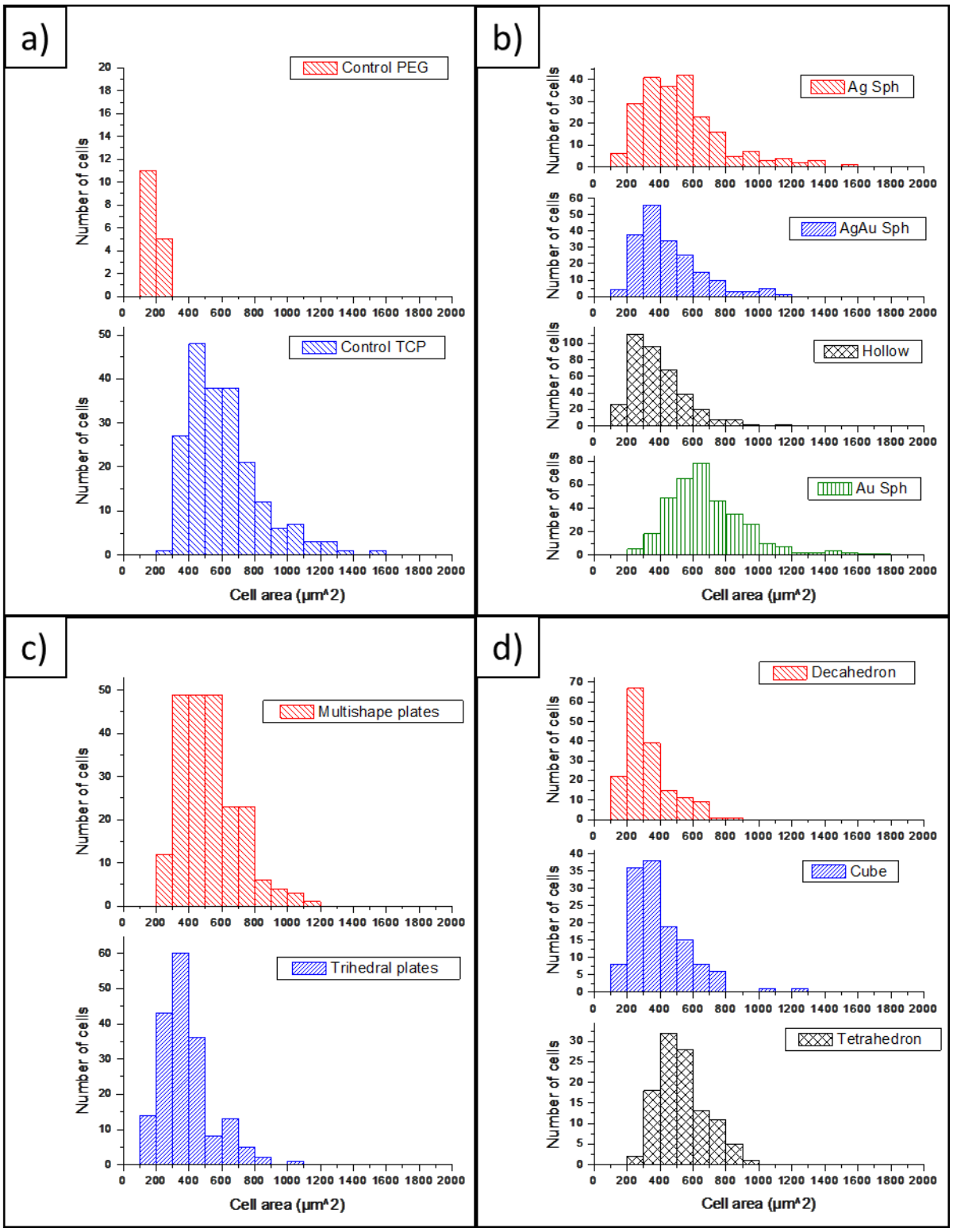

Figure 6.6: Histogram of the cell area of fibroblasts cultured on: a) control substrates, b) composites with spherical nanoparticles, c) 2D nanostructures and d) 3D nanostructures.

As expected, the composite materials **PEG-NP** showed better adherent properties than pure **PEG** samples. In all cases, cells adhered and spread with only a small percentage of

round shaped cells observed. Both optical and SEM analysis confirmed the expectations (Figure 6.7). The shape and size of the cells were similar to those of cells cultured on TCP.

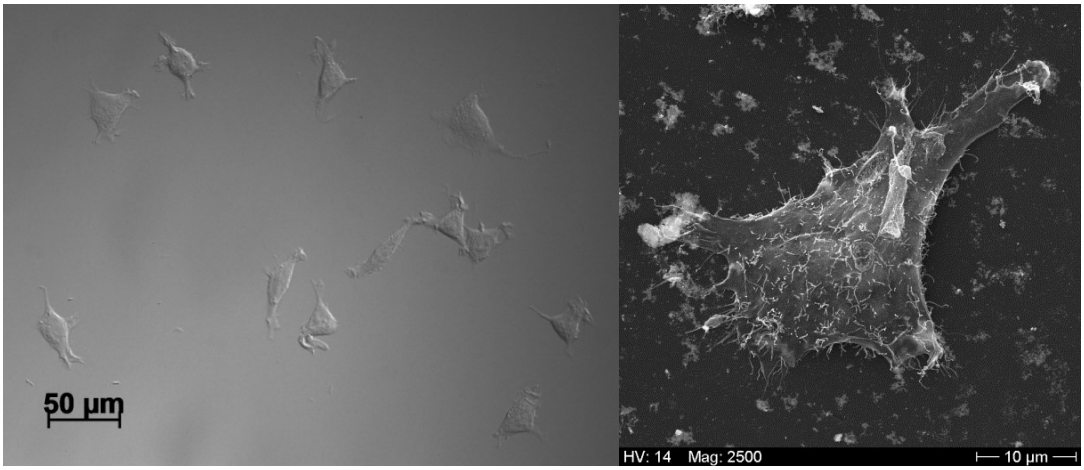

Figure 6.7: Fibroblast adhering on composite sample PEG-Au nanospheres (Left: Optical image, Right: SEM image).

Regarding the histogram of cell areas (Figure 6.6) it can be seen that on 2D gold structures (Figure 6.6c) the cells had areas close to those of non-adherent cells. These shapes induced adhesion but did not enhance spreading. A similar situation occurred with 3D structures (Figure 6.6d); the maximum of the histogram was located around 300 μm^2. Only tetrahedral nanoparticles showed to increase slightly the spreading. However, fibroblast cultured on samples containing spherical nanoparticles, especially Ag and Au nanospheres (142 nm and 21 nm respectively), spread more than on the other cases with an average area of 688 ± 238 μm^2 and maximum values of 1795 μm^2. These sizes were even larger than those obtained on TCPs.

Once the capacity of modifying the adhesive properties of **PEG** with metallic nanoparticles was established, the next logical step was to apply these composite materials in more complex samples. Au nanospheres stood out among the tested nanoparticles as the material which induced greater degrees of spreading (other shapes and sizes tested in this work showed similar results). For this reason, further experimentation was carried out using exclusively this kind of nanoparticles.

6.3.2 Patterning with **PEG-AuNP** composite materials:

Patterns are interesting because they enable researchers to create contrast zones and study the preference of the cells for one or another area. In this section, we present several

methods to generate micropatterns (lines) of AuNPs on **PEG** samples with the aim of being able to control the adhesion site for the adhesion of fibroblast cells.

*6.3.2.1 **PEG-AuNP** as filler for FIMIC samples:* [3]

As previously stated (see Chapter 1), the FIMIC method is a useful tool to generate surface patterns with UV-curable polymers. In this case, AuNPs were mixed with the liquid pre-polymer of **PEG** and used as filler to generate FIMIC samples. The samples were prepared and characterized, proving that the Au was present only at the filler lines of the samples [68]. Fibroblasts were seeded on these samples and incubated for 24 hours as outlined in the experimental section.

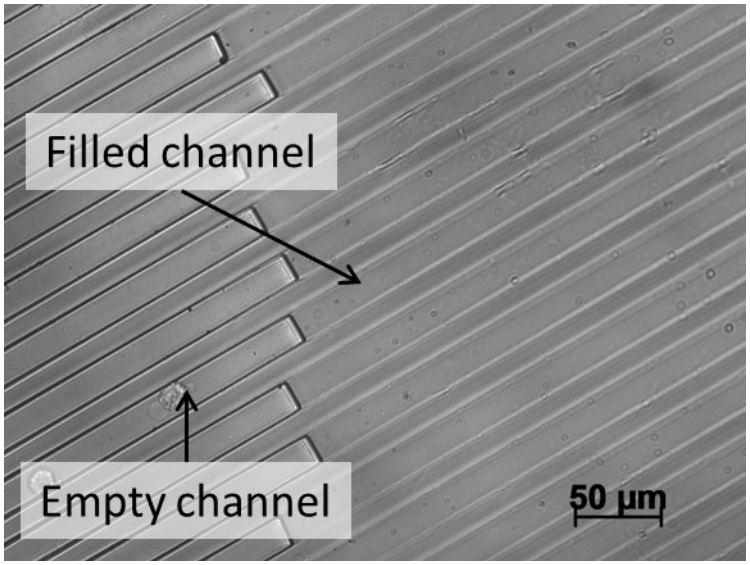

Figure 6.8: Adhesion experiment on a FIMIC sample with PEG 575 0% CL as mold and composite PEG-AuNP as filler.

Cell adhesion experiments showed, contrary to our expectations, no adhesion on the FIMIC samples (Figure 6.8). A plausible explanation is that the content of accessible Au on the surface was too low; the mix **PEG-AuNP** filled the channels, incorporating AuNPs inside the whole volume of the grooves, including the cell-accessible surface (Figure 6.9). With this method, a lot of AuNPs were "wasted" inside the channel, where they cannot be reached by the cells, leaving only a small fraction arising on the surface of the substrate.

[3] The work described in this section was done in collaboration with Dr. Manar Arafeh.

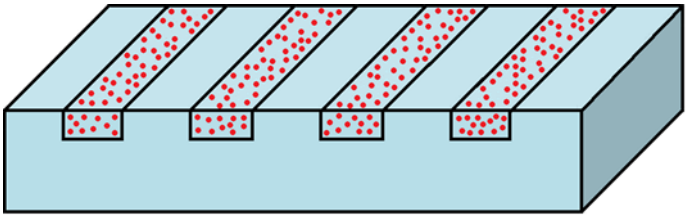

Figure 6.9: Schematic representation of a FIMIC sample with PEG-AuNP composite mix as filler. The AuNPs (red dots) are distributed inside the channel and on the surface of the sample.

These gold inclusions modified the elastic properties of the surface of the sample [68], however this did not seem to affect the adhesive behavior of the fibroblasts.

The preparation of FIMIC samples using **PEG-AuNP** composite mix as filler presented several disadvantages. One of them, as explained above, was the loss of the active component inside the volume of the filled channel. To solve this, the concentration of AuNPs in the mix should be increased, but this presented another problem, namely the agglomeration of the AuNPs. It was decided to develop a new strategy to reduce the necessary amount of AuNPs to achieve satisfactory modification of the substrate to induce adhesion.

6.3.2.2 FIMIC-transferring: [4]

This method is a combination of the FIMIC procedure and the transferring used in the Section 6.3.1. Our hypothesis was that if a FIMIC sample is prepared on a SiO_2 wafer coated with AuNPs instead of a glass slide as usual, the gold will be transferred to the filled lines after polymerization, because the acrylate groups of the liquid filler are all available to react with the linker of the gold during UV-curing. After peeling the sample from the SiO_2, the stripes of AuNPs corresponding to the filled lines should be transferred to the surface of the polymeric substrate (Figure 6.10).

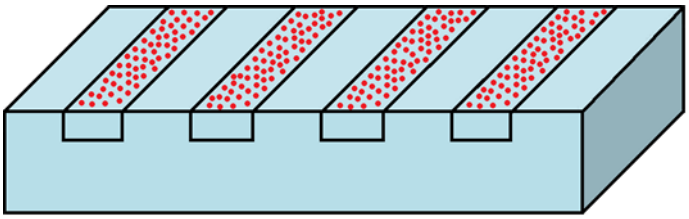

Figure 6.10: Schematic representation of a FIMIC-transferring sample with the AuNPs (red dots) on the surface of the filler lines.

[4] The work described in this section was done in collaboration with Çiğdem Yeşildağ

On these samples, the AuNPs should be located directly in contact with the cells, ensuring the cell-substrate interaction. At the same time, these substrates enjoyed the advantages of the FIMIC method, for example the versatility to use different materials for mold and filler.

Figure 6.11 is a representative image of the adhesion experiments on FIMIC-transferring samples. Fibroblasts adhered on the FIMIC area ignoring the pattern. The cells were located equally on the filled lines and on the mold lines. The adhesion of fibroblasts on **PEG** substrates verified the transferring of the AuNPs, however, this transfer occurred on the whole surface of the substrate and not only to the filled lines as expected. This was corroborated by AFM measurements of the silicon substrate after transferring (Figure 6.12). The height image was taken on an area not reached by the capillary filling (outside the FIMIC zone). Topographic features of 20 nm were detected, corresponding to the size of the AuNPs. The topography formed a pattern of 10 µm with a separation of 50 µm, which were the sizes of channel and mold lines respectively. This confirmed that on areas not reached by the filler, the gold was transferred to the mold lines as well.

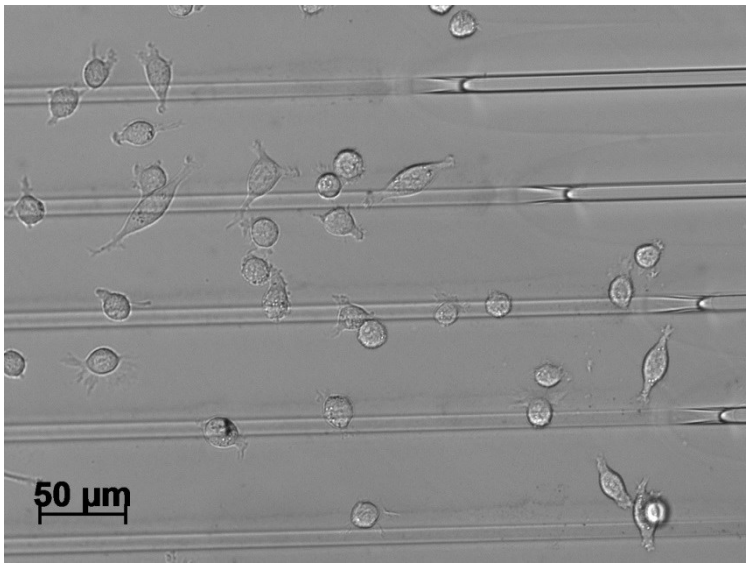

Figure 6.11: Fibroblasts L929 cultured on a FIMIC-transferring sample. The filled lines are 10 µm width with a separation of 50 µm.

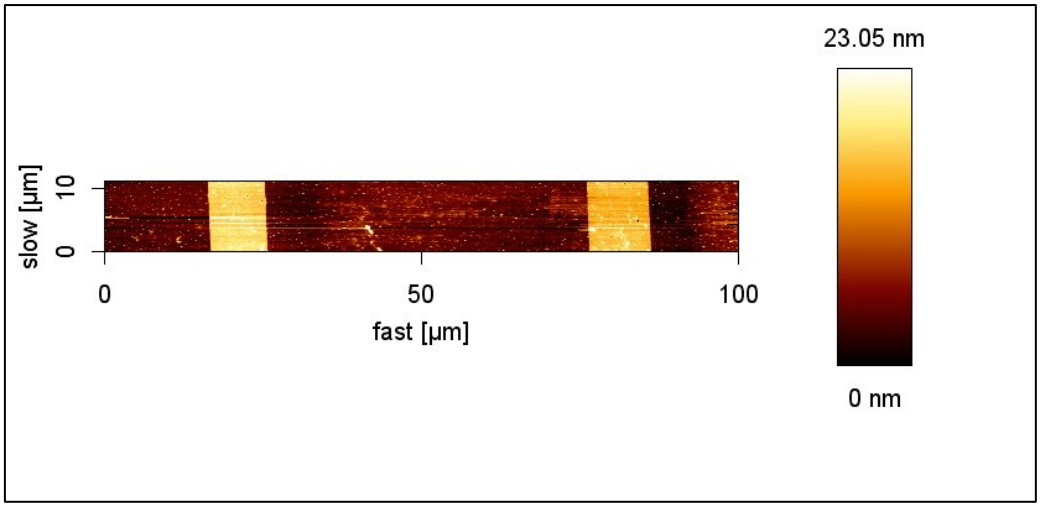

Figure 6.12: Height image of a silicon substrate after FIMIC-transferring obtained by AFM analysis. In the analyzed area, the substrate was in contact with a PEG mold with dimensions 10-50, where 10 µm was the width of the empty channels and 50 µm was the area in contact with the silicon substrate.

A possible reason for this unselective transfer may be the presence of a thin scum-layer on the surface of the sample. The AuNPs on the SiO_2 wafer increased the roughness of the substrate and, consequently, the contact between mold and the surface may not have been good enough to avoid the appearance of a scum-layer (see Chapter 1).

Another cause could be the presence of free acrylate groups on the mold lines. As seen in Chapter 2, to avoid delamination of the FIMIC samples, the mold was irradiated with UV for a short period to obtain a solid sample with free acrylate groups to react with those belonging to the filler material. Free acrylates on the surface of the mold contacting with the SiO_2 were, therefore, also available to react with the AuNPs, transferring them to those areas as well.

Both situations were difficult to avoid. Therefore, a different approach was conceived to generate surface patterns.

6.3.2.3 Pattern-transferring: [5]

The idea behind this method is to generate patterns of AuNPs on SiO_2 wafers and to transfer them into **PEG** hydrogels. After transferring, a flat substrate with a clearly defined pattern of AuNPs on the surface was obtained (Figure 6.13).

[5] The work described in this section was done in collaboration with Çiğdem Yeşildağ and Christoph Bartsch.

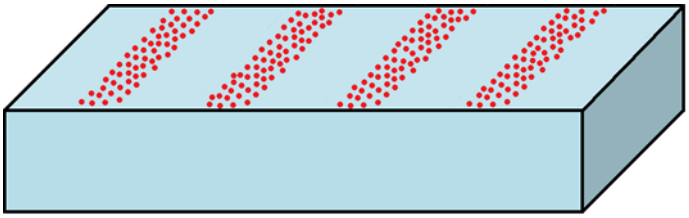

Figure 6.13: Schematic representation of a pattern-transferring sample. The AuNPs (red dots) are located on the surface of the gel forming a pattern.

The transfer of the AuNPs could already be confirmed by eye observation; the sample acquired a ruby-red coloring typical for gold spheres of 20 nm [68].

Fibroblasts were seeded on the hydrogels and incubated for 24 hours. As predicted, optical images of the samples showed adhesion only on the areas of the hydrogel patterned with AuNPs (Figure 6.14). Cells adhered, spread and aligned to the direction of the pattern.

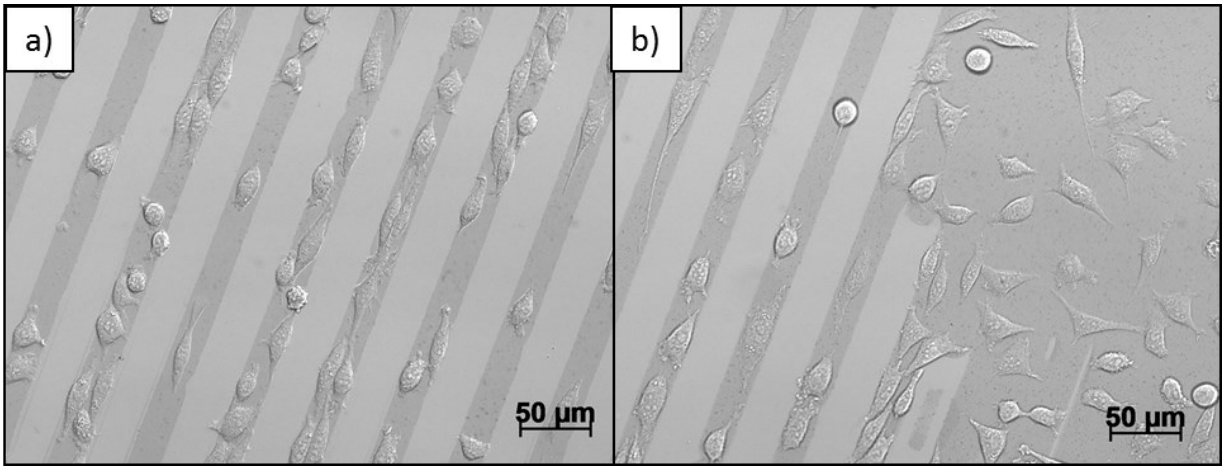

Figure 6.14: Optical image of fibroblast adhering on a pattern-transferring sample. The darker lines correspond to the patterns of AuNPs.

The pattern of AuNPs could already be recognized on the optical images as darker lines (Figure 6.14). AFM analysis showed no gold nanoparticles on the surface of the silicon wafer after transferring (image not shown), confirming complete transfer of the gold particles. Height images of the hydrogel in swollen state showed topography of 20 nm in lines of 25 µm width (Figure 6.15). These values correspond to the height of the gold nanoparticles and the size of the pattern created on the silicon wafer respectively. The phase image confirmed that the pattern was generated by different materials, namely gold and **PEG**.

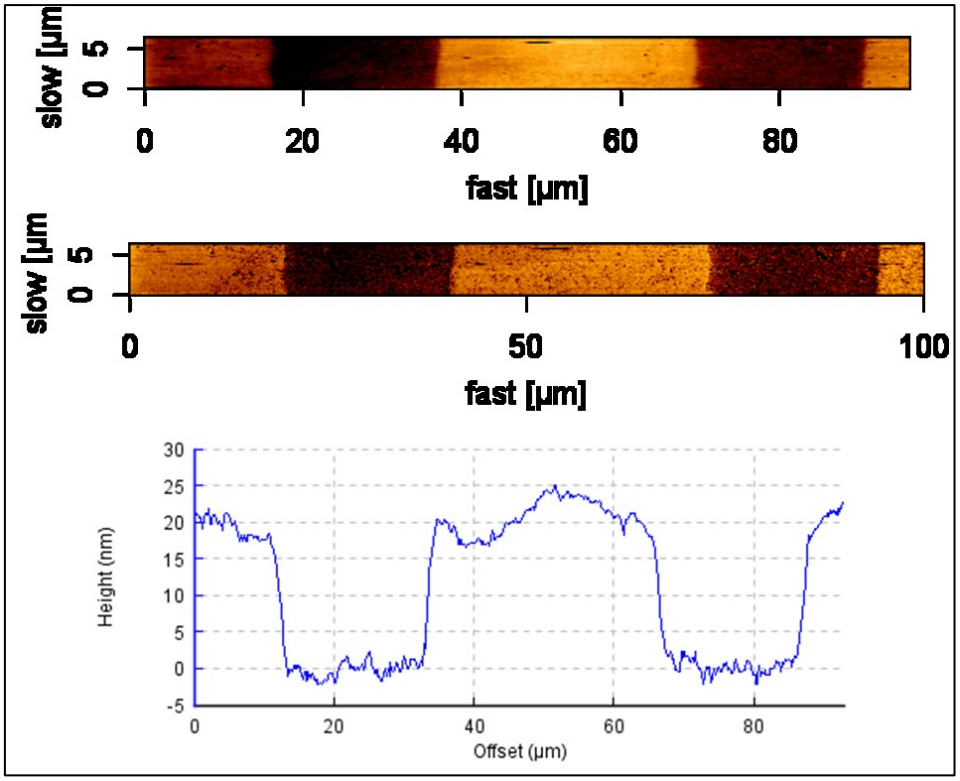

Figure 6.15: AFM height image (Top), phase image (Middle) and cross-section profile (Bottom) of a pattern-transferring sample with a gold pattern of 25 µm. Measured in swollen state.

In Figure 6.14b the edge of the pattern can be seen. On the non-patterned zone fibroblasts adhered everywhere, as happened on hydrogels with transferred metallic nanoparticles (see Section 6.3.1.2). This image confirmed that the dark areas corresponded to transferred gold, while the bright ones were pure, anti-adhesive **PEG**.

In this case, the size of the pattern (25 µm) was wide enough to allow a cell to completely sit on it and even up to two cells can fit inside the pattern next to each other. At the same time, the separation between lines (25 µm) was sufficient to avoid line bridging (cells spread connecting two adjacent Au-patterned lines). Different pattern sizes may also be interesting to, indeed, induce line crossing and promote migration perpendicularly to the pattern direction. These samples can, therefore, be used as templates to control and direct cell migration.

These samples successfully generated a surface pattern on PEG substrates that can be recognized by fibroblast, inducing cell adhesion exclusively on the patterned sites. They were also easier to be manufactured and overcame the limitations of the previously presented methods, i.e. low efficiency due to loss of active material in the volume, risk of

formation of scum-layer, risk of delamination and uncontrolled transfer of the gold nanoparticles.

6.4 Conclusions

In the first part of this chapter, the cytocompatibility of composite materials of **PEG** containing transferred metallic nanoparticles on the surface was tested with fibroblast cells. Nine different shapes of nanoparticles were used: gold spheres, silver spheres, gold/silver (core/shell) spheres, gold hollow spheres, gold multishape plates, gold triangular plates and three-dimensional gold tetrahedrons, cubes and decahedrons. All materials showed high cytocompatibility (99% cell viability) after 24 hours.

The modification of the anti-adhesive properties of the substrate material (**PEG**) by the addition of the metallic nanoparticles was investigated. Fibroblasts cultured on composite materials adhered and spread, contrary to the observations on pure **PEG** samples. Substrates containing 20 nm gold nanospheres showed the best results, with cells spreading areas even greater than those measured on tissue culture plates.

Once the effectiveness and cytocompatibility of the composite materials was verified, different methods to generate patterned samples applying these materials were investigated.

FIMIC samples prepared with a mix of **PEG** and gold nanospheres as filler material were cultured with fibroblasts. After the incubation time, the samples were investigated and no cell adhesion was detected. Our suggestion for this is that the amount of gold nanoparticles present on the surface of the substrate, ergo in contact with the cells, was too low, because the nanoparticles were distributed inside the whole volume of the channels and not preferentially located on the surface.

A new approach was then pursued; to prepare a FIMIC sample on a SiO_2 wafer coated with gold nanoparticles and make use of the free acrylate groups of the liquid filler to link with the gold nanoparticles and transfer them solely to the filler lines of the FIMIC samples (FIMIC-transferring). Our measurements indicated that the gold was not only transferred to the filler lines but also to the mold ones, obscuring the pattern. Two phenomena may be

behind this effect: The formation of scum-layer due to a bad contact between mold and silicon wafer or the reaction between acrylate groups of the mold (left free to react with the filler and avoid delamination) and the linker of the gold nanoparticles.

Another strategy was suggested; the pattern of gold nanoparticles was generated on the silicon substrate and transferred afterwards to the PEG hydrogel (pattern-transferring). We proved that the transfer of the patterned lines of gold nanospheres was effective and fibroblast adhesion experiments showed that those patterns created specific anchoring sites for cell adhesion in contrast with the anti-adhesive **PEG** background. This method overcame the limitations of the previously presented ones and was a good candidate for the preparation of chemically patterned substrates to control and direct cell migration.

Despite the good initial results, the pattern-transferring method could be improved. If the presence of acrylate groups in the shortly UV-cured mold of **PEG** caused transfer of gold to the mold lines in the FIMIC-transferring samples, what was initially an inconvenience can become useful. Patterns much larger than those obtained by removing the gold with the **PEG** filled channels of micro-molding in capillaries samples can be generated by deprinting the gold nanospheres from the silicon wafer simply by using **PEG** molds (micro-molding deprinting is limited by the maximal length of the capillary filling). This would manifest another variation of the micro-contact deprinting method (μCdP) developed in our group [162].

Chapter 7:

Immobilization of polymeric capsules by Fill-Molding in Capillaries for controlled interaction with adherent cells

7.1 Introduction:

Targeted drug delivery is a relatively young research area yet of great importance for human health improvement [163]. Traditional approaches for drug treatments present several challenges, like the maintenance of the therapeutic effect or the specificity of the delivery. These problems can be solved by using carrier systems.

Suitable carriers must fulfil some requirements [164]: i) Controlled load of the drug; to ensure the correct efficiency of the treatment, every carrier must contain the correct amount of drugs. Controlled load permits, as well, multi-load of different drugs for complementary treatment in the same carrier [165–167]. ii) Chemical and physical stability to resist enzymatic or chemical attacks inside the body as well as pH inactivation [164,168,169] or mechanical deformation due to cellular uptake [170]. iii) Specific targeting of the affected tissue to increase the efficiency and reduce undesired side effects [171,172]. iv) Controlled release of the drug to maintain the concentration along the cure or control the dose, timing and duration of the treatment [163,171].

In the past decades, several types of carries have been developed with the aim of fulfilling most of these requirements for drug delivery, e.g. polymeric micelles [173], liposomes [174], gels [175] or colloidal particles [176]. Among these methods, encapsulation in polyelectrolyte multilayer microcapsules stands out as a very promising technique. Capsules synthesized by the Layer-by-Layer method (**LbL**) present several advantages over other encapsulation techniques [71], such as the capacity to control the mechanical properties as well as the thickness of the capsule in the range of nm to µm [71], their loading capacity or the possibility to tune the biodegradability of the capsule by changing the material used for the shell [177,178].

One of the most important properties of **LbL** capsules is the possibility of modification of the shell [179]. Different types of materials and molecules can be added to the shell to accomplish a specific function:

Targeting of the cells can be achieved by several methods: Magnetic nanoparticles can be used to control the location of the capsules by applying a magnetic field, increasing the

concentration of capsules and, therefore, increasing the possibilities of cell uptake [180,181]. Biofunctionalization of the shell with antibodies has shown to achieve targeting of cells with a high specificity [172]; only cells containing the corresponding antigen will react to the capsule. This specificity has a great significance not only for targeting the desired tissue, but also at the cellular level. For example, for cancer treatments only tumor cells should be attacked while the surrounding healthy cells should remain unaffected.

To assess the effectiveness of the capsule uptake, it is necessary to confirm their location. Capsules can be detected by recognition of the electromagnetic spectrum of noble metals incorporated to the surface [179]. Other components such as quantum dots [182], or fluorescent dyes [183] can be used as well to track the position of the capsules by fluorescent analysis. Fluorescent dyes are also used as a model system to analyze the release of the load [184].

Controlled release of the capsules is of capital importance for *in vivo* applications, because it is a non-invasive method and no surgery is required. Noble metal nanoparticles can be used for remote release by laser induction, transforming the light energy into heat [184]. Near-infrared absorbing dyes apply the same principle to induce disruption of the capsule multilayer [185]. A laser source can also activate Photo Dynamic Therapy (PDT) agents which will destabilize the shell of the capsule and release the content [186]. Capsules containing magnetic nanoparticles showed a variable permeability when exposed to magnetic fields. This behavior has been also exploited for load and release of the charge [187]. Capsules containing DNA molecules on their shells decompose in solutions with high ionic strength, liberating their content [188]. Biodegradable capsules will also decompose when exposed to enzymatic activity inside the cell [178].

Other functionalities can be incorporated to the capsules by modification of the shell components: Silver nanoparticles can prevent bacterial adsorption and growth [189]. The addition of polymers like **PEG** can prevent the recognition of the capsules by phagocytic cells [18]. Liposomes can also be added to the shell to create multi-compartment capsules where two components can maintained separated until their reaction is required [190].

As previously stated, cell targeting plays a principle role in drug delivery. Drug vehicles in suspension must be labelled for recognition and uptake by the cells. At the same time,

unspecific administration of drug carriers requires an elevated concentration to ensure interaction with cells prior to uptake [183] We can use the opposite approach; inspired on Francis Bacon`s cite “If the hill will not come to Mohammed, Mohammed will go to the hill” [191] we aim to use soft lithographic methods to immobilize the carriers at the surface of cytocompatible materials, controlling the horizontal and vertical distribution, and thereby inducing controlled cell adhesion. In this way, contact between cells and capsules will take place without functionalizing the surface of the capsules with specific receptors and, at the same time, it is possible to reduce the necessary amount of carriers, approaching to an ideal situation, i.e. direct addition of drugs inside the cells. Once the capsule and cell are brought into contact, the capsule can be opened and the load released.

To prepare such materials, we propose the use of the FIMIC method. This technique has been previously employed in our group to generate composite materials of PEG-based polymers and nanoparticles, such as calcium phosphate or gold, thus introducing biofunctional particles inside the channels [67,68]. With this method, the particles can be horizontally distributed (Figure 7.1a), i.e. along the filled channels, as well as vertically (Figure 7.1b). To generate specific locations for cell interaction it is important to locate the particles close to the patterned surface, since particles inside the bulk material are not accessible for the cells and no advantage will be taken of their functionality.

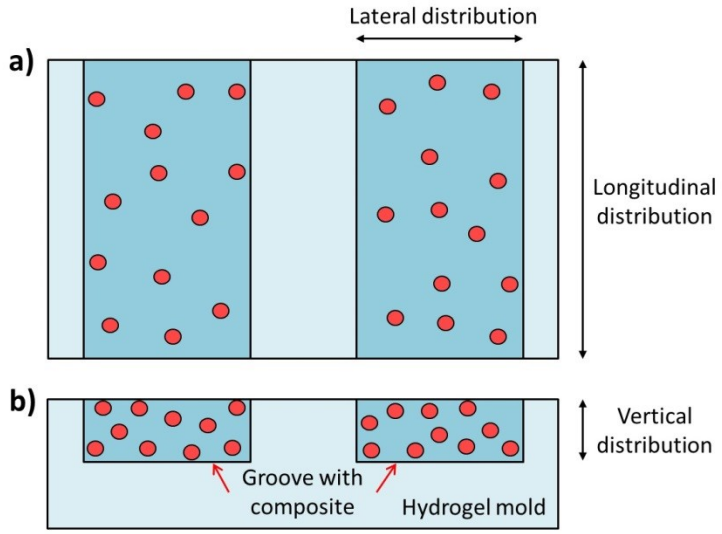

Figure 7.1: Schematic representation of a composite FIMIC sample: a) Top view showing the horizontal distribution of the particles, b) Cross-section showing the vertical distribution.

In this chapter, we present the formation of composite materials using PEG-based polymers and novel solid and hollow microparticles in combination with our recently

developed FIMIC method. Particles with a solid core of $CaCO_3$ were more robust than hollow capsules and for this reason **PEG** samples containing those particles were used as model system to explore the applicability of this method using microparticle composite materials. Hollow capsules were, however, more interesting than solid particles because of the capacity to load them with molecules to deliver to the cells and therefore they were used to investigate the interaction between cells and the composite material.

Two different approaches were applied regarding the polymer used as filler material in the FIMIC method: Composites of **PEG** with solid particles (**PEG-µP**) and with hollow capsules (**PEG-µCap**) were used. When both the mold and the filler are made of **PEG**, we had the advantage of presenting to the cells an anti-adhesive surface which was chemically, elastically and topographically homogeneous. It was expected that the microparticles in the filler locally modified the properties of the surface and induced cell adhesion, changing the traditional behavior of cells on **PEG** substrates.

A composite of **3BC** containing capsules (**3BC-µCap**) was also employed as filler. Using **3BC** as a base material for the composite, cell adhesion could be induced specifically on the filled lines, where the capsules were located. With this method, targeting of the cells can take place without the necessity of functionalization of the capsules for specific, biochemical targeting.

With these strategies, we aimed to investigate the feasibility of the immobilization of **LbL** capsules on the surface of cytocompatible hydrogels prepared by soft lithographic methods, and their effect on the interaction between the cell and the biomaterial. These composite materials presented two functionalities: First, the substrate could act as scaffold for tissue regeneration and migration. Second, the capsules could be used as drug carriers loaded with (bio)molecules such as nucleotides, peptides, growth factors or analgesics [192–195], as well as transfection vehicles when loaded with genetic material [196,197]. This kind of material could be extremely useful for tissue engineering, since these drugs can, among others, induce or suppress the expression of proteins [198] or enhance the healing process [199].

7.2 Materials and methods:

7.2.1 Microparticles:

As already specified in Chapter 2, we worked with two types of microparticles, i.e. hollow capsules of 3 µm in diameter and particles with solid core of $CaCO_3$ with sizes from 3 µm to 5 µm.

The shell of the microparticles was formed by layers of polyelectrolytes with opposite charge, namely poly(diallyldimethylammonium) (PDADMAC, positive) and poly(sodium styrene sulfonate) (PSS, negative).

To determine the concentration of the stock solution of capsules and particles, an aliquot was diluted 10 times in deionized water and 10 µL were placed in a counting chamber (Marienfeld Superior, Paul Marienfeld GmbH & Co. KG). The concentration obtained for the capsules was $2.4 \cdot 10^4$ capsules/mL and for the particles $6 \cdot 10^4$ particles/mL.

7.2.2 Composite materials:

Composite materials of **PEG** and solid $CaCO_3$ (**PEG-µP**) were prepared by direct mixing of the polymer and the stock solution of solid particles ($6 \cdot 10^4$ particles/mL). Acetone was added in order to increase the working volume and to facilitate the mixing and was subsequently removed by a stream of N_2. Three suspensions **PEG-µP** of 60 µL were prepared (Table 7.1):

Table 7.1: Suspensions of particles in PEG used for the experiments.

Volume of particle stock (µL)	Volume of PEG (µL)	Dilution rate	Concentration (particles/mL)
3	57	1/20	$3.0 \cdot 10^3$
12	48	1/5	$1.2 \cdot 10^4$
30	30	1/2	$3.0 \cdot 10^4$

With this method, the concentration of the stock solution was always reduced by the addition of the liquid polymer.

For these experiments two composites polymer/capsules were used; one using **PEG** as a base material (**PEG-µCap**) and another using **3BC** (**3BC-µCap**). To prepare them, 100 µL of the stock solution ($2.4 \cdot 10^4$ capsules/mL) were centrifuged at 5000 rpm during 5 minutes. The supernatant was removed and the pellet was immediately re-suspended with 50 µL of the liquid polymer. The resulting concentration was $4.8 \cdot 10^4$ capsules/mL.

For better analysis with confocal microscopy, the concentration was further increased, ensuring a larger presence of capsules inside the channels. In this case, the pellet was re-suspended in 25 µL of **PEG** obtaining a suspension of $9.6 \cdot 10^4$capsules/mL.

7.2.3 Preparation of the FIMIC samples:

FIMIC samples were prepared as described in Chapter 2. In this section, the mold was always prepared with **PEG** and the channels were filled with the corresponding composite material, i.e. **PEG-µP**, **PEG-µCap** or **3BC-µCap**. The curing times were 8 minutes for the mold and 20 minutes for the filled sample.

7.2.4 Fluorescence microscopy:

Fluorescence images were obtained using the equipment described in Chapter 2.

To determine the position of the surface of the sample while taking cross-section pictures, the hydrogels were submerged in an aqueous solution containing 1 mg/L of fluorescein sodium salt (Sigma-Aldrich) and left overnight. With this strategy the fluorescently-labelled hydrogel could be recognized by fluorescent microscopy and the interface microscope slide/hydrogel was clearer. As an alternative method to improve the contrast between the edges and the bulk material, the same samples were dried at atmospheric conditions. In this way, we avoided noise signals caused by fluorescein solution surrounding the sample.

Confocal and 3D images were made using a Leica TCS SP5 II Confocal Microscope (Leica, Wetzlar, Germany) with a 20x and a water immersion 63x objective. Excitation wavelengths used were 561 nm and 488 nm and detectors were set in the range of 637-666 nm and 508-537 nm for TRITC-dextran and fluorescein respectively. On the fluorescence images, the

capsules were represented by red dots and the fluorescein by green fluorescence. The scan speed used was 10 Hz for images and 100 Hz for 3D series. Images were analyzed and processed using the program Bioimage XD (Free software).

7.2.5 Cell studies:

Cell adhesion experiments were carried out following the instructions recorded in Chapter 2. Briefly, the samples were sterilized in ethanol and left overnight in PBS for complete hydration. A suspension containing mouse fibroblasts L929 (50000cell/mL) was dropped on the samples. After seeding, cells were incubated 24 hours at 37°C and 5% CO_2. Finally, the cells were fixed with formaldehyde for 30 minutes and observed under the microscope.

7.3 Results and discussion

7.3.1 FIMIC with particles:

The particles had better mechanical stability than the capsules due to their solid cores and were therefore used for the preliminary studies, i.e. application of the FIMIC method to fill the channels with the composite polymer/microparticle material.

Several channel widths narrow (10 µm), medium (20 µm) and wide grooves (50 µm), were analyzed to verify that the particles were carried by the polymer all along the filled channel (longitudinal distribution). **PEG** was used as a mold with **PEG-µP** as filler. The sizes of the molds and the concentration of particles used are summarized in Table 7.2.

Table 7.2: Experiments to determine the distribution and the optimal concentration of particles.

Exp.	Dimensions of the mold (w-d-h)	Concentration (particles/mL)
1	10-20-10	$3.0 \cdot 10^3$
2	50-10-10	$1.2 \cdot 10^4$
3	25-25-10	$3.0 \cdot 10^4$

The concentration of particles in the composite was increased progressively in order to guarantee a homogeneous distribution of the particles over the surface of the sample as well as a sufficient number of particles for cell interaction. The first two concentrations, i.e. $3 \cdot 10^3$ particles/mL and $1.2 \cdot 10^4$ particles/mL were too low and the channels were almost empty (Figure 7.2a and b respectively). When the composite contained $3 \cdot 10^4$ particles/mL (Figure 7.2c), the particles showed a good longitudinal distribution over the channels. According to these results, concentrations below $3 \cdot 10^4$ particles/mL were not recommended.

Regarding the size of the channel, it was confirmed that in all cases the particles reached the filling front (Figure 7.2b and c). This demonstrates that the capillary force was strong enough to carry the particles all along the channels. As was expected, this preparation method was applicable for particles of sizes in the order of 3 to 5 µm. It is interesting to note that some of the particles were outside of the FIMIC, i.e. on the empty channels (Figure 7.2b and c); however, they were always close to the border of the filled area. A feasible explanation might be that, during UV-curing, the volume of the polymer was reduced due to shrinking [63] and the particles could have been deposited on the empty areas. This phenomenon is comparable to the deposition of seaweed on the beach when the tide goes out.

When the lateral distribution of the particles, i.e. along the width of the channels, was analyzed, it was seen that they tended to accumulate close to the sides of the filled channels, especially in the case of wide channels (Figure 7.2b).

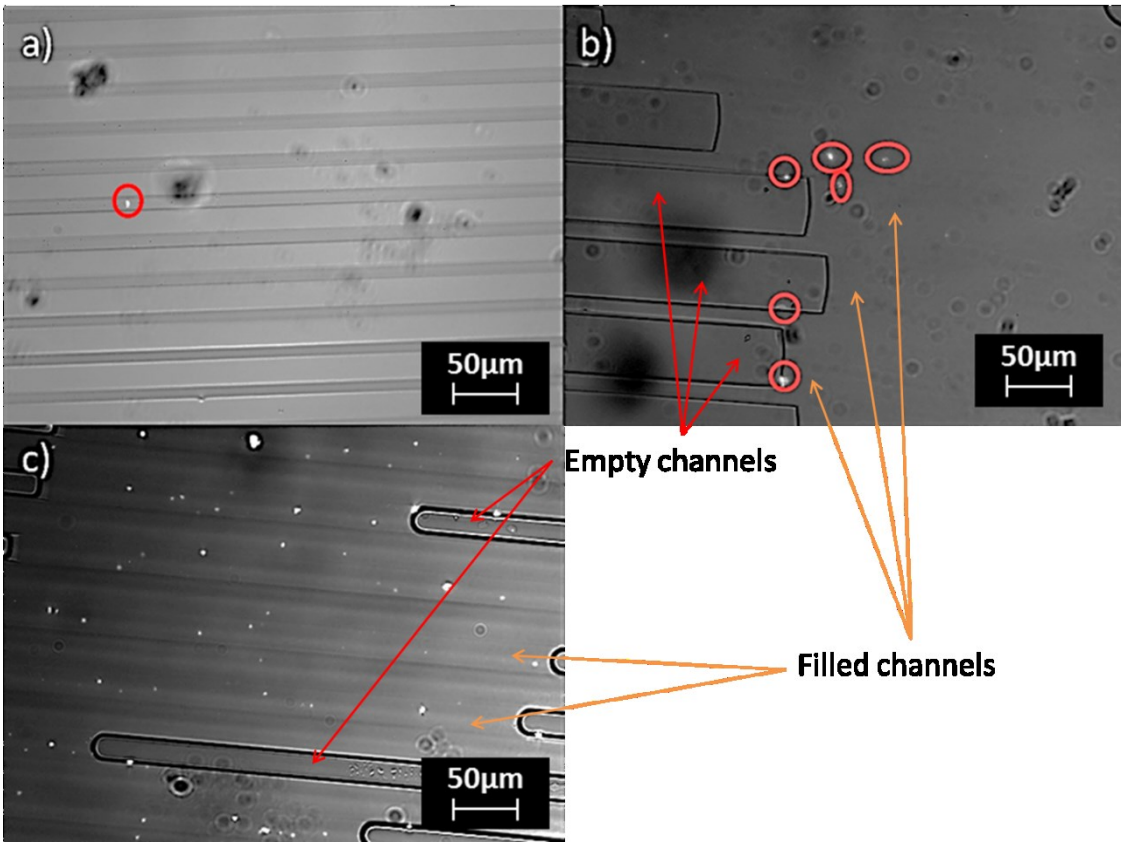

Figure 7.2: Merged fluorescent and optical images of the FIMIC samples a) 10-20-10 (3·103 particles/mL), b) 50-10-10 (1.2·104 particles/mL) and c) 25-25-10 (3·104 particles/mL). The bright dots represent fluorescent particles or clusters of them (Encircled in a) and b) for easier recognition).

The $CaCO_3$ particles formed aggregates (Figure 7.3b). Accumulation of particles was undesirable for several reasons: A homogeneous distribution of the particles would maximize the area for interaction between cell and material. At the same time, the formation of agglomerates could modify the size of the particle ensembles. The observed aggregates had sizes of the order of tens of micrometers and, therefore, the size of the channels may have become a limiting factor for the filling process. Figure 7.3a illustrates this phenomenon; a sample 10-20-10 was prepared using **PEG-µP** with the highest concentration, i.e. $3 \cdot 10^4$ particles/mL. Despite the relatively high concentration, only a low fraction of the particles entered the channels.

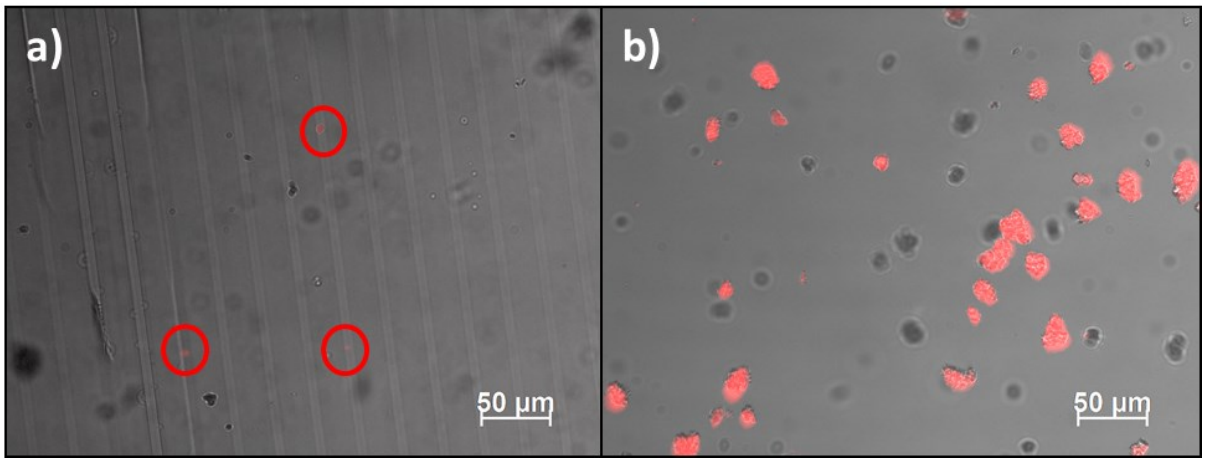

Figure 7.3: Combined optical and fluorescent images of a) a FIMIC sample filled with PEG-µP (Particles encircled for ease of recognition) and b) the drop of composite used to fill the grooves.

7.3.2 FIMIC with capsules:

Once the efficacy of the FIMIC technique had been demonstrated with $CaCO_3$ particles, the feasibility of the method using the capsules, which can be employed as potential drug carriers or transfection vehicles, was tested. The suspension of capsules was centrifuged and re-suspended in **PEG**, obtaining a composite **PEG-µCap** with a final concentration of $4.8 \cdot 10^4$ capsules/mL.

PEG molds with relatively narrow channels (10 µm) were prepared and filled with the composite material (**PEG-µCap**) (Figure 7.4). The hollow capsules had a diameter of 3 µm and, in contrast to the $CaCo_3$ particles, they did not form aggregates. In accordance with what was expected and in agreement with the results obtained for solid particles, the small monodisperse capsules entered inside the narrow channels (Figure 7.4). The capsules showed a good longitudinal distribution and capsules could be found at any position of the filled channels. Samples with shallow channels were also employed, i.e. with a channel depth close to the capsule size (Figure 7.4b). Even in this case, the size of the channel did not interfere with the filling process and the capsules were distributed homogeneously. These observations imply that a large variety of pattern sizes can be successfully used with the size of the capsule as a minimum, and only the concentration must be controlled to obtain a good distribution of capsules over the sample.

The previous observation of particles located at the empty channels was also seen using capsules. Regarding the lateral distribution, a preference for the side walls of the channels was observed as well.

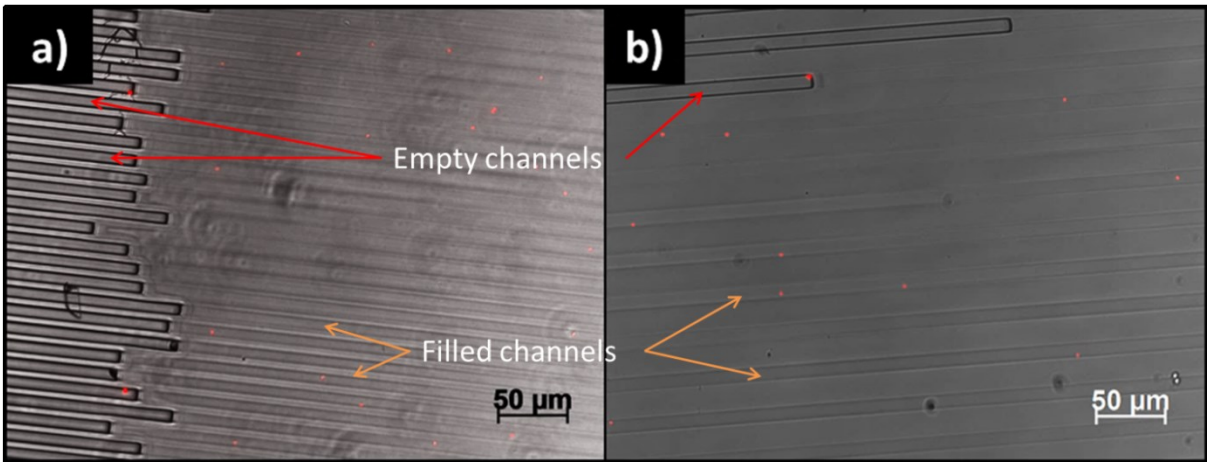

Figure 7.4: Combined optical and fluorescent images of a FIMIC sample a) 10-5-10 and b) 10-20-5 filled with PEG-µCap (4.8·104 capsules/mL).

For better understanding of the distribution of the capsules inside the channels, notably concerning their vertical distribution, confocal microscopy was employed. A suspension of capsules containing $9.6 \cdot 10^4$capsules/mL was then used on two different samples: one with 5 µm and another with 15 µm deep channels. In all cases the mold was prepared with **PEG** and the filler material used was **PEG-µCap**.

Capsules present in samples with 5 µm deep grooves were located close to the patterned surface (Figure 7.5). As could be expected, the shallow channel depth (5 µm) was not sufficient to create significant differences in the vertical distribution of the capsules (with diameters of 3 µm). Nevertheless, Figure 7.6 shows that the capsule on the right was closer to the surface than the one on the left, confirming that, in these samples, some degree of vertical distribution was possible.

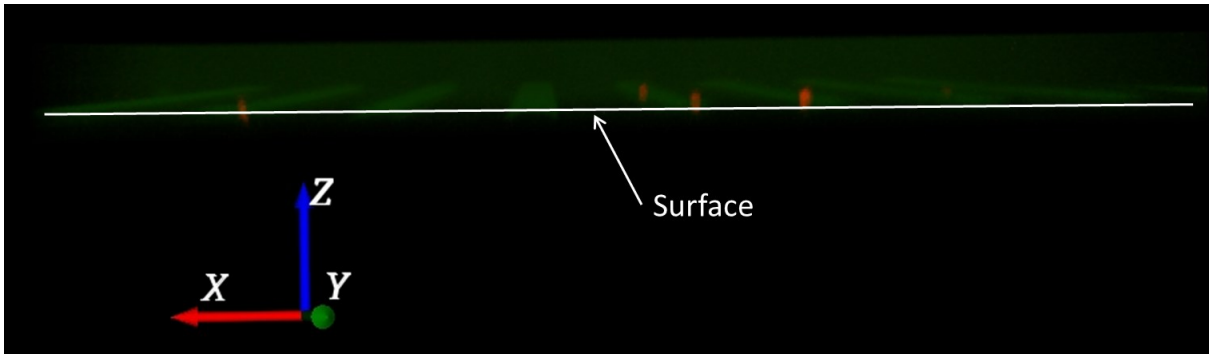

Figure 7.5: 3D representation of the fluorescent confocal image of a FIMIC sample (PEG-µCap in PEG) 10-20-5 containing fluorescent capsules (red dots). Green fluorescence corresponds to the volume of the hydrogel, which was stained with fluorescein. The position of the surface is indicated with a white line.

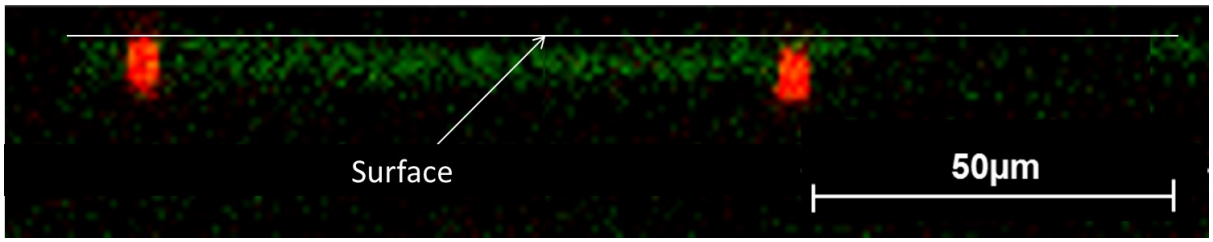

Figure 7.6: Cross-section of a FIMIC sample (PEG-µCap in PEG) 10-20-5 made using confocal microscopy. The surface is represented by the green fluorescence (Highlighted with a white line).

In the case of 15 µm deep channels, the differences in the vertical position of the capsules were easily noticeable (Figure 7.7). When greater depths were used, the capsules were randomly distributed in the vertical direction, without preference for the bottom of the channel or the surface.

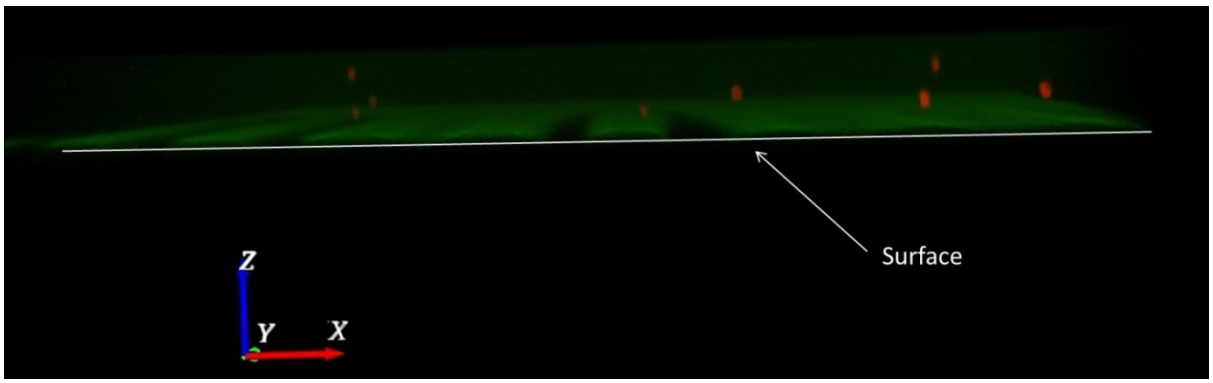

Figure 7.7: 3D representation of the fluorescent confocal image of a FIMIC sample (PEG-µCap in PEG) 10-20-15 containing fluorescent capsules (red dots). Green fluorescence corresponds to the volume of the hydrogel. The position of the surface is indicated with a white line.

Figure 7.8 shows cross-sections of a 10-20-15 sample at different points. The patterned surface is recognized by green fluorescence and marked by a white line. Three capsules can be seen at different distances from the surface, confirming that the capsules can be located at any vertical position of the filled channel.

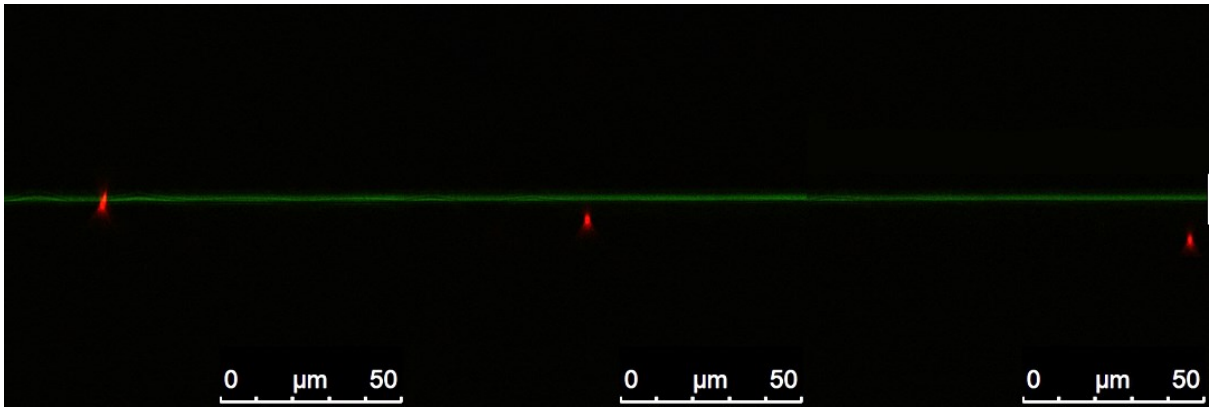

Figure 7.8: Cross-section image obtained by confocal microscopy at three different positions of a FIMIC sample 10-20-15. The green line corresponds to the fluorescently-dyed surface. The red points correspond to capsules.

Atomic force microscopy analysis of the substrate surface was carried out in order to investigate possible modifications of the surface induced by the addition of the microparticles. AFM images can show topographic features down to the nanometer scale, therefore, capsules placed on the surface of the sample should be detected. Several samples were investigated in locations where capsules were optically recognized. However, height images did not reveal the presence of capsules (Figure 7.9).

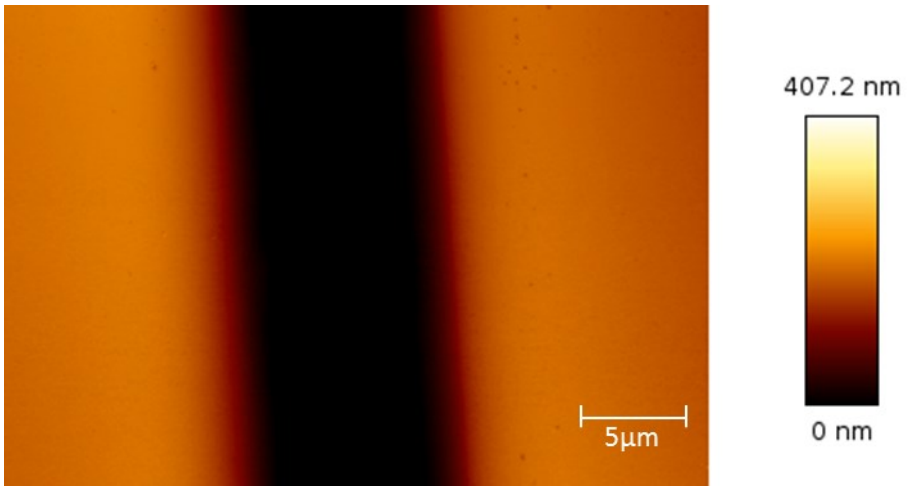

Figure 7.9: Height image of a FIMIC sample 10-20-5 showing a topographical difference between the mold and the filler. Dark area: Filler PEG 575 0%CL. Bright area: Mold PEG 575 10%CL. Sample measured in dry state.

Analyses in the intermittent contact mode can also show the surface properties of the sample; lock-in phase images represent differences in the interaction between the surface material and the AFM tip. If, for instance, the lock-in phase image of the section scanned in Figure 7.9 was observed, two clearly defined areas with different surface properties, i.e. the mold of **PEG** 10% CL (dark) and the filler of **PEG** 0% CL (bright) were detected and could be

discriminated from each other (Figure 7.10). A darker point inside the filler line was also recorded. This point corresponded to a capsule (Confirmed by optical imaging, image not shown) and demonstrates that inclusion of the capsules in the FIMIC samples modified the surface properties of the sample when close to the surface.

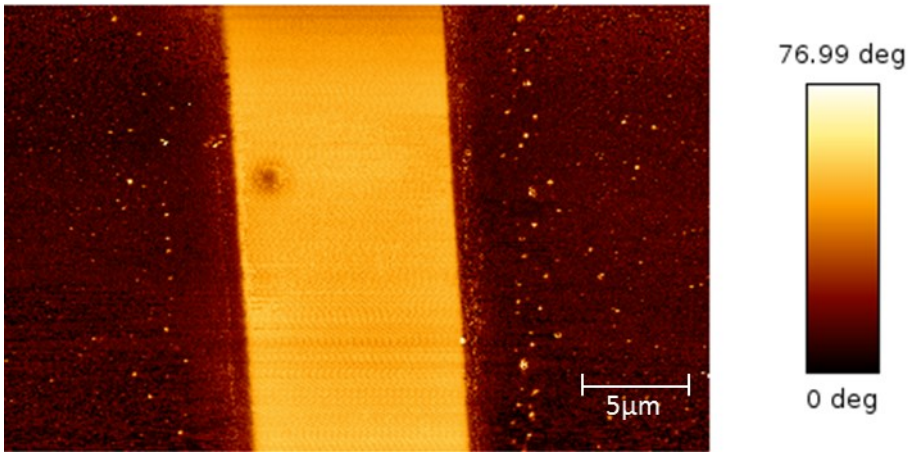

Figure 7.10: Phase image of a FIMIC sample 10-20-5 showing a capsule that modifies the hardness of the filler material. Dark area: Mold PEG 575 10%CL. Bright area: Filler PEG 575 0%CL. Sample measured in dry state.

This capsule, as for the others, was undetectable on the height image (Figure 7.9). In other words, the capsule was close to the surface but not protruding from it. These results highlighted that, despite the vertical distribution of the capsules, they were rarely exposed on the surface and did not modify the topography of the FIMIC sample.

As already explained in the introduction, the interest in using **3BC** as filler material in combination with capsules relies on the adhesive properties of this polymer. Nevertheless, the physical properties of **3BC** are different to those of **PEG** and they may affect the capillary filling of the channels. Consequently, the applicability of this method with the **3BC** system had to be confirmed. The concentration of capsules used for this experimentation was of $4.8 \cdot 10^4$ capsule/mL.

Figure 7.11 shows that, also when using **3BC-µCap** as the filler, the capsules were well distributed along the channels. As observed for **PEG**, some capsules were located at the filling edge and even outside the filled areas. The capsules were mainly positioned on the walls of the filled channels.

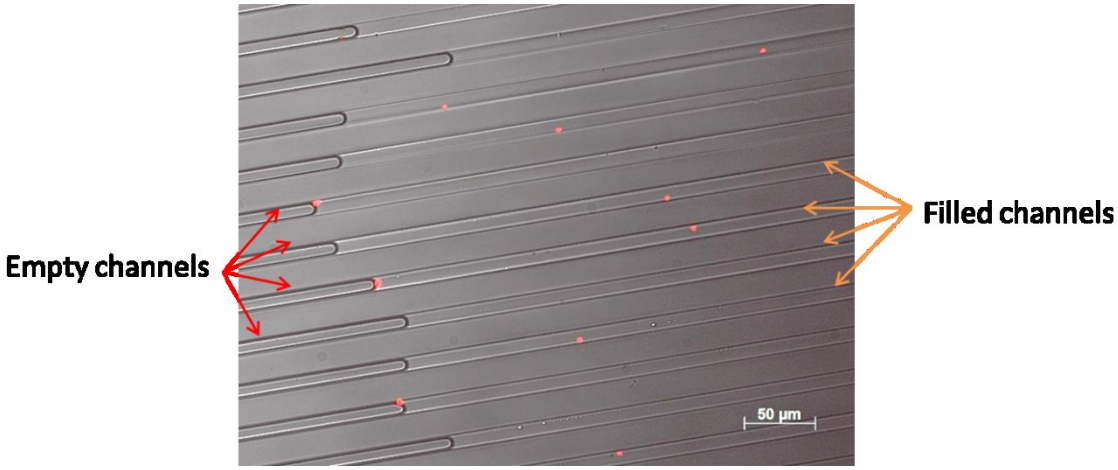

Figure 7.11: Combined optical and fluorescent image of a FIMIC sample 10-20-5 using PEG as the mold and 3BC-µCap as the filler.

7.3.3 Cell adhesion experiments:

One of the hypotheses of this work was that only capsules exposed at the surface could modify the chemical properties of the anti-adhesive **PEG**, thereby acting as anchoring sites for cell adhesion (the shell of the capsules is formed by layers of poly(diallyldimethylammonium) and poly(sodium styrene sulfonate)). Besides altering the chemical properties, exposed capsules could slightly modify other local properties as well, e.g. the surface topography and elasticity, which may also induce cell adhesion on intrinsically anti-adhesive PEG surfaces, as has been seen previously [22,64]. The adhesive behavior of fibroblasts on FIMIC samples prepared with **PEG-µCap** was analyzed to verify this hypothesis. According to the observed distribution of the capsules, it was decided to use molds with 5 µm deep channels aiming to locate the capsules as close to the patterned surface as possible.

The cells were incubated for 24 hours, fixed and observed under microscope. Sparse fibroblast adhesion was seen (image not shown), corresponding to the behavior previously observed on FIMIC samples prepared with pure **PEG** [66]. The presence of capsules in the filled lines showed no effect on the adhesiveness of the material. An explanation could be that using shallow channels alone was not enough to guarantee the presence of capsules on the surface. Only those capsules placed on the surface of the material can act as anchoring points for the cells since no other cues for cell adhesion are present.

Since the incorporation of capsules was not sufficient to induce cell adhesion onto the non-adhesive base material, **3BC-µCap** was also used as the filler material, taking advantage of the adhesive contrast between **PEG** and **3BC** for inducing adhesion specifically on the areas where the capsules were present. Figure 7.12 shows that the cells adhered exclusively onto **3BC-µCap** stripes. Cells that were found on top of the mold lines were in fact anchoring to the adjacent composite lines, practically bridging over the anti-adhesive **PEG** lines. The strategy was successful. As expected, cells adhered onto **3BC** stripes, thus at the areas where the capsules were present (Figure 7.12a) without the necessity of biofunctionalization. Nevertheless, the cells were not necessary adhering right on top of the capsules, as seen in Figure 7.12b. Again, it could be reasoned that capsules do not act as sites for preferential adhesion because they were likely not protruding from the surface and, therefore, not accessible for the cells.

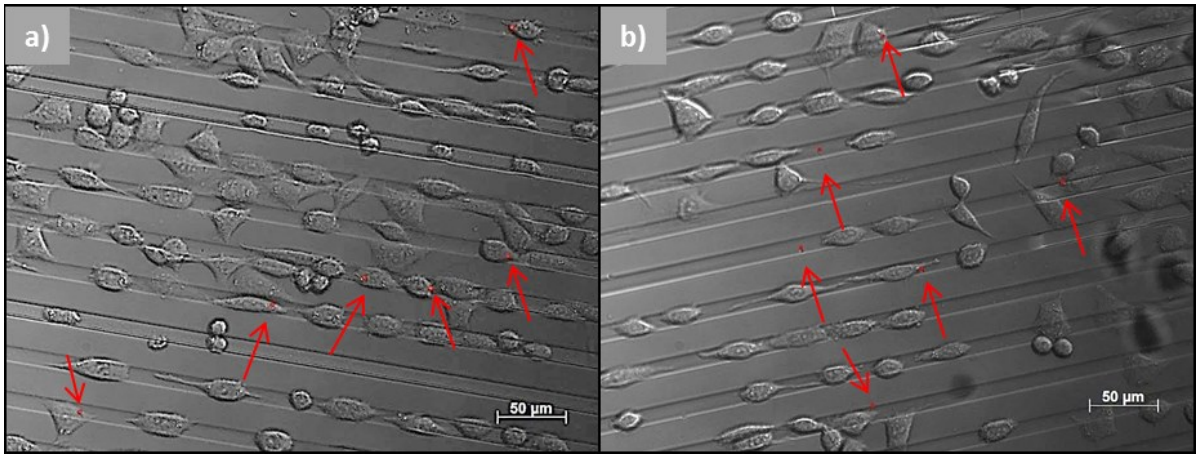

Figure 7.12: Combined optical and fluorescent image of fibroblast adhesion after 24 hours on a FIMIC sample (3BC-µCap in PEG) 10-20-5. Capsules are represented by red dots and marked by arrows.

7.4 Conclusions

Composite materials of PEG-based polymers, namely poly(ethylene glycol) (**PEG**) and a block co-polymer of PEG and poly(propylene glycol) (**3BC)** and microparticles were generated, demonstrating that both $CaCO_3$ particles and hollow capsules were robust enough to resist the centrifugation process necessary to achieve the working concentration required without being destroyed.

The FIMIC method was successfully applied to locate those microparticles with microscopic precision at the surface of an intrinsically cell-repellent hydrogel. A

homogeneous longitudinal and vertical distribution of the microparticles within the channels of the mold was confirmed, regardless of the polymer used for the composite material, i.e. no preference for any specific position inside the filled channel. It was observed that not only the concentration but also the size of the channel became a limiting factor for the efficiency of the filling process when solid particles were used, due to their tendency to agglomerate.

Intriguingly, the mere addition of capsules to pure **PEG** did not modify the cell-repellent properties of the hydrogel. Samples combining **PEG** as a mold and **3BC** with capsules (**3BC-µCap)** as filler material corroborated previous observations, i.e. adhesion of fibroblasts exclusively on the **3BC** lines. Generating an adhesive pattern on the surface, direct adhesion of fibroblast onto regions containing capsules immobilized on the surface of the gel was achieved without necessity of biofunctionalization. This is an advantage compared with the unspecific administration of capsules in suspension, where the concentration has to be elevated to ensure interaction and further uptake of the capsules by the cells. Nevertheless, the cells did not preferentially adhere to the capsules. A feasible explanation is that, due to the vertical distribution of the capsules, they are not sufficiently exposed at the patterned surface and, therefore, they remain inaccessible to the cells.

As was hypothesized, superficial capsules could be detected by cells; hence methods to induce capsules to reach the surface should be developed. For further studies, we suggest the use of a higher concentration of capsules in the filler material combined with samples with channels of shallow depth. That should increase the probability of finding capsules exposed at the surface and interacting with adhesive cells. Another approach would be the use of magnetically modified capsules, which can be attracted to the surface via magnetic fields during the FIMIC processing.

After positive recognition of the capsules by the cells, the next necessary step will be to prove the viability of the release of the load and its uptake by cells. This could be of great interest, for example, to deliver growth factors and, at the same time, provide an adequate scaffold to migrating cells during wound healing or to introduce genetic material inside the cells for transfection.

Bibliography

[1] J.B. Park, R.S. Lakes, Biomaterials: An Introduction, 3rd ed., Springer, New York, 2007.

[2] D.F. Williams, Definitions in biomaterials. Proceedings of a consensus conference of the european society for biomaterials., Vol. 4, Elsevier, New York, 1987.

[3] M. Epple, Biomaterialien und Biomineralisation, B.G. Teubner, Wiesbaden, 2003.

[4] S.A. Guelcher, J.O. Hollinger, An Introduction to Biomaterials, CRC Press Taylor & Francis, 2005.

[5] C. Migliaresi, Composites, in: B.D. Ratner, A.S. Hoffman, F.J. Schoen, J.E. Lemons (Eds.), Biomater. Sci. An Intoduction to Mater. Med., 3rd ed., Academic Press, 2012.

[6] E. Salernitano, C. Migliaresi, Composite materials for biomedical applications: a review., J. Appl. Biomater. Biomech. 1 (2003) 3–18.

[7] O. Wichterle, D. Lim, Hydrophilic Gels for Biological Use, Nature. 185 (1960) 117–118.

[8] J. Kopeček, Hydrogel Biomaterials: A Smart Future?, Biomaterials. 28 (2007) 5185–5192.

[9] A.M. Kloxin, M.W. Tibbitt, A.M. Kasko, J.A. Fairbairn, K.S. Anseth, Tunable hydrogels for external manipulation of cellular microenvironments through controlled photodegradation, Adv. Mater. 22 (2010) 61–66.

[10] M. Bindu Sri, V. Ashok, C. Arkendu, As A Review on Hydrogels as Drug Delivery in the Pharmaceutical Field, Int. J. Pharm. Chem. Sci. 1 (2012) 642–661.

[11] J.L. Drury, D.J. Mooney, Hydrogels for tissue engineering: scaffold design variables and applications, Biomaterials. 24 (2003) 4337–4351.

[12] Y. Yagci, S. Jockusch, N.J. Turro, Photoinitiated Polymerization: Advances, Challenges, and Opportunities, Macromolecules. 43 (2010) 6245–6260.

[13] Z. Drira, V.K. Yadavalli, Nanomechanical measurements of polyethylene glycol hydrogels using atomic force microscopy., J. Mech. Behav. Biomed. Mater. 18 (2013) 20–8.

[14] J.M. Harris, Poly(Ethylene Glycol) Chemistry: Biotechnical and Biomedical Applications, Plenum Press, New York, 1992.

[15] C.M. Lo, H.B. Wang, M. Dembo, Y.L. Wang, Cell movement is guided by the rigidity of the substrate., Biophys. J. 79 (2000) 144–52.

[16] G.M. Whitesides, E. Ostuni, S. Takayama, X. Jiang, D.E. Ingber, Soft lithography in biology and biochemistry, Annu. Rev. Biomed. Eng. 3 (2001) 335–373.

[17] S.R. Peyton, C.B. Raub, V.P. Keschrumrus, A.J. Putnam, The use of poly(ethylene glycol) hydrogels to investigate the impact of ECM chemistry and mechanics on smooth muscle cells., Biomaterials. 27 (2006) 4881–4893.

[18] U. Wattendorf, O. Kreft, M. Textor, G.B. Sukhorukov, H.P. Merkle, Stable stealth function for hollow polyelectrolyte microcapsules through a poly(ethylene glycol) grafted polyelectrolyte adlayer., Biomacromolecules. 9 (2008) 100–108.

[19] J. Blümmel, N. Perschmann, D. Aydin, J. Drinjakovic, T. Surrey, M. Lopez-Garcia, et al., Protein repellent properties of covalently attached PEG coatings on nanostructured SiO(2)-based interfaces., Biomaterials. 28 (2007) 4739–4747.

[20] Y. Wang, G. Subbiahdoss, J. Swartjes, H.C. van der Mei, H.J. Busscher, M. Libera, Length-scale mediated differential adhesion of mammalian cells and microbes, Adv. Funct. Mater. 21 (2011) 3916–3923.

[21] P. Kim, D.-H. Kim, B. Kim, S.K. Choi, S.H. Lee, A. Khademhosseini, et al., Fabrication of nanostructures of polyethylene glycol for applications to protein adsorption and cell adhesion, Nanotechnology. 16 (2005) 2420–2426.

[22] V.A. Schulte, M. Díez, M. Möller, M.C. Lensen, Surface topography induces fibroblast adhesion on intrinsically nonadhesive poly(ethylene glycol) substrates., Biomacromolecules. 10 (2009) 2795–801.

[23] M.C. Lensen, V.A. Schulte, J. Salber, M. Díez, F. Menges, M. Möller, Cellular responses to novel, micropatterned biomaterials, Pure Appl. Chem. 80 (2008) 2479–2487.

[24] V.A. Schulte, M. Díez, M. Möller, M.C. Lensen, Cellular responses to physically and mechanically patterned biomaterials, Eur. Cells Mater. 20 (2010) 157.

[25] P. Roach, D. Farrar, C.C. Perry, Surface tailoring for controlled protein adsorption: effect of topography at the nanometer scale and chemistry., J. Am. Chem. Soc. 128 (2006) 3939–3945.

[26] M. Amiji, K. Park, Prevention of protein adsorption and platelet adhesion on surfaces by PEO/PPO/PEO triblock copolymers, Biomaterials. 13 (1992) 682–692.

[27] S. Hsu, C.-M. Tang, J.-J. Chiu, T.-C. Liao, C.-C. Lin, H. Iwata, Cell migration rate on poly(epsilon-caprolactone)/poly(ethylene glycol) diblock copolymers and correlation with the material sliding angle., Macromol. Biosci. 7 (2007) 482–490.

[28] S.M. Kelleher, Z. Zhang, A. Löbus, C. Strehmel, M.C. Lensen, Blending PEG-based polymers and their use in surface micro-patterning by the FIMIC method to obtain topographically smooth patterns of elasticity, Biomater. Sci. 2 (2014) 410.

[29] S.A. DeLong, J.J. Moon, J.L. West, Covalently immobilized gradients of bFGF on hydrogel scaffolds for directed cell migration, Biomaterials. 26 (2005) 3227–3234.

[30] A.J. Engler, S. Sen, H.L. Sweeney, D.E. Discher, Matrix elasticity directs stem cell lineage specification, Cell. 126 (2006) 677–689.

[31] H.B. Wang, M. Dembo, Y.L. Wang, Substrate flexibility regulates growth and apoptosis of normal but not transformed cells., Am. J. Physiol. Cell Physiol. 279 (2000) C1345–C1350.

[32] Migration 101 - An Introduction to Cell Migration, https://www.cellmigration.org/science/index.shtml.

[33] R. Horwitz, D. Webb, Cell migration, Curr. Biol. 13 (2003) R756–R759.

[34] M.E. Mycielska, M.B.A. Djamgoz, Cellular mechanisms of direct-current electric field effects: galvanotaxis and metastatic disease., J. Cell Sci. 117 (2004) 1631–9.

[35] P. Weiss, Guiding principles in cell locomotion and cell aggregation, in: Exp. Cell Res., 1961: pp. 260–281.

[36] A. Buck, A.F. Horwitz, Cell Surface Receptors for Extracellular Matrix Molecules, Annu. Rev. Cell Biol. 3 (1987) 179–205.

[37] D.C. Worth, M. Parsons, Advances in imaging cell-matrix adhesions, J. Cell Sci. 123 (2010) 3629–3638.

[38] N.Q. Balaban, U.S. Schwarz, D. Riveline, P. Goichberg, G. Tzur, I. Sabanay, et al., Force and focal adhesion assembly: a close relationship studied using elastic micropatterned substrates., Nat. Cell Biol. 3 (2001) 466–72.

[39] B. Geiger, A. Bershadsky, R. Pankov, K.M. Yamada, B.G. Correspondence, Transmembrane extracellular matrix– cytoskeleton crosstalk, Nat. Rev. Mol. Cell Biol. 2 (2001) 793–805.

[40] B. Geiger, J.P. Spatz, A.D. Bershadsky, Environmental sensing through focal adhesions, Nat. Rev. Mol. Cell Biol. 10 (2009) 21–33.

[41] R.J. Pelham, Y.-L. Wang, Cell locomotion and focal adhesions are regulated by substrate flexibility, Proc. Natl. Acad. Sci. 94 (1997) 13661–13665.

[42] J. Wu, Z. Mao, C. Gao, Controlling the migration behaviors of vascular smooth muscle cells by methoxy poly(ethylene glycol) brushes of different molecular weight and density, Biomaterials. 33 (2012) 810–820.

[43] C.A. Reinhart-King, M. Dembo, D.A. Hammer, Endothelial Cell Traction Forces on RGD-Derivatized Polyacrylamide Substrata, Langmuir. 11 (2003) 1573–1579.

[44] R.J. Petrie, A.D. Doyle, K.M. Yamada, Random versus directionally persistent cell migration, Nat. Rev. Mol. Cell Biol. 10 (2009) 538–549.

[45] S.B. Carter, Principles of Cell Motility: The Direction of Cell Movement and Cancer Invasion, Nature. 208 (1965) 1183–1187.

[46] A. Harris, Behavior of cultured cells on substrata of variable adhesiveness, Exp. Cell Res. 77 (1973) 285–297.

[47] R.G. Flemming, C.J. Murphy, G.A. Abrams, S.L. Goodman, P.F. Nealey, Effects of synthetic micro- and nano-structured surfaces on cell behavior, Biomaterials. 20 (1999) 573–588.

[48] A.I. Teixeira, G.A. Abrams, P.J. Bertics, C.J. Murphy, P.F. Nealey, Epithelial contact guidance on well-defined micro- and nanostructured substrates, J. Cell Sci. 116 (2003) 1881–1892.

[49] P. Weiss, Experiments on cell and axon orientation in vitro: The role of colloidal exudates in tissue organization, J. Exp. Zool. 100 (1945) 353–386.

[50] D. Choquet, D.P. Felsenfeld, M.P. Sheetz, Extracellular Matrix Rigidity Causes Strengthening of Integrin–Cytoskeleton Linkages, Cell. 88 (1997) 39–48.

[51] B. Cortese, M. Riehle, R. Cingolani, G. Gigli, Cells response sensing durotaxis by varying mechanical rigidity, Eur. Cells Mater. 16 (2008) 44.

[52] E. Wallraff, H.G. Wallraff, Migration and bidirectional phototaxis in Dictyostelium discoideum slugs lacking the actin cross-linking 120 kDa gelation factor., J. Exp. Biol. 200 (1997) 3213–3220.

[53] A. Bahat, M. Eisenbach, Sperm thermotaxis, Mol. Cell. Endocrinol. 252 (2006) 115–119.

[54] U. Lins, D.A. Bazylinski, Encyclopedia of Microbiology, Elsevier, 2009.

[55] I. Wheeldon, A. Farhadi, A.G. Bick, E. Jabbari, A. Khademhosseini, Nanoscale tissue engineering: spatial control over cell-materials interactions, Nanotechnology. 22 (2011) 212001.

[56] D. Hoffman-Kim, J.A. Mitchel, R. V Bellamkonda, Topography, cell response, and nerve regeneration., Annu. Rev. Biomed. Eng. 12 (2010) 203–31.

[57] L.F. Reynolds, M.C. Bren, B.C. Wilson, G.D. Gibson, M.S. Shoichet, R.J.L. Murphy, Transplantation of porous tubes following spinal cord transection improves hindlimb function in the rat, Spinal Cord. 46 (2008) 58–64.

[58] J. Cai, X. Peng, K.D. Nelson, R. Eberhart, G.M. Smith, Permeable guidance channels containing microfilament scaffolds enhance axon growth and maturation, J. Biomed. Mater. Res. Part A. 75A (2005) 374–386.

[59] Y. Xia, G.M. Whitesides, Soft Lithography, Annu. Rev. Mater. Sci. 28 (1998) 153–184.

[60] B.D. Terris, H.J. Mamin, M.E. Best, J. a. Logan, D. Rugar, S. a. Rishton, Nanoscale replication for scanning probe data storage, Appl. Phys. Lett. 69 (1996) 4262–4264.

[61] M.C. Lensen, P. Mela, A. Mourran, J. Groll, J. Heuts, H. Rong, et al., Micro- and nanopatterned star Poly(ethylene glycol) (PEG) materials prepared by UV-based imprint lithography, Langmuir. 23 (2007) 7841–7846.

[62] B. Cortese, G. Gigli, M. Riehle, Mechanical Gradient Cues for Guided Cell Motility and Control of Cell Behavior on Uniform Substrates, Adv. Funct. Mater. 19 (2009) 2961–2968.

[63] E. Pezron, B. Magny, Modeling of UV Oligomers and Monomers Properties: Viscosity and Shrinkage, Eur. Coat. J. 9 (1996) 602–606.

[64] M. Diez, V.A. Schulte, F. Stefanoni, C.F. Natale, F. Mollica, C.M. Cesa, et al., Molding Micropatterns of Elasticity on PEG-Based Hydrogels to Control Cell Adhesion and Migration, Adv. Eng. Mater. 13 (2011) B395–B404.

[65] E. Kim, Y. Xia, G.M. Whitesides, Micromolding in capillaries: Applications in materials science, J. Am. Chem. Soc. 118 (1996) 5722–5731.

[66] S. Kelleher, A. Jongerius, A. Loebus, C. Strehmel, Z. Zhang, M.C. Lensen, AFM Characterization of Elastically Micropatterned Surfaces Fabricated by Fill-Molding In Capillaries (FIMIC) and Investigation of the Topographical Influence on Cell Adhesion to the Patterns, Adv. Eng. Mater. 14 (2012) B56–B66.

[67] A. Loebus, Patterning Strategies of Poly(ethylene glycol) Based Hydroxyapatite Composites for Biomedical Applications, Dissertation Technische Universität Berlin, 2013.

[68] M. Arafeh, Micro- and Nano-patterned Gold Structures for Selective Immobilization of Proteins, Dissertation Technische Universität Berlin, 2014.

[69] J.Y. Park, D.H. Lee, E.J. Lee, S.-H. Lee, Study of cellular behaviors on concave and convex microstructures fabricated from elastic PDMS membranes., Lab Chip. 9 (2009) 2043–9.

[70] M.F. Bédard, D. Braun, G.B. Sukhorukov, A.G. Skirtach, Toward Self-Assembly of Nanoparticles on Polymeric Microshells: Near-IR Release and Permeability, ACS Nano. 2 (2008) 1807–1816.

[71] M.M. de Villiers, D.P. Otto, S.J. Strydom, Y.M. Lvov, Introduction to nanocoatings produced by layer-by-layer (LbL) self-assembly, Adv. Drug Deliv. Rev. 63 (2011) 701–715.

[72] J. Turkevich, P.C. Stevenson, J. Hiller, A Study of the Nucleation and Growth Processes in the Synthesis of Colloidal Gold, Discuss. Faraday Soc. 11 (1951) 55–75.

[73] W. Wang, Y. Pang, J. Yan, G. Wang, H. Suo, C. Zhao, et al., Facile synthesis of hollow urchin-like gold nanoparticles and their catalytic activity, Gold Bull. 45 (2012) 91–98.

[74] C. Wang, S. Peng, R. Chan, S. Sun, Synthesis of AuAg alloy nanoparticles from core/shell-structured Ag/Au., Small. 5 (2009) 567–570.

[75] J.-H. Lee, K. Kamada, N. Enomoto, J. Hojo, Polyhedral Gold Nanoplate: High Fraction Synthesis of Two-Dimensional Nanoparticles through Rapid Heating Process, Cryst. Growth Des. 8 (2008) 2638–2645.

[76] F. Kim, S. Connor, H. Song, T. Kuykendall, P. Yang, Platonic gold nanocrystals., Angew. Chemie Int. Ed. 43 (2004) 3673–7.

[77] Y. Chen, X. Gu, C.-G. Nie, Z.-Y. Jiang, Z.-X. Xie, C.-J. Lin, Shape controlled growth of gold nanoparticles by a solution synthesis., Chem. Commun. 1 (2005) 4181–4183.

[78] X.-M. Zhao, Y. Xia, G.M. Whitesides, Fabrication of three-dimensional micro-structures: Microtransfer molding, Adv. Mater. 8 (1996) 837–840.

[79] R. Merkel, N. Kirchgeßner, C.M. Cesa, B. Hoffmann, Cell Force Microscopy on Elastic Layers of Finite Thickness, Biophys. J. 93 (2007) 3314–3323.

[80] D.E.I. 10993-5, Biological evaluation of medical devices - Part 5: Test for in vitro cytotoxicity, (2009).

[81] E.A. Codling, M.J. Plank, S. Benhamou, Random walk models in biology., J. R. Soc. Interface. 5 (2008) 813–834.

[82] G.A. Dunn, A.F. Brown, A Unified Approach to Analysing Cell Motility, J. Cell Sci. Suppl. 8 (1987) 81–102.

[83] M.H. Gail, C.W. Boone, The Locomotion of Mouse Fibroblasts in Tissue Culture, Biophys. J. 10 (1970) 980–993.

[84] P.A. DiMilla, J.A. Quinn, S.M. Albelda, D.A. Lauffenburger, Measurement of individual cell migration parameters for human tissue cells, AIChE J. 38 (1992) 1092–1104.

[85] B.C. Isenberg, P.A. Dimilla, M. Walker, S. Kim, J.Y. Wong, Vascular smooth muscle cell durotaxis depends on substrate stiffness gradient strength., Biophys. J. 97 (2009) 1313–22.

[86] H. Jeon, H. Hidai, D.J. Hwang, K.E. Healy, C.P. Grigoropoulos, The effect of micronscale anisotropic cross patterns on fibroblast migration., Biomaterials. 31 (2010) 4286–95.

[87] G.P. Raeber, M.P. Lutolf, J.A. Hubbell, Part II: Fibroblasts preferentially migrate in the direction of principal strain., Biomech. Model. Mechanobiol. 7 (2008) 215–25.

[88] D. House, M.L. Walker, Z. Wu, J.Y. Wong, M. Betke, Tracking of cell populations to understand their spatio-temporal behavior in response to physical stimuli, in: 2012 IEEE Comput. Soc. Conf. Comput. Vis. Pattern Recognit. Work., 2009: pp. 186–193.

[89] E. Batschelet, Circular Statistics in Biology, Academic Press, London, UK, 1981.

[90] S. Benhamou, How to reliably estimate the tortuosity of an animal's path: straightness, sinuosity, or fractal dimension?, J. Theor. Biol. 229 (2004) 209–20.

[91] J.-P. Kaiser, A. Bruinink, Investigating cell-material interactions by monitoring and analysing cell migration., J. Mater. Sci. Mater. Med. 15 (2004) 429–35.

[92] F. Stefanoni, M. Ventre, F. Mollica, P.A. Netti, A numerical model for durotaxis, J. Theor. Biol. 280 (2011) 150–158.

[93] J.-P. Kaiser, A. Reinmann, A. Bruinink, The effect of topographic characteristics on cell migration velocity., Biomaterials. 27 (2006) 5230–41.

[94] F. Milde, D. Franco, A. Ferrari, V. Kurtcuoglu, D. Poulikakos, P. Koumoutsakos, Cell Image Velocimetry (CIV): boosting the automated quantification of cell migration in wound healing assays., Integr. Biol. (Camb). 4 (2012) 1437–47.

[95] R.G. Harrison, The cultivation of tissues in extraneous media as a method of morpho-genetic study, Anat. Rec. 6 (1912) 181–193.

[96] S.P. Khan, G.G. Auner, G.M. Newaz, Influence of nanoscale surface roughness on neural cell attachment on silicon., Nanomedicine. 1 (2005) 125–129.

[97] M. Chiquet, L. Gelman, R. Lutz, S. Maier, From mechanotransduction to extracellular matrix gene expression in fibroblasts, Biochim. Biophys. Acta - Mol. Cell Res. 1793 (2009) 911–920.

[98] D.E. Discher, P.A. Janmey, Y. Wang, Tissue cells feel and respond to the stiffness of their substrate, Science. 310 (2005) 1139–1143.

[99] D.W. Hamilton, C. Oakley, N.A.F. Jaeger, D.M. Brunette, Directional change produced by perpendicularly-oriented microgrooves is microtubule-dependent for fibroblasts and epithelium., Cell Motil. Cytoskeleton. 66 (2009) 260–71.

[100] N. Gomez, S. Chen, C.E. Schmidt, Polarization of hippocampal neurons with competitive surface stimuli: contact guidance cues are preferred over chemical ligands., J. R. Soc. Interface. 4 (2007) 223–33.

[101] C. Oakley, D.M. Brunette, The sequence of alignment of microtubules, focal contacts and actin filaments in fibroblasts spreading on smooth and grooved titanium substrata., J. Cell Sci. 106 (1993) 343–54.

[102] M.J. Dalby, M.J.P. Biggs, N. Gadegaard, G. Kalna, C.D.W. Wilkinson, A.S.G. Curtis, Nanotopographical stimulation of mechanotransduction and changes in interphase centromere positioning., J. Cell. Biochem. 100 (2007) 326–38.

[103] M.J. Dalby, M.O. Riehle, S.J. Yarwood, C.D.. Wilkinson, A.S.. Curtis, Nucleus alignment and cell signaling in fibroblasts: response to a micro-grooved topography, Exp. Cell Res. 284 (2003) 272–280.

[104] M.J. Dalby, Topographically induced direct cell mechanotransduction., Med. Eng. Phys. 27 (2005) 730–42.

[105] K.N. Dahl, A.J.S. Ribeiro, J. Lammerding, Nuclear shape, mechanics, and mechanotransduction, Circ. Res. 102 (2008) 1307–1318.

[106] A. Curtis, C. Wilkinson, Topographical control of cells, Biomaterials. 18 (1997) 1573–1583.

[107] D.W. Hamilton, B. Chehroudi, D.M. Brunette, Comparative response of epithelial cells and osteoblasts to microfabricated tapered pit topographies in vitro and in vivo., Biomaterials. 28 (2007) 2281–93.

[108] S. Al-Haque, J.W. Miklas, N. Feric, L.L.Y. Chiu, W.L.K. Chen, C.A. Simmons, et al., Hydrogel substrate stiffness and topography interact to induce contact guidance in cardiac fibroblasts., Macromol. Biosci. 12 (2012) 1342–53.

[109] N.M. Alves, I. Pashkuleva, R.L. Reis, J.F. Mano, Controlling cell behavior through the design of polymer surfaces, Small. 6 (2010) 2208–2220.

[110] D.-H. Kim, K. Han, K. Gupta, K.W. Kwon, K.-Y. Suh, A. Levchenko, Mechanosensitivity of fibroblast cell shape and movement to anisotropic substratum topography gradients., Biomaterials. 30 (2009) 5433–44.

[111] A. Buxboim, I.L. Ivanovska, D.E. Discher, Matrix elasticity, cytoskeletal forces and physics of the nucleus: how deeply do cells “feel” outside and in?, J. Cell Sci. 123 (2010) 297–308.

[112] P. Kuntanawat, C. Wilkinson, M. Riehle, Observation of durotaxis on a well-defined continuous gradient of stiffness, Comp. Biochem. Physiol. Part A Mol. Integr. Physiol. 146 (2007) S192.

[113] S.-Y. Chou, C.-M. Cheng, P.R. LeDuc, Composite polymer systems with control of local substrate elasticity and their effect on cytoskeletal and morphological characteristics of adherent cells., Biomaterials. 30 (2009) 3136–42.

[114] A. Saez, M. Ghibaudo, A. Buguin, P. Silberzan, B. Ladoux, Rigidity-driven growth and migration of epithelial cells on microstructured anisotropic substrates., Proc. Natl. Acad. Sci. U. S. A. 104 (2007) 8281–6.

[115] H.G. Sundararaghavan, G.A. Monteiro, B.L. Firestein, D.I. Shreiber, Neurite growth in 3D collagen gels with gradients of mechanical properties, Biotechnol. Bioeng. 102 (2009) 632–643.

[116] J.A. Burdick, A. Khademhosseini, R.S. Langer, Fabrication of gradient hydrogels using a microfluidics/photopolymerization process, Langmuir. 20 (2004) 5153–5156.

[117] C.-H.R. Kuo, J. Xian, J.D. Brenton, K. Franze, E. Sivaniah, Complex stiffness gradient substrates for studying mechanotactic cell migration., Adv. Mater. 24 (2012) 6059–64.

[118] S. Degand, B. Knoops, C.C. Dupont-Gillain, Design and characterization of surfaces presenting mechanical nanoheterogeneities for a better control of cell–material interactions, Colloids Surfaces A Physicochem. Eng. Asp. 442 (2014) 164–172.

[119] S. Nemir, H.N. Hayenga, J.L. West, PEGDA hydrogels with patterned elasticity: Novel tools for the study of cell response to substrate rigidity., Biotechnol. Bioeng. 105 (2010) 636–644.

[120] M.S. Hahn, J.S. Miller, J.L. West, Three-Dimensional Biochemical and Biomechanical Patterning of Hydrogels for Guiding Cell Behavior, Adv. Mater. 18 (2006) 2679–2684.

[121] J.T. Smith, J.T. Elkin, W.M. Reichert, Directed cell migration on fibronectin gradients: effect of gradient slope., Exp. Cell Res. 312 (2006) 2424–2432.

[122] A.S. Sarvestani, E. Jabbari, Analysis of cell locomotion on ligand gradient substrates, Biotechnol. Bioeng. 103 (2009) 424–429.

[123] S.P. Palecek, J.C. Loftus, M.H. Ginsberg, D.A. Lauffenburger, A.R. Horwitz, Integrin-ligand binding properties govern cell migration speed through cell-substratum adhesiveness, Nature. 385 (1997) 537–540.

[124] X. Jiang, D.A. Bruzewicz, A.P. Wong, M. Piel, G.M. Whitesides, Directing cell migration with asymmetric micropatterns, Proc. Natl. Acad. Sci. 102 (2005) 975–978.

[125] K. Theerakittayakorn, T. Bunprasert, Differentiation capacity of mouse L929 fibroblastic cell line compare with human dermal fibroblast, World Acad. Sci. Eng. Technol. 74 (2011) 378–381.

[126] C. Strehmel, Zelluläre Reaktionen muriner Fibroblasten auf planaren und strukturierten Polyethylenglykol-basierten Biomaterialien, Dissertation Technische Universität Berlin, 2013.

[127] R. Milo, P. Jorgensen, U. Moran, G. Weber, M. Springer, BioNumbers--the database of key numbers in molecular and cell biology., Nucleic Acids Res. 38 (2010) D750–753.

[128] E. Hadjipanayi, V. Mudera, R.A. Brown, Close dependence of fibroblast proliferation on collagen scaffold matrix stiffness, J. Tissue Eng. Regen. Med. 3 (2009) 77–84.

[129] J. Boussinesq, Application des potentiels à l'étude de l'équilibre et du mouvement des solides élastiques, Gauthier-Villars, Paris, France, 1885.

[130] J.M. Maloney, E.B. Walton, C.M. Bruce, K.J. Van Vliet, Influence of finite thickness and stiffness on cellular adhesion-induced deformation of compliant substrata, Phys. Rev. E. 78 (2008) 41923.

[131] J.P. Butler, I.M. Tolić-Nørrelykke, B. Fabry, J.J. Fredberg, Traction fields, moments, and strain energy that cells exert on their surroundings., Am. J. Physiol. Cell Physiol. 282 (2002) C595–605.

[132] Z. Yang, J.-S. Lin, J. Chen, J.H.-C. Wang, Determining substrate displacement and cell traction fields - a new approach, J. Theor. Biol. 242 (2006) 607–616.

[133] J.C. Del Alamo, R. Meili, B. Alonso-Latorre, J. Rodríguez-Rodríguez, A. Aliseda, R. a Firtel, et al., Spatio-temporal analysis of eukaryotic cell motility by improved force cytometry., Proc. Natl. Acad. Sci. 104 (2007) 13343–13348.

[134] S. Sen, A.J. Engler, D.E. Discher, Matrix strains induced by cells: Computing how far cells can feel, Cell. Mol. Bioeng. 2 (2009) 39–48.

[135] U.S. Schwarz, N.Q. Balaban, D. Riveline, A.D. Bershadsky, B. Geiger, S. Safran, Calculation of forces at focal adhesions from elastic substrate data: the effect of localized force and the need for regularization., Biophys. J. 83 (2002) 1380–94.

[136] A.J. Engler, L. Richert, J.Y. Wong, C. Picart, D.E. Discher, Surface probe measurements of the elasticity of sectioned tissue, thin gels and polyelectrolyte multilayer films: Correlations between substrate stiffness and cell adhesion, Surf. Sci. 570 (2004) 142–154.

[137] S.A. Maskarinec, C. Franck, D.A. Tirrell, G. Ravichandran, Quantifying cellular traction forces in three dimensions, Proc. Natl. Acad. Sci. 106 (2009) 22108–22113.

[138] A. Buxboim, K. Rajagopal, A.E.X. Brown, D.E. Discher, How deeply cells feel: methods for thin gels, J. Phys. Condens. Matter. 22 (2010) 194116.

[139] C. Roduit, S. Sekatski, G. Dietler, S. Catsicas, F. Lafont, S. Kasas, Stiffness tomography by atomic force microscopy, Biophys. J. 97 (2009) 674–7.

[140] E. Bertrand, T.D. Blake, J. De Coninck, Dynamics of dewetting, Colloids Surfaces A Physicochem. Eng. Asp. 369 (2010) 141–147.

[141] F.R. Menges, Wetting of micro- and nanostructured hydrophobic surfaces, Rheinisch-Westfälische Technische Hochschule Aachen, 2008.

[142] D.W. Schubert, T. Dunkel, Spin coating from a molecular point of view: its concentration regimes, influence of molar mass and distribution, Mater. Res. Innov. 7 (2003) 314–321. d

[143] A. Revzin, R.J. Russell, V.K. Yadavalli, W.-G. Koh, C. Deister, D.D. Hile, et al., Fabrication of poly(ethylene glycol) hydrogel microstructures using photolithography., Langmuir. 17 (2001) 5440–7.

[144] K.Y. Suh, J. Seong, A. Khademhosseini, P.E. Laibinis, R. Langer, A simple soft lithographic route to fabrication of poly(ethylene glycol) microstructures for protein and cell patterning, Biomaterials. 25 (2004) 557–563.

[145] B.S.E. Equipement, Spin Coater Theory, http://www.brewerscience.com/research/processing-theory/spin-coater-theory.

[146] R. Bhattacharya, P. Mukherjee, Biological properties of “naked” metal nanoparticles., Adv. Drug Deliv. Rev. 60 (2008) 1289–1306.

[147] J.Z. Zhang, Biomedical Applications of Shape-Controlled Plasmonic Nanostructures: A Case Study of Hollow Gold Nanospheres for Photothermal Ablation Therapy of Cancer, J. Phys. Chem. Lett. 1 (2010) 686–695.

[148] M. Turner, V.B. Golovko, O.P.H. Vaughan, P. Abdulkin, A. Berenguer-Murcia, M.S. Tikhov, et al., Selective oxidation with dioxygen by gold nanoparticle catalysts derived from 55-atom clusters., Nature. 454 (2008) 981–983.

[149] G. a Petkova, C.K.C. Záruba, P. Zvátora, V. Král, Gold and silver nanoparticles for biomolecule immobilization and enzymatic catalysis., Nanoscale Res. Lett. 7 (2012) 287.

[150] J.R. Morones-Ramirez, J.A. Winkler, C.S. Spina, J.J. Collins, Silver Enhances Antibiotic Activity Against Gram-Negative Bacteria, Sci. Transl. Med. . 5 (2013) 190ra81–190ra81.

[151] A.S. Nikolov, N.N. Nedyalkov, R.G. Nikov, P.A. Atanasov, M.T. Alexandrov, Characterization of Ag and Au nanoparticles created by nanosecond pulsed laser ablation in double distilled water, Appl. Surf. Sci. 257 (2011) 5278–5282.

[152] R. Weissleder, A clearer vision for in vivo imaging, Nat. Biotechnol. 19 (2001) 316–317.

[153] K.-S. Lee, M.A. El-Sayed, Gold and silver nanoparticles in sensing and imaging: sensitivity of plasmon response to size, shape, and metal composition., J. Phys. Chem. B. 110 (2006) 19220–19225.

[154] M. Arnold, E.A. Cavalcanti-Adam, R. Glass, J. Blümmel, W. Eck, M. Kantlehner, et al., Activation of integrin function by nanopatterned adhesive interfaces., Chemphyschem. 5 (2004) 383–388.

[155] X. Ye, L. Jin, H. Caglayan, J. Chen, G. Xing, C. Zheng, et al., Improved size-tunable synthesis of monodisperse gold nanorods through the use of aromatic additives., ACS Nano. 6 (2012) 2804–2817.

[156] S.R. Saptarshi, A. Duschl, A.L. Lopata, Interaction of nanoparticles with proteins: relation to bio-reactivity of the nanoparticle., J. Nanobiotechnology. 11 (2013) 26.

[157] A.M. Alkilany, C.J. Murphy, Toxicity and cellular uptake of gold nanoparticles: what we have learned so far?, J. Nanopart. Res. 12 (2010) 2313–2333.

[158] A.G. Tkachenko, H. Xie, D. Coleman, W. Glomm, J. Ryan, M.F. Anderson, et al., Multifunctional gold nanoparticle-peptide complexes for nuclear targeting, J. Am. Chem. Soc. 215 (2003) 4700–4701.

[159] Y. Pan, S. Neuss, A. Leifert, M. Fischler, F. Wen, U. Simon, et al., Size-dependent cytotoxicity of gold nanoparticles., Small. 3 (2007) 1941–9.

[160] R. de Lima, A.B. Seabra, N. Durán, Silver nanoparticles: a brief review of cytotoxicity and genotoxicity of chemically and biogenically synthesized nanoparticles., J. Appl. Toxicol. 32 (2012) 867–879.

[161] F. Ren, Study of Cytotoxic Effects of Different Sizes of AuNPs and their Applications (Dissertation in preparation), Technische Universität Berlin, n.d.

[162] J. Chen, P. Mela, M. Möller, M.C. Lensen, Microcontact Deprinting : A Technique to Pattern Gold Nanoparticles, ACS Nano. 3 (2009) 1451–1456.

[163] B.P. Timko, K. Whitehead, W. Gao, D.S. Kohane, O. Farokhzad, D. Anderson, et al., Advances in Drug Delivery, Annu. Rev. Mater. Res. 41 (2011) 1–20.

[164] A.S. Angelatos, B. Radt, F. Caruso, Light-Responsive Polyelectrolyte/Gold Nanoparticle Microcapsules, J. Phys. Chem. B. 109 (2005) 3071–3076.

[165] M. Delcea, A. Yashchenok, K. Videnova, O. Kreft, H. Möhwald, A.G. Skirtach, Multicompartmental micro- and nanocapsules: hierarchy and applications in biosciences., Macromol. Biosci. 10 (2010) 465–474.

[166] O. Kreft, A.G. Skirtach, G.B. Sukhorukov, H. Möhwald, Remote Control of Bioreactions in Multicompartment Capsules, Adv. Mater. 19 (2007) 3142–3145.

[167] J. Swarbrick, ed., Encyclopedia of Pharmaceutical Technology, 3rd ed., 2006.

[168] B. Wang, T.J. Siahaan, R. Soltero, eds., Drug Delivery: Principles and Applications, John Wiley & Sons, Inc., Ney Jersey, 2005.

[169] J. Weyermann, D. Lochmann, C. Georgens, A. Zimmer, Albumin–protamine–oligonucleotide-nanoparticles as a new antisense delivery system. Part 2: cellular uptake and effect, Eur. J. Pharm. Biopharm. 59 (2005) 431–438.

[170] M. Delcea, S. Schmidt, R. Palankar, P.A.L. Fernandes, A. Fery, H. Möhwald, et al., Mechanobiology: Correlation Between Mechanical Stability of Microcapsules Studied by AFM and Impact of Cell-Induced Stresses, Small. 6 (2010) 2858–2862.

[171] K.E. Uhrich, S.M. Cannizzaro, R.S. Langer, K.M. Shakesheff, Polymeric Systems for Controlled Drug Release, Chem. Rev. 99 (1999) 3181–3198.

[172] C. Cortez, E. Tomaskovic-Crook, A.P.R. Johnston, B. Radt, S.H. Cody, A.M. Scott, et al., Targeting and Uptake of Multilayered Particles to Colorectal Cancer Cells, Adv. Mater. 18 (2006) 1998–2003.

[173] C. Scholz, M. Iijima, Y. Nagasaki, K. Kataoka, Polymeric Micelles as Drug Delivery Systems : a Reactive Polymeric Micelle Carrying Aldehyde Groups, Polym. Adv. Technol. 9 (1998) 768–776.

[174] M. Michel, M. Winterhalter, L. Darbois, J. Hemmerle, J.C. Voegel, P. Schaaf, et al., Giant liposome microreactors for controlled production of calcium phosphate crystals., Langmuir. 20 (2004) 6127–6133.

[175] A.P. Nowak, V. Breedveld, L. Pakstis, B. Ozbas, D.J. Pine, D. Pochan, et al., Rapidly recovering hydrogel scaffolds from self-assembling diblock copolypeptide amphiphiles, Nature. 417 (2002) 424–428.

[176] S. Faraasen, J. Vörös, G. Csúcs, M. Textor, H.P. Merkle, E. Walter, Ligand-Specific Targeting of Microspheres to Phagocytes by Surface Modification with Poly(L-Lysine)-Grafted Poly(Ethylene Glycol) Conjugate, Pharm. Res. 20 (2003) 237–246.

[177] B.G. De Geest, A.G. Skirtach, A.A. Mamedov, A.A. Antipov, N.A. Kotov, S.C. De Smedt, et al., Ultrasound-triggered release from multilayered capsules., Small. 3 (2007) 804–808.

[178] B.G. De Geest, R.E. Vandenbroucke, A.M. Guenther, G.B. Sukhorukov, W.E. Hennink, N.N. Sanders, et al., Intracellularly Degradable Polyelectrolyte Microcapsules, Adv. Mater. 18 (2006) 1005–1009.

[179] A.G. Skirtach, A.M. Yashchenok, H. Möhwald, Encapsulation, release and applications of LbL polyelectrolyte multilayer capsules., Chem. Commun. 47 (2011) 12736–12746.

[180] D.A. Gorin, S.A. Portnov, O.A. Inozemtseva, Z. Luklinska, A.M. Yashchenok, A.M. Pavlov, et al., Magnetic/gold nanoparticle functionaliyed biocompatible microcapsules with sensitivity to laser irradiation, Phys. Chem. Chem. Phys. 10 (2008) 6899–6905.

[181] B. Zebli, A.S. Susha, G.B. Sukhorukov, A.L. Rogach, W.J. Parak, Magnetic targeting and cellular uptake of polymer microcapsules simultaneously functionalized with magnetic and luminescent nanocrystals., Langmuir. 21 (2005) 4262–4265.

[182] G.B. Sukhorukov, A.L. Rogach, M. Garstka, S. Springer, W.J. Parak, A.M. Javier, et al., Multifunctionalized Polymer Microcapsules: Novel Tools for Biological and Pharmacological Applications, Small. 3 (2007) 944–955.

[183] A. Muñoz Javier, O. Kreft, M. Semmling, S. Kempter, A.G. Skirtach, O.T. Bruns, et al., Uptake of Colloidal Polyelectrolyte-Coated Particles and Polyelectrolyte Multilayer Capsules by Living Cells, Adv. Mater. 20 (2008) 4281–4287.

[184] A.G. Skirtach, C. Déjugnat, D. Braun, A.S. Susha, A.L. Rogach, W.J. Parak, et al., The role of metal nanoparticles in remote release of encapsulated materials., Nano Lett. 5 (2005) 1371–1377.

[185] A.G. Skirtach, A. a Antipov, D.G. Shchukin, G.B. Sukhorukov, Remote activation of capsules containing Ag nanoparticles and IR dye by laser light., Langmuir. 20 (2004) 6988–6992.

[186] M.F. Bédard, S. Sadasivan, G.B. Sukhorukov, A.G. Skirtach, Assembling polyelectrolytes and porphyrins into hollow capsules with laser-responsive oxidative properties, J. Mater. Chem. 19 (2009) 2226–2233.

[187] Z. Lu, M.D. Prouty, Z. Guo, V.O. Golub, C.S.S.R. Kumar, Y.M. Lvov, Magnetic switch of permeability for polyelectrolyte microcapsules embedded with Co@Au nanoparticles., Langmuir. 21 (2005) 2042–2050.

[188] C. Schüler, F. Caruso, Decomposable hollow biopolymer-based capsules., Biomacromolecules. 2 (2001) 921–926.

[189] C.M. Dvoracek, G. Sukhonosova, M.J. Benedik, J.C. Grunlan, Antimicrobial behavior of polyelectrolyte-surfactant thin film assemblies., Langmuir. 25 (2009) 10322–10328.

[190] B. Städler, R. Chandrawati, K. Goldie, F. Caruso, Capsosomes: subcompartmentalizing polyelectrolyte capsules using liposomes., Langmuir. 25 (2009) 6725–6732.

[191] F. Bacon, Essays, Orbis, 1696.

[192] M.N. Singh, K.S.Y. Hemant, M. Ram, H.. Shivakumar, Microencapsulation: A promising technique for controlled drug delivery, Res. Pharm. Sci. 5 (2010) 65–77.

[193] H. Ai, S. a Jones, M.M. de Villiers, Y.M. Lvov, Nano-encapsulation of furosemide microcrystals for controlled drug release., J. Control. Release. 86 (2003) 59–68.

[194] O.L. Johnson, H. Auer, H. Bernstein, M.M. Ganmukhi, A. Khan, Composition for sustained release of human growth hormone, EP 0831787B1, 2001.

[195] X. Qiu, S. Leporatti, E. Donath, H. Möhwald, Studies on the Drug Release Properties of Polysaccharide Multilayers Encapsulated Ibuprofen Microparticles, Langmuir. 17 (2001) 5375–5380.

[196] J.L. Santos, A. Nouri, T. Fernandes, J. Rodrigues, H. Tomás, Gene delivery using biodegradable polyelectrolyte microcapsules prepared through the layer-by-layer technique., Biotechnol. Prog. 28 (2012) 1088–94.

[197] A.L. Becker, A.P.R. Johnston, F. Caruso, Layer-by-layer-assembled capsules and films for therapeutic delivery., Small. 6 (2010) 1836–52.

[198] M.L. Stephenson, P.C. Zamecnik, Inhibition of Rous sarcoma viral RNA translation by a specific oligodeoxyribonucleotide., Proc. Natl. Acad. Sci. 75 (1978) 285–288.

[199] P. Martin, Wound Healing-Aiming for Perfect Skin Regeneration, Science. 276 (1997) 75–81.

Appendix

Main subroutine “Run”

```
Global Cancel As Integer
Global Angle
Global TimeLapse As Integer
Global TrackNum As Range
Global X As Range
Global Y As Range
Global XMod As Range
Global YMod As Range
Global AngPos As Range
Global Ang090 As Range
Global dx As Range
Global dy As Range
Global Dist As Range
Global Speed As Range
Global Pers As Range
Global L As Range
Global Cosine As Range
Global N As Integer
Global Ncell As Integer
Global Pi As Double
Global NSlides As Integer
Global Ini As Integer
Global Fin As Integer
-------------------------------------------------------------------------------
Sub Run()
  Application.ScreenUpdating = False
  Cancel = 0
  Call LoadFile
     If Cancel = 1 Then
       Exit Sub
     End If
  Call Parameters(Angle, TimeLapse, Cancel)
     If Cancel = 1 Then
       Exit Sub
     End If
  Scaling.Show 'Opens a user form to indicate the used objective
     If Cancel = 1 Then
       Exit Sub
     End If
  Set TrackNum = Rows(1).Find("Track n°").Columns.EntireColumn
  Set X = Rows(1).Find("X").Columns.EntireColumn
  Set Y = Rows(1).Find("Y corrected").Columns.EntireColumn
  Set XMod = Rows(1).Find("Xmod (µm)").Columns.EntireColumn
  Set YMod = Rows(1).Find("Ymod (µm)").Columns.EntireColumn
  Set AngPos = Rows(1).Find("Angle pos, ?pos (°)").Columns.EntireColumn
  Set Ang090 = Rows(1).Find("Ang (0°-90°)").Columns.EntireColumn
  Set dx = Rows(1).Find("dx (µm)").Columns.EntireColumn
  Set dy = Rows(1).Find("dy (µm)").Columns.EntireColumn
  Set Dist = Rows(1).Find("Distance (µm)").Columns.EntireColumn
  Set Speed = Rows(1).Find("Speed (µm/min)").Columns.EntireColumn
  Set Pers = Rows.Find("Time persist").Columns.EntireColumn
  N = WorksheetFunction.Max(Range("A:A"))
  Ncell = WorksheetFunction.Max(TrackNum)
  Pi = WorksheetFunction.Pi
```

```
  Call Process
  Call GrafTracks.TracksIm
  Call GrafTracks.TrackOrig
  Call GrafAng.GrafAng
  Call Correl.Correl
  Call Results.Results
  Call Save
End Sub
```

Function LoadFile

```
'Loads the raw data from the saved file
Function LoadFile()
  Dim Dataworkbook As Workbook
  Dim Resultworkbook As Workbook

  Cancel = 0
  Set Resultworkbook = ActiveWorkbook
  Application.CutCopyMode = False

  'Opens a dialog to select the file
  With Application.FileDialog(msoFileDialogOpen)
     .Filters.Clear
     .Filters.Add "Excel 2002-03", "*.xls", 1
     .Filters.Add "Excel 2007", "*.xlsx; *.xlsm; *.xlsa", 2
     .AllowMultiSelect = False
     If .Show = False Then
       Cancel = 1
     Else
       Workbooks.Open .SelectedItems(1)
       Set Dataworkbook = ActiveWorkbook
       Set DataRange = Dataworkbook.Sheets(1).Range("A:E")
       Set DestinationRange = Resultworkbook.Sheets("Data").Range("A:E")
       DataRange.Copy DestinationRange
       Dataworkbook.Close False
     End If
  End With
End Function
```

Function Parameters

```
'Introduces the data of pattern angle and frame lapse
Function Parameters(Angle, TimeLapse, Cancel)
  Cancel = 0
  Do
    Angle = InputBox("Angle of the pattern (-90°/90°): ", "Introduce
              parameter", " ")
    If Angle = "" Then
      Cancel = 1
      Exit Function
    ElseIf Angle <= -90 Or Angle > 90 Then
      MsgBox "Angle with respect to the horizontal. It must be between -
              90° and 90°", vbInformation
    End If
  Loop Until Angle <= 90 And Angle > -90

  Do
```

```
    TimeLapse = InputBox("Video time lapse (min/Frames): ", "Introduce
                parameter", "10")
    If TimeLapse = "" Then
      Cancel = 1
      Exit Function
    End If
  Loop Until TimeLapse > 0 And TimeLapse <> " "

  Worksheets("Data").Activate
  Rows.Find("Pattern angle, ? (°)").Cells.Offset(, 1).Value = Angle
  Rows.Find("min/frame").Cells.Offset(, 1).Value = TimeLapse
End Function
```

Subroutine Process

```
'Processes the data and calculates the parameters
Sub Process()
  Worksheets("Data").Activate
  For clmnnum = Y.Column To Pers.Column
    Cells(2, clmnnum).AutoFill Destination:=Range(Cells(2, clmnnum),
                Cells(N + 1, clmnnum))
  Next
End Sub
```

User Form “Scaling” code

```
Sub CommandButton1_Click()
  Worksheets("Data").Activate
    If OptionButton1.Value = True Then
      Cells(5, 22).Value = 0.626
    ElseIf OptionButton2.Value = True Then
      Cells(5, 22).Value = 0.313
    ElseIf OptionButton3.Value = True Then
      Cells(5, 22).Value = TextBox1.Value
      If TextBox1.Value = "" Then
        MsgBox "Introduce the scaling factor", vbInformation
        Cancel = 1
      End If
    End If
    Unload Me
  End Sub

Sub CommandButton2_Click()
  Cancel = 1
  Unload Me
End Sub
```

Subroutine TracksIm

```
'Draws the tracks of the cell migration
Sub TracksIm()
  Dim XVal As Range
  Dim YVal As Range
  Dim MaxVal As Integer
  Dim MinVal As Integer
  Dim RangGraf As Integer
  Dim IntGraf As Integer
  Dim Graph As Integer
```

```
Worksheets("Data").Activate
ActiveWorkbook.Sheets.Add before:=Worksheets("Data")
With ActiveSheet
   .Name = "Tracks"
End With
TrackNum.Copy
Sheets("Tracks").Columns(1).Select
Selection.PasteSpecial Paste:=xlPasteValues, Operation:=xlNone,
              SkipBlanks:=False, Transpose:=False
X.Copy
Sheets("Tracks").Columns(2).Select
Selection.PasteSpecial Paste:=xlPasteValues, Operation:=xlNone,
              SkipBlanks:=False, Transpose:=False
Y.Copy
Sheets("Tracks").Columns(3).Select
Selection.PasteSpecial Paste:=xlPasteValues, Operation:=xlNone,
              SkipBlanks:=False, Transpose:=False
With Worksheets("Tracks")
   Set TNumGraf = Columns(1).EntireColumn
   Set XGraf = Columns(2).EntireColumn
   Set YGraf = Columns(3).EntireColumn
   TNumGraf.ColumnWidth = "0.08"
   XGraf.ColumnWidth = "0.08"
   YGraf.ColumnWidth = "0.08"
   Cells(1, 4) = " "
End With

Set Tracks = ActiveSheet.ChartObjects.Add _
         (Left:=250, Width:=550, Top:=25, Height:=400)
With Tracks.Chart
   .ChartType = xlXYScatterLinesNoMarkers
   .ChartArea.Font.Size = 14
   .Parent.Name = "Tracks"
   .Axes(xlCategory).MinimumScale = 0
   .Axes(xlCategory).MaximumScale = 1400
   .Axes(xlCategory).MajorUnit = 200
   .Axes(xlCategory).HasTitle = True
   .Axes(xlCategory).AxisTitle.text = "µm"
   .Axes(xlValue).MinimumScale = 0
   .Axes(xlValue).MaximumScale = 1040
   .Axes(xlValue).MajorUnit = 208
   .Axes(xlValue).HasTitle = True
   .Axes(xlValue).AxisTitle.text = "µm"
End With

For Cell = 1 To Ncell
   Call Func.RangeCell(Cell, N, TrackNum)
   With ActiveSheet
      Set XVal = Range(XGraf.Cells(Ini), XGraf.Cells(Fin))
      Set YVal = Range(YGraf.Cells(Ini), YGraf.Cells(Fin))
      ActiveSheet.ChartObjects("Tracks").Activate
   End With

   With ActiveChart
      With .SeriesCollection.NewSeries
         .Values = YVal
         .XValues = XVal
         .Name = Cell
      End With
   End With
Next
```

```
ActiveSheet.ChartObjects("Tracks").Activate
For Each s In ActiveChart.SeriesCollection
  NSlides = s.Points.Count
  For a = 1 To NSlides
    If a = 1 Or a = NSlides Then
      s.Points(a).ApplyDataLabels
      With s.Points(a).DataLabel
        .text = a
        .Format.TextFrame2.TextRange.Font.Bold = msoTrue
        .Format.TextFrame2.TextRange.Font.Size = 10
        .Format.Fill.ForeColor.RGB = RGB(255, 255, 255)
        .Format.Fill.Transparency = 0.4
        .Position = xlLabelPositionCenter
      End With
    End If
  Next
Next
With ActiveChart
  Iter = 0
  Do Until 7 * Iter >= Ncell
    Iter = Iter + 1
    For R = 1 To Ncell
      With .SeriesCollection(R)
        Select Case R
          Case 1 + (Iter - 1) * 7
          .Format.Line.ForeColor.RGB = RGB(79, 129, 189)
          Case 2 + (Iter - 1) * 7
          .Format.Line.ForeColor.RGB = RGB(155, 187, 89)
          Case 3 + (Iter - 1) * 7
          .Format.Line.ForeColor.RGB = RGB(255, 0, 0)
          Case 4 + (Iter - 1) * 7
          .Format.Line.ForeColor.RGB = RGB(0, 255, 255)
          Case 5 + (Iter - 1) * 7
          .Format.Line.ForeColor.RGB = RGB(255, 51, 204)
          Case 6 + (Iter - 1) * 7
          .Format.Line.ForeColor.RGB = RGB(255, 255, 0)
          Case 7 + (Iter - 1) * 7
          .Format.Line.ForeColor.RGB = RGB(0, 0, 0)
        End Select
      End With
    Next
  Loop
End With

For i = 1 To Ncell
ActiveSheet.CheckBoxes.Add(845, 30 + 20 * i, 47, 17).Select
  With Selection
    .Caption = i
    .Name = "Checkbox" & i
    .Interior.Color = RGB(192, 192, 192)
    .Border.Color = RGB(0, 0, 0)
    .Display3DShading = True
    .Value = Checked
    .OnAction = "'" & ThisWorkbook.Name & "'!" & "ShowTrack.ShowTrack"
  End With
Next
ActiveSheet.Shapes.AddLabel(msoTextOrientationHorizontal, 818, 28, 110,
             25).Select
Selection.ShapeRange.TextFrame2.TextRange.Characters.text = "Show/Hide
             Track n.:"
```

```
  ActiveSheet.Shapes.AddShape(msoShapeRectangle, 222.75, 12.75, 714,
              424.5).Select
  Selection.ShapeRange.ZOrder msoSendToBack
  With Selection.ShapeRange
    .Fill.ForeColor.RGB = RGB(166, 166, 166)
    .Line.ForeColor.RGB = RGB(0, 0, 0)
    .Name = "Background"
  End With
  ActiveSheet.Shapes.SelectAll
  Selection.ShapeRange.Group.Select
  Selection.Placement = xlFreeFloating
End Sub
```

Subroutine TrackOrig

```
'Draws the windrose representation of the tracks
Sub TrackOrig()
  Worksheets("Data").Activate
  ActiveWorkbook.Sheets.Add before:=Worksheets("Data")
  With ActiveSheet
    .Name = "Tracks 0.0"
  End With
  TrackNum.Copy
  Sheets("Tracks 0.0").Columns(1).Select
  Selection.PasteSpecial Paste:=xlPasteValues, Operation:=xlNone,
              SkipBlanks:=False, Transpose:=False
  XMod.Copy
  Sheets("Tracks 0.0").Columns(2).Select
  Selection.PasteSpecial Paste:=xlPasteValues, Operation:=xlNone,
              SkipBlanks:=False, Transpose:=False
  YMod.Copy
  Sheets("Tracks 0.0").Columns(3).Select
  Selection.PasteSpecial Paste:=xlPasteValues, Operation:=xlNone,
              SkipBlanks:=False, Transpose:=False
  With Worksheets("Tracks 0.0")
    Set TNumGraf = Columns(1).EntireColumn
    Set XGraf = Columns(2).EntireColumn
    Set YGraf = Columns(3).EntireColumn
    TNumGraf.ColumnWidth = "0.08"
    XGraf.ColumnWidth = "0.08"
    YGraf.ColumnWidth = "0.08"
    Cells(1, 4) = " "
  End With

  'Defines the Range and interval for the axis of Chart TracksOrig
  MaxVal = WorksheetFunction.Max(Range(XGraf, YGraf))
  MinVal = WorksheetFunction.Min(Range(XGraf, YGraf))
  RangGraf = WorksheetFunction.Max(MaxVal, -MinVal)
  RangGraf = WorksheetFunction.Ceiling(RangGraf, 20)
  IntGraf = RangGraf / 4

  'Adds the direction of the pattern on Chart TracksOrig
  If Angle > -45 And Angle < 45 Then
    XPat1 = Array(-RangGraf, 0, RangGraf)
    XPat2 = XPat1
    YPat1 = Array(IntGraf - RangGraf * Tan(Angle * Pi / 180), IntGraf,
              IntGraf + RangGraf * Tan(Angle * Pi / 180))
    Ypat2 = Array(-IntGraf - RangGraf * Tan(Angle * Pi / 180), -IntGraf, -
              IntGraf + RangGraf * Tan(Angle * Pi / 180))
```

```
Else
   YPat1 = Array(-RangGraf, 0, RangGraf)
   Ypat2 = YPat1
   XPat1 = Array(IntGraf - RangGraf / Tan(Angle * Pi / 180), IntGraf,
               IntGraf + RangGraf / Tan(Angle * Pi / 180))
   XPat2 = Array(-IntGraf - RangGraf / Tan(Angle * Pi / 180), -IntGraf, -
               IntGraf + RangGraf / Tan(Angle * Pi / 180))
End If

Set TracksOrig = ActiveSheet.ChartObjects.Add(Left:=250, Width:=550,
               Top:=25, Height:=400)
With TracksOrig.Chart
   .ChartType = xlXYScatterLinesNoMarkers
   .ChartArea.Font.Size = 14
   .Parent.Name = "TracksOrig"
   With .Axes(xlCategory)
      .MinimumScale = -RangGraf
      .MaximumScale = RangGraf
      .MajorUnit = IntGraf
      .MajorTickMark = xlCross
      .HasTitle = True
      With .AxisTitle
         .text = "Distance (µm)"
         .Left = 361
         .Top = 215
      End With
   End With
   With .Axes(xlValue)
      .MinimumScale = -RangGraf
      .MaximumScale = RangGraf
      .MajorUnit = IntGraf
      .MajorTickMark = xlCross
      .MajorGridlines.Format.Line.Visible = msoFalse
   End With
End With

For Cell = 1 To Ncell
   Call Func.RangeCell(Cell, N, TrackNum)
   With ActiveSheet
      Set XVal = Range(XGraf.Cells(Ini), XGraf.Cells(Fin))
      Set YVal = Range(YGraf.Cells(Ini), YGraf.Cells(Fin))
      ActiveSheet.ChartObjects("TracksOrig").Activate
   End With
   With ActiveChart
      With .SeriesCollection.NewSeries
         .Values = YVal
         .XValues = XVal
         .Name = Cell
      End With
   End With
Next

'Adds Pattern lines
With TracksOrig.Chart
   With .SeriesCollection.NewSeries
      .Values = YPat1
      .XValues = XPat1
      .Name = "Pattern"
      With .Format.Line
         .Weight = 0.25
         .ForeColor.RGB = RGB(0, 0, 0)
```

```
        .DashStyle = msoLineDash
      End With
    End With
    With .SeriesCollection.NewSeries
      .Values = Ypat2
      .XValues = XPat2
      .Name = "Pattern"
      With .Format.Line
        .Weight = 0.25
        .ForeColor.RGB = RGB(0, 0, 0)
        .DashStyle = msoLineDash
      End With
    End With
    .Legend.LegendEntries(Ncell + 2).Delete
  End With

  With ActiveChart
    Iter = 0
    Do Until 7 * Iter >= Ncell
      Iter = Iter + 1
      For R = 1 To Ncell
        With .SeriesCollection(R)
          Select Case R
            Case 1 + (Iter - 1) * 7
            .Format.Line.ForeColor.RGB = RGB(79, 129, 189)
            Case 2 + (Iter - 1) * 7
            .Format.Line.ForeColor.RGB = RGB(155, 187, 89)
            Case 3 + (Iter - 1) * 7
            .Format.Line.ForeColor.RGB = RGB(255, 0, 0)
            Case 4 + (Iter - 1) * 7
            .Format.Line.ForeColor.RGB = RGB(0, 255, 255)
            Case 5 + (Iter - 1) * 7
            .Format.Line.ForeColor.RGB = RGB(255, 51, 204)
            Case 6 + (Iter - 1) * 7
            .Format.Line.ForeColor.RGB = RGB(255, 255, 0)
            Case 7 + (Iter - 1) * 7
            .Format.Line.ForeColor.RGB = RGB(0, 0, 0)
          End Select
        End With
      Next
    Loop
  End With

  For i = 1 To Ncell
    ActiveSheet.CheckBoxes.Add(845, 30 + 20 * i, 47, 17).Select
    With Selection
      .Caption = i
      .Name = "Checkbox" & i
      .Interior.Color = RGB(192, 192, 192)
      .Border.Color = RGB(0, 0, 0)
      .Display3DShading = True
      .Value = Checked
      .OnAction = "'" & ThisWorkbook.Name & "'!" & "ShowTrack.ShowTrack"
    End With
  Next
  ActiveSheet.Shapes.AddLabel(msoTextOrientationHorizontal, 818, 28, 110,
              25).Select
  Selection.ShapeRange.TextFrame2.TextRange.Characters.text = "Show/Hide
              Track n.:"
  ActiveSheet.Shapes.AddShape(msoShapeRectangle, 222.75, 12.75, 714,
              424.5).Select
```

```
  Selection.ShapeRange.ZOrder msoSendToBack
  With Selection.ShapeRange
    .Fill.ForeColor.RGB = RGB(166, 166, 166)
    .Line.ForeColor.RGB = RGB(0, 0, 0)
    .Name = "Background"
  End With
  ActiveSheet.Shapes.SelectAll
  Selection.ShapeRange.Group.Select
  Selection.Placement = xlFreeFloating
  'Draws the chart TrackOrig with black background
  Blck = MsgBox("Draw the tracks on black background?", vbYesNo, "Tracks
              Origin 0.0")
  If Blck = vbYes Then
    Call Blackback
  End If
End Sub
```

Subroutine Blackback

```
'Draws the chart TrackOrig with black background
Sub Blackback()
  Worksheets("Tracks 0.0").Select
  With ActiveSheet.ChartObjects("TracksOrig").Chart
    .ChartArea.Format.Fill.ForeColor.RGB = RGB(0, 0, 0)
    .PlotArea.Format.Fill.ForeColor.RGB = RGB(0, 0, 0)
    .Legend.Format.Line.ForeColor.RGB = RGB(255, 255, 255)
    .Legend.Format.TextFrame2.TextRange.Font.Fill.ForeColor.RGB = RGB(255,
              255, 255)
    Iter = 1
    Do Until 7 * Iter >= Ncell
      .SeriesCollection(7 + (Iter - 1) * 7).Format.Line.ForeColor.RGB =
              RGB(255, 255, 255)
      Iter = Iter + 1
    Loop
    .SeriesCollection(Ncell + 1).Format.Line.ForeColor.RGB = RGB(255, 255,
              255)
    .SeriesCollection(Ncell + 2).Format.Line.ForeColor.RGB = RGB(255, 255,
              255)
    .Axes(xlCategory).AxisTitle.Format.TextFrame2.TextRange.Font.Fill.Fore
              Color.RGB = RGB(255, 255, 255)
    For Each a In .Axes
      a.Format.Line.ForeColor.RGB = RGB(255, 255, 255)
      a.TickLabels.Font.Color = RGB(255, 255, 255)
    Next a
  End With
End Sub
```

Subroutine GrafAng

```
'Draws the histogram of step angle frequency
Sub GrafAng()
  ActiveWorkbook.Sheets.Add before:=Worksheets("Data")
  With ActiveSheet
    .Name = "Graphics angles"
  End With
  Cells(1, 1) = "Cell"
  Cells(1, 2) = "Angle (°)"
```

```
Cells(1, 2).AddComment.text text:="The range is +/-15° of the indicated
            centre"
Cells(1, 3) = "Frequency of occurence"
Columns(3).ColumnWidth = 11.57
Columns(3).WrapText = True
Columns(3).NumberFormat = "0.00"
ActiveSheet.Shapes.AddLabel(msoTextOrientationHorizontal, 818, 28, 110,
            25).Select
Selection.ShapeRange.TextFrame2.TextRange.Characters.text = "Show/Hide
            Track n.:"
ActiveSheet.Shapes.AddShape(msoShapeRectangle, 222.75, 12.75, 714,
            424.5).Select
Selection.ShapeRange.ZOrder msoSendToBack
With Selection.ShapeRange
   .Fill.ForeColor.RGB = RGB(166, 166, 166)
   .Line.ForeColor.RGB = RGB(0, 0, 0)
   .Name = "Background"
End With

Set AngChart = ActiveSheet.ChartObjects.Add(Left:=250, Width:=550,
            Top:=25, Height:=400)
With AngChart.Chart
   .Parent.Name = "Ang Chart"
   .ChartType = xlColumnClustered
   .ChartArea.Font.Size = 14
   .ChartGroups(1).GapWidth = 200
   .ChartGroups(1).Overlap = 0
   .Axes(xlValue).MaximumScale = 100
   .Axes(xlValue).TickLabels.NumberFormat = "0"
   .Axes(xlValue).HasTitle = True
   .Axes(xlValue).AxisTitle.text = "Frequency (%)"
   .Axes(xlCategory).HasTitle = True
   .Axes(xlCategory).AxisTitle.text = "Angle (°)"
   .Axes(xlCategory).HasMajorGridlines = True
End With

For Cell = 1 To Ncell
   Call Func.RangeCell(Cell, N, TrackNum)
   Set TrackSerie = Range(Ang090.Cells(Ini), Ang090.Cells(Fin))
   RAngFin = Cell * 4 + 1
   Ang0 = 0
   For rownum = RAngFin - 3 To RAngFin
      Cells(rownum, 1) = Cell
      Cells(rownum, 2) = Ang0
      Ang0 = Ang0 + 30
   Next
   With AngChart.Chart.SeriesCollection.NewSeries
      .XValues = Range(Cells(RAngFin - 3, 2), Cells(RAngFin, 2))
      .Values = Range(Cells(RAngFin - 3, 3), Cells(RAngFin, 3))
      .Name = Cell
   End With
   For rownum = 1 To Ncell * 4 + 1
      Iter = 0
      Do Until 7 * Iter >= Ncell
         Iter = Iter + 1
         Select Case Cells(rownum, 1)
            Case 1 + (Iter - 1) * 7
            Range(Cells(rownum, 1), Cells(rownum, 3)).Interior.Color =
                RGB(220, 230, 241)
            Case 2 + (Iter - 1) * 7
```

```
            Range(Cells(rownum, 1), Cells(rownum, 3)).Interior.Color =
                RGB(216, 228, 188)
            Case 3 + (Iter - 1) * 7
            Range(Cells(rownum, 1), Cells(rownum, 3)).Interior.Color =
                RGB(242, 220, 219)
            Case 4 + (Iter - 1) * 7
            Range(Cells(rownum, 1), Cells(rownum, 3)).Interior.Color =
                RGB(0, 255, 255)
            Case 5 + (Iter - 1) * 7
            Range(Cells(rownum, 1), Cells(rownum, 3)).Interior.Color =
                RGB(255, 51, 204)
            Case 6 + (Iter - 1) * 7
            Range(Cells(rownum, 1), Cells(rownum, 3)).Interior.Color =
                RGB(255, 255, 0)
            Case 7 + (Iter - 1) * 7
            Range(Cells(rownum, 1), Cells(rownum, 3)).Borders.LineStyle =
                xlYes
          End Select
        Loop
'Calculates the amount of angles belongs to each interval
        If Cells(rownum, 1) = Cell Then
          Tot = Application.WorksheetFunction.Count(TrackSerie)
          If Cells(rownum, 2) <> 0 Then
            Cells(rownum, 3) =
                (Application.WorksheetFunction.CountIfs(TrackSerie, ">=" &
                (Cells(rownum, 2) - 15)) -
                Application.WorksheetFunction.CountIfs(TrackSerie, ">=" &
                (Cells(rownum, 2) + 15)) +
                Application.WorksheetFunction.CountIfs(TrackSerie, ">=" &
                (Cells(rownum, 2) + 180 - 15)) -
                Application.WorksheetFunction.CountIfs(TrackSerie, ">=" &
                (Cells(rownum, 2) + 180 + 15))) / Tot * 100
          Else
            Cells(rownum, 3) =
                (Application.WorksheetFunction.CountIfs(TrackSerie, "<15")
                + Application.WorksheetFunction.CountIfs(TrackSerie,
                ">=165") -
                Application.WorksheetFunction.CountIfs(TrackSerie, ">=195")
                + Application.WorksheetFunction.CountIfs(TrackSerie,
                ">=345")) / Tot * 100
          End If
        End If
      Next
    Next

    With AngChart.Chart
      Iter = 0
      Do Until 7 * Iter >= Ncell
        Iter = Iter + 1
        For R = 1 To Ncell
          With .SeriesCollection(R).Format
            Select Case R
              Case 1 + (Iter - 1) * 7
              .Line.ForeColor.RGB = RGB(79, 129, 189)
              .Fill.ForeColor.RGB = RGB(79, 129, 189)
              Case 2 + (Iter - 1) * 7
              .Line.ForeColor.RGB = RGB(155, 187, 89)
              .Fill.ForeColor.RGB = RGB(155, 187, 89)
              Case 3 + (Iter - 1) * 7
              .Line.ForeColor.RGB = RGB(255, 0, 0)
              .Fill.ForeColor.RGB = RGB(255, 0, 0)
```

```
            Case 4 + (Iter - 1) * 7
            .Line.ForeColor.RGB = RGB(0, 255, 255)
            .Fill.ForeColor.RGB = RGB(0, 255, 255)
            Case 5 + (Iter - 1) * 7
            .Line.ForeColor.RGB = RGB(255, 51, 204)
            .Fill.ForeColor.RGB = RGB(255, 51, 204)
            Case 6 + (Iter - 1) * 7
            .Line.ForeColor.RGB = RGB(255, 255, 0)
            .Fill.ForeColor.RGB = RGB(255, 255, 0)
            Case 7 + (Iter - 1) * 7
            .Line.ForeColor.RGB = RGB(0, 0, 0)
            .Fill.ForeColor.RGB = RGB(0, 0, 0)
          End Select
        End With
      Next
    Loop
  End With

  For i = 1 To Ncell
    ActiveSheet.CheckBoxes.Add(845, 30 + 20 * i, 47, 17).Select
    With Selection
      .Caption = i
      .Name = "Checkbox" & i
      .Interior.Color = RGB(192, 192, 192)
      .Border.Color = RGB(0, 0, 0)
      .Display3DShading = True
      .Value = Checked
      .OnAction = "'" & ThisWorkbook.Name & "'!" & "ShowTrack.ShowTrack"
    End With
  Next
  ActiveSheet.Shapes.SelectAll
  Selection.ShapeRange.Group.Select
  Selection.Placement = xlFreeFloating
End Sub
```

Subroutine Correl

```
'Draws the position vector of each step
Sub Correl()
  Worksheets("Data").Activate
  ActiveWorkbook.Sheets.Add before:=Worksheets("Data")
  With ActiveSheet
    .Name = "Correlation"
  End With
  TrackNum.Copy
  Sheets("Correlation").Columns(1).Select
  Selection.PasteSpecial Paste:=xlPasteValues, Operation:=xlNone,
              SkipBlanks:=False, Transpose:=False
  dx.Copy
  Sheets("Correlation").Columns(2).Select
  Selection.PasteSpecial Paste:=xlPasteValues, Operation:=xlNone,
              SkipBlanks:=False, Transpose:=False
  dy.Copy
  Sheets("Correlation").Columns(3).Select
  Selection.PasteSpecial Paste:=xlPasteValues, Operation:=xlNone,
              SkipBlanks:=False, Transpose:=False
  With Worksheets("Correlation")
    Set TNumGraf = Columns(1).EntireColumn
    Set XGraf = Columns(2).EntireColumn
    Set YGraf = Columns(3).EntireColumn
```

```
   TNumGraf.ColumnWidth = "0.08"
   XGraf.ColumnWidth = "0.08"
   YGraf.ColumnWidth = "0.08"
   Cells(1, 4) = " "
End With

MaxVal = WorksheetFunction.Max(Range(XGraf, YGraf))
MinVal = WorksheetFunction.Min(Range(XGraf, YGraf))
RangGraf = WorksheetFunction.Max(MaxVal, -MinVal)
RangGraf = WorksheetFunction.Ceiling(RangGraf, 20)

Set Correlation = ActiveSheet.ChartObjects.Add(Left:=250, Width:=550,
             Top:=25, Height:=400)
With Correlation.Chart
   .ChartType = xlXYScatter
   .ChartArea.Font.Size = 14
   .Parent.Name = "Correlation"
   With .Axes(xlCategory)
      .MinimumScale = -RangGraf
      .MaximumScale = RangGraf
      .MajorTickMark = xlCross
      .HasTitle = True
      With .AxisTitle
         .text = "µm"
         .Left = 432
         .Top = 215
      End With
   End With
   With .Axes(xlValue)
      .MinimumScale = -RangGraf
      .MaximumScale = RangGraf
      .MajorTickMark = xlCross
      .MajorGridlines.Format.Line.Visible = msoFalse
   End With
End With

For Cell = 1 To Ncell
   Call Func.RangeCell(Cell, N, TrackNum)
   With ActiveSheet
      Set XVal = Range(XGraf.Cells(Ini), XGraf.Cells(Fin))
      Set YVal = Range(YGraf.Cells(Ini), YGraf.Cells(Fin))
      ActiveSheet.ChartObjects("Correlation").Activate
   End With
   With ActiveChart
      With .SeriesCollection.NewSeries
         .Values = YVal
         .XValues = XVal
         .Name = Cell
         .ChartType = xlXYScatter
         .MarkerStyle = 8
      End With
   End With
Next
With ActiveChart
   Iter = 0
   Do Until 7 * Iter >= Ncell
      Iter = Iter + 1
      For R = 1 To Ncell
         With .SeriesCollection(R)
            Select Case R
               Case 1 + (Iter - 1) * 7
```

```
            .Format.Fill.ForeColor.RGB = RGB(79, 129, 189)
            Case 2 + (Iter - 1) * 7
            .Format.Fill.ForeColor.RGB = RGB(155, 187, 89)
            Case 3 + (Iter - 1) * 7
            .Format.Fill.ForeColor.RGB = RGB(255, 0, 0)
            Case 4 + (Iter - 1) * 7
            .Format.Fill.ForeColor.RGB = RGB(0, 255, 255)
            Case 5 + (Iter - 1) * 7
            .Format.Fill.ForeColor.RGB = RGB(255, 51, 204)
            Case 6 + (Iter - 1) * 7
            .Format.Fill.ForeColor.RGB = RGB(255, 255, 0) 'Yellow
            Case 7 + (Iter - 1) * 7
            .Format.Fill.ForeColor.RGB = RGB(0, 0, 0) 'Black
          End Select
        End With
      Next
    Loop
    With .SeriesCollection.NewSeries
      .Values = Array(-RangGraf / 2 * Sin(Angle * Pi / 180), RangGraf / 2
                * Sin(Angle * Pi / 180))
      .XValues = Array(-RangGraf / 2 * Cos(Angle * Pi / 180), RangGraf / 2
                * Cos(Angle * Pi / 180))
      .Name = "Pattern"
      .ChartType = xlXYScatterLinesNoMarkers
      With .Format.Line
        .Weight = 2
        .ForeColor.RGB = RGB(0, 0, 0)
        .BeginArrowheadStyle = msoArrowheadStealth
        .BeginArrowheadLength = msoArrowheadLong
        .BeginArrowheadWidth = msoArrowheadWide
        .EndArrowheadStyle = msoArrowheadStealth
        .EndArrowheadLength = msoArrowheadLong
        .EndArrowheadWidth = msoArrowheadWide
      End With
    End With
  End With

  For i = 1 To Ncell
    ActiveSheet.CheckBoxes.Add(845, 30 + 20 * i, 47, 17).Select
    With Selection
      .Caption = i
      .Name = "Checkbox" & i
      .Interior.Color = RGB(192, 192, 192)
      .Border.Color = RGB(0, 0, 0)
      .Display3DShading = True
      .Value = Checked
      .OnAction = "'" & ThisWorkbook.Name & "'!" & "ShowTrack.ShowTrack"
    End With
  Next
  ActiveSheet.Shapes.AddLabel(msoTextOrientationHorizontal, 818, 28, 110,
              25).Select
  Selection.ShapeRange.TextFrame2.TextRange.Characters.text = "Show/Hide
              Track n.:"
  ActiveSheet.Shapes.AddShape(msoShapeRectangle, 222.75, 12.75, 714,
              424.5).Select
  Selection.ShapeRange.ZOrder msoSendToBack
  With Selection.ShapeRange
    .Fill.ForeColor.RGB = RGB(166, 166, 166)
    .Line.ForeColor.RGB = RGB(0, 0, 0)
    .Name = "Background"
  End With
```

```
  ActiveSheet.Shapes.SelectAll
  Selection.ShapeRange.Group.Select
  Selection.Placement = xlFreeFloating
End Sub
```

Subroutine Results

```
'Adds worksheet of results
Sub Results()
  ActiveWorkbook.Sheets.Add before:=Worksheets("Data")
  With ActiveSheet
    .Name = "Results"
  End With
  Cells(1, 1) = "Cell"
  Cells(1, 2) = "Colour"
  Cells(1, 3) = "N. Slides"
  Cells(1, 4) = "Migration time (min)"
  Cells(1, 5) = "Euclidean distance D (µm)"
  Cells(1, 5).AddComment.text text:="Straight displacement from Pos0 to
              Pos final"
  Cells(1, 6) = "Total path length L (µm)"
  Cells(1, 7) = "Straightness index"
  Cells(1, 8) = "Mean cosine c"
  Cells(1, 9) = "Average speed (µm/min)"
  Cells(1, 10) = "Persistence time (min)"
  Set Eucl = Rows(1).Find("Euclidean distance D
              (µm)").Columns.EntireColumn
  Set L = Rows(1).Find("Total path length L (µm)").Columns.EntireColumn
  Set Tiemp = Rows(1).Find("Migration time (min)").Columns.EntireColumn
  Set Cosine = Rows(1).Find("Mean cosine c").Columns.EntireColumn
  AngRad = WorksheetFunction.Radians(Angle)

  For Cell = 1 To Ncell
    Call Func.RangeCell(Cell, N, TrackNum)
    For Col = 1 To 14
      Cells(Cell + 1, Col).NumberFormat = "0.00"
      Select Case Col
        Case Rows(1).Find("Cell").Column
          Cells(Cell + 1, Col) = Cell
          Cells(Cell + 1, Col).NumberFormat = "0"
        Case Rows(1).Find("Colour").Column
          With Cells(Cell + 1, Col)
            Iter = 0
            Do Until 7 * Iter >= Ncell
              Iter = Iter + 1
              Select Case Cells(Cell + 1, 1)
                Case 1 + (Iter - 1) * 7
                .Interior.Color = RGB(220, 230, 241)
                .Value = "Blue"
                Case 2 + (Iter - 1) * 7
                .Interior.Color = RGB(216, 228, 188)
                .Value = "Green"
                Case 3 + (Iter - 1) * 7
                .Interior.Color = RGB(242, 220, 219)
                .Value = "Red"
                Case 4 + (Iter - 1) * 7
                .Interior.Color = RGB(0, 255, 255)
                .Value = "Cyan"
                Case 5 + (Iter - 1) * 7
                .Interior.Color = RGB(255, 51, 204)
```

```
                .Value = "Pink"
                Case 6 + (Iter - 1) * 7
                .Interior.Color = RGB(255, 255, 0)
                .Value = "Yellow"
                Case 7 + (Iter - 1) * 7
                .Interior.Color = RGB(255, 255, 255)
                .Value = "White"
              End Select
            Loop
          End With
        Case Rows(1).Find("N. Slides").Column
          Cells(Cell + 1, Col) = NSlides
          Cells(Cell + 1, Col).NumberFormat = "0"
        Case Tiemp.Column
          Cells(Cell + 1, Col) = (NSlides - 1) * TimeLapse
          Cells(Cell + 1, Col).NumberFormat = "0"
          Columns(Col).ColumnWidth = "9.86"
        Case Eucl.Column
          Cells(Cell + 1, Col) = Sqr((XMod.Cells(Fin) - XMod.Cells(Ini))
              ^ 2 + (YMod.Cells(Fin) - YMod.Cells(Ini)) ^ 2)
          Columns(Col).ColumnWidth = "14.29"
        Case L.Column
          Cells(Cell + 1, Col) = Application.Sum(Range(Dist.Cells(Ini),
              Dist.Cells(Fin)))
          Columns(Col).ColumnWidth = "12.57"
        Case Rows(1).Find("Straightness index").Column
          Cells(Cell + 1, Col) = Cells(Cell + 1, Eucl.Column) /
              Cells(Cell + 1, L.Column)
          Columns(Col).ColumnWidth = "11.57"
        Case Rows(1).Find("Mean cosine c").Column
          Cells(Cell + 1, Col) = Func.c(Ini, Fin, Cell)
          Columns(Col).ColumnWidth = "8.14"
        Case Rows(1).Find("Average speed (µm/min)", , , xlWhole).Column
          Cells(Cell + 1, Col) =
              WorksheetFunction.AverageIf(Range(Speed.Cells(Ini),
              Speed.Cells(Fin)), "<>0")
          Columns(Col).ColumnWidth = "14"
        Case Rows.Find("Persistence time (min)").Column
          Cells(Cell + 1, Col) = TimeLapse *
              WorksheetFunction.Max(Range(Pers.Cells(Ini),
              Pers.Cells(Fin)))
          Cells(Cell + 1, Col).NumberFormat = "0"
          Columns(Col).ColumnWidth = "11"
      End Select
    Next
  Next
  Range(Columns(1), Columns(14)).WrapText = True
End Sub
```

Subroutine ShowTrack

```
'Shows and hides the tracks on the different charts
Sub ShowTrack()
  Application.ScreenUpdating = False
  Set myCBX = ActiveSheet.CheckBoxes(Application.Caller)
  Ind = myCBX.Caption
  LastRow = ActiveSheet.Columns(1).Find("").Row
  Call Func.RangeCell(Val(Ind), LastRow - 1, Columns(1))

  Range(Rows(Ini), Rows(Fin)).Select
```

```
  If myCBX = xlOn Then
    Selection.Rows.EntireRow.Hidden = False
    Cells(1, 1).Select
  Else
    Selection.Rows.EntireRow.Hidden = True
    Cells(1, 1).Select
  End If
End Sub
```

Function RangeCell

```
'Defines the 1st and last row of the data corresponding to that cell and
    the number of slides
Function RangeCell(CellNumber, MaxRows, TrackColumn)
  NSlides = 0
  For i = 2 To MaxRows + 1
    If TrackColumn.Cells(i) = CellNumber Then
      NSlides = NSlides + 1
      If TrackColumn.Cells(i) <> TrackColumn.Cells(i - 1) Then
        Ini = i
      End If
    End If
  Next
  Fin = Ini + NSlides - 1
End Function
```

Function c

```
'Calculates the value for sinuosity
Function c(InitialPoint, EndPoint, CellNumber)
  Sumat = 0
  For rownum = InitialPoint + 1 To EndPoint
    If AngPos.Cells(rownum) <> "" Then
      Sumat = Sumat + Dist.Cells(rownum) * Cos(AngPos.Cells(rownum) * Pi /
              180)
    End If
  Next
  c = Sumat / L.Cells(CellNumber + 1) 'Mean cosin
End Function
```

Subroutine Save

```
Sub Save()
  Worksheets("Data").Select
  ActiveSheet.Shapes.Range(Array("Button 1", "Button 2")).Select
  Selection.Delete
  Do
    fname = Application.GetSaveAsFilename("", "Excel Macro-Enabled
            Workbook (*.xlsm),*.xlsm")
  Loop Until fname <> False
  ActiveWorkbook.SaveAs Filename:=fname
End Sub
```

Abstract

The main goal of this thesis is the control of the migratory behavior of fibroblasts by modifying the pattern dimensions of single external triggers. Controlling cell migration opens a wide range of possibilities in the field of regenerative therapies and cancer treatment. To accomplish this goal, migration on three types of substrates was investigated; topographically, elastically and chemically patterned hydrogels. These external signals constitute some of the most important migration triggers of the extracellular matrix. Samples were prepared using poly(ethylene glycol) (PEG) hydrogels. This polymer had been widely used as biomaterial because of its anti-adhesive properties. However, our group recently proved that the presence of micrometric topographic and mechanical patterns induces the adhesion of mouse fibroblasts (L929) on such materials. At the same time, smooth PEG hydrogels serve as an excellent inert background for chemical patterning.

For a scientific and comparable analysis of migratory behavior, specific migration parameters are required. Extensive research of the analysis methods has shown that any of the available software solutions was suitable for our system. For this reason, it was decided to program our own analysis tool (CellMAT) incorporating the main parameters used by other researchers to describe cell migration. CellMAT was able to process large amounts of data, saving calculation time and simplifying the interpretation of the migration tracks.

Fibroblasts migrating on channel-like topographically patterned substrates aligned to the pattern when the size of the grooves was similar to the cell size. On wider channels, the cells migrated randomly as if they were on a flat surface. Due to the properties of the PEG substrates, only the cells inside the channels adhered strongly enough to stay, avoiding line-crossing (in other words, perpendicular migration). On the other hand, when the spacing between grooves was in the order of the cell size or below, the cells were able to attach simultaneously to two adjacent channels and migrate outside them.

Mechanical patterns were prepared using the **Fi**ll-**M**olding **I**n **C**apillaries (**FIMIC**) method. This soft lithographic technique permits well-defined binary patterns of elasticity to be created using polymers with different degrees of cross-linking. In this method, a topographically patterned hydrogel (mold) was filled with the secondary material (filler) via

capillary force. Early experiments using pure PEG polymers highlighted that the fibroblasts showed a tendency to adhere and migrate on the mold lines, contradicting in some cases the expected durotactic behavior, namely, migration on the stiffer areas. Atomic force microscopy (AFM) analysis of the properties of the surface revealed that in those cases where the cells migrated on the softer mold lines non-negligible topography was present. This topography was a result of the different levels of swelling of the two components of the substrate.

In order to remove the topography of the FIMIC samples, blend materials of PEG and PEG-based polymers were used. These blends already showed their efficiency, when swollen, to level out the initial topography measured in FIMIC samples in the dry state. Experimentation on such substrates confirmed the observations from pure PEG samples. The analysis of the topography of the surface confirmed that those samples where the migration agreed with the durotaxis theory were found to be smooth, while on those where the migration occurred on the soft mold lines, the cells adhered on the convex structures of the surface, in agreement with the findings of Park and colleagues. These results indicate that the geometric cues may overrule underlying mechanical signals; this finding helps to elucidate the hierarchy between topographic and mechanical cues.

Interestingly, when the separation between attractive lines was larger than the typical size of a spread cell the migration was geometrically confined to those lines, without the existence of physical barriers.

In an attempt to generate substrates completely free of topographic features, but with a mechanical pattern, three approaches were investigated: spin-coating on topographic and FIMIC substrates, filling of channels and removal of the excess via scraping with a razor blade (razor-blading) and filling of channels and removal of the excess via spilling under pressure (sandwich method). These three procedures were intended to embed the pattern of elasticity under a homogenous layer of controlled thickness. Spin-coating and razor-blading presented several complications associated with dewetting and handling. The sandwich method successfully generated substrates with an embedded pattern of elasticity (seen via AFM) and the thickness of the blanket layer could be controlled by modifying the pressure exerted on the sample (load). Surprisingly, despite completely coating the original topographic substrate, topographic structures were still detectable when the samples were

hydrated. A possible explanation for this is that the different degree of swelling of both polymeric components was responsible for these alterations of the surface.

Chemical patterns were created using an inert PEG background in contact with a more adhesive PEG-based polymer (3BC) which contains poly(propylene glycol). As expected, selective adhesion onto the 3BC lines was observed. A similar behavior as on topographically and elastically patterned substrates was observed; cells migrated parallel to the pattern on narrow stripes (< 20 µm) while the degree of randomness increased with the width of the lines. On the other hand, perpendicular migration was enhanced by using moderately sized adherent lines (10-20 µm) with reduced spacing in between (< 10 µm).

Other kinds of chemical patterns were also used in this work. The adhesive properties and cytotoxicity of composite materials prepared with gold nanoparticles and PEG (PEG-AuNP) were tested. The incorporation of the nanoparticles modified the anti-adhesive nature of the PEG hydrogel and the immobilization of the particles in the polymeric network eliminated the toxicity of the small-sized nanoparticles. Several methods for patterning well-defined lines of gold nanoparticles on a PEG background were investigated: application of the FIMIC method using the composite PEG-AuNP as filler, selective transfer of gold to the filler lines during the FIMIC process (FIMIC-transferring) and transferring of a previously created gold pattern. Of these approaches the last one was the most promising; cells selectively adhered on clearly defined stripes where the gold was transferred.

A composite of microcapsules and PEG (PEG-µCap) was also used as filler for the FIMIC method. The incorporation of microcapsules into the hydrogel was expected to modify the surface properties of the hydrogel itself (i.e. topography and elasticity) and, therefore, induce cell adhesion exclusively at the location of those capsules. These capsules are potential drug carries for growth factors or transduction agents, which can improve the migration of cells as well as the tissue regeneration process. Confocal fluorescence imaging showed that the capsules were distributed inside the volume of the filled channels. AFM analysis showed that the properties of the surface can be effectively modified by the presence of capsules close to the surface. Unexpectedly, only a low fraction of the capsules were located close to the surface for interaction with cells and fibroblast adhesion on these materials was no different to that observed on similar samples without microcapsules. This project, despite it is at an early stage of development, is very promising. To solve some of

the current issues, improvements have been suggested, such as the incorporation of magnetic nanoparticles to the microcapsules in order to induce accumulation on the surface of the substrate during the FIMIC process.

Zusammenfassung

Das Hauptziel dieser Promotionsarbeit ist die Kontrolle des Wanderungsverhaltens von Fibroblasten durch die Modifizierung der Musterabmaße von einzelnen externen Auslösern. Die Bedeutung von Zellwanderung wurde von vielen Autoren unterstrichen. Infolgedessen erweitert die Kontrolle der Zellwanderung die Möglichkeiten im Bereich regenerativer Therapien und Krebsbehandlung. Um dieses Ziel zu erreichen, wurde die Zellwanderung auf drei verschiedenen Substraten untersucht: Topographisch, elastisch und chemisch gemusterte Hydrogele. Diese drei externen Signale stellen einige der wichtigsten Auslöser in der extrazellulären Matrix dar. Die Proben wurden mit Polyethylen Glykol (PEG) Hydrogelen vorbereitet. Dieses Polymer wird wegen seiner antiadhäsiven Eigenschaften häufig benutzt. Trotzdem wurde vor kurzem von unserer Gruppe nachgewiesen, dass die Präsenz von mikrometrischen Topographien und elastische Mustern die Adhäsion von Mausfibroblasten (L929) auf solchen Materialien induziert. Gleichzeitig stellen glatte PEG Hydrogele einen exzellenten Untergrund für chemische Muster dar.

Um eine reproduzier- und vergleichbare Analyse des Wanderungsverhaltens zu leisten, werden spezifische Zellwanderungsparameter benötigt. Eine ausführliche Untersuchung der analytischen Methoden zeigte, dass keine der verfügbaren Softwarelösungen für die Analyse der Zellwanderung für unser System geeignet war. Aus diesem Grund wurde entschieden, ein eigenes analytisches Werkzeug zu entwickeln (CellMAT), das die wichtigsten Zellwanderungsparameter enthält. CellMAT kann große Datenmengen verarbeiten, Zeit einsparen und vereinfacht die Auswertung der Wanderungsspuren.

Fibroblasten, die auf kanal-mäßigen Topographien wandern, orientieren sich an dem Muster, wenn die Größe der Kanäle ähnlich der der Zellgröße ist. Auf breiten Kanälen wandern die Zellen so orientierungslos, als ob sie auf einer flachen Oberfläche wären. Auf Grund der Eigenschaften der PEG-Substrate bleiben nur die Zellen haften, die sich innerhalb des Kanals befinden. Deswegen wandern sie nicht außerhalb der Kanäle senkrecht zum Muster. Andererseits ist Wanderung auf der externen Oberfläche des Substrates möglich, wenn der Abstand zwischen den Kanälen im Bereich der Zellgröße oder geringer ist. Dann

können die Zellen sich gleichzeitig an zwei nebeneinanderliegenden Kanälen festhalten und außerhalb von diesen wandern.

Elastische Muster wurden mit der **F**ill-**M**olding-**I**n-**C**apillaries (**FIMIC**) Methode vorbereitet. Diese Soft-lithographische Methode ermöglicht die Herstellung von eindeutig definierten binären elastischen Mustern, dank der Nutzung von Polymeren mit verschiedenem Vernetzungsgrad. Für diese Methode wurde ein topographisch gemustertes Hydrogel (Mold) mit einem sekundären Polymer (Filler) durch Nutzung des Kapillareffektes ausgefüllt. Frühe Zellwanderungsuntersuchungen mit reinen PEG Polymeren zeigten eine Tendenz zu Adhäsion und Zellwanderung auf den Moldlinien zuweilen im Gegensatz zur Durotaxistheorie, d.h. Zellwanderung auf den steiferen Zeilen. Die rasterkraftmikroskopische (AFM) Analyse der Oberflächeneigenschaften zeigte, dass in den Fällen, wo die Zellen auf weicheren Moldlinien gewandert sind, eine nicht vernachlässigbare Topographie vorhanden war. Diese Topographie folgte aus dem unterschiedlichen Quellverhalten der zwei Substratkomponenten.

Um die Topographie der FIMIC-Proben zu beseitigen, wurden Mischmaterialien aus PEG und PEG-basierten Polymeren benutzt. Experimente auf solchen Substraten bestätigten die Beobachtungen auf reinen PEG-Proben. Die Analyse der Oberflächentopographie bestätigte, dass auf den Proben, wo die Topographie ausgeglichen wurde, die Zellwanderung mit der Durotaxistheorie übereinstimmte. Wenn die Zellwanderung hingegen auf den weicheren Moldlinien stattfand, adhärierten die Zellen auf den konvexen Strukturen der Oberfläche. Diese Ergebnisse deuten an, dass geometrische Signale grundlegende elastische Signale maskieren können. Diese Entdeckung könnte helfen, die Hierarchie zwischen topographischen und elastischen Signalen aufzuklären.

Interessanterweise wurde die Zellwanderung nur durch die Separation zwischen attraktiven Linien geometrisch begrenzt, wenn deren Abstand größer als die typische Zellgröße war.

Um eine ganz flache Oberfläche herzustellen, wurden drei Methoden untersucht: Spin-coating auf topographischen und FIMIC Substraten, Verfüllung der Kanäle und Entfernen des Überschusses via Kratzen mit einem Messer (Razor-blading) und Verfüllung der Kanäle sowie das Entfernen des Überschusses via Überlaufen unter Druck (Sandwich Methode). Diese drei Methoden dienten dem Zweck, das elastische Muster unter eine

homogene Schicht mit kontrollierter Dicke einzubetten. Spin-coating und Razor-blading zeigten verschiedene Komplikationen verbunden mit der Entnetzung und der Handhabung. Die Sandwich Methode stellte erfolgreiche Substrate mit eingebettetem elastischem Muster her. Die Dicke der Schicht wurde mit der Modifizierung des Druckes kontrolliert. Trotz der Bedeckung der Topographie waren die Strukturen auf den hydratisierten Proben noch erkennbar. Wir stellten die Hypothese auf, dass das unterschiedliche Quellverhalten von beiden Materialien für diese Strukturen verantwortlich ist.

Chemische Muster wurden bei der Gegenübereinstellung von inertem PEG Hintergrund mit einem adhäsiver PEG-basierte Polymer (3BC) hergestellt. Wie erwartet, wurde selektive Adhäsion auf den 3BC Linien beobachtet. Die Zellen wanderten ähnlich wie die auf topographischen und elastischen Mustern; Zellen wanderten parallel zum Muster auf engen Linien (< 20 µm), während die Orientierungslosigkeit mit der Breite der Linien steigerte. Die perpendikulare Wanderung wurde durch die Nutzung von mittelgroßen adhärenten Linien (10-20 µm) und kleinen Abständen dazwischen (< 10 µm) gefördert.

Die adhäsiven Eigenschaften und die Zytotoxizität von Hydrogel Komposite aus Goldnanopartikeln und PEG (PEG-AuNP) wurde getestet. Die Einbringung der Nanopartikel modifizierte den antiadhäsiven Charakter des PEG und die Immobilisierung im polymerischen Netzwerk eliminierte die Toxizität von kleinen Nanopartikeln. Mehrere Methoden wurden untersucht, um wohldefinierte Linien aus Goldnanopartikeln auf PEG Hintergründen zu untersuchen: Anwendung der FIMIC-Methode mit Komposite PEG-AuNP als Filler, selektiver Transfer von Gold zu den Filler Linien während des FIMIC Prozesses (FIMIC-transferring) und der Transfer eines vorher hergestellten Goldmusters (Pattern transferring). Von diesen Ansätzen war der letzte der vielversprechendste; die Zellen adhärierten gezielt auf klar definierten Linien, wohin das Gold transferiert wurde.

Komposite Materialen aus Mikrokapseln und PEG (PEG-µCap) wurden auch als Filler für die FIMIC Methode benutzt. Von der Einfügung der Mikrokapseln in das Hydrogel wurde eine Modifikation der Oberflächeneigenschaften (d.h. Topographie und Elastizität) erwartet und damit die exklusive Zelladhäsion an den Stellen, wo die Mikrokapseln lokalisiert waren. Konfokal Mikroskopie zeigte, dass die Kapseln innerhalb des Volumens der gefüllten Kanäle verteilt wurden. AFM Analyse zeigte, dass die Oberflächeneigenschaften durch nah zur Oberfläche liegende Kapseln tatsächlich modifiziert werden können. Unerwarteter Weise

waren nur wenige Kapseln nah genug an der Oberfläche, um die Zelladhäsion zu beeinflussen.

Acknowledgments

First of all, I would like to thank Prof. Dr. Marga C. Lensen for giving me the opportunity to work with her in the field of biomaterials these last three years. Thank to her support, patience and corrections, I learned many things during this time and this helped to improve myself. I will also want to thank Prof. Dr. Holger Stark and Prof. Dr. Eva M. Eisenbarth for accepting to form part of the proofing committee and for having the patience of reading my thesis.

I also want to thank the member of the LensenLab for the help they offered me when I joined the group, for explaining my how to use the different equipment (and their tricks), for the long and nice chats about everything and nothing. My special acknowledgment to Dr. Susan Gaffney for introducing me the LensenLab and for becoming to me not only a mentor but also a friend.

I also want to thank Dr. Gaffney and Dr. Rhys Dowler for correcting my grammar, trying the not insignificant task of making a Spanish to improve his English.

Of course, I do not want to forget the support of Zuleyha Yenice, Andreas Klee, Carsten Hirschfeld and the people of the Werkstatt.

Ich möchte auch mich bei Prof. Dr. Peter Hufnagl für die konstruktive Diskussion und seine Unterstützung bedanken. Gleichzeitig will ich die gesamte Hufnagl Familie bedanken, dass sie eine zweite Familie für mich gewesen sind.

También quiero agradecer a la Dra. Victoria E. Santos por haberme ayudado a dar mis primeros pasos en el loco mundo de la investigación, a los laboristas, que, aunque no han hecho demasiado (o más bien nada) relacionado con este trabajo, han ayudado con su amistad a hacer de mí una mejor persona. A Bender, por enseñarme que por viejo que sea el material de laboratorio, siempre hay laboratorios con peores equipos, y que esos equipos pueden, a veces, ser tu salvación.

A mi familia, por haber hecho de mi lo que soy; a mis padres por la educación que me han dado y por darme la oportunidad de llegar hasta donde estoy y a mi hermano por sus consejos y sus siempre constructivas críticas.

Finalmente quiero agradecer a mi hija Paula por todos los buenos momentos al llegar a casa después del trabajo y por vigilar mi trabajo desde la foto en mi despacho. Ebenso will ich meine Verlobte Charlotte für ihre Unterstützung, für ihre Gesellschaft und für wollen ihre Leben mit mir zu verbringen bedanken.

List of publications

Published and submitted manuscripts:

de Vicente Lucas, G.; Lensen M.C. Topographically and elastically micropatterned PEG-based hydrogels to control cell adhesion and migration. *Submitted to European Polymer Journal; special issue Hydrogels (on invitation).*

Zhang, Z. ‡; Loebus, A. ‡; **de Vicente Lucas, G.**; Ren, F.; Arafeh, M.; Ouyang, Z.; Lensen, M.C. Synthesis of Poly(ethylene glycol)-based Hydrogels via Amine-Michael Type Addition with Tunable Stiffness and Postgelation Chemical Functionality. *Chemistry of Materials, 2014, vol. 26 (12), pp. 3524-3630.*

Manuscripts In preparation:

Zhang, Z.; Kelleher, S.; Strehmel, C.; Loebus, A.; **de Vicente, G.**; Schlesener, C.; Steinhilber, D Haag, R.; Lensen, M.C. Fabrication of hydrogels from star-shaped and hyperbranched polyether macromonomers with tuneable degradation properties via click chemistry. *Ready to be submitted to Polymer Chemistry*.

Loebus, A.‡; Zhang, Z.‡; Strehmel, C; **de Vicente Lucas, G.**; Lensen, M.C. Soft lithographic surface patterning of in-situ PEG Nanocomposite Hydrogels for selective interface interaction. *To be submitted.*

de Vicente Lucas, G.; Skirtach, A.G.; Lensen, M.C. Immobilization of polymeric capsules by Fill-Molding in Capillaries for controlled interaction with adherent cells. *To be submitted.*

de Vicente Lucas, G.; Lensen, M.C. Analysis tool for processing of cell migration tracks data (CellMAT). *Manuscript in preparation*.

de Vicente Lucas, G.; Gruner, P.; Lensen, M.C. Embedding of patterns of elasticity for controlling cell migration. *Manuscript in preparation*.

de Vicente Lucas, G. ‡; Yeşildağ, Ç. ‡; Bartsch, C., Lensen, M.C. Micro-transfer patterning strategies for selective control of cell adhesion on PEG-based hydrogels. *Manuscript in preparation*.

Arafeh, M.; **de Vicente Lucas, G.**; Loebus, A.; Lensen, M.C. Embedded Micro-pattern of PEG-Gold Nanoparticles Composite Hydrogel for Biomedical Applications. *Manuscript in preparation*.

Contributions to Scientific Conferences

Poster Contribution:

Genipin-Crosslinked Chitosan/Au Nanocomposite Hydrogels for Cancer Treatment Applications. Ren, F., **de Vicente Lucas, G.**, Zhang, Z., Lensen, M.C. *Materials Science and Engineering* 2014, Darmstadt, Germany

Micro- and Nano-patterned Surfaces for Selective Immobilization of Enzymes. Arafeh, M., Chen, J., Guiet, A., Loebus, A., Felkel, D., Zhang, Z., **de Vicente Lucas, G.**, Kelleher, S., Fischer, A., Lensen, M.C. *13th Dresden Polymer Discussion and 8th Max Bergmann Symposium– "Molecular Bioengineering Meets Polymer Science"* 2012, Dresden, Germany.

Bioconversion of glycerol into 2,3-butanediol employing different strains of *Klebsiella oxytoca* under aerobic conditions. Ripoll, V., **de Vicente, G.**, Morán, B., Ladero, M., Santos, V.E. *European Congress of Applied Biotechnology*. 2011, Berlin, Germany.

Oral contribution:

Controlling cell migration via topographical, mechanical and chemical surface patterns. **de Vicente Lucas, G.**, Strehmel, C., Zhang, Z., Loebus, A., Kelleher, S., Lensen, M.C. *Material Science and Engineering* 2012, Darmstadt, Germany